©Copyright 2012
Chunsheng Zhao

Investigation of Surface Interactions between Cytochrome b_5 and Major Cytochrome P450 Isoforms

Chunsheng Zhao

A dissertation
Submitted in partial fulfillment of the
Requirements for the degree of

Doctor of Philosophy

University of Washington
2012

Reading Committee:
William M. Atkins, Chair
Sidney D. Nelson, Honorary Chair
David R. Goodlett
Kenneth E. Thummel

Program Authorized to Offer Degree:
Medicinal Chemistry

University of Washington

Abstract

Investigation of Surface Interactions between Cytochrome b_5 and
Major Cytochrome P450 Isoforms

Chunsheng Zhao

Chair of the Supervisory Committee:
Professor: William M. Atkins
Honorary Chair:
Professor: Sidney D. Nelson
Department of Medicinal Chemistry

Cytochrome b_5 (cyt b5 or holo b5) is known as one of the key components in the microsomal cytochrome P450 (CYP) monooxygenase system that metabolizes structurally diverse endogenous and exogenous compounds. It has been reported to modulate many CYPs activity and the effect is both CYP isoform and substrate dependent. However, to date no consensus has been made on the underlying mechanism. In the present study, the surface interactions between cyt b5 and major hepatic CYP isoforms 3A4, 2C9, 2A6 and 2D6 were investigated. Chemical cross-linking coupled with mass spectrometric analysis was used to identify the potential electrostatic interactions on protein surfaces of cyt b5 and CYPs. Subsequently, the interaction models of cyt b5-CYPs were built using these identified cross-linking sites as constraints. For the first time, holo b5 and apo b5 (cyt b5 devoid of heme) surface interactions with CYPs were compared. The models suggest both of them bind to the same the groove on CYPs with very small difference in their orientations. The closest distances between the heme groups of cyt b5 and each CYP isoform are beyond direct electron transfer distance, indicating that cyt b5 likely modulates these CYP isoforms

activity through allosteric effect, in addition to the potential electron transfer role. In order to confirm that the residues involved in cross-linking are functionally important for cyt b5-CYP interaction, site-directed mutagenesis of CYP3A4 were carried out with the identified Lys residues on CYP3A4 being substituted with neutral residue Ala. In addition, the importance of Arg446 on CYP3A4 at the interface of the cyt b5-CYP3A4 complex model was also accessed by single-point mutation. Mutation of these residues reduced or abolished cyt b5 binding affinity, suggesting that electrostatic interactions at the interface of the two proteins are functionally important and the chemical cross-linking coupled with mass spectrometric analysis serves as a useful tool to study protein-protein interaction.

Table of Contents

List of Figures v

List of Tables ix

Chapter 1. Human cytochrome P450s and their redox partners 1

1.1 Human Cytochrome P450 1

1.1.1 Introduction of cytochrome P450s 1

1.1.2 P450 catalytic cycle 2

1.2 Interaction between P450s and CPR 3

1.2.1 CPR structure 3

1.2.2 Kinetics of electron transfer between CPR and P450s 5

1.2.3 P450-CPR complex formation 7

1.2.4 P450 topology in interactions with CPR 9

1.3 Cytochrome b5 10

1.3.1 Structure of cytochrome b5 10

1.3.2 Cytochrome b5 modulation of P450 catalyzed reactions 11

1.3.3 Cytb5-P450 complex formation 12

1.3.4 P450 topology in interactions with b5 15

1.3.5 Structural comparison of holocytochrome b5 and apocytochrome b5 16

1.4 In vivo role of cytochrome b5 17

1.4.1 Cytochrome b5 knockout animal models 17

1.4.2 Pharmacogenetics of cytochrome b5 19

1.4.3 Cytochrome b5 - P450 interaction in regulatory pathways 21

1.5 Mechanism of cytochrome b5 action 21

1.5.1 Auxiliary source of electrons for P450s in substitute of CPR 21

1.5.2 Fast second electron input 23

1.5.3 Electron Transfer with P450 as a two-electron acceptor 24

1.5.4 Enhancement of the coupling efficiency of the P450 catalytic cycle 25

1.5.5 Allosteric effects on P450 conformation 26
1.6 Cyt b5 competes with CPR for binding to P450s 28
1.7 Cross-linking studies of the interaction between P450 and its redox partners 29
1.8 Cross-linking reagent and P450 isoform selection for the current investigation 30
Chapter 2. Cyt b5-CYP3A4 Interaction Study 38
2.1 CYP3A4 interaction with redox partners 38
2.1.1 CYP3A4 introduction 38
2.1.2 Cyt b5 modulation effect on CYP3A4 39
2.1.3 CYP3A4 structure 41
2.1.4 CYP3A4 topology for binding of redox partners 44
2.2 Experimental procedures 46
2.2.1 Materials 46
2.2.2 Protein Expression and Purification 46
2.2.3 Site-Directed Mutagenesis of CYP3A4 51
2.2.4 Cross-linking Reactions 52
2.2.5 Proteolytic Digestion and Mass Spectrometric Analysis 52
2.2.6 Testosterone 6β-Hydroxylation Catalyzed by CYP3A4 Wild Type and Mutant 53
2.2.7 Equilibrium binding of cyt b5. 53
2.2.8 Molecular Docking and Energy Minimization. 54
2.3 Results 54
2.3.1 Chemical Cross-linking. 54
2.3.2 Apo b5 and CYP3A4 Interactions by Mass Spectrometric Analysis. 54
2.3.3 Modeling of Holo b5-CYP3A4 and Apo b5-CYP3A4 Complex 55
2.3.4 Site-directed mutagenesis of CYP3A4 and protein purification 56
2.3.5 Effect of the Mutations on Catalytic Activities of CYP3A4 57
2.3.6 Effect of the Mutations on CYP3A4 binding to Cyt b5 57
2.3.7 Effect of the mutations on CRP interaction with CYP3A4 58

2.4 Discussion 59
Chapter 3. Cyt b5-CYP2C9 Interaction Study 81
3.1 CYP2C9 interaction with its redox partners 81
3.1.1 CYP2C9 introduction 81
3.1.2 Cyt b5 modulation effect on CYP2C9 82
3.1.3 CYP2C9 structure and topology in interaction with its redox partners 83
3.1.4 Hypothesis for the study of cyt b5-CYP2C9 interaction 87
3.2 Materials and experimental procedures 87
3.2.1 Materials 87
3.2.2 Protein Expression and Purification 88
3.2.3 Cross-linking Reactions 89
3.2.4 Proteolytic Digestion and LTQ-Orbitrap Mass Spectrometric Analysis 90
3.2.5 Data Processing and Database Searching 91
3.2.6 Molecular Docking 92
3.3 Results 92
3.3.1 Chemical Cross-Linking 92
3.3.2 Holo b5 and CYP2C9 Interactions 93
3.3.3 Apo b5 and CYP2C9 Interactions by Mass Spectrometric Analysis 95
3.3.4 Modeling of Holo b5-CYP2C9 and Apo b5-CYP2C9 Complex 96
3.4 Discussion 99
Chapter 4. Cyt b5-CYP2A6 Interaction Study 131
4.1 CYP2A6 interaction with its redox partners 131
4.1.1 CYP2A6 introduction 131
4.1.2 Cyt b5 modulation on CYP2A6 activity 132
4.1.3 CYP2A6 structure and topology in binding to redox partners 133
4.1.4 Goals of the study of cyt b5-CYP2A6 interaction 135
4.2 Materials and experimental procedures 135

4.2.1 Materials 135
4.2.2 Protein Expression and Purification 135
4.2.3 Cross-linking reactions, mass spectrometric analysis and data processing 137
4.2.4 Molecular Docking 137
4.3 Results 138
4.3.1 Chemical Cross-Linking 138
4.3.2 Holo b5 and CYP2A6 Cross-linking Results 138
4.3.3 Apo b5 and CYP2A6 Cross-linking Results 141
4.3.4 Modeling of Holo b5-CYP2A6 and Apo b5-CYP2A6 Interactions 143
4.4 Discussion 146
Chapter 5. CYP2D6 Interactions with Cyt b5 and Conclusions 187
5.1 Control experiments for crosslinking studies using CYP2D6-cyt b5 and CYPs-C-terminal truncated cyt b5 187
5.1.1 Rationale of control experiments 187
5.1.2 Methods 187
5.1.3 Results 188
5.1.4 Discussion 189
5.2 Summary of cyt b5-CYP interactions 189
5.3 Future direction of cyt b5-CYP interaction study 192
Bibliography 193

List of Figures

Figure 1.1. Catalytic cycle of P450s. 33

Figure 1.2. Three-dimensional model illustrating the features of surface sites in CYP2C5 involved in redox-partner interactions. 34

Figure 1.3. Ribbon diagram of the crystal structure of cyt b5. 35

Figure 1.4. Rationale of activation of carboxylic acid group by EDC to react with primary amine group. 36

Figure 2.1. Interface between the holo b5-CYP3A4 complex model. 65

Figure 2.2. Comparison of effect of holo/apo b5 on NADPH-dependent formation of 6β-hydroxyl testosterone by CYP3A4. 65

Figure 2.3. SDS-PAGE analysis of the cross-linking reactions of apo b5 and CYP3A4 using EDC 66

Figure 2.4. Precursor ion MS spectra for cross-linked peptide apo b_5: ^{35}FLEEHPGGEEVLR^{47} – CYP3A4: ^{116}SAISIAEDEEWKR^{128}. 67

Figure 2.5. Precursor ion MS spectra for cross-linked peptide apo b_5: ^{48}EQAGGDATENFEDVGHSTDAR^{68} - CYP3A4: ^{71}VWGFYDGQQPVLAITDPDM IKTVLVK^{96} 68

Figure 2.6. Tandem mass spectra for two cross-linked peptide precursor ions identified from apo b5-CYP3A4 complex. 70

Figure 2.7. Top views of apo b5-CYP3A4 complex models. 71

Figure 2.8. Sequence alignment of CYPs 2B4, 2E1, 2C19, 2D6, 3A4, 3A5 and 2J2. 71

Figure 2.9. CO-ferrous binding difference spectra of wild-type CYP3A4 and its mutants 72

Figure 2.10. Testosterone binding affinity with CYP3A4 and its mutants. 72

Figure 2. 11. NADPH-dependent formation of 6β-hydroxyl testosterone by CYP3A4 and its mutants. 73

Figure 2.12. NADPH-dependent formation of Vivid Green® from Vivid DBOMF by CYP3A4 and its mutants. 74

Figure 2.13. Titration of cyt b5 to wild-type CYP3A4 and mutants and apo b5 to wild-type CYP3A4. 75

Figure 2.14. Effect of cyt b5 on formation of 6β-hydroxyl testosterone by CYP3A4 and its mutants. 75

Figure 2.15. Effect of CPR on formation of 6β-hydroxyl testosterone by CYP3A4 and its mutants. 76

Figure 2.16. Orientations of CYP3A4 and holo/apo b5 in membranes. 77

Figure 3.1. Precursor ion MS spectra for cross-linked peptide holo b_5: ^{48}EQAGGDATENFEDVGHSTDAR^{68} - CYP2C9: ^{421}KSK^{423} 103

Figure 3.2. Precursor ion MS spectra for cross-linked peptide holo b_5: ^{35}FLEEHPGGEEVLR^{47} - CYP2C9: ^{421}KSK^{423}. 105

Figure 3.3. Precursor ion MS spectra for cross-linked peptide holo b5: ^{48}EQAGGDATENFEDVGHSTDAR^{68} - CYP2C9: ^{109}GFGIVFSNGKK^{119} 106

Figure 3.4. Precursor ion MS spectra for cross-linked peptide holo b5: ^{35}FLEEHPGGEEVLR^{47} - CYP2C9: ^{158}KTK^{160} 106

Figure 3.5. Precursor ion MS spectra for cross-linked peptide holo: ^{48}EQAGGDATENFEDVGHSTDAR^{68} - CYP2C9: ^{271}MEKEK^{275}. 107

Figure 3.6. Tandem mass spectra for five cross-linked peptide precursor ions identified from holo b5-CYP2C9 complex. 112

Figure 3.7. Precursor ion MS spectra for cross-linked peptide apo b_5: ^{35}FLEEHPGGEEVLR^{47} - CYP2C9: ^{421}KSK^{423} 113

Figure 3.8. Precursor ion MS spectra for cross-linked peptide apo b_5: ^{48}EQAGGDATENFEDVGHSTDAR^{68} - CYP2C9: ^{119}KWK^{121} 113

Figure 3.9. Precursor ion MS spectra for cross-linked peptide apo b_5: ^{48}EQAGGDATENFEDVGHSTDAR^{68} - CYP2C9: ^{27}GKLPPGPTPLPVIGNILQIGIK^{48} ... 114

Figure 3.10. Precursor ion MS spectra for cross-linked peptide apo b_5: ^{48}EQAGGDATENFEDVGHSTDAR^{68} - CYP2C9: ^{233}LLKNVAFMK^{241} 114

Figure 3.11. Tandem mass spectra for five cross-linked peptide precursor ions identified from apo b5-CYP2C9 complex. 118

Figure 3.12. Holo/apo b5-CYP2C9 complex models. 119

Figure 4.1. Precursor ion MS spectra for cross-linked peptide holo b_5: ^{48}EQAGGDATENFEDVGHSTDAR^{68} - CYP2A6: ^{124}AKQLR^{128}. 150

Figure 4.2 Precursor ion MS spectra for cross-linked peptide holo b_5: ^{48}EQAGGDATENFEDVGHSTDAR^{68} - CYP2A6: ^{376}KDTKFR^{381}. 150

Figure 4.3 Precursor ion MS spectra for cross-linked peptide holo b_5: ^{48}EQAGGDATENFEDVGHSTDAR^{68} - CYP2A6: ^{425}KSDAFVPFSIGKR^{437}..... 151

Figure 4.4. Precursor ion MS spectra for cross-linked peptide holo b_5: ^{48}EQAGGDATENFEDVGHSTDAR^{68} - CYP2A6: ^{462}LKSSQSPK^{469}. 151

Figure 4.5. Precursor ion MS spectra for cross-linked peptide holo b5: 48EQAGGDATENFEDVGHSTDAR68 - CYP2A6: 275MQEEEKNPNTEFYLK289..... 152

Figure 4.6. Precursor ion MS spectra for cross-linked peptide holo b_5: ^{35}FLEEHPGGEEVLR^{47} - CYP2A6: ^{425}KSDAFVPFSIGKR^{437}. 152

Figure 4.7. Precursor ion MS spectra for cross-linked peptide holo b_5: ^{35}FLEEHPGGEEVLR^{47} - CYP2A6: ^{376}KDTKFR^{381}..... 153

Figure 4.8. Precursor ion MS spectra for cross-linked peptide holo b_5: ^{35}FLEEHPGGEEVLR^{47} - CYP2A6: ^{334}VIGKNR^{339} 154

Figure 4.9. Tandem mass spectra for the cross-linked peptide precursor ion No.1 in Table 4.1 155

Figure 4.10. Tandem mass spectra for the cross-linked peptide precursor ion No.2 in Table 4.1..... 156

Figure 4.11. Tandem mass spectra for the cross-linked peptide precursor ion No.3 in Table 4.1..... 157

Figure 4.12 Tandem mass spectra for the cross-linked peptide precursor ion No.4 in Table 4.1..... 158

Figure 4.13 Tandem mass spectra for the cross-linked peptide precursor ion No.5 in Table 4.1..... 159

Figure 4.14. Tandem mass spectra for the cross-linked peptide precursor ion No.6 in Table 4.1..... 160

Figure 4. 15. Tandem mass spectra for the cross-linked peptide precursor ion No.7 in Table 4.1..... 161

Figure 4.16. Tandem mass spectra for the cross-linked peptide precursor ion No.8 in Table 4.1 162

Figure 4.17. Precursor ion MS spectra for cross-linked peptide apo b_5: ^{48}EQAGGDATENFEDVGHSTDAR^{68} - CYP2A6: ^{124}AKQLR^{128} 163

Figure 4.18. Precursor ion MS spectra for cross-linked peptide apo b_5: ^{48}EQAGGDATENFEDVGHSTDAR^{68} - CYP2A6: ^{376}KDTK^{379} 163

Figure 4.19. Precursor ion MS spectra for cross-linked peptide apo b_5: ^{35}FLEEHPGGEEVLR^{47} - CYP2A6: ^{374}VKK^{376} 164

Figure 4.20. Precursor ion MS spectra for cross-linked peptide apo b_5: ^{35}FLEEHPGGEEVLR^{47}- CYP2A6: ^{334}VIGKNR^{339} 164

Figure 4.21. Precursor ion MS spectra for cross-linked peptide apo b_5: ^{35}FLEEHPGGEEVLR^{47} - CYP2A6: ^{334}VIGKNR^{339} 165

Figure 4.22. Precursor ion MS spectra for cross-linked apo b_5: ^{35}FLEEHPGGEEVLR^{47} - CYP2A6: ^{251}KVEHNQR^{257} 165

Figure 4.23 Tandem mass spectra for cross-linked peptide precursor ion No.1 in Table 4.2 166

Figure 4.24. Tandem mass spectra for cross-linked peptide precursor ion No.2 in Table 4.2 167

Figure 4. 25. Tandem mass spectra for cross-linked peptide precursor ion No.3 in Table 4.10 168

Figure 4.26. Tandem mass spectra for cross-linked peptide precursor ion No.4 in Table 4.10 169

Figure 4.27. Tandem mass spectra for cross-linked peptide precursor ion No.5 in Table 4.1 170

Figure 4.28. Figure 4.28 Tandem mass spectra for cross-linked peptide precursor ion No.6 in Table 4.10 171

Figure 4.29. Holo/apo b5-CYP2A6 complex models. 173

List of Tables

Table 2.1 Inter-molecular cross-linked peptide candidates in the complex of CYP3A4-apob_5. 78

Table 2.2 Assignment of tandem mass spectrum for the quadruple-charged ion of cross-linked peptide apo b5:^{35}Phe-Arg^{47}-CYP3A4:^{116}Ser-Arg^{128} with m/z of 757.3763. 79

Table 2.3 Assignment of tandem mass spectrum for the quintuple-charged ion of the cross-linked peptide apo b5:^{48}Glu-Arg^{68}-CYP3A4: ^{71}Val-Lys^{96} with m/z of 1024.8989. 80

Table 3.1 Inter-molecular cross-linked peptides in the complex of holo cytb_5-CYP2C9. 120

Table 3.2 Inter-molecular cross-linked peptides in the complex of apo cytb_5-CYP2C9. 121

Table 3.3. Assignment tandem MS spectra of precursor ion $[M+4H]^{4+}$=638.0406 for holo b5: ^{48}EQAGGDATENFEDVGHSTDAR^{68} - CYP2C9: ^{421}KSK^{423} 122

Table 3.4 Assignment of tandem MS spectra of precursor ion $[M+4H]^{4+}$=464.4965 for holo b5: ^{35}FLEEHPGGEEVLR^{47} - CYP2C9: ^{421}KSK^{423} 123

Table 3.5 Assignment of tandem MS spectra of ion $[M+5H]^{5+}$=668.9106 for cross-linking peptide holo human b5: ^{48}EQAGGDATENFEDVGHSTDAR^{68} - CYP2C9: ^{109}GFGIVFSNGKK^{119} 124

Table 3.6 Assignment of tandem MS spectra of ion $[M+4H]^{4+}$=468.0014 for cross-linked peptide holo b5: ^{35}FLEEHPGGEEVLR^{47} - CYP2C9: ^{158}KTK^{160} 125

Table 3.7 Assignment of tandem MS spectra of ion $[M+5H]^{5+}$=571.0525 for cross-linked peptide holo human b5: ^{48}EQAGGDATENFEDVGHSTDAR^{68} - CYP2C9: ^{271}MEKEK^{275} 126

Table 3.8 Assignment of tandem MS spectra of ion $[M+4H]^{4+}$=464.4986 for cross-linking peptide apo b_5: ^{35}FLEEHPGGEEVLR^{47} - CYP2C9: ^{421}KSK^{423} 127

Table 3.9 Assignment of tandem MS spectra of ion $[M+4H]^{4+}$=662.8094 for apo b5: ^{48}EQAGGDAT ENFEDVGHSTDAR^{68} - CYP2C9: ^{119}KWK^{121} 128

Table 3.10 Assignment of tandem MS spectra of ion $[M+4H]^{4+}$=1103.0741 for cross-linking peptide apo b5: ^{48}EQAGGDATENFEDVGHSTDAR^{68} - CYP2C9: ^{27}GKLPPGPTPLPVIGNILQIGI K^{48} 129

Table 3.11 Assignment of tandem MS spectra of ion $[M+5H]^{5+}$=650.9129 for cross-linking peptide apo b5: ^{48}EQAGGDATENFEDVGHSTDAR^{68} - CYP2C9: ^{233}LLKNVAFMK^{241} 130

Table 4.1 Inter-molecular cross-linked peptides in the complex of holo b_5-CYP2A6. 174

Table 4.2 Assignment tandem MS spectra of precursor ion 561.2653 z=5 for cross-linked peptide holo b_5: ^{48}EQAGGDATENFEDVGHSTDAR^{68} - CYP2A6: ^{124}AKQLR^{128} 175

Table 4.3 Assignment tandem MS spectra of precursor ion 597.0750 z=5 for cross-linked peptide holo b_5: ^{48}EQAGGDATENFEDVGHSTDAR^{68} - CYP2A6: ^{376}KDTKFR^{381} 176

Table 4.4 Assignment tandem MS spectra of precursor ion 728.5439 z=5 for cross-linked peptide holo b_5: ^{48}EQAGGDATENFEDVGHSTDAR^{68} - CYP2A6: ^{425}KSDAFVPFSIGKR^{437}) 177

Table 4.5 Assignment tandem MS spectra of precursor ion 613.0852 z=5 for cross-linked peptide holo b_5: ^{48}EQAGGDATENFEDVGHSTDAR^{68} - CYP2A6: ^{462}LKSSQSPK^{469} 178

Table 4.6 Assignment tandem MS spectra of precursor ion 818.1609 z=5 for holo b5: ^{48}EQAGGDATENFEDVGHSTDAR^{68} - CYP2A6: ^{275} MQEEEKNPNTEFYLK ^{289}..... 179

Table 4.7 Assignment tandem MS spectra of precursor ion 697.8615 z=4 for cross-linked peptide holo b_5: ^{35}FLEEHPGGEEVLR^{47} - CYP2A6: ^{425}KSDAFVPFSIGK^{436} 180

Table 4.8 Assignment tandem MS spectra of precursor ion 458.2413 z=5 for cross-linked peptide holo b_5: ^{35}FLEEHPGGEEVLR^{47} - CYP2A6: ^{376}KDTKFR^{381} 181

Table 4.9 Assignment tandem MS spectra of precursor ion 436.6376 z=5 for cross-linked peptide holo b_5: ^{35}FLEEHPGGEEVLR^{47} - CYP2A6: ^{334}VIGKNR^{339} , NO. 8 in Table 4.1. 181

Table 4.10 Inter-molecular cross-linked peptides in the complex of apo cytb_5-CYP2A6. 182

Table 4.11 Assignment tandem MS spectra of precursor ion 561.2653 z=5 for cross-linked peptide apo b_5: ^{48}EQAGGDATENFEDVGHSTDAR^{68} - CYP2A6: ^{124}AKQLR^{128} 183

Table 4.12 Assignment tandem MS spectra of precursor ion 597.0750 z=5 for cross-linked peptide apo b_5: ^{48}EQAGGDATENFEDVGHSTDAR^{68} - CYP2A6: ^{376}KDTK^{379} 183

Table 4.13 Assignment tandem MS spectra of precursor ion 728.5439 z=5 for cross-linked peptide apo b_5: ^{35}FLEEHPGGEEVLR^{47} - CYP2A6: ^{374}VKK^{376} 184

Table 4.14 Assignment tandem MS spectra of precursor ion 613.0852 z=5 for cross-linked peptide apo b_5: ^{48}EQAGGDATENFEDVGHSTDAR^{68} - CYP2A6: ^{334}VIGKNR^{339} 185

Table 4.15 Assignment tandem MS spectra of precursor ion 818.1609 z=5 for apo b_5: : ^{35}FLEEHPGGEEVLR^{47}- CYP2A6: ^{334}VIGKNR^{339} 186

Table 4.16 Assignment tandem MS spectra of precursor ion 818.1609 z=5 for apo b_5: ^{35}FLEEHPGGEEVLR^{47}- CYP2A6: ^{251}KVEHNQR^{257} 186

Acknowledgments

I owe my sincere thanks to all the people who have helped make this dissertation possible: the faculty, staff, my colleagues and friends in the Department of Medicinal Chemistry and Pharmaceutics, and the UW Proteomics Center. It is their guidance, support and helps that made my graduate study experience the one I will cherish forever. I specifically would like to express my deepest gratitude to the following people:

Dr. Sidney D. Nelson, my advisor for the past five years before he suddenly passed away last year. He guided me into the field of drug metabolism, and had been so patient and encouraging to allow me to explore and learn different things. He will always be missed.

Dr. William M. Atkins, who has been providing me support and advice on my thesis research, and guided me through my defense and dissertation preparation with great patience. His passion and insight in science have been great inspiration to me.

Dr. David R. Goodlett, who has been providing mentoring to me in proteomics research. His guidance and support are invaluable.

Dr. Kenneth E. Thummel, for his advice, suggestions and helps on my scientific development.

Dr. Rheem A. Totah, for her significant help during my research as well as dissertation preparation.

My GSR, Dr. Thomas Hazlet, for his warm helps and support.

Dr. Allan E. Rettie, for his support and advice during all my graduate study.

Dr. Priska von Haller, for providing me the mass spectrometer training and technical support.

The current and previous Nelson lab members Michelle Wahlin, Dr. Hideo Takakusa and Dr. Klarissa Hardy, etc., for the many helpful discussions, support and friendship.

Dr. Mariko Nakano, for her kindly help through my graduate study.

The Atkins lab, the Goodlett lab and the Totah lab members, for their scientific helps and friendship.

It was great pleasure to work with these wonderful people, who have made my graduate journey so meaningful.

Dedication

To my husband Zhanglin,

For his support and encouragement, and the sacrifices he made during my graduate study, as well as the many scientific discussions and company during late nights of my writing.

To my parents and parents-in-law,

For their endless love and support.

To my children,

For everything they brought to me.

Chapter 1. Human cytochrome P450s and their redox partners

1.1 Human Cytochrome P450

1.1.1 Introduction of cytochrome P450s

Cytochrome P450s (P450s, CYPs) are heme-containing enzymes ubiquitous in nature found in a wide range of phyla, constituting a large superfamily with over 8000 named genes (http://www.genomesonline.org/). Humans have 115 P450 genes with ~50% being full-length. The 57 functional human P450s are assigned into 18 families that are conserved in all mammals on the basis of primary amino acid sequence similarity (Ortiz de Montellano, 2005).

P450s can metabolize a large number of structurally different endogenous and exogenous compounds. About 15 major isoforms of the 57 known human P450s are responsible for over 90% of the oxidative metabolism of all pharmaceuticals in current clinical use. These isoforms are mainly from families 1, 2, or 3; they are CYPs 1A1, 1A2, 1B1, 2A6, 2B6, 2C8, 2C9, 2C19, 2D6, 2E1 and 3A4 (Farooq and Roberts, 2010; Ortiz de Montellano, 2005,). P450s contain a heme cofactor which conducts redox reactions, resulting in the activation of one molecule of oxygen, with bond scission and one oxygen atom inserted into an organic substrate while the other one is reduced to form water. The stoichiometry is:

$$R\text{-}H + O_2 + 2e^- + 2H^+ \xrightarrow{P450} R\text{-}OH + H_2O$$

This monooxygenation reaction requires a redox partner to supply reducing equivalents during the catalysis. On the basis of different types of electron transfer systems used during

the catalytic cycle, P450s are divided into two major classes. The Class I family includes bacterial and mitochondria P450s, which use a two-component shuttle system consisting of an iron-sulfur protein and ferredoxin reductase. The Class II family includes microsomal P450s, receiving electrons from NADPH-dependent cytochrome P450 reductase (CPR), a membrane-bound protein containing FAD and FMN cofactors. Cytochrome b_5 (cyt b5) may also modify rates of catalysis of some P450 isoforms in class II (Ortiz de Montellano, 2005).

1.1.2 P450 catalytic cycle

The P450 catalytic cycle includes the introduction of two electrons and a typical reaction cycle is shown in Fig. 1.1. The resting state P450 is in the ferric iron form and can reversably bind a substrate. The substrate bound complex accepts the 1st electron transferred by Cytochrome P 450 Reductase (CPR) from NADPH, during which the heme iron is reduced to the ferrous state. This ferrous species then binds molecular oxygen to form a ferrous-dioxy species, which readily accepts a second electron. This second electron usually is delivered by CPR from NADPH, but in some circumstances, it can also be delivered by cyt b5. The mechanism of the second electron transfer by cyt b5 has been under extensive investigation, yet it is still is under debate and awaits further elucidation. With the second electron transfer, ferrous-dioxy species is further reduced to ferrous-peroxyl species. Next, protons provided by water can bind to the distal oxygen in this species followed by cleavage of the di-oxygen bond. The perferryl species is thus formed with one oxygen atom bound to the heme iron. The perferryl species is also known as compound I, a long-sought principal intermediate involved in P450 catalysis whose spectroscopic and kinetic characterization were recently reported (Jung et al., 2011; Rittle and Green, 2010; Rittle et al., 2010). After

inserting one oxygen atom into the substrate, the perferryl species releases the oxidized product with the heme iron simultaneously reduced to ferric state. Thus the resting state ferric P450 species is regenerated for the next catalytic cycle (Ortiz de Montellano, 2005). In this catalytic cycle, there are three shunting pathways, also called uncoupling pathways. The uncoupling can happen at three steps. One is at the ferrous-dioxy state; auto-oxidation results in the super oxide release and the generation of the ferric enzyme. The other uncoupling pathway happens at the step when the hydroperoxo species is forming perferryl species. The proximal oxygen atom can be protonated to release a hydrogen peroxide molecule resulting in the loss of oxidizing ability and generation of ferric enzyme (Ortiz de Montellano, 2005). A third point of uncoupling is possible via two electron reduction of the compound I intermediate to yield additional water. Different P450s may have different coupling efficiency depending on substrates. In the catalytic cycle, interactions between P450 and its coenzymes are key factors in facilitating the electron transfer and the coupling of the cycle. Therefore, these interactions have attracted significant attention. A brief review of studies on the interaction of P450s with the redox partners are summarized below.

1.2 Interaction between P450s and CPR

1.2.1 CPR structure

For microsomal P450s, CPR is an obligatory coenzyme, catalyzing the transfer of electrons to all microsomal P450s (Farooq and Roberts, 2010; Hamdane et al., 2009; Zhang et al., 2009). CPR cycles between the one- and three-electron reduced forms in vivo (Hamdane et al., 2009).

CPR belongs to the family of electron transfer flavoproteins, using both FAD and FMN as tightly binding cofactors. CPR is ~78 kDa with three functional domains: an FMN-binding domain, an FAD binding domain, an NADPH binding domain, with a linker domain as an insert in the FAD-binding domain and an N-terminal membrane-binding domain (Ortiz de Montellano, 2005). It is anchored by the hydrophobic N-terminus to the endoplasmic reticulum membrane, which contains a single α-helix. The cytosolic domain of CPR is responsible for its redox capability. N-terminally-truncated CPR is still able to catalyze the electron transfer reactions with CPR redox partners. In addition to a membrane-binding domain and a cytosolic domain, CPR contains a linker domain between them, which possesses a unique sequence and structure, connecting and orienting the FMN and FAD domains (Ellis et al., 2009; Xia et al., 2011).

The crystal structure of CPR has been resolved using the cytosolic domain of CPR (Wang et al., 1997), which shows a conformation suited for interflavin electron transfer, but not for a subsequent transfer to an acceptor protein. Further study provided evidence showing that internal electron transfers in CPR between the two domains are limited by the motion of the domain, which can cause the open-close conformation change of CPR. When crystallized with a deletion of 4-amino acid in the linker domain, CPR showed three remarkably extended conformations, which clearly demonstrated that the FMN domain undergoes a structural rearrangement that separates it from the FAD and therefore exposes the FMN to allow interaction with its redox partners (Ellis et al., 2009; Hamdane et al., 2009). A most recent study (Xia et al., 2011), using an engineered protein with two cysteine residues in replacement of Asp147 and Arg514 in the FMN and FAD domains to form a disulfide bond between them, further proved that conformational changes of CPR are essential for catalysis

and cofactor binding. The cross-linked form of the mutant CPR exhibited a significant decrease both in the rate of interflavin electron transfer and electron transfer to its redox partners.

1.2.2 Kinetics of electron transfer between CPR and P450s

It is reported that CPR forms a 1:1 (M/M) functional complex with P450s (Miwa and Lu, 1984; Miwa et al., 1979). In human liver endoplasmic reticulum, the ratio of P450s to CPR is about 10:1-20:1, with P450s in excess (Estabrook et al., 1971). This stoichiometry, along with the N-terminal membrane arrangement of the two enzymes, is considered to be of great importance for the electron transfer process facilitated by CPR to P450s (Farooq and Roberts, 2010). Since CPR is an obligatory component for all P450s for their catalytic activity, it is speculated that in the human body, there is a special mechanism permitting CPR to interact with those P450s that have less affinity for CPR compared with others (Backes and Kelley, 2003). Although the kinetics of electron transfer between CPR and P450s were also studied widely in reconstituted systems (Farooq and Roberts, 2010), debate still exists concerning the mechanism by which CPR and P450s interact with each other functionally in the membrane.

As mentioned earlier, the first electron transfer in the P450 cycle is facilitated by CPR to reduce the heme iron of P450s from ferric state to ferrous state. This process is generally considered to be rapid with a unique characteristic of biphasic kinetics (Gigon et al., 1969). Different hypotheses about the biphasic nature of P450 reduction have been proposed over the years. For example, Backes et al. suggested that the rate of a functional complex formation of CPR with P450s is a controlling factor for the slow phase of reduction (Backes

and Eyer, 1989; Eyer and Backes, 1992). Peterson et al. (Peterson et al., 1976) found that the temperature dependence of the electron transfer process from CPR to microsomal P450s was unusual for membrane-bound enzymes. The fast phase is not temperature-dependent while slow phase is. It was considered that the hepatic microsomal drug-metabolizing system exists as clusters, with most of the P450 molecules arranged around a central CPR molecule and the central CPR is able to randomly reduce those P450s within the cluster without motion through the membrane (Peterson et al., 1976). However, a study using saturated reductase compared with P450s in a reconstituted system showed that the first electron transfer by CPR to P450 still maintains a biphasic nature, indicating that the slow phase of electron transfer rate is not due to a limited supply of CPR (Backes and Kelley, 2003). Tamburini et al. (Tamburini et al., 1984) found that the high-spin form of ferric P450 is more rapidly reduced than the low-spin form and suggested that the high-spin form was a prerequisite for CPR reduction and the low- to high-spin transition due to substrate binding could account for the apparent activation energy observed for the reduction of high-spin P450. This has now been challenged.

In a most recent study, Farooq et al proved that the biphasic nature of the first electron transfer for CYP3A4 facilitated by CPR is not a simple sum of high-spin rate and low-spin rate (Farooq and Roberts, 2010), because erythromycin, which induces less spin state change for the heme iron compared with testosterone, can still significantly increase the rate of CYP3A4 reduction by CPR. Farooq et al also studied the effect of the CPR/CYP3A4 ratio on CYP3A4 reduction, and found that CPR and CYP3A4 exist in complexes with a 1:1 stoichiometry. The rate of CYP3A4 reduction was independent of the CPR/CYP3A4 ratio, while the amplitude of the change in spectral absorbance was increased to a maximum with

the increase of the ratio. The result supported the view that a relatively stable CPR-P450 complex facilitated the first electron transfer followed by dissociation and reformation before the much slower second electron transfer takes place.

1.2.3 P450-CPR complex formation

Interactions between CPR and P450s have been widely studied using different P450 isoforms with complex results. It has been found that the characteristics of this complex, such as the affinity of the CPR-P450 complex, the dissociation rate of the complex, etc., can be influenced differently depending on the P450 isoform, the ionic strength of the buffer in the metabolism system, as well as different substrates (Backes and Eyer, 1989; Eyer and Backes, 1992; French et al., 1980; Voznesensky and Schenkman, 1992; 1994).

Complementary charge pairing interactions are found to be important for CPR-P450 complex formation with a large amount of supporting evidence. Bernhardt et al (Bernhardt et al., 1984) modified lysine residues on CYP2B4 with 2-methoxy-5-nitrotropone and fluorescein isoocyanate, and found that CPR-supported CYP2B4 activity and the percent of aerobic reduction decreased, while there was no effect on cumene hydroperoxide- or hydrogen peroxide-supported CYP2B4 activities. Since cumene hydroperoxide/hydrogen peroxide can directly oxidize the heme iron to the ferrous-dioxy species without the facilitation by CPR, this suggested that only the first electron transfer by CPR to CYP2B4 is affected, which necessitates the CPR-P450 complex formation. When carboxyl groups on CPR were modified by 1-ethyl-3-(dimethylaminopropyl)carbodiimide hydrochloride (EDC), the CYP2B4 activity and catalytic efficiency were inhibited by approximately 85% (Bernhardt et

al., 1987). In addition, Bernhardt et al. and Nadler et al. reported respectively that CYP2B4 could protect CPR from being modified by EDC. Further site-directed mutagenesis on CPR modifying specific acidic residues to neutral residues at two acidic clusters demonstrated that the cluster 207Asp-Asp-Asp209 is specifically important for CPR interaction with P450 (Shen et al., 1995). Similarly, when surface basic residues on P450s were modified or mutated, the interaction between CPR and P450s were also reduced (Cvrk et al., 1996). Mutation of the P450 surface residues that are proposed to interact with CPR was also reported to reduce of the CPR-supported P450 activities (Cvrk et al., 1996).

Voznesensky and Schenkman have argued that increasing ionic strength increases the rate of first electron transfer by CPR to CYP2B4, even though it was expected to decrease the rate. In their study, the increase in reaction rate was proposed to be due to the increase of the fraction of P450 reduced in the fast phase, in addition to the increase of fast-phase rate constant (Voznesensky and Schenkman, 1992). Davydov et al. later introduced a fluorescent probe into CPR and used fluorescence energy transfer to evaluate more directly the interactions between CPR and CYP2B4. The results clearly indicated that the K_d for the complex was increased with the increase of ionic strength, supporting the contention that electrostatic force is the driving force for interactions (Davydov et al., 1996). Davydov et al. also pointed out that in the early study of Voznesensky and Schenkman, an increase in the rate of electron flow through those complexes overcame the decrease of affinity by stronger ion strength in the buffer that resulted in an increase of the P450 activity.

Hydrophobic forces are also considered to play an important role in CPR-P450 complex formation. In an earlier study, Johnson et al. truncated the CPR N-terminal hydrophobic region. This truncation caused the loss of activity of CPR for P450 due to inability to accept

electrons from NADPH (Johnson and Muller-Eberhard, 1977). Black et al. further reported that hydrophobic CPR fragments could inhibit association of full-length CPR association with P450 (Black et al., 1979). Later Estabrook et al. elucidated the mechanism by which truncated CPR lacks the ability to facilitate electron transfer and suggested that the hydrophobic N-terminus of CPR is important for CPR to accept electrons from NADPH. On the other hand, in a more recent study (Kenaan et al., 2011), Kanaan et al. used fluorescence labeling and stopped-flow spectroscopy to study hydrophobic residues on CYP2B4 surface in contribution to CPR binding. Their study revealed that hydrophobic residues Val267 and Leu270 on the proximal surface of CYP2B4 are of great importance in mediating CYP2B4-CPR interactions. These sites on P450 exhibited the greatest changes in fluorescence intensity upon binding CPR, the greatest increases in the Km values of the P450 variants for CPR and the greatest decreases in the rates and extents of reduced P450-CO formation upon CPR binding.

1.2.4 P450 topology in interactions with CPR

In 2003, Hlavica et al. reviewed the topology of P450 in the electron-transfer complex formation with its redox partners (Hlavica et al., 2003). P450s share common overall folds and a common catalytic cycle even though their active-site architectures differ from each other quite markedly (Ortiz de Montellano, 2005). P450s are believed to have a common conserved core fold that constitutes part of their proximal surface (Graham-Lorence and Peterson, 1996; Graham and Peterson, 1999), which is proposed to represent the major site for redox partner interactions. Hlavica used CYP102 as a paradigm for modeling donor-docking regions in eukaryotic P450s to map the interaction sites that are involved in the

redox partner interaction onto the structure of CYP102, providing a picture of the overall distribution of contact sites (Hlavica et al., 2003). A homology modeling study using CP2C5 as a template (Fig. 1.2) for constructing a selective map of surface regions on members of the CYP2 family showed that there are divergent contact sites on CYPs that interact with redox partners. This suggested that, depending on the P450 isoforms, there are conformational alterations which induce a shift in the topology of donor interaction (Hlavica et al., 2003). Overall, the authors suggested that the proximal surface structural elements which are dominant by positive charged residues are likely to be the redox partner recognition sites. The model also suggests that CPR and cyt b5 have overlapped binding sites in the proximal surface of CYPs.

Most recently, Im and Waskell reviewed the interaction of CYP 2B4 with CPR and cyt b5 including studies using mutagenesis, kinetic experiments, computer modeling, resonance Raman studies etc., and concluded that CPR binds to the basic, positively-charged, proximal surface of CYP2B4 (Im and Waskell, 2011), and has overlapped binding sites with cyt b5.

1.3 Cytochrome b5

1.3.1 Structure of cytochrome b5

Microsomal cytochrome b5 (cyt b5) is the other redox partner of microsomal P450s, which is also a heme-containing protein with a molecular weight of ~16.7 kD. Cyt b5 exists widely in various organisms in both a soluble form and a membrane bound form; the soluble form found in erythrocytes functions in reducing hemoglobin, and the membrane bound form is in mitochondria or endoplasmic reticulum (Vergeres and Waskell, 1995). It is highly conserved

among species including yeast, insects, avian species, and pig erythrocytes (Schenkman and Jansson, 2003). Mammalian species share over 80% sequence identity in their cyt b5, and substitutions are highly conserved (Schenkman and Jansson, 2003). Also, it is notable that the acidic residues in cyt b5 account for 25% of the total amino acid sequence, resulting in the cyt b5 surface being negatively charged at physiological conditions, which can induce charge paring between cyt b5 and its partner proteins. Cyt b5 can accept and transfer electrons with a variety of acceptor proteins, such as cytochrome c, P450s, metmyoglobin, methemoglobin, etc. (Schenkman and Jansson, 2003).

Microsomal cyt b5 contains a large N-terminal hydrophilic cytosolic domain and a small C-terminal hydrophobic transmenbrane domain with a linker region between. The heme is located in a hydrophobic pocket where the iron is coordinated at the proximal and distal position with two histidine residues, His44 and His68, which are completely conserved among species (Schenkman and Jansson, 2003). The catalytic region contains 4 α-helices forming a cleft into which the heme is inserted, with a heme edge exposed to the environment (Fig. 1.3). Acidic residues Glu49 and Asp65 are well conserved in all species except bacteria (Gly and Thr, instead).

1.3.2 Cytochrome b5 modulation of P450 catalyzed reactions

Cyt b5 can increase, decrease, or have no effect on P450 catalyzed reactions, depending on the P450 isoforms studied and the substrates used (Porter, 2002; Schenkman and Jansson, 2003). The first evidence of cyt b5 modulating P450 activity came from the study demonstrating that NADH stimulated NADPH-supported metabolism of drugs in rat

microsomes (Correia and Mannering, 1973; Hildebrandt and Estabrook, 1971). To date it has been reported that cyt b5 can modulate over 20 CYP isoforms, and the effect is both isoform and substrate dependent (Porter, 2002; Schenkman and Jansson, 2003). Cyt b5 is not essential for most P450 species; however, addition of cyt b5 to a reconstituted P450 system can have considerable effects on the coupling of the system and the activity of some P450 isoforms (Gruenke et al., 1995; Hlavica, 1984; Hlavica and Lewis, 2001; Morgan and Coon, 1984; Perret and Pompon, 1998; Pompon, 1987; Yamazaki et al., 1996). A summary of cyt b5 modulation effect on different P450 isoforms and substrates can be found in the review articles by Porter et al. and Schenkman et al. and many other publications. Examples of cyt b5 effects include: the metabolism of methoxyflurane, prostaglandins A1, E1, and E2 by CYP2B4 (Vatsis et al., 1982), 7-ethoxycoumarin, chlorzoxazone, aniline, and N-nitrosodimethylamine by CYP2E1 (Yamazaki et al., 1996b), p-nitrophenetole O-deethylation by CYP2B1 (Kuwahara and Omura, 1980), and arachidonate by CYP4A7 (Loughran et al., 2001), show an absolute reqirement of cyt b5. On the other hand, some CYPs show higher activity in the presence of cyt b5 than in the absence of cyt b5, such as CYP2A6-catalyzed coumarin 7-hydroxylation, CYP3A4-catalyzed testosterone (TST) 6β-hydroxylation, CYP2C19-catalyzed S-mephenytoin 4'-hydroxylation (Yamazaki et al., 1997; Yamazaki et al., 2002), etc.. Reactions inhibited by cyt b5 include CYP2B4-catalyzed benzphetaminene demethylation (Gruenke et al., 1995). In contrast, cyt b5 shows no effect on CYP1A2- and CYP2D6-catalyzed reactions (Yamazaki et al., 1997), as well as benzo[a]pyrene hydroxylation by CYP2B4 (Gruenke et al., 1995).

1.3.3 Cytb5-P450 complex formation

A number of investigations have shown that cyt b5 and P450s can associate to form a complex, inducing a low- to high-spin transition of the P450 and increasing P450's affinity for CPR and substrates. The magnitude of cyt b5 effect varies with different P450 isoforms (Gruenke et al., 1995; Schenkman and Jansson, 2003; Yamazaki et al., 1997; Yamazaki et al., 2002). Regarding the stoichiometry of cyt b5 interacting with P450s, there are several proposals. An early proposal was that a productive ternary complex could be formed. Later, protein binding and dissociation reactions in an ordered sequence during catalysis were suggested from observations that carbodiimidation of CYP2B4 in the presence of a mixture of CPR and cyt b5 failed to form heterotrimers. Tamburini et al. used a cross-linking reagent in reconstituted systems and found that a 1:1 molar heterodimeric complex of cyt b5 and CYP2B4 could form. In the presence of substrate, the complex formation was increased in liver microsomes as indicated by the increase of the high spin fraction of P450s in the presence of substrate (Jansson and Schenkman, 1996). Additional support was obtained from the observation that CPR and cyt b5 functionally antagonize each other in electron donation to CYP2B4, suggesting that CYP2B4 might have multiple domains for CPR binding and therefore, cyt b5 lacks the ability to interfere with productive anchoring of CPR to CYP2B4 to properly orient the redox partners to promote electro-chemical flow.

Charge pairing forces are believed to be the driving force for cyt b5 to interact with P450s. Increasing the ionic strength of the buffer eliminates the stimulating effects of cyt b5 on P450 catalysis. In earlier studies, it has been found that the conserved acidic residues Glu49, 53 and Asp65, around the exposed heme edge on cyt b5, together with one of the heme propionate residues, protrude into a common plane, forming an anionic charge region under physiological conditions. This region is believed to provide a charge-pairing network for

interactions with cyt b5 partners (Schenkman and Jansson, 2003). The complex formation process results from the exposure of new charges on the surface of the P450s from dissociation of several intermolecular salt bridges (Di Primo et al., 1997). Therefore, cyt b5 is supposed to induce a direct conformational change of P450. A more complicated kinetic model was proposed by Perret et al, which involves a CYP3A4-b5 complex formation and electron shuttling between the proteins in the complex within a single productive P450 cycle (Louerat-Oriou et al., 1998).

Vergeres et al. (Vergeres et al., 1995) reported that, cyt b5 modified with nitro groups was less able to shift the spin equilibrium of CYP2B4 to the high-spin conformer compared with the control. Mass spectrometric analysis of the cyt b5 after modification detected three nitrated tyrosine residues located at positions 11, 34 and 129, and the latter two modifications could be protected in the presence of CYP2B4, suggesting that Tyr34 and Tyr129 might contribute to the complex of cyt b5 and CYP2B4.

In addition, Naffin-Olivos et al. mutated 14 charged or polar residues on the cyt b5 surface to glycine and found that mutation of Glu48, Glu49 or Arg52 reduced the maximal stimulation of CYP17 17, 20-lyase activity, suggesting that these residues mediated the binding of cyt b5 with CYP17 (Naffin-Olivos and Auchus, 2006).

In addition to the charge pairing, the hydrophobic C-terminal membrane anchor domain of cyt b5 is also necessary for binding to P450s. Cleavage of the linker region by proteolysis resulted in the loss of electron transfer ability to microsomal P450s, though the truncated cyt b5 was still able to transfer electron to soluble electron acceptor proteins such as cytochrome c, metmyoglobin, or met-hemoglobin (Vergeres and Waskell, 1992). When the C-terminus

was deleted by 19 amino acids, cyt b5 only retained 20% activity with CYP2B4 (Clarke et al., 2004). In addition, the length of the membrane anchor domain is important for cyt b5 to be targeted to intracellular organelles. Shortening the anchor by 11 amino acids resulted in the loss of ability to anchor to the endoplasmic reticulum, whereas lengthening it by 5 amino acids lead the protein to be transported to the plasma membrane of COS cells. In vitro, this α-helical membrane spanning domain has been demonstrated to be important for the interaction of cyt b5 with P450s to exert its modulatory effect (Chudaev et al., 2001; Vergeres and Waskell, 1992). This interaction is more likely via non-specific interactions (Conner et al., 2011).

1.3.4 P450 topology in interactions with b5

Hlavica et al. have compiled a comprehensive review investigating the topology of surface sites of P450s that interact with cyt b5 based on studies using chemical modification of key amino acid residues, immunolocalization studies, targeted mutagenesis experiments, molecular modeling, as well as topology of membrane-embedded sites based on the functional importance of the hydrophobic tails of P450s and electron-donating proteins. The readers are referred to this review in 2003 for a complete account of P450 interactions with both of its redox partners CPR and cyt b5 (Hlavica et al., 2003). In this chapter of this thesis, a list of P450 topological interactions with cyt b5 along with updated information since 2003 is presented in Table 1. Both a surface map of the interacting sites onto CYP102 crystal structure and a computer model based on a CYP2C5 crystal structure showed that sites that are involved in cyt b5 binding cluster on the center of the proximal face near the heme ligand. This cluster was found to overlap with the CPR-docking regions as well (Hlavica et al.,

2003). A recent review of CYP2B4 interaction with cyt b5 and CPR (Im and Waskell, 2011) reported that the cyt b5 binding site on CYP2B4 is primarily on the C-helix and β-bulge, the edge of the concavity on the proximal surface. Cyt b5 and CPR both bind to the basic, positively-charged, proximal surface of CYP2B4 on distinct but overlapping sites.

1.3.5 Structural comparison of holocytochrome b5 and apocytochrome b5

Apocytochrome b5 (apo b5) is cyt b5 devoid of heme. Holocytochrome b5 (holo b5), the cyt b5 with iron protoporphyrin-IX liganded to His44 and His68, consists of six α-helices, five strands (one β-sheet, and various β-turns) in the sequence of β1-α1-β4-β3-α2-α3-β5-α4-α5-β2-α6 (Mathews, 1979) (Falzone et al., 1996). These secondary structures form two hydrophobic cores in the molecule, one binding the heme group (core 1, Fig. 1.3); the other is remote from the heme, and believed to be important for maintenance of the structural integrity of the protein (core 2).

Apo b5 has been used as a control for cyt b5 effects on CYPs (Yamazaki et al., 1997; Yamazaki et al., 1996a; Yamazaki et al., 2002) and its structure has been extensively studied. Due to heme removal, the secondary structure around the heme is locally disturbed and apo b5 was considered to be less stable than the holoprotein in solution (Huntley & Strittmatter, 1972; Tajima et al., 1976; Pfeil, 1993). However, Moore and Lecomte (Moore and Lecomte, 1990) reported that in apo b5 the key element of the second core forms a stable hydrophobic cluster stabilizing these structural units. Further investigation showed that the apoprotein contains a stable four-stranded β-sheet encompassing β1, β2, β3,and β4 and three α-helices, corresponding to α1, α2, and α6 in holo b5, the two short helices α3 and α5 formed partially and α4 was non-detectable, among which the latter three helices along with β5 bordered the

heme binding pocket. In apo b5, the most flexible region, other than the termini, was found to be Ala50 (in β5) - Glu69 (in α5). The polypeptide segment α4-loop-α5 bearing His68 exhibited faster internal motions than that α2 bearing His44, as the latter heme anchor can only move within a restricted region, whereas the former can adopt many orientations with respect to the stable core. Therefore, heme removal seems to affect the structure and dynamics of core 1 whereas its removal leaves core 2 largely intact. According to the experimental results, Falzone et al. (Falzone et al., 1996) speculated that apo b5 might be viewed as being constructed of two closely associated modules, one providing a stable well-defined core and minimal elements for heme binding, and the other, a partly folded, fluctuating cluster of residues making up the larger part of the heme pocket. In summary, these studies suggested that apo b5 largely maintained its secondary structure and, when used in studies of modulation of P450s activities, it serves as a good comparison with holo cyt b5 for the role of heme.

1.4 In vivo role of cytochrome b5

1.4.1 Cytochrome b5 knockout animal models

The in vivo relevance of cyt b5 has remained uninvestigated until recently. Emoto et al. have reported that coexpression of cyt b5 with recombinant human P450s yielded a more accurate estimate of intrinsic drug clearance (Emoto and Iwasaki, 2007). Therefore, understanding the in vivo role of cytochrome b5 is of significance to more accurately predict clearance from in vitro experiments.

Finn et al. in 2008 reported their study of conditional deletion of liver microsomal cyt b5 in mice, indicating that microsomal cyt b5 plays a major role in the in vivo metabolism of

certain drugs and chemicals in a P450 isoform and substrate dependent manner. The hepatic cyt b5 null (HBN) mice were able to develop and breed normally, having no overt phenotype. In vitro assays showed that metabolism of a range of substrates by different P450 isoforms was essentially abolished and the NADPH-dependent metabolism of many substrates was reduced by 50-90%, including CYP3A-catalyzed 7-benzyloxy-4-trifluoromethylcoumarin (BFC) metabolism, CYP2C-catalyzed 7-methoxy-4-trifluoromethylcoumarin metabolism, CYP1A/2B-catalyzed 7-ethoxy-4-trifluoromethylcoumarin metabolism, CYP1A1/2-catalyzed ethoxyresorufin metabolism, CYP2B/3A-catalyzed7-benzyloxy-4-trifluoromethylcoumarin metabolism, CYPP2E1-catalyzed chlorzoxazone metabolism and CYP2D6-catalyzed bufuralol metabolism. Supplementation with exogenous recombinant cyt b5 to HBN microsomes restored BFC or chlorzoxazone metabolism to wild-type levels. In vivo elimination profiles of several drugs were also evaluated, and the pharmacokinetics of some drugs were markedly altered, e.g. maximum plasma concentration of midazolam was increased by 2.5 fold and clearance decreased by 3.6-fold; half-life of chlorzoxazone, metoprolol and tolbutamide was increased to ~3, 3, and 1.6 fold (Finn et al., 2008).

In 2010, Mclaughlin from the same group reported a further study using cyt b5 complete null mice (BCN). Despite cyt b5's significant role in lipid and steroid hormone metabolism and reduction of methemoglobin, cyt b5 complete null mice were viable. However, increases of hepatic P450s at the neonatal mRNA expression and protein levels were seen for some P450 isoforms. In vitro assays showed that hepatic activities for chlorzoxazone (CYP2E1), midazolam (CYP2C, CYP3A), metoprolol (CYP2D), and tolbutamide (CYP2C) were markedly reduced. Metabolism in lung, kidney and small intestines was also reduced profoundly. In vivo, metoprolol metabolism by CYP2D6 was significantly altered, in contrast

to the liver-specific cyt b5 null mice, suggesting that extra-hepatic cyt b5 plays a significant role in drug disposition. Testicular testosterone levels were significantly lowered due to the deletion of cyt b5 causing lowered lyase activities of testicular CYP17 (McLaughlin et al., 2010).

Li et al. reported an evaluation of cholorzoxazone hydroxylation using liver microsomes and hepatocytes prepared from hepatic CPR-null mice and the result supported that the cyt b5 electron transfer pathway can support a low but measurable level of CYP2E1 activity under physiological conditions. An in vivo study is needed to further understand cyt b5‘s role.

1.4.2 Pharmacogenetics of cytochrome b5

As mentioned earlier, cyt b5 is highly conserved among all species. Its expression level is fairly consistent between individuals and could serve as an indicator for the integrity of the microsomal samples (Forrester et al., 1992). To date, only four cases were reported related to naturally occurring cyt b5 mutations in humans.

In 1994, Giordano reported a case in which the patient showed congenital methemoglobinemia and pseudohermaphrodism. A splicing mutation in the cyt b5 gene was identified as a 16-bp deletion in the cDNA which leads to a new in-frame stop codon and results in a truncated protein of 45 amino acids. The genomic DNA molecular lesion is an AG to GG alteration in the 3′ splicing junction of intron 1. The patient was homozygous for the lesion (Giordano et al., 1994).

In 2007, Kurian et al. (Kurian et al., 2007) reported a naturally occurring variant in a healthy subject with the mutation A178G in cyt b5. The subject was heterozygous. The predicted

amino acid substitution was T60A, which lead to dramatically reduced cyt b5 expression (70%) but modestly altered affinity for hydroxylamine substrates. The diminished expression is attributable to enhanced susceptibility of the variant to proteolysis degradation.

In 2010, Kok et al. (Kok et al., 2010) reported a newborn subject with defective 17, 20-lyase activity, who has a homozygous W27X mutation on the *CYB5A* gene (*CYPB5A* refers to genes coding microsomal cyt b5; *CYPB5B* refers to genes coding mitochondrial cyt b5), leading to the formation of a premature stop codon. The subject's parents were both heterozygous carriers of this mutation. This mutation results in the loss of residues Glu48 and 49 of Cyt b5, which are necessary for an intact 17, 20-lyase activity (Naffin-Olivos and Auchus, 2006). In this case, mutations in the CYP17A1 gene explaining the 17, 20-lyase deficiency were not found.

Most recently, Idkowiak et al. (Idkowiak et al., 2012) reported a missense mutation in the human cyt b5 gene, which causes 46, XY disorder of sex development (46,XY DSD) due to 17,20 lyase deficiency. The 46,XY DSD is characterized by ambiguous or female external genitalia (Mendonca et al., 2009). Three affected siblings in the homozygous state had greatly reduced 17, 20 lyase activities but completely preserved 17α-hydroxylase activity. This is the first human *CYB5A* missense mutation (p.H44L identified). This mutation is likely to cause the loss of heme binding to cyt b5, suggesting that the presence of heme is crucial to support 17, 20 lyase activity. However, this is in contradiction with an in vitro study, which showed that both apo b5 and holo b5 can stimulate the 17, 20-lyase activity of CYP17 (Auchus et al., 1997). Further study is necessary in order to fully understand the mechanism and importance of cyt b5 in vivo.

1.4.3 Cytochrome b5 - P450 interaction in regulatory pathways

Cyt b5-P450 interactions are responsive to major pathways of hormonal regulation, including glucagon, thyroid, and other hormones (Mkrtchian and Andersson, 1990). Cytochrome P450 can be phosphorylated, which impairs the ability of P450 to interact with cyt b5 and results in the down-regulation of P450s activities, leading to an increase of reactive oxygen stress (Zangar et al., 2004).

In addition, Davydov et al. (Davydov, 2001) suggested that interactions of cyt b5 with cytochrome c may be a pathway for regulation of P450s. Cyt b5 and cyt c can form a complex which has been a classic model for the mechanistic studies on the interactions of electron-transfer proteins (Mauk et al., 1995). However, this complex has been considered as unnatural and without physiological meaning, even though Archakov et al. (Archakov et al., 1974) proposed a hypothesis of ‘‘intermembrane electron transfer’’, which suggests that these interactions serve as a regulatory connection between mitochondrial and microsomal electron transfer chains. Recent reports provided additional evidence of cytochromes b5 and c interaction in the crosstalk between mitochondria and ER, regulation of cytochrome P450-dependent oxygen activation, and apoptosis (Davydov, 2001).

1.5 Mechanism of cytochrome b5 action

1.5.1 Auxiliary source of electrons for P450s in substitute of CPR

NADH cytochrome b5 reductase (CBR) is the natural redox partner of cyt b5, shuttling electrons from NADH to cyt b5 to generate reduced ferrous cyt b5 for participation in many

redox cycles (Vergeres and Waskell, 1995). This process is much faster compared with CPR in reducing cyt b5 (Porter, 2002). Cyt b5 is therefore proposed to contribute to the NADH supported electron transfer pathway from CBR to P450, facilitating the transfer of both required electrons, which is separate and independent of CPR (Porter, 2002a).

Porter has reviewed the mechanism of cyt b5-dependent transfer of both electrons to P450s in the absence of CPR (Porter, 2002).This electron transfer pathway is: NADH →CBR→ cyt b5→P450s, and was found effective for CYP3A4- and CYP2E1-catalyzed reactions. In CYP3A4-catalyzed oxidation of testosterone and nifedipine, Yamazaki et al. found that in the NADH→CBR→b5→CYP3A4 reactions were at rates greater than the NADPH→CPR→CYP3A4 system (Yamazaki et al., 1996c). The same group also found that for CYP2E1 catalyzed 7-ethoxycoumarin deethylation, this pathway supported the reaction at about one-fourth the rate of the NADPH→CPR→CYP2E1 pathway. In addition, in human liver microsomes, an anti-CPR antibody only exerted a modest reduction in NADH driven 7-ethoxycoumarin deethylation, indicating that CPR was not a major facilitator for electron transfer. Recently, Li et al. (Li and Porter, 2009) used liver microsomes and hepatocytes from hepatic CPR-null mice to evaluate the ability of the NADH→CBR→b5 pathway in supporting CYP2E1-catalyzed chlorzoxazone hydroxylation and found that NADPH-supported activity was almost absent in liver microsomes from hepatic CPR-null mice, while NADH-supported activity was about two fold higher than in wild-type liver microsomes (partially due to a certain increase of P450 expression level). In hepatocytes from CPR-null mice, chlorzoxazone hydroxylation was about 5% of that from wild-type mice, consistent with results obtained using microsomes, in which the NADH-supported reaction rate was about 5% of that in the presence of both NADH and NADPH in the reaction mixture. These

results using whole cells support the view that under physiological conditions, the NADH→CBR→cyt b5 electron transfer pathway is able to support a measurable level of CYP2E1 activity in the absence of CPR (Li, 2009).

1.5.2 Fast second electron input

In the P450-catalytic cycle, the mechanism of the second electron transfer is not well understood. One reason for this is that it is not possible to isolate the second electron transfer process from the first electron transfer. The second electron can be transferred by CPR from NADPH, and in some cases, cyt b5 can also facilitate the process.

Cyt b5 has a midpoint potential around -20 to +5 mV and CPR has a potential of -350 mV. The former is considered unlikely to directly contribute the 1st electron to P450s, which have a potential around -230 mV in the substrate bound form. In comparison, the dioxy-ferrous P450 species has a midpoint potential around +50 mV. Therefore, ferrous b5 is capable of transferring a reducing equivalent to the dioxy-ferrous species (Guengerich, 1983). This electron transfer is proposed to occur through CPR to cyt b5 and then to the P450 species, as CPR can readily reduce cyt b5 without the need of NADH or CBR (Schenkman and Jansson, 2003).

Using heme analogs to substitute natural heme of cyt b5 showed that cyt b5 must undergo redox changes to stimulate CYP2B4 catalyzed oxidation reactions for specific substrates. For example, manganous heme-cyt b5 loses its ability to undergo redox change and therefore is unable to stimulate CYP2B4-catalyzed oxidation of p-nitroanisole, benzphetamine, ethoxycoumarin, and acetanilide, though it was able to influence substrate affinity for CYP2B4 through interaction with it (Morgan and Coon, 1984; Tamburini and Schenkman,

1987). Similarly, manganous-heme b5 and cobaltous-heme b5 both failed to support CYP2B4- and CYP3A-catalyzed oxidation reactions respectively (Canova-Davis et al., 1985; Sugiyama et al., 1982). Further, apo b5 was not effective in stimulation of CYP2E1 and some P450 isoforms as afforded by the holo b5 (Imai & Sato, 1977; Morgan & Coon, 1984; Sugiyama et al., 1982; Vatsis et al., 1982).

1.5.3 Electron Transfer with P450 as a two-electron acceptor

According to one hypothesis the cyt b5 stimulatory effect is the result of the two hemoprotein complex accepting two electrons during a single interaction with CPR. In this process, CPR transfers two electrons to the Cyt b5-P450 complex before dissociating from it, followed by ferrous P450 binding oxygen and accepting the second electron from the bound cyt b5. In the absence of cyt b5, ferrous P450 would have to dissociate from CPR after accepting the first electron and later associate with CPR again for the second electron transfer (Perret and Pompon, 1998; Tamburini and Schenkman, 1987). According to this hypothesis, cyt b5 associates with P450 to form a complex as a "buffer" for the excess electron. The ferric P450 upon reduction by the 1st electron transferred by CPR, can quickly pass this electron to cyt b5 to reduce its heme iron to the ferrous state, simultaneously, P450 is recovered to the ferric state, ready to accept the 2nd electron from CPR and undergo further catalytic cycle to from an oxy-ferrous species. This species can be reduced by ferrous cyt b5 and therefore the electron kept by cyt b5 is transferred back to the P450.

This mechanism was proposed first by Tamburini et al. in their study of a covalently linked CYP2B4-b5 complex, which was fully functional in the presence of NADPH, while CBR was not able to efficiently reduce cyt b5. Since earlier studies have suggested that the

electron transfer site on cyt b5 is unavailable for interaction with another redox partner when it was complexed with one (Nisimoto and Lambeth, 1985), it was speculated that cyt b5 in the complex would have to obtain an electron from the P450 in the complex. A more complex kinetic model was proposed by Perret et al. (Perret and Pompon, 1998) involving a CYP3A4-cyt b5 electron shuttle within a single productive P450 cycle. Rapid kinetic analysis of cyt b5 reduction upon NADPH addition suggested that cyt b5 was reduced by the CYP3A4 ferrous-dioxygen complex and reoxidized by subsequent P450 oxygenated intermediates. The core of this hypothesis is consistent to the two-electron acceptor proposal.

1.5.4 Enhancement of the coupling efficiency of the P450 catalytic cycle

Cyt b5 may be able to improve the coupling of NADPH oxidation to substrate oxidation (Imai and Sato, 1977). This mechanism of function was carefully reviewed by Schenkman (Schenkman and Jansson, 2003). As described earlier, in the P450 catalytic cycle, there are three uncoupling pathways. One of these uncoupling pathways is the leakage of superoxide from the ferrous-dioxy species, which dismutates to hydrogen-peroxide. In the presence of cyt b5, release of superoxide is decreased, while NADPH consumption is either decreased or unaffected, allowing an increase in product formation. This uncoupling depends both on the P450 isoform and the substrate. The stoichiometry relates the consumption of NADPH and oxygen with the formation of hydrogen peroxide and product, showing that cyt b5 enhances drug oxidation at the expense of hydrogen peroxide production by providing the second electron faster than the rate of peroxide release in the uncoupling pathway (Gorsky et al., 1984; Jansson and Schenkman, 1987; Qian et al., 1998).

Locuson studied the effects on the coupling of CYP2C9 catalysis by both holo and apo b5 and found that for (*S*)-flurbiprofen metabolism, with the increase of holo/apo b5, both the rate of NADPH consumption and hydroperoxide formation decreased with the production formation rate increased, which suggested that both holo and apo b5 were able to increase the reaction coupling efficiency (Locuson et al., 2007b).

1.5.5 Allosteric effects on P450 conformation

The mechanism by which cyt b5 modulates the conformation of P450s and acts as an effector for P450 catalysis has been heavily studied and discussed over the years (Porter, 2002; Schenkman and Jansson, 2003). Documented allosteric stimulation by cyt b5 includes a number of P450 isoforms: CYP3A4, 2C9, 4A7, 2A6, 2B6, 2C8, 2C19, 3A5 and 17(Auchus et al., 1998b; Yamazaki et al., 2002). This allosteric effect on CYPs activities is generally modest (less than 5 fold).

The very first evidence of cyt b5's role of non-electron transfer is shown by Morgan et al. (Morgan and Coon, 1984) in their study to substitute the heme iron by manganese which showed that Mn-b5 was not able to accept or transfer electrons, but was still able to decrease the Km of some substrates for CYP2B4 or 1A2. Further evidence was provided later by Yamazaki et al., showing that apo b5 was still effective in stimulating catalysis of several P450 isoforms, such as CYP3A4, 2C9 and 2A6 (Yamazaki et al., 1997; Yamazaki et al., 1996a; Yamazaki et al., 2002). This revealed that cyt b5 did not have to undergo redox changes to exert its effect on P450s, and so modulation of the P450 conformation might be the dominating factor contributing to its effect.

Strong evidence of an allosteric effect of cyt b5 came from the study on CYP17A 17,20-lyase activity (Auchus et al., 1998a; Auchus et al., 1998b; Geller et al., 1999). CYP17A catalyzes 17α-hydroxylation of pregnenolone (17α-hydroxylase activity) and the further conversion of 17α-hydroxypergnenolone to dehydroisoandrosterone (17, 20-lyase activity). For its 17, 20-lyase activity, CPR is both necessary and sufficient. The addition of apo b5 had the same effect as holo b5 in stimulating the lyase activity, but neither had any effect on 17α-hydroxylase activity. Therefore, cyt b5 functions to direct the route of steroid synthesis between androgens and corticosteroids

Further evidence for allosteric effects of cyt b5 comes from studies with CYP4A7 (Loughran et al., 2001), a fatty acid metabolizing P450 isoform in rabbit kidney. Substrates arachidonate, laurate, and myristate were all metabolized by CYP4A7 in the presence of cyt b5; however, in the absence of cyt b5, only laurate and myristate were metabolized at a much lower rate, with no metabolism of arachidonate. Apo b5 stimulated CYP4A7-catalyzed metabolism of laurate and myristate to the same extent as holo b5, which strongly suggested that cyt b5 plays a conformational role.

This mechanism was challenged later: the stimulatory effect of apo b5 was suggested to be due to the transfer of excess heme in CYP3A4 and CYP17A preparations to apo b5, and addition of heme scavenger myoglobin depleted the stimulatory effect of apo b5 (Gilep et al., 2001; Guryev et al., 2001). A holo b5 mutant with heme binding histidine residue 68 mutated to alanine as well as the Zinc-substituted-heme form (Zn-b5) did not stimulate the activity of either CYP3A4 or CYP17A. However, Yamazaki et al. (Yamazaki et al., 2001) argued that in the presence of heme scavenger apo-myoglobin, apo b5 was still able to stimulate CYP3A4 catalyzed testosterone or nifedipine oxidation, indicating that the stimulatory effect

of apo b5 is not due to its conversion to holo b5. The apo b5 mechanism therefore remains to be elucidated by further evidences.

1.6 Cyt b5 competes with CPR for binding to P450s

The Waskell group has long used CYP2B4 as a model P450 to study its interaction with both cyt b5 and CPR and they recently reviewed CYP2B4 interactions with both cyt b5 and CPR. They propose several seemingly contradictory phenomenon in their hypothesized mechanism, such as different effects on the same P450 for different substrates and different effects at different enzyme ratios. The CYP2B4 catalytic cycle follows the multi-step reaction cycle similar to that observed in the majority of other P450s. Cyt b5 stimulates its activity 10-100-fold by reducing the formation of superoxide and hydrogen peroxide, and improving the coupling of NADPH consumption to drug oxidation. In addition, cyt b5 competes with CPR for an overlapping binding site on the proximal surface of CYP2B4. These two characteristics of cyt b5 can explain the isoform and substrate-dependent effect on CYP2B4 (Im and Waskell, 2011). For example, when the cyt b5/CPR molar ratio is less than 1, cyt b5 causes a CYP2B4 conformational change allowing for rapid delivery of the second proton to the hydroperoxo intermediate and subsequent rapid formation of the active oxidizing perferryl species, and substrate metabolism is increased; at high molar ratios, cyt b5 binds to the proximal surface of CYP2B4 and prevents CPR from binding and reducing ferric P450 species, abolishing the catalytic cycle. When the stimulatory and inhibitory effects of cyt b5 are relatively equal, it will "appear" to have no effect on the enzymatic activity. A conformational change in the active site of CYP2B4 induced by cyt b5 binding that allows a

more rapid formation of perferral species than in the absence of it was also proposed in addition to cyt b5's electron transfer role in the catalytic cycle.

1.7 Cross-linking studies of the interaction between P450 and its redox partners

Chemical cross-linking has been widely used for detection of protein-protein interactions (Phizicky and Fields, 1995). Cross-linking studies on interactions related to P450 and its redox partners have been documented since the 1980s. In 1984, cyt b5 interaction with its redox partner CBR was reported (Hackett and Strittmatter, 1984) using the water-soluble chemical cross-linking reagent 1-ethyl-3-[3-dimethylaminopropyl]carbodiimide hydrochloride (EDC). Investigation of the kinetics of the complex suggested that in the complex, the two enzymes were cross-linked at surfaces where protein-protein contacts allowed for electron transfer, with an orientation similar to that assumed for the two free proteins in binding for electron transfer (Hackett and Strittmatter, 1984). In 1985, Nisimoto (Nisimoto and Lambeth, 1985) reported a study of CPR-cyt b5 interactions wherein an EDC cross-linked complex containing one molecule of CPR and one molecule of cyt b5 was identified. The purified 1:1 complex showed no activity in reducing cytochrome c, but it was partly reducible by NADPH. This study suggests that CPR sites for donating rather than the accepting electrons were blocked by the covalently bound of cyt b5. Tamburini et al. (Tamburini et al., 1985) used EDC to cross-link CYP2B4 and cyt b5 and characterized the covalent complex, in which the two cytochromes were covalently bound at the interface where functional electron transfer happens. Gao et al. in our group (Gao et al., 2006) reported a successful identification of the interacting sites between cytochrome P450 2E1 and cyt b5 using EDC as a cross-linking reagent coupled with isotope labeling and mass spectrometric

analysis, which revealed the interacting surfaces on the two enzymes. Despite these efforts in applying chemical cross-linking into the protein-protein interaction in P450 catalytic system, many questions remain. For example: what is the orientation of the proteins when they interact with each other? Is this orientation isoform dependent? What is the mechanism of cyt b5's substrate and isoform dependent effects in modulation of P450 activities?

Recently, chemical cross-linking coupled with mass spectrometric analysis has become an even more powerful tool for the investigation of protein-protein interactions (Sinz, 2003; Tang et al., 2005; Young et al., 2000). The increase in the power of this approach results from its high through-put format, the requirement for minimal protein, the increase in the size of complexes that can be studied, so that there is no significant restriction on the size of the individual proteins, and a great variety of choices in cross-linking reagents (Pierce Biotechnology, 2005). The difficulty in applying this method lies in the usually low abundance of the cross-linked peptides in the reaction mixtures. Sometimes, isolation or enrichment methods become necessary. The chapters of this thesis represent further application of these methods to the important questions concerning cyt b5-P450 interactions.

1.8 Cross-linking reagent and P450 isoform selection for the current investigation

A great variety of chemical cross-linking reagents have been developed for protein-protein interaction study (Thermo Scientific, 2009), such as homobifunctional, amine-reactive NHS-esters or imidates, and heterobifunctional, amine-reactive, and photoactivatable phenyl azides. If one or both the two proteins contain sulfhydryls, a sulfhydryl- and amine-reactive cross-linker, such as Sulfo-SMCC, can be used. In some situations, distances between two proteins

are not known and selection of a cross-linker with the optimal length of the spacer arm is important.

In the current investigation, EDC was chosen as it can cross-link basic (Lys) and acidic (Asp or Glu) residues that come into very close proximity and generate amide bonds, with "zero-length" linker between the two cross-linked molecules (Fig. 1.4). The "zero-length" linker limits the number of orientations that must be considered in structural models based on cross-linking data.

Among the major hepatic P450s, CYPs 3A4, 2C9 and 2A6 were selected for the current investigation. Cyt b5 has similar stimulatory effect on these three enzymes compared with CYP2D6 and CYP2E1 (Yamazaki et al., 1997; Yamazaki et al., 2002). Both holo and apo b5 are able to stimulate these three isoforms to a similar extent, for example, CYP2C9-catalyzed (S)-warfarin 7-hydroxylation were stimulated 5 fold, CYP3A4-catalyzed nifedipine oxidation was stimulated 2 fold, CYP2A6-catalyzed coumarin 7-hydroxylatio was stimulated 2.5 fold. In comparison, neither holo b5 nor apo b5 affects CYP2D6 activity; holo b5 significantly stimulates CYP2E1-catalyzed chlorzoxazone 6-hydroxylation while apo b5 does not.

Earlier, our laboratory has investigated surface interaction between CYP2E1 and cyt b5 and constructed a model of their interaction, which is consistent with cyt b5's electron transfer role for CYP2E1. In the current study, these three isoforms that possibly are modulated by cyt b5 through a different mechanism from CYP2E1 were selected, in order to understand all possible effects of cyt b5 on these isoforms. At the same time, the CYP2D6 and cyt b5 surface interactions were also investigated. Since CYP2D6 activity is not affected by cyt b5, it serves as a negative control for the study.

The hypothesis of the investigation is that cyt b5 activation of CYP3A4, CYP2C9 and CYP2A6 is due, in part, to induced conformational changes throughout the protein that lead to a smaller CYP active site volume and decreased uncoupling. Cyt b5 has no specific interaction with CYP2D6. The goal of the project is: 1) to map the protein-protein contact surfaces between cyt b5 and CYP isoforms 3A4, 2C9, 2A6 and 2D6 via chemical cross-linking and mass spectrometry; 2) to confirm that cross-linking sites on CYPs are functionally involved in cyt b5-CYP isoform interactions using site-directed mutagenesis; 3) to compare the conformational changes induced by cyt b5 on CYPs in 10 nsec molecular dynamics simulations, using the chemical cross-linking data as distance constraints. This thesis is focused on the first two specific aims with chapters 2, 3 and 4 dedicated to the study of surface interaction between cyt b5 and CYP3A4, CYP2C9 and CYP2A6, respectively. In the end of the thesis, the third goal for this project is briefly discussed.

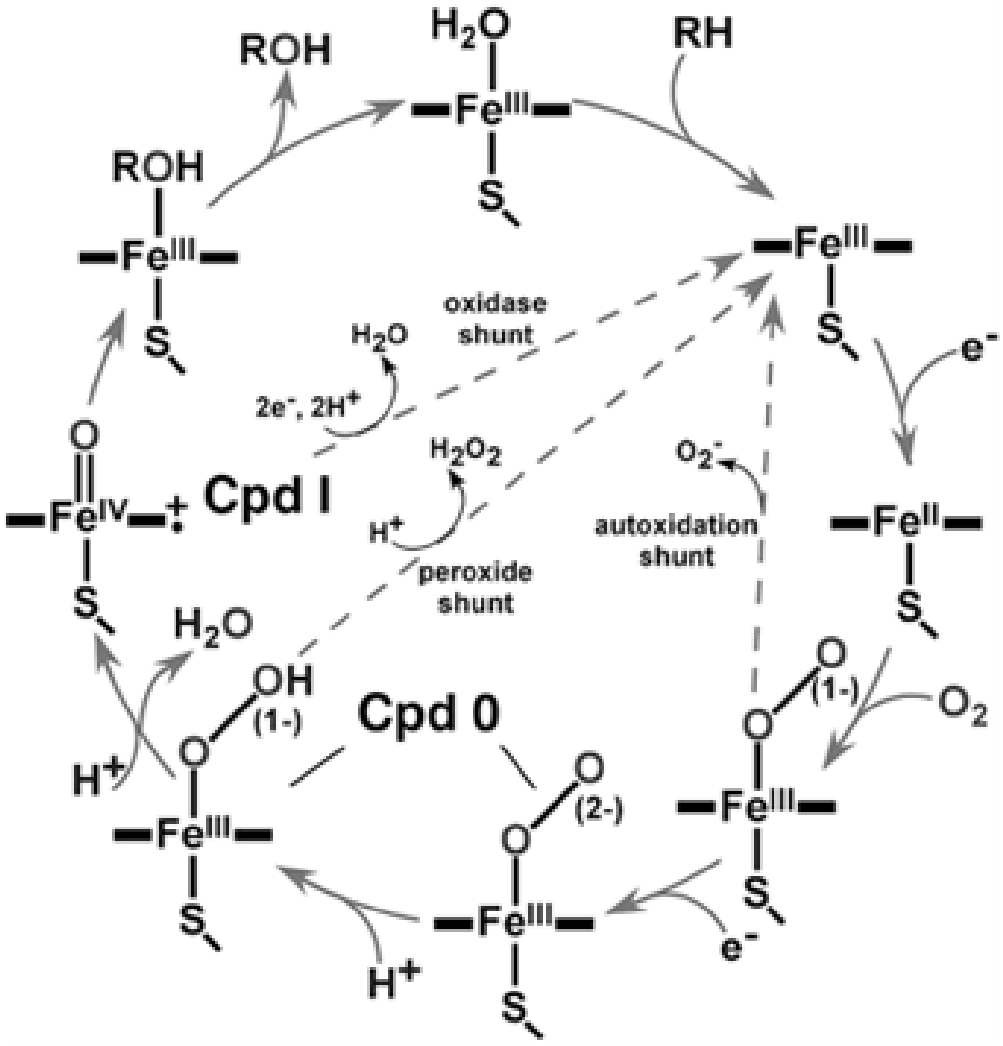

Figure 1.1. Catalytic cycle of P450s. (Adapted from reference (Denisov et al., 2005))

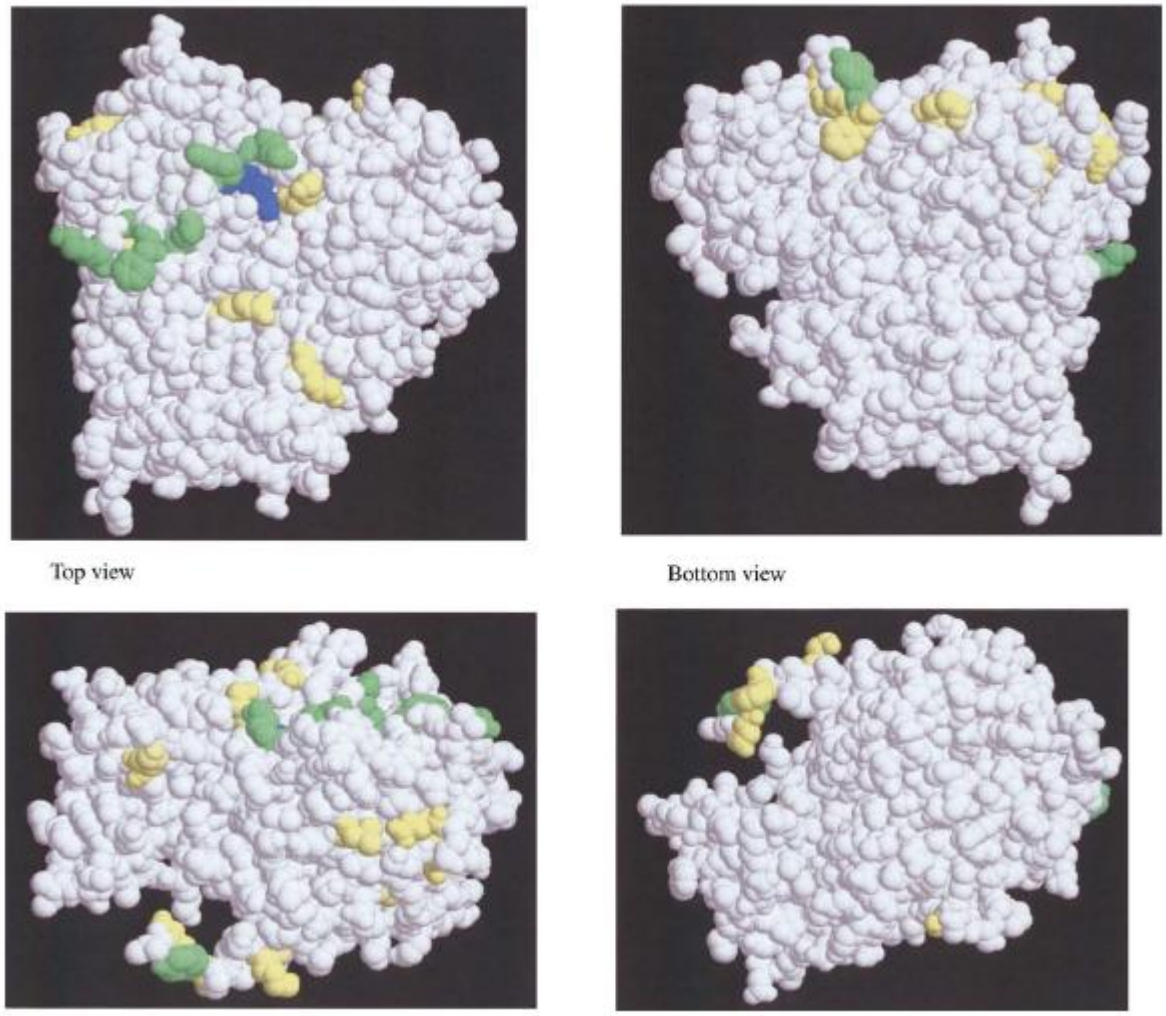

Figure 1.2. Three-dimensional model illustrating the features of surface sites in CYP2C5 involved in redox-partner interactions. The composite profile was generated by mapping the key residues identified for interactions with redox partners (CPR/cyt b5) onto the crystal structures of CYP2C5 (PDB code 1dt6) with progesterone docked in the active site. The color code indicates: yellow spheres, CPR-binding sites; blue spheres, b5-binding sites; green spheres, sites common to CPR and b5.The images were created using the RasWin 2.7.2.1 molecular visualization programmed and rendered by ray tracing. For top and bottom views, the coordinates were rotated by 908 in the x-axis. (Adapted from reference Hlavica et al., 2003)

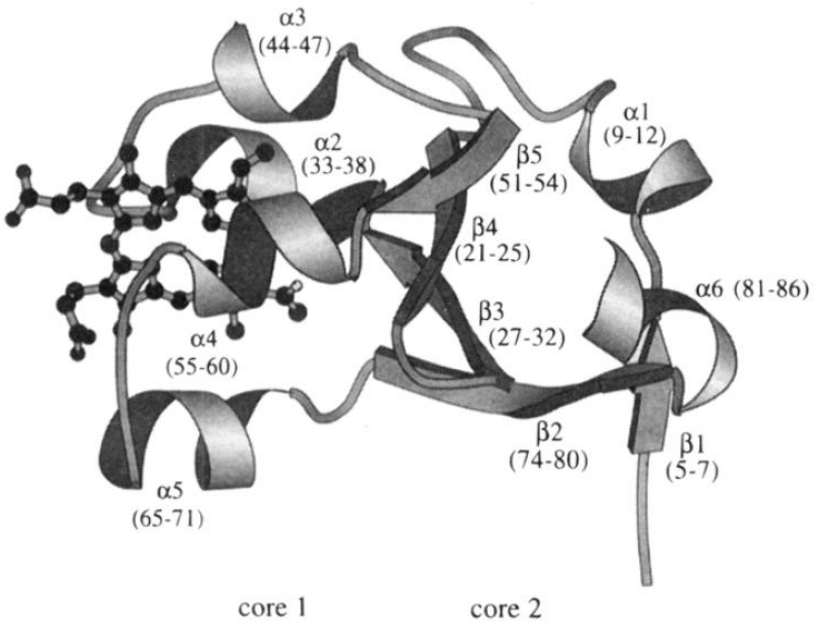

Figure 1.3. Ribbon diagram of the crystal structure of cyt b5. (Matthews eta., 1972). The residues involved in the secondary structure are given in parentheses. The bovine numbering scheme is used, which is 5 numbers lower than human cyt b5. The secondary structure in cyt b5 in a sequence is: β1-α1-β4-β3-α2-α3-β5-α4-α5-β2-α6. (Adapted from reference (Storch and Daggett, 1995)).

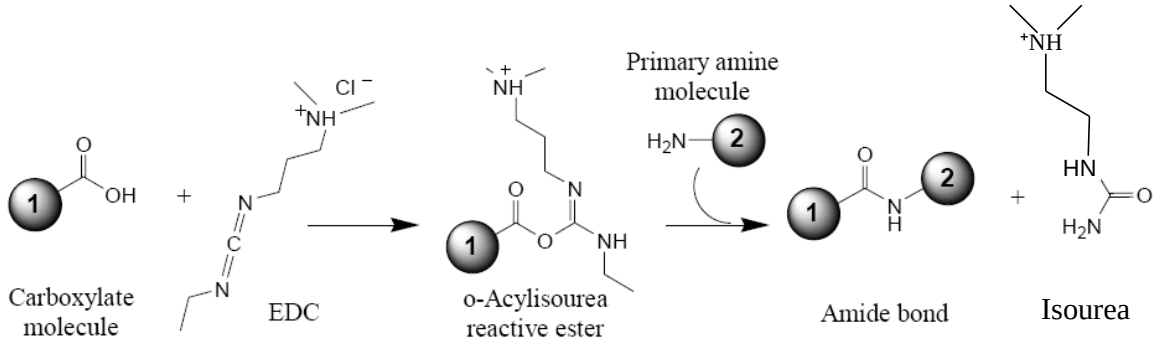

Figure 1.4. Rationale of activation of carboxylic acid group by EDC to react with primary amine group. (Adapted from Pierce Biotechnology product instructions.)

Table 1.1 Chemical modification and genetic engineering of various P450s: identification of key residues involved in redox partner binding. (Adapted and modified with update from reference Hlavica et al., 2003)

CYP isoform	residue identified	location in 2nd structure
17A1	K83	αB
101	R72	αB
17A1	K88	αB
2B1	K122	αC
2B4	R122	αC
2B1	K122-T231	αC
2A5	R129	αC
2B4	R126	αC
2B2	S128	αC
2B4	S128	αC
2B4	R133	αC1
2B4	F135	αC1
2B4	M137	αC1
2B4	K139	αC1
2B4	H226	αG
2B4	V267	αH
2B4	L270	αH
17A1	R347	αJ
11A1	K338	αJ'
27A1	K354	αK
27A2	k358	αK
101	K344	MR
2B4	K433	HBR
17A1	R449	αL

Chapter 2. Cyt b5-CYP3A4 Interaction Study

2.1 CYP3A4 interaction with redox partners

2.1.1 CYP3A4 introduction

Human CYP3A4 is the most abundant P450 isoform expressed in liver and intestine, accounting for ~25-30% of the total liver P450 and even higher in small intestine (Ortiz de Montellano, 2005; Paine et al., 2006). It is also expressed in extra hepatic tissues including lung, stomach, colon, and adrenal. It belongs to CYP3A family, which also include CYPs 3A5, 3A7 and 3A43 in humans (Ortiz de Montellano, 2005).

CYP3A4 contributes to the metabolism of almost 50% of all known pharmaceuticals on the market, including many important therapeutics such as lovastatin and other statins, prostate hypertrophy inhibitor finasteride, immune suppressant cyclosporin, protease inhibitor indinavir and sildenafil, etc. (Ortiz de Montellano, 2005). CYP3A4 also catalyzes the metabolism of endogenous substrates, such as retinoic acid, bile acids, and steroid hormones testosterone and oestrogen (Bozina et al., 2009). In addition, CYP3A4 participates in the metabolism and activation of dietary and environmental chemicals such as PAH-diols, mycotoxins, aflatoxins B1, G1, and sterigmatocystin, pesticides, flavonoids, as well as a number of food additives (Bozina et al., 2009), though its catalytic efficiency in PAH activation is lower than that of the CYP1 family enzymes. CYP3A4 has structure- and size-diverse substrates. Midazolam 1'-hydroxylation), erythromycin N-demethylation, cortisol 6β-hydroxylation (in vivo) and testosterone 6β-hydroxylation (in vitro) are used as probe assays (Bozina et al., 2009).

CYP3A4 has been found able to simultaneously bind to multiple molecules (Khan et al., 2002; Williams et al., 2004), giving rise to cooperative functional behavior. For example, CYP3A4 crystal structure shows a peripheral binding site, and midazolam oxidation by CYP3A4 indicates partially overlapping binding site in the active site of CYP3A4 (Khan et al., 2002; Williams et al., 2004). Therefore, CYP3A4 activity can be altered by substrates, as well as inhibitors and inducers, leading to either sub-optimal therapeutic efficacy or toxicity. In addition, CYP3A4 is subject to genetic polymorphism. As of 2011, 22 alleles have been identified (http://www.cypalleles.ki.se/). Different CYP3A4 variant proteins were found with decreased (*8,*11,*13*17), none (*20), or increased activity (*18A) in vitro. To date, it is still unclear how important these mutations are in vivo (Bozina et al., 2009). Among the variants, *CYP3A4 *1B/*1B* genotype was found significantly associated with aggressive prostate cancer in African-American men (Bozina et al., 2009). CYP3A4 is also highly inducible, leading to high chance of drug-drug interaction and toxicity (Bozina et al., 2009).

2.1.2 Cyt b5 modulation effect on CYP3A4

Cyt b5 can modulate CYP3A4 activity and its effect is substrate-dependent. For example, the presence of cyt b5 can stimulate testosterone 6β-hydroxylation and nifendipine oxidation, but not ethylmorphine metabolism (Yamazaki et al., 1997; Yamazaki et al., 1996a; Yamazaki et al., 2002). Regarding the mechanism of cyt b5 modulation, there are several proposals as discussed previously in chapter 1.

Yamazaki et al first compared apo b5 and holo b5 in their effect on CYP3A4-catlayzed testosterone 6β-hydroxylation and nifendipine oxidation and found that both can modestly

stimulate CYP3A4 activity ~2-5 fold (Johnson et al., 1997; Yamazaki et al., 1997; Yamazaki et al., 2002). This revealed that electron transfer facilitated by cyt b5 is not necessary to exert a stimulatory effect. However, for ethylmorphine metabolism, neither apo or holo b5 provides additional benefit (Schenkman and Jansson, 2003). In addition, the substrate inhibition effect of triazolam using human liver microsomes was attenuated with supplementation of exogenous human cyt b5, resulting in increase of 1'-OH triazolam formation and the corresponding decrease of the 4-OH triazolam to 1'-OH triazolam ratio (Schrag and Wienkers, 2001). This suggests that conformational change occurred upon cyt b5 binding and caused the altered regioselectivity.

Using phenyldiazene as a probe, the active site topology of CYP3A4 was examined by Yamaguchi et al. (Yamaguchi et al., 2004) with four potential N-phenylprotoporphyrin IX regioisomers derived from adduct on the nitrogen atom in pyrrole rings B, A, C, or D. The regioisomer formation was compared in the absence/presence of CPR, cyt b5, or both, and the results clearly showed a difference, suggesting that conformational change occurs, with the structural elements around pyrrole ring C the most prominent.

In another study conducted by the same group, evidence for the existence of two distinct conformers of CYP3A4 with different sensitivity to hydroperoxide-caused heme loss was reported (Kumar et al., 2005). The stimulatory effect of cyt b5 on CYP3A4 in H_2O_2-supported 7-benzyloxyquinoline debenzylation and its ability to reverse the α-NF inhibition effect suggests an important role of cyt b5 as an allosteric modulator. Furthermore, in the absence of cyt b5, up to 66% CYP3A4 was destroyed by hydrogen-peroxide in the fast phase, compared to only ~16% in the presence of cyt b5, suggesting cyt b5 interaction with

CYP3A4 results in ratio change of the two distinct populations of CYP3A4 with different susceptibility to H_2O_2-caused destruction.

2.1.3 CYP3A4 structure

Similar to all other human P450s, CYP3A4 is membrane-associated at the N-terminus. Its crystal structure was first solved in 2004 by William et al. (Williams et al., 2004). As of March 2012, there are a total number of 9 crystal structures reported , 7 of which are with a variety of substrate/inhibitor bound: 1TQN (progesterone bound), 1W0G (metyrapone bound), 2J0D (erythromycin bound), 2V0M (ketoconazole bound), 3NXU (ritonavir bound), 3UA1 (bromoergocryptine bound), 3TJS (desthiazolylmethyloxycarbonyl ritonavir bound) and 2 of which are substrate free form: 1TQN and 1W0E. CYP3A4 is known to metabolize large substrates such as erythromycin and cyclosporine, therefore its active site volume has been considered to be relatively large. According to the calculation of Yano et al., CYP3A4 active site volume is 1386 $Å^3$ and docking studies have indicated that both α-napthoflavone and testosterone can be accommodated by the active site. In addition, its active site contains multiple substrate binding sites, which could be occupied by more than one substrate simultaneously and result in cooperative kinetic behavior of CYP3A4. Moreover, the shape of CYP3A4 active site is considered crucial for its activity because the residues adjacent to the heme of CYP3A4 could provide space for multiple compounds binding without competitively inhibiting each other. A seven phenylalanine "Phe-cluster" (Phe108, 213, 215, 219, 220, 241, 304 on the loop of F-F', G-G' and I helix) was identified lining the top of the active site, playing an important role in both regioselectivity and stereoselectivity (Wang et al., 2009).

The two substrate-free forms have little backbone difference with only Arg212 showing a different conformation. Comparing the substrate-free and substrate-bound forms reveals that CYP3A4 has a dramatic flexibility to adapt to different substrates in the active site (Ekroos and Sjogren, 2006). Binding of ketoconazole induced the shift of the position of secondary structure elements relative to their positions in the structures of ligand-free CYP3A4, including not only those secondary elements defining the active site, but also those further away from the active site (Ekroos and Sjogren, 2006). The most prominent changes take place in the F, G helices and the loop between them. The hydrophobic Phe-cluster identified in the ligand-free structures is found broken up with several Phe side chains exposed to the surface (Ekroos and Sjogren, 2006). In addition, residues 210–213 (on F-F' loop) in the ligand-free structure show lack of secondary structure, but form a helix extending the F helix by one extra turn. Arg212 on F-F' loop which lines the active site in ligand-free structures, is found relocated on the surface of CYP3A4 in the ketoconazole complex. In comparison, its adjacent residue Leu211, which is on CYP3A4 surface in the ligand-free structures, is found inside the active site in the ketoconazole complex (Ekroos and Sjogren, 2006). Substitution of Leu211 and Asp214 with Phe and Glu, respectively, resulted in the elimination of both homotropic and heterotropic cooperativity in steroid hydroxylation reactions, and a reduced response to ANF. Testosterone has a hyperbolic binding isotherm with the mutant, compared with a sigmoidal binding isotherm with the wild-type, which indicates that the mutant possessed a single steroid binding site instead of more than one binding site as in wild-type (Harlow and Halpert, 1998). Erythromycin was also found to induce CYP3A4 conformational change, though to a lesser degree compared with ketoconazole, with the most prominent difference around the F-G loop area. The recent published structure 3NXU with

ritonavir bound also showed conformational change in the same region. Another recent published structure "3UA1" identifies the shift of residues 107-109 on B'-C' loop for binding of bromoergocryptine (Sevrioukova and Poulos, 2012). Overall, the positional and conformational changes of the regions of F-G helix/loop and B-C loop, and the N- and C-terminal loops of CYP3A4 lining the cavity boundaries contribute to the malleable active site of CYP3A4 to accommodate different-sized substrates.

In addition, CYP3A4 structural flexibility was demonstrated in many other studies. In a study of CYP3A4-catalyzed pyrene metabolism, it is found that in the presence of $MgCl_2$, pyrene kinetics were biphasic instead of hyperbolic, suggesting that CYP3A4 is conformationally sensitive to its environment (Schrag and Wienkers, 2000). Anzenbacherova et al. (Anzenbacherova et al., 2000) studied the compressibility and suggested that the CYP3A4 structure was quite flexible and denatured to in active P420 form relatively easily. Substrate binding does not seem to be a stabilizing factor, as in the presence of substrates, the CYP3A4 active site exhibits even more compressibility (Anzenbacherova et al., 2000). Computer dynamic modeling also provides evidence on CYP3A4 malleability (Hendrychova et al., 2012). The active site of CYP3A4 was significantly flexible with the motion of the secondary structure elements. Solvent channels and substrate access/egress channels were found open during the simulation. It was found that in CYP3A4 substrate egress is primarily through the B–C loop from the active site (pw2e), and secondly from the channel between the F – G loop, B′ helix/B – B′ loop/B – C loop and the β1 sheet (pw2a) (Hendrychova et al., 2012). These regions are highly variable in both primary sequence and structure among different P450s (Skopalik et al., 2008) (Li et al., 2007).

2.1.4 CYP3A4 topology for binding of redox partners

Kumar et al. substituted amino acid residues on SRSs 1, 4, and 5 with larger Phe or Trp to probe the structural basis of cyt b5-mediated allosteric modulation (Kumar et al., 2005). Mutation of Ser119, Ile301, Ala305, Ile369, or Ala370 decreased or even abolished the stimulatory effect of cyt b5. Ser119 is in the B-C loop; Ile301 and Ala-305 are in I helix closest to the heme; Ile369 and Ala370 are in the loop of K helix-$\beta 2_1$ sheet. However, these residues are buried in the enzyme in the crystal structure of CYP3A4.

Previous study by our laboratory (Wen et al., 2006) showed that Cys98 located in B-C loop region plays an important role for conformational integrity required for the CYP3A4-CPR interaction. Using the photo-affinity substrate lapachenole and site-directed mutagenesis, Cys98 was found photo-labeled resulting in CYP3A4 loss of CO-binding capacity and decrease in activity, indicating that this residue plays an important role in substrate access/egress. Substitution of Cys98 to Phe or Trp resulted in the nucleophile residues for photo-affinity labeling, suggesting the induction of conformational change. C98W exhibited decreased maximum electron flow rate between CYP3A4 and CPR (Wen et al., 2006). The Cys98 residue is in the B-C loop close to the C-terminus of B helix on the proximal surface of CYP3A4.

As discussed above, although efforts have been devoted to the study of the mechanism of cyt b5 modulation of CYP activity with the observation that the cyt b5 effect on CYP is both substrate and CYP isoform dependent, limited studies have been conducted on the investigation of the role of surface residues contributing to the interaction of cyt b5 with CYP3A4. Thus information of the structural organization of the complex is very limited. A thorough elucidation of the structural organization of cyt b5 and CYP3A4 in the interaction

complex will greatly facilitate our understanding of the differential roles of cyt b5 in modulating catalytic efficiency of different CYPs. Our laboratory has further studied cyt b5 interaction with CYP3A4 using chemical cross-linking and isotopic labeling coupled with mass spectrometric analysis (Gao, 2007). Residues Lys96 (on Helix B), Lys127 (on Helix C) and Lys421 (on K''-L loop) were found cross-linked with cyt b5. All these residues are on the proximal surface of CYP3A4. The model shows that cyt b5 interacts with the B-C loop of CYP3A4, which is a highly flexible structural element and involved in substrate recognition (Gao, 2007). As apo b5 has also been reported to stimulate CYP3A4 activity to a similar degree as holo b5, it is proposed that cyt b5 mainly play an allosteric role in CYP3A4 activity. The current study is aimed to further investigate surface interaction between apo b5 and CYP3A4 by using chemical cross-linking coupled with mass spectrometric analysis, and construct an interaction model of apo b5-CYP3A4 interaction to compare with the model of holo b5-CYP3A4, in order to understand the mechanism by which apo b5 exerts a similar effect on CYP3A4 compared with holo b5. Site-directed mutagenesis on the cross-linking sites on CYP3A4 with holo b5 was used to confirm the functional importance of the cross-linking sites on CYP3A4 in binding with cyt b5. In addition, in the holo b5-CYP3A4 interaction model, Arg446 on CYP3A4 is in close contact with holo b5 (Fig. 2.1). This residue is also conserved among several other P450 isoforms, and has been identified as an important component of binding with CPR for CYP2B4 in previous studies (Im and Waskell, 2011). Therefore, Arg446 is also included in the mutagenesis study in order to evaluate its importance in cyt b5 binding to CYP3A4.

2.2 Experimental procedures

2.2.1 Materials

E. coli strain DH5α containing the expression vector pCWhum3A4$(His)_6$ was kindly provided by Dr. Ronald W. Estabrook and plasmid $(His)_4$HMWHuman-cyt b5 by Dr. Richard J. Auchus, University of Michigan (Guryev, 2001; Holmans, 1994). Restriction enzymes were from New England BioLabs (Beverly, MA). Platinum Pfx DNA polymerase, T4 DNA ligase, Histidine-tagged recombinant human cyt b5 were from Invitrogen (Carlsbad, CA). *E. coli* C41 OverExpress™ Competent cells were from Lucigen (Middleton, WI). QuikChange mutagenesis kit was from Stratagene (La Jolla, CA). Bactotryptone, bactopeptone, and bactoyeast extract were from BD Biosciences Clontech (Palo Alto, CA). Emulgen 911 was from Kao Chemicals (Tokyo, Japan). IPTG, δ-ALA, thiamine, imidazole hydrochloride, protease inhibitor cocktail, sodium cholate and dithiothreitol were from Sigma-Aldrich (St. Louis, MO). CHT ceramic hydroxyapatite, type I, 40 μm particle size was from Bio-Rad (Hercules, CA). L-α-dilauroyl-sn-glycero-3-phosphocholine (DLPC), L-α-dioleoyl-sn-glycero-3-phosphocholine (DOPC), L-α-dilauroyl-sn-glycero-3-phosphoserine (DLPS) were from Avanti Polar-lipids, Inc. (Alabaster, AL). Ni-NTA Superflow was from Qiagen (Valencia, CA). Reagent 1-Ethyl-3-[3-dimethylaminopropyl]carbodiimide hydrochloride (EDC) was from Pierce Biotechnology, Inc. (Rockford, IL). Sequencing grade modified trypsin was from Roche Applied Science (Indianapolis, IN). ^{18}O-labeled water (99 atom % ^{18}O) was from Isotec (Miamisburg, OH). HPLC solvents were of the HPLC-grade. All other reagents were analytical grade.

2.2.2 Protein Expression and Purification

CYP3A4 and mutants were produced in *E. coli* C41 cells using the expression plasmid pCWhum3A4 $(His)_6$ as described previously (Gillam E. M., 1993). Briefly, single colonies on LB-agar plate containing 50 μg/mL ampicillin were inoculated into a ~3 mL LB-ampicillin (50 μg/mL) medium for overnight culture at 37 °C. The overnight culture was then seeded to 500 mL of Terrific Bloth medium supplemented with ampicillin (50 μg/mL) and thiamine (1mM) at 37 ℃ and shaken at 225 rpm. When the A_{600} of the culture reached 0.4, 0.5 mL of 1 M δ-ALA was supplemented, and protein expression was induced by 0.5 mL of 1 M IPTG with further growth at 27 ℃ and 125 rpm for ~40 hours. Cells were harvested by centrifugation and stored at -80 ^{o}C until further use.

Cells pellets were thawed and resuspended in ice-cold resuspension buffer (50 mM KPi, 20% glycerol, 20 mM β-mercaptoethanol (BME), pH 7.4) supplemented with 50 μM testosterone (TST) and protease inhibitor cocktail to a final 250 μL per liter culture. The cell suspension was passed through French Press twice. Then, subcellular fraction was stirred at 4 ℃ for 1 h in the presence of 10% Emulgen 911, and centrifuged at 37000 rpm and 4 ℃ for 60 min with the resulting red supernatant collected. For purification, a final concentration of 50 μM TST was used in buffers for Ni-NTA column chromatography. The supernatant was loaded onto Ni-NTA affinity column equilibrated with resuspension buffer, and the column was washed extensively with wash buffer (50 mM KPi, 300 mM NaCl, 40 mM imidazole, 100 mM glycine, 20% glycerol, 2 mM BME, and 0.2% Emulgen 911, pH 7.4), protein was eluted with elution buffer (50 mM KPi, 20% glycerol, 2 mM BME, 0.2% cholate, and 400 mM imidazole). Eluted protein was dialyzed against hydroxyapatite (HA) equilibration buffer (10 mM KPi, 2 mM BME, 0.2% cholate, and 20% glycerol) at 4 ℃ and loaded onto the hydroxyapatite column, and washed with HA wash buffer (25 mM KPi, 2 mM BME, and

20% glycerol, pH 7.4). Protein was eluted with elution buffer (400 mM KPi and 20% glycerol, pH 7.4) and dialyzed into storage buffer (50 mM KPi, 20% glycerol, 0.5 mM EDTA, 0.1 mM DTT and 1 mM EDTA, pH 7.4). Protein was aliquot and stored at −80 °C for further use. CO-binding difference spectra were used to determine protein concentrations with an extinction coefficient of 91 mM^{-1} cm^{-1}. Purity of protein was examined using SDS–PAGE.

Recombinant rat CPR was expressed as previously described (Shen et al., 1989) with little modifications. Basically, cultures were grown as described above except that LB was used for culture instead of Terrific Broth. LB medium was supplemented with 1 μg/mL riboflavin, 1 mM thiamine, and 100 μg/mL ampicillin. Expression was induced with 1 mM IPTG when A_{550} reached 0.8, and cultures were grown for a further 16 h at 27 ℃ and shaking at 125 rpm. Cells were harvested by centrifugation at 4 °C, stored at −80 °C. Subcellular membrane was prepared with cells resuspended in cold lysis buffer (50 mM Tris (pH 8), 0.25 M sucrose, 0.5 mM EDTA, 200 μM FMN, 0.02 mg/mL lysozyme, and 50 μM DTT) supplemented with protease inhibitor cocktail (250 μL per liter culture) and passed through a French pressure cell twice. Then the mixture was centrifuged at 37000 rpm for 45 min with the pellet collected. The pellet was then resuspended with homogenization buffer (50 mM Tris (pH 7.7), 0.1 mM EDTA, 50 μM DTT, 10% glycerol, and 0.1% Triton X-100) and stirred for 1 hour at 4 ℃, and centrifuged again at 37000 rpm for 60 min with the yellow-greenish supernatant collected. The supernatant was loaded onto a 2', 5'-ADP Sepharose affinity column equilibrated with homogenization buffer and washed with 20 column volumes of wash buffer. Protein was then eluted with a 5 mM $NADP^+$ in wash buffer with 0.1% Triton X-100 and dialyzed against storage buffer (100 mM KPi, 0.1 mM EDTA, and 20% glycerol,

pH 7.5). rCPR was shown >95% pure by SDS–PAGE on an 8% reducing acrylamide gel stained with Coomassie blue. The rCPR concentration was determined by measuring the difference in absorbance between 456 and 550 nm of the purified protein in a solution of 0.01 mM $K_3Fe(CN)6$ in 100 mM KPi using an extinction coefficient of 21.1 $mM^{-1}cm^{-1}$.

Human cyt b5 was prepared according to previously published protocol (Yamazaki et al., 1996). Protein expression and purification were carried out according to previously reported protocol (Holmans et al., 1994) (Naffin-Olivos and Auchus, 2006). Plasmid $(His)_4$HMWHuman-cyt b5 was used to express wild-type human b5 in E. coli. Briefly, plasmids were transformed into C41(DE3) cells and spread onto Luria-Bertani medium plates containing 0.1 mg/mL carbenicillin and incubated overnight at 37 ℃. Then ~3 mL of the overnight culture was seeded into 500 mL of Terrific Broth supplemented with 0.5 mM δ-aminolevulinic acid (δ-ALA) and 0.1 mg/mL carbenicillin and incubated at 37 ℃ with shaking at 140 rpm. When the A600 reached 0.35-0.4, cells were induced with 10 μM isopropyl-β-D-thiogalactopyranoside (IPTG) and allowed to shake at 125 rpm at 37 ℃ for 16-20 hours. Then cells were harvested at 4 ℃ by centrifugation. The cell pellet was resuspended in buffer A (10 mM potassium phosphate and 1 mM EDTA, pH 7) with 250 μL protease inhibitor cocktail per liter culture. The cells were lysed by two passages through the French Press cell and centrifuged at 125 000g for 1 h at 4 ℃ with bright red gelatinous pellet collected. The cell lysate was divided into two parts, one for holo cyt b5 preparation and the other one for apo b5 preparation.

For holo cyt b5 preparation, a 50 μL aliquot of lysed cells was diluted in buffer containing 20 mM Tris, 1 mM EDTA, pH 8, and 0.1% CHAPS and titrated with the hemin chloride solution to allow the heme to reconstitute the potential apoprotein. The hemin chloride

solution was prepared in 50:50 v/v ethanol/water. During titration, the absorbance spectrum from 350 to 600 nm was monitored and the titration was complete when a distinct increase in absorbance at 385 nm is observed which is a result of the accumulation of Tris-ligated heme. The amount of heme needed to reconstitute the total cell lysate with a 10% molar excess was calculated and added to the cell lysate. The pellet was then resuspended in buffer B (10 mM potassium phosphate, pH 8, 2 mM 2-mercaptoethanol, and 20% glycerol) with final concentration of 1% (w/v) CHAPS added and stirred at 4 ℃ for 1 hour. The mixture was then centrifuged again at 109, 000g for 1 h at 4 ℃ with supernatant collected. Ni-NTA agarose column equilibrated with buffer B was used for purification. The supernatant was loaded onto the column with 20 column volumes washing using buffer B supplemented with 0.1% CHAPS, 10 mM imidazole, and 400 mM KCl. Protein was eluted with buffer B supplemented with 0.1% CHAPS and 100 mM imidazole and then dialyzed against buffer C (10 mM potassium phosphate, pH 7.5, 20% glycerol, 0.5 mM EDTA, 0.1 mM dithiothreitol, and 0.05% CHAPS) with one buffer exchange. Concnetration of cyt b5 was determined by monitoring the difference spectroscopy from 350 to 500 nm before and after reduction by sodium dithionite. The concentration of the cyt b5 was calculated using the difference between $\Delta A_{(424-409\ )}$ after the addition of sodium dithionite and $\Delta A_{(424-409)}$) before the addition of sodium dithionite with extinction coefficient of 180 $mM^{-1}cm^{-1}$.

Apo b5 preparation was according to a published protocol (Yamazaki et al., 1996a). Cyt b5 was added drop-wise to 25 ml of cold acetone containing 0.2% HCl at -20 ℃ in ice-salt bath and then stirred for 15 min. The white precipitate was collected by centrifugation (3700 rpm 15 min, 4 ℃) and dried under an N2 stream. Dried precipitate was homogenized using a hand-held Teflon/glass device in ~4.0 ml of 0.20 M potassium phosphate buffer (pH 7.25)

containing 0.4% sodium cholate. The insoluble precipitate was then removed by centrifugation, and the supernatant was collected and dialyzed twice against 0.10 M potassium phosphate buffer containing 0.1 mM EDTA at 4 ℃. Protein concentration was determined by the BCA method (Kotrbová et al., 2009).

2.2.3 Site-Directed Mutagenesis of CYP3A4

The oligonucleotide primers used in the generation of CYP3A4 mutants K96A, K127A, K421A and R446Awere as the following (mismatches indicated by the underlined bases):

K96A forward	5’ CAA AAC AGT GCT AGT GGC AGA ATG TTA TTC TGT CTT C3’
K96A reverse	5’ GAA GAC AGA ATA ACA TTC TGC CAC TAG CAC TGT TTT G 3’
K127A forward	5’ GCT GAG GAT GAA GAA TGG GCG AGA TTA CGA TCA TTG C3’
K127A reverse	5’ GCA ATG ATC GTA ATC TCG CCC ATT CTT CAT CCT CAG C 3’
K421A forward	5’ CTC CCT GAA AGA TTC AGC GCG AAG AAC AAG GAC AAC 3’
K421A reverse	5’ GTT GTC CTT GTT CTT CGC GCT GAA TCT TTC AGG GAG 3’
R446A forward	5’-CCA GAA ACT GCA TTG GCA TGG CGT TTG CTC TCA TG-3’
R446A reverse	5’- CAT GAG AGC AAA CGC CAT GCC AAT GCA GTT TCT GG -3’

For construction of a CYP3A4 triple mutant K96A/K127A /K421A, a CYP3A4 double mutant K96A/ K421A was first constructed using the K421A single mutant plasmid as the template and the K96A forward and reverse primers, afterwards, the triple mutant K96A/K127A /K421A was constructed using the K96A/ K421A plasmid as the template and the K127A forward and reverse primers. The mutagenesis was performed using QuikChange mutagenesis kit according to the manufacturer’s protocol. The full-length cDNAs of CYP3A4 sequence containing the desired mutations were analyzed at University of Washington Sequencing Facility.

2.2.4 Cross-linking Reactions

CYP3A4 and apo b5 were reconstituted at a molar ratio of 1:1 in 100 uL 50 mM KPi buffer in the presence of lipids mixture of DLPC/DSPC/DOPC (1/1/1) with final concentration of 10 μM for each enzyme. The lipid mixture was prepared using DLPC:DSPC:DOPC in a ratio of 1:1:1 (w:w:w).The solution was gently stirred for 10 min and held at room temperature for 2 hr. Then the chemical cross-linking reagent EDC was added to a final concentration of 10 mM from a 100 mM stock. The reaction was allowed to proceed at room temperature for 2 hr followed by dialysis against 50 mM KPi buffer followed by a second dialysis against 50 mM ammonium bicarbonate buffer to remove EDC and isourea that was generated.

2.2.5 Proteolytic Digestion and Mass Spectrometric Analysis

Digestion of the cross-linked protein complex was performed as previously described (Gao, 2007; Gao et al., 2006). Mass spectrometric analysis for apo b5 and CYP3A4 chemical cross-linking was according to a published method (Singh et al., 2008). The Orbitrap mass analyzer of an LTQ-Orbitrap was used to acquire data, whose high mass accuracy provides great specificity in limiting false positives due to the explosion of possible sequence combination in the cross-linked complex candidates. Only precursors with charge state of +3 and above were targeted for MS2 fragmentation, as cross-linked peptides tend to form higher charge states due to the its longer length. The data were analyzed with the open-modification algorithm Popitam. Tandem mass data were analyzed manually with the MS3D collaboratory portal (Schilling et al., 2003; Yu et al., 2008) and University of Washington Proteomics Center web tools as references.

2.2.6 Testosterone 6β-Hydroxylation Catalyzed by CYP3A4 Wild Type and Mutant.

CYP3A4 catalyzed testosterone 6β-Hydroxylation was carried out according to a published protocol (Shaw, 1997). The final reaction buffer contains 0.2 μM CYP3A4, 0.4 μM NADPH-dependent cyt P450 reductase, 0.2 μM cyt b5, 0.5 mg/mL CHAPS, 0.033 mg/mL of L-α-dilauroyl-sn-glycero-3-phosphocholine (DLPC), 0.033 mg/mL of L-α-dioleoyl-sn-glycero-3-phosphocholine (DOPC), 0.033 mg/mL of L-α-dilauroyl-sn-glycero-3-phosphoserine (DLPS), and 3 mM GSH in 50 mM potassium HEPES buffer at pH 7.4. Testosterone 6β-hydroxylation assay was carried out according to a previously described procedure (Guengerich, 1986; Shaw, 1997). Vivid Green™ assay was carried out according to the protocol that comes with the purchase of the substrate. Both assays were conducted at a fixed enzymes ratio of 1:2:1 for CYP3A4/CPR/cyt b5 unless otherwise noted.

2.2.7 Equilibrium binding of cyt b5.

Experiments were conducted using the method described earlier with buffer conditions slightly modified (Gilep et al., 2001; Tamburini et al., 1985). The dissociation constant (Kd) was determined using the equation as described in (Clarke et al., 2004):

$$\Delta A = \Delta Amax\{\frac{[Kd + [CYP3A4] + [b5])}{2} - \sqrt{\left[\frac{(Kd + [CYP3A4] + [b5])^2}{4} - [CYP3A4][b5]\right]}\}$$

The ΔA is the change in absorbance difference between 390 nm and 418 nm, and ΔAmax is the maximal absorbance change; [CYP3A4] is 200 nM in the assay; [b5] is the concentration of holo b5 or apo b5, respectively; and the Kd is the spectral dissociation constant of the CYP3A4-b5 complex.

For TST binding affinity assay, the change in absorbance difference between 390 nm and 418 nm (ΔA) was plotted as a function of TST concentration (Farooq and Roberts, 2010; Roberts et al., 2005). Apparent dissociation constants were estimated using the Hill equation: $\Delta A = Amax \times S^n / [Kd(app) + S^n]$ with GraphPad software. The Amax is the maximal absorbance change, S is the TST concentration, Kd(app) is the apparent dissociation constant (the substrate concentration that gives an absorbance change of 50% of Amax), and n is the Hill coefficient.

2.2.8 Molecular Docking and Energy Minimization.

X-ray crystallographic structures of bovine cyt b5 (PDB "1CYO") (Cunane et al., 1996) and human CYP3A4 (PDB "1TQN") (Yano, 2004) were used to construct the model of the CYP3A4-cyt b5 complex. ZDOCK SERVER was used to predict apo b5-CYP3A4 interaction model with identified sites as constraints (Pierce et al., 2011).

2.3 Results

2.3.1 Chemical Cross-linking.

The apo b5 preparation showed a stimulatory effect on CYP3A4 activity to a similar extent as holo b5 (Fig. 2.2). Treatment of an equimolar mixture of CYP3A4 and apo b5 with EDC resulted in the formation of cross-linked protein complexes, with major complexes being ~73 kDa according to SDS-PAGE (Fig. 2.3).

2.3.2 Apo b5 and CYP3A4 Interactions by Mass Spectrometric Analysis.

Two cross-linked peptide complexes between apo b5 and CYP3A4 were successfully identified (Table 2.1 and Fig. 2.4-2.6) and confirmed by their corresponding tandem mass spectra (Table 2.2-2.3 and Fig. 2.6).

For the first cross-linked peptide apo b5: ^{35}FLEEHPGGEEVLR^{47} - CYP3A4: ^{116}SAISIAEDEEWKR^{128}, its quadruple-charged precursor with an m/z of 757.3763 and quintuple-charged precursor with an m/z of 606.1026 were both found (Table 2.1). The tandem spectrum of the ion with m/z of 757.3763 shows the linear y9 ion of cyt b5 indicating the first Glu residue is the only possible site that is cross-linked with apo b5 (Fig. 2.6A and Table 2.2). Therefore, the cross-linking sites between apo b5 and CYP3A4 were determined to be Glu37 and Lys127, respectively.

For the second cross-linked peptide apo b5: ^{48}EQAGGDATENFEDVGHSTDAR^{58} - CYP3A4: ^{71}VWGFYDGQQPVLAITDPDMIKTVLVK^{96}, only the quintuply-charged precursor ion with an m/z of 1024.8989 was observed (Table 2.1). The observance of y8 ion of apo b5 indicates that those acidic residues included in y8 cannot be cross-linked, leaving only residues Glu48, Asp53, Glu56, Glu59 and Asp60 as possible targets (Fig. 2.6B and Table 2.3). Further differentiation between them is difficult due to lack of sufficient fragmentation. Lys91 on CYP3A4 is the only possible site to be the cross-linked as terminal Lys residue cannot be the site both cross-linked and cleaved by trypsin.

2.3.3 Modeling of Holo b5-CYP3A4 and Apo b5-CYP3A4 Complex

The docked models of apo b5-CYP3A4 complexes were constructed with the identified cross-linking sites as constraints (Fig. 2.7). The interacting surface on apo b5 consists of the

segments α2-loop-α3 and α4-loop-α5, the major segments for the hydrophobic core 1 where heme is inserted. According to the apo b5-CYP3A4 model, apo b5 is predicted to bind to the same groove on CYP3A4 as holo b5 with common contacting regions despite the different orientations. The contact regions on CYP3A4 for apo b5 are the B helix, B-B' loop, C helix, C-D loop, D helix, K''-L meander region, and the β-bulge (Fig. 2.7). Apo b5 α4 and α5 helices approach the B-B' loop region and the C helix of CYP3A4, respectively

2.3.4 Site-directed mutagenesis of CYP3A4 and protein purification

Site-directed single-point and multiple substitutions of the cationic Lys residues on CYP3A4 (Lys96, Lys127 and Lys421) with Ala were carried out in order to confirm the functional importance of these identified cross-linked sites. From the holo b5-CYP3A4 interaction model our laboratory previously constructed (Gao, 2007), Arg446 was predicted to be of importance in interacting with cyt b5 by forming an ionic hydrogen bond with Gly residue in cyt b5 (Fig. 2.1). In addition, Arg446 is found conserved through several P450 species (CYP2A6, 2C19, 2D6, 2E1, 3A4, 2J2 and rabbit CYP2B4 (Fig. 2.8). Therefore, single-point mutagenesis study of this site was also included.

The purified CYP3A4 wild-type, single-point mutants K96A, K421A, R446A and the triple mutant K96A/K127A/K421A all showed a homogenous 450 nm soret in the reduced CO-ferrous binding difference spectra (Fig. 2.9). The expression level of K127A was extremely low for unknown reasons, so it was not further studied. A testosterone binding affinity assay was carried out to examine the active sites of the mutants (Fig. 2.10). Analysis of the data using the Hill equation yielded Kd(app) values of 25 μM (N=1.53, R2=0.99), 71 μM (N=1.45, R2=0.99), 108 μM (N=1.07, R2=0.995), 30 μM (N=1.34, R2=0.997), and 42

μM (N=1.31, R2=0.99) for CYP3A4 wild-type, K96A, K421A, R446A and triple mutant, respectively. The wild-type apparent dissociation constant is comparable to that previously reported (Farooq and Roberts, 2010; Roberts et al., 2005). All mutants showed significant binding with testosterone, indicating that the heme environment of the mutants remains unchanged and their active sites were not impacted by the mutations.

2.3.5 Effect of the Mutations on Catalytic Activities of CYP3A4

Cyt b5 stimulatory effects on CYP3A4 wild-type and mutants catalyzed testosterone 6β-hydroxylation are shown in Fig. 2.11. Catalytic efficiency of wild-type CYP3A4, K421A and K96A was increased by cyt b5 2.5-fold, 1.7-fold and 1.3-fold, respectively. Interestingly, the triple mutant K96A/K127A/K421A displayed very low catalytic activity both in the absence and presence of b5, suggesting that the simultaneous substitution of the three sites abolished the activity of CYP3A4, which was not rescued by cyt b5. Significantly, R446A also abolished CYP3A4 activity. In addition, another CYP3A4 substrate fluorogenic Vivid™, was also tested to compare the activities of wild-type CYP3A4 and its mutants (Fig. 2.12). The results were consistent with testosterone 6β-hydroxylation activities.

2.3.6 Effect of the Mutations on CYP3A4 binding to Cyt b5

The affinity of cyt b5 with wild-type CYP3A4 and its mutants is shown in Fig. 2.13. Cyt b5 binds wild-type CYP3A4, K96A and K421A with K_d values of 140 μM, 346 μM and 287 μM, which are in accordance with the stimulatory effects of cyt b5 on wild-type CYP3A4, K96A and K421A in testosterone 6β-hydroxylation and Vivid™ substrate metabolism. The

affinity of cyt b5 with R446A showed a drastically decrease, with a K_d value greater than 1000 μM.

In addition, it has been reported that the ratio of cyt b5/CYP can affect the catalytic efficiency for some CYPs (Locuson et al., 2007b; Zhang et al., 2008; Zhang et al., 2005), which is due to cyt b5 competing with CPR for the overlapping but distinct binding sites on CYPs. This ratio-dependent effect of cyt b5 on CYP3A4 activities was also revealed in the results shown in Fig. 2.14, with a stimulating effect at low ratios, but an inhibitory effect with increase of b5/CYP3A4 ratios. Both wild-type CYP3A4 and K421A showed maximal activities at the ratio of 2:1. K96A reached the maximal activity at the b5/CYP3A4 ratio of 3:1, consistent with previous cyt b5 binding assays. Both the triple mutant and R446A showed very low activity either in the presence or absence of cyt b5 as expected because the triple substitution significantly reduced the charge-pair driving force for interaction and the mutation of Arg446 was predicted to be important for redox partner binding.

2.3.7 Effect of the mutations on CRP interaction with CYP3A4

Since residue Lys127 and Arg446 appear to be of importance for CPR binding as well, as shown in testosterone 6β-hydroxylation and Vivd Green™ substrate metabolism in the absence of cyt b5, the effect of the mutations on CYP3A4 activity in the presence of varying concentrations of CPR were determined (Fig. 2.15). Apparent $K'_{m,CPR}$ was used to illustrate the affinity of CYP3A4-CPR interaction, as testosterone 6β-hydroxylation exhibited Michaelis-Menten kinetics dependent on CPR concentrations. Wild-type CYP3A4, K96A and K421A have comparable binding $K'_{m,CPR}$ values as shown in Fig. 2.15, suggesting

neither Lys96 nor Lys421 play a significant role for CPR binding. In comparison, CPR binding to R446A and the triple mutant was abolished. This agrees with the earlier proposal that cyt b5 and CPR have overlapped binding sites on P450s and they compete with each other for binding to P450s (Im and Waskell, 2011; Zhang et al., 2007; Zhang et al., 2005).

2.4 Discussion

In a previous study from our laboratory (Gao et al., 2006), surface residues involved in the interaction between cyt b5 and CYP2E1 were identified and a model of their interaction was constructed based on the crystal structures of CYP2E1 and homology model of human cyt b5. The model suggests an involvement of heme groups of cyt b5 and CYP2E1 during their interaction, which is consistent with cyt b5's electron transfer role for CYP2E1 catalysis (Gao, 2006). In addition, surface residues on CYP3A4 interacting with cyt b5 were also studied (Gao, 2007). The results of this investigation support the previous proposal that cyt b5 exerts its effect on CYP3A4 through an allosteric effect in addition to possible electron transfer, as indicated by their heme groups being apart in the model of cyt b5-CYP3A4 (Gao, 2007). In this current study, surface residues of CYP3A4 and apo b5 in close contact during their interaction were cross-linked by the chemical cross-linking reagent EDC via covalent binding, and these cross-linked sites were identified by mass spectrometric analysis. Using these sites as constraints, the apo b5-CYP3A4 interaction models were constructed using protein docking calculations based on the crystal structures of the two enzymes. In addition, comparison of the interaction between holo cyt b5-CYP3A4 (Gao, 2007) and apo b5-CYP3A4 were illustrated.

Interestingly, the two peptide segments identified on apo b5 involved in interaction with CYP3A4 are the same ones on holo b5 cross-linked with CYP3A4. This suggests that these two structural elements paly significant roles in interacting with P450s. Likewise, on CYP3A4, the residue Lys127 were found to be cross-linked with both apo and holo b5; Lys91 is cross-linked with the same segment of cyt b5 as Lys96 is. The interaction models of holo b5-CYP3A4 and apo b5-CYP3A4 suggest that although apo b5 lacks the heme group, the surfaces of apo b5 and holo cyt b5 that interact with CYP3A4 overlap, with different orientations. More significantly, in the two models, both holo and apo b5 are in direct contact with the B-B' loop region of CYP3A4. The B-B' loop region is located on the boundary of the CYP3A4 proximal and distal face, and is considered as the substrate recognition sites (SRSs) of CYP3A4 (Roussel F, 2000). As discussed in the introduction of this chapter, this loop region showed high flexiblity in computer dynamic simulation studies. Through conformational changes, it is speculated to be involved in regulation of substrate access/egress channel in CYP3A4, e.g., previous studies have shown that lapachenole, a substrate of CYP3A4, covalently binds to this loop region (Wen, 2005).Therefore, the interaction of cyt b5 with this structural element of CYP3A4 may initiate a conformational change of it, which can further induce an allosteric effect on the active site of CYP3A4, resulting the change in substrate metabolism. Similar conformational modulation effect of cyt b5 on CYP enzymes has been reported for CYP101 ($P450_{cam}$), where cyt b5 can stimulate 5-exo-hydroxycamphor formation by $P450_{cam}$. The conformational perturbations of $P450_{cam}$ upon cyt b5 binding onto the proximal surface were found transmitted to regions even in the distal surface, including regions for substrate access and orientation (Rui et al., 2006). Consequently, the association of cyt b5 with CYP gives rise to the allosteric effect on the

CYP. This is further supported by our results (Fig. 2.2), as well as previous reports that apo b5 can increase the catalytic activity of CYP3A4 to the extent comparable to holo b5 (Yamazaki et al., 1997; Yamazaki et al., 2002).

As has described in Chapter 1 on CYPs structures, CYP3A4 is anchored on the membrane by its N-terminal membrane anchor. In addition, analysis of the crystal structures suggests that the hydrophobic residues on the F-G loop of CYPs are embedded in the membrane as an additional support of the protein (Berka et al., 2011; Ohta et al., 1992). Previous reports have indicated that the angle between heme plane of CYPs and the membrane is between 38 to 78^{o} depending on the CYP isoforms. Cyt b5 is believed to be anchored in the membrane with its C-terminal trans-membrane domain (Clarke et al., 2004; Vergeres and Waskell, 1995). Between the cytosolic functional domain and the trans-membrane domain, cyt b5 has a flexible 15 amino acid linker domain, which allows cyt b5 functional domain to adjust its position to interact with CYPs effectively (Banci et al., 2000; Clarke et al., 2004). In addition, human cyt b5 in solution NMR structure (PDB: 2I9R) showed that the linker domain can adopt various conformations. In our models of holo/apo b5-CYP3A4 interaction, when CYP3A4 is positioned on the membrane within the range of 38^{o} - 78^{o} as shown in Fig. 2.16 (Berka et al., 2011), if holo/apo b5 are allowed to adopt an orientation as in the NMR structure, both linker domains of holo/apo b5 are capable of reaching the membrane. This indicates that under physiological conditions, when holo/apo b5 are anchored on the membrane with their C-terminal trans-membrane domain, their linker regions provide them enough flexibility to allow them to interact with CYP3A4 in the productive orientation. Therefore, the orientations of holo/apo b5 relative to CYP3A4 in our models are reasonable under the physiological conditions.

Both holo b5 and apo b5 cause a spin state change of CYP3A4 from low spin to high spin to a comparable extent (Fig. 2.13). The affinity of apo b5 to CYP3A4 is also similar to holo b5 as shown in Fig. 2.13. This is consistent with the results of activity assays wherein apo b5 stimulates CYP3A4 activity to a similar extent as holo b5, and supports the computer models of apo b5-CYP3A4, in which apo b5 interacts with CYP3A4 by binding the same sites on CYP3A4 with a different orientation than holo b5 (Gao, 2007).

Site-directed mutagenesis and assessment of the CYP3A4 catalytic activities using one of its classical substrate testosterone and a fluorescence substrate Vivid Green™ confirmed the functional importance of the identified residues on CYP3A4 in cyt b5-CYP3A4 interaction. In the activity assays with the above two substrates, cyt b5 showed a stimulatory effect on the catalytic efficiency (Vmax/Km) of wild-type CYP3A4 to 2.6-fold and 1.8-fold, and K421A to 1.7-fold and 1.6-fold, respectively (Fig. 2.11 and 2.12). In contrast, the stimulatory effect on the catalytic efficiency of K96A was 1.3-fold and 1.2-fold, respectively. This indicates that the substitution of Lys96 had a greater impact on the stimulatory effect of cyt b5 than Lys421, in parallel with the lower cyt b5 binding affinity of K96A than that of K421A. It has been reported that cyt b5 and CRP have distinct but overlapping binding sites on CYPs, and compete with each other to bind to CYPs (Zhang et al., 2007). Since the apparent binding affinity ($K_{m,app}$) of CPR to K96A and K421A appeared to be undisturbed, it is likely that the change in cyt b5 stimulatory effect is due to the decreased affinity of cyt b5 with K96A.

An interesting finding is that at higher ratio of cyt b5 to CYP3A4, CYP3A4 catalytic activity decreased, while it increased at lower ratios. Similar observations were also reported for CYP2C9, which showed a decreased activity at high cyt b5 to CYP2C9 ratio (above 4) (Locuson et al., 2007b), when competition between CPR and cyt b5 would diminish the

essential binding of CRP and the transfer of electrons from NADPH and resulted in a decrease in overall oxidase activity (Locuson et al., 2007a). In the current study, when cyt b5/CYP3A4 ratio was varied, at a 3:1 ratio K96A showed a maximal catalytic activity. Cyt b5 stimulatory effects on K96A catalytic efficiency are slightly lower than for K421A, possibly due to the higher K_d value of cyt b5 with K96A than that with K421A (Fig. 2.14), since CRP has a comparable affinity with both K96A and K421A.

The triple (K96A/K127A/K421A) mutant exhibited only minimal activity on testosterone and Vivid Green™ substrate metabolism. As mentioned previously, both K96A and K421A retained CPR binding capability and catalytic activity for both substrates; we therefore speculated that Lys127 might be more important in CPR-CYP3A4 binding. Another possibility is that the three sites synergistically play a pivotal role in CPR-CYP3A4 binding, and the simultaneous mutation resulted in more prominent effect than single mutation on the CRP binding.

A significant finding was that R446A showed very low turnover rates for metabolism of both TST and the fluorogenic Vivid ™ substrate. Arg446 was found to be conserved among CYP species such as 2A6, 2C19, 2D6, 2E1, 3A5, 2J2 and rabbit 2B4. In both the holo b5/apo b5-CYP3A4 interaction models, Arg446 residue appeared to be in close contact with the CYP3A4 redox partner. The substitution of this single residue resulted in a dramatic reduction in the CYP3A4 activity, suggesting that neither cyt b5 nor CPR binds to R446A productively. Since cyt b5 and CPR have been reported to compete with each other in binding with CYPs (Im and Waskell, 2011; Locuson et al., 2007b; Zhang et al., 2005), and computer molecular model of cyt b5-CYP2B4 indicates that cyt b5 and CPR have distinct but overlapping binding sites on CYP2B4 (Im and Waskell, 2011), it is not surprising that

residue Arg446 would play a significant role in CPR binding as well. This is consistent with previous report that Arg443 residue on CYP2B4 was found to contribute to CPR binding (Bridges et al., 1998).

In conclusion, in the current study, we identified the interacting sites between apo b5 and CYP3A4 using chemical cross-linking coupled with mass spectrometric analysis, and determined the functional importance of the residues on CYP3A4 using site-directed mutagenesis and metabolic assays. Results also suggest that mass spectrometry coupled with cross-linking serves as a useful tool to understand protein-protein interactions. Computer models of the apo b5-CYP3A4 complex was constructed and compared with our laboratory's previous model of holo b5-CYP2E1. The study further illustrated how both the holo- and apo-cyt b5 can affect CYP3A4 with similar effect and suggests that cyt b5 has an allosteric effect on CYP3A4 catalytic activity, in addition to possible electron transfer. The critical role of Arg446 residue in interactions with both cyt b5 and CRP was discovered and demonstrated. These findings may facilitate a better understanding of the complex mechanisms of cyt b5 modulation. The interaction models based on cross-linking results could lead to a better understanding of the modulation of CYP activity by cyt b5, and eventually better prediction of drug clearance, drug toxicity, drug-drug interactions and in vitro-in vivo extrapolation.

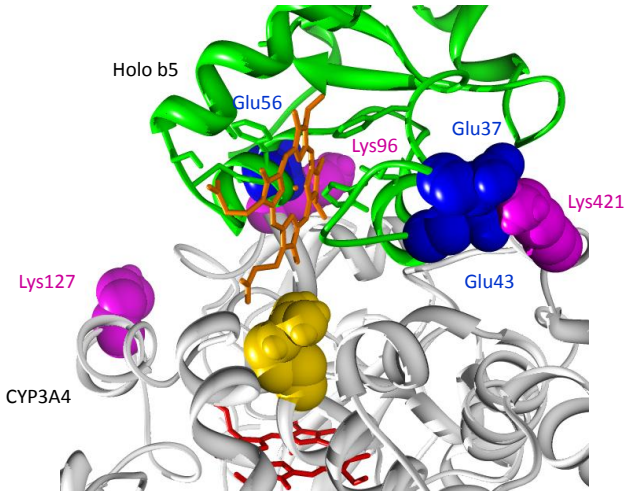

Figure 2.1. Interface between the holo b5-CYP3A4 complex model. Arg446 (golden) illustrated in the holo b5-CYP3A4 model (modified according to (Gao, 2007)). CYP3A4 is white; b5 is green. The interacting residues on CYP3A4 and cyt b5 are magenta and blue, respectively.

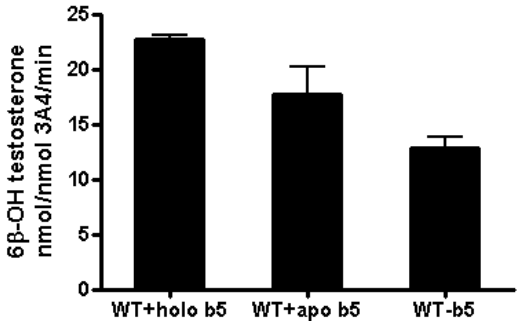

Figure 2.2. Comparison of effect of holo/apo b5 on NADPH-dependent formation of 6β-hydroxyl testosterone by CYP3A4. Reactions were carried out using 40 pmol CYP3A4, 80 pmol CPR in the presence and absence of 40 pmol holo/apo b5. The substrate testosterone is 500 μM.

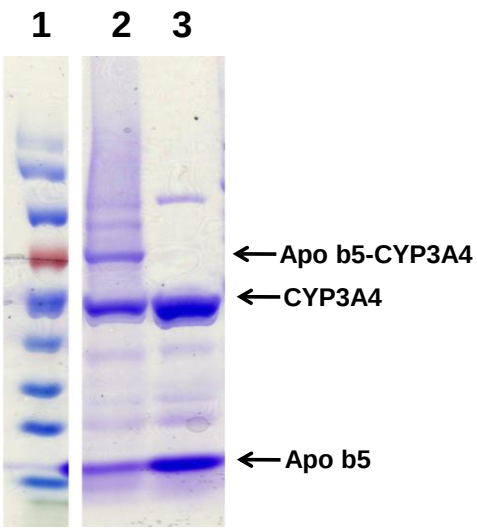

Figure 2.3. SDS-PAGE analysis of the cross-linking reactions of apo b5 and CYP3A4 using EDC. Apo b5 and CYP3A4 were in a 1:1 mole ratio in the absence and presence of EDC. Lane 1, protein ladder; lane 2, apo b5 + CYP3A4 with EDC; lane 3, apo b5 + CYP3A4 without EDC.

(A)

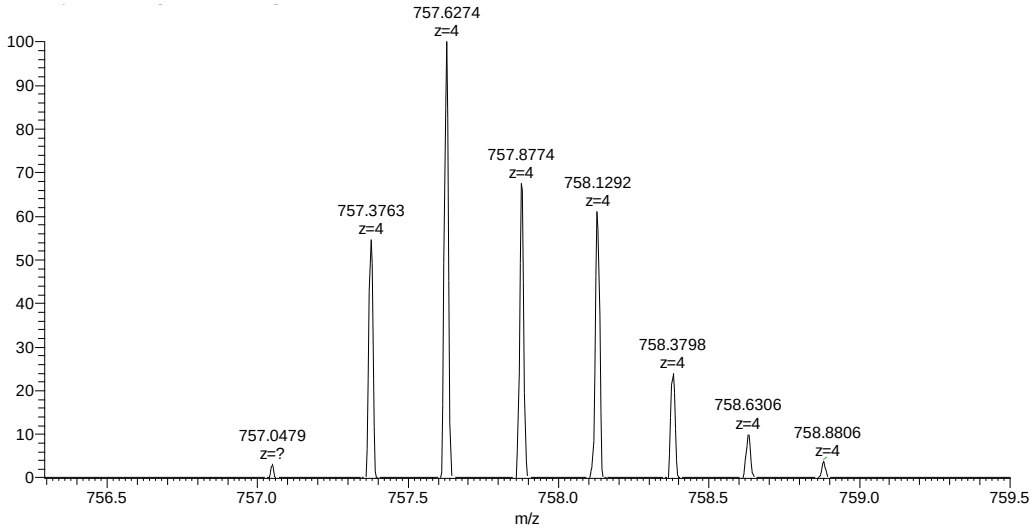

(B)

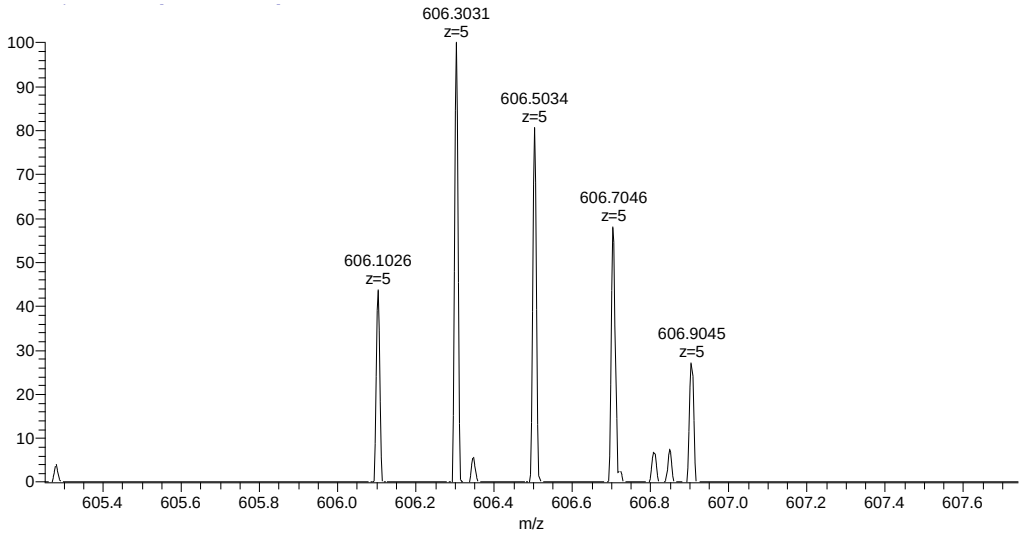

Figure 2.4. Precursor ion MS spectra for cross-linked peptide apo b_5: ^{35}FLEEHPGGEEVLR^{47} – CYP3A4: ^{116}SAISIAEDEEWKR^{128}. (A) Quadruple charged ion $[M + 4H]^{4+}$ = 757.3763 (ion No.1 in Table 1); (B) Quintuple charged ion $[M + 5H]^{5+}$ = 606.1026 (ion No.2 in Table 1).

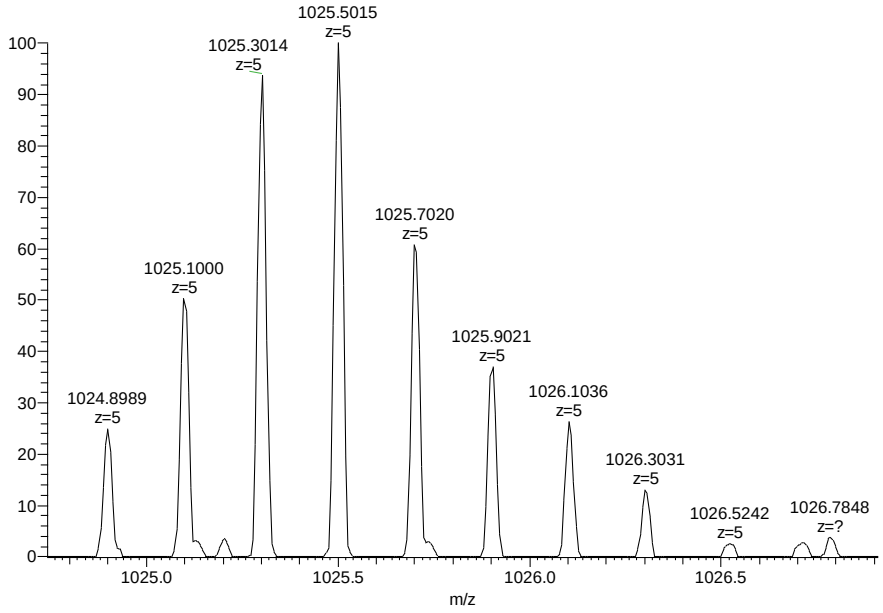

Figure 2.5. Precursor ion MS spectra for cross-linked peptide apo b_5: ^{48}EQAGGDATENFEDVGHSTDAR^{68} - CYP3A4: ^{71}VWGFYDGQQPVLAITDPDM IKTVLVK^{96} with quintuple charge ($[M + 4H]^{4+}$ = 1024.8998, ion No.3 in Table 1)

(A)

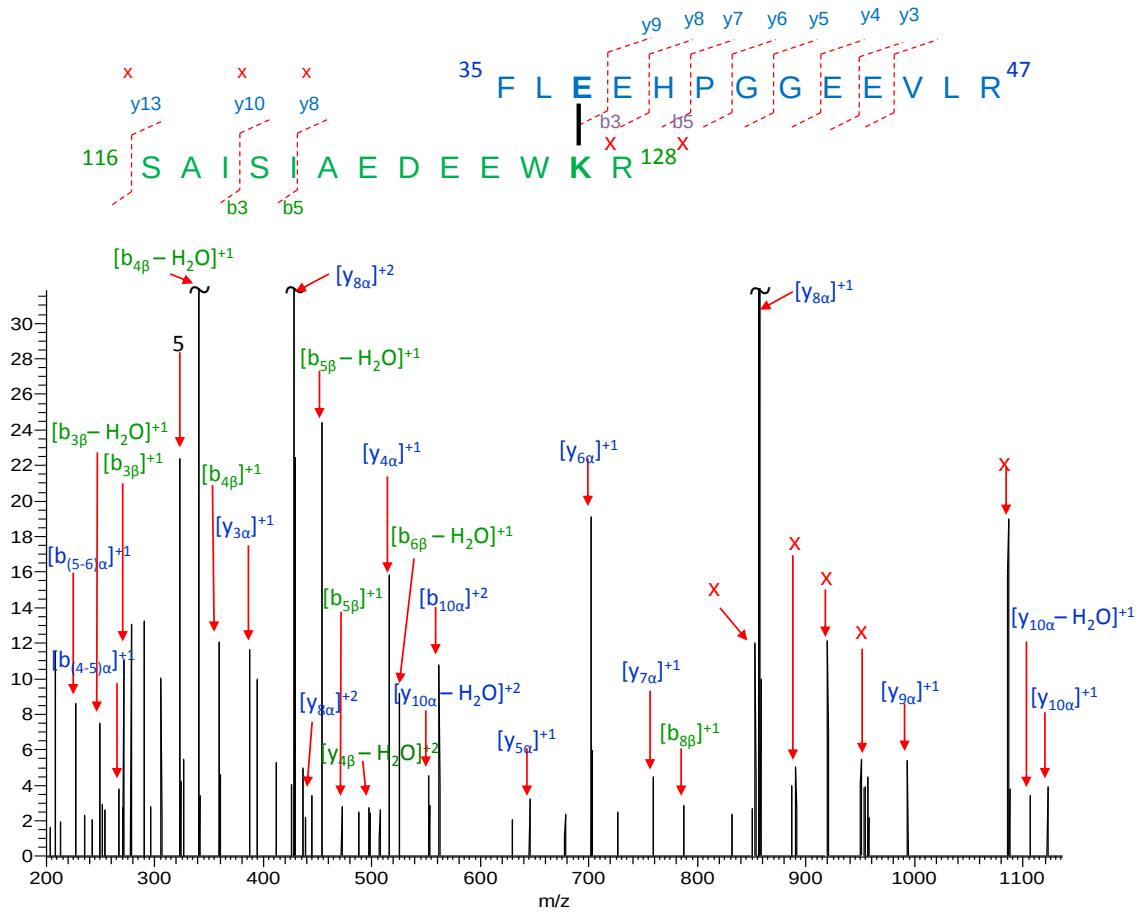
35 F L E E H P G G E E V L R 47
116 S A I S I A E D E E W K R 128
y9 y8 y7 y6 y5 y4 y3
y13 y10 y8
b3 b5
[b4β – H2O]+1
[y8α]+2
[y8α]+1
[b5β – H2O]+1
[b3β – H2O]+1
[b3β]+1
[y4α]+1
[y6α]+1
[b4β]+1
[y3α]+1
[b6β – H2O]+1
[b(5-6)α]+1
[b5β]+1
[b10α]+2
[b(4-5)α]+1
[y8α]+2
[y10α – H2O]+2
[y7α]+1
[y9α]+1
[y10α – H2O]+1
[y10α]+1
[y5α]+1
[b8β]+1
[y4β – H2O]+2
m/z

(B)

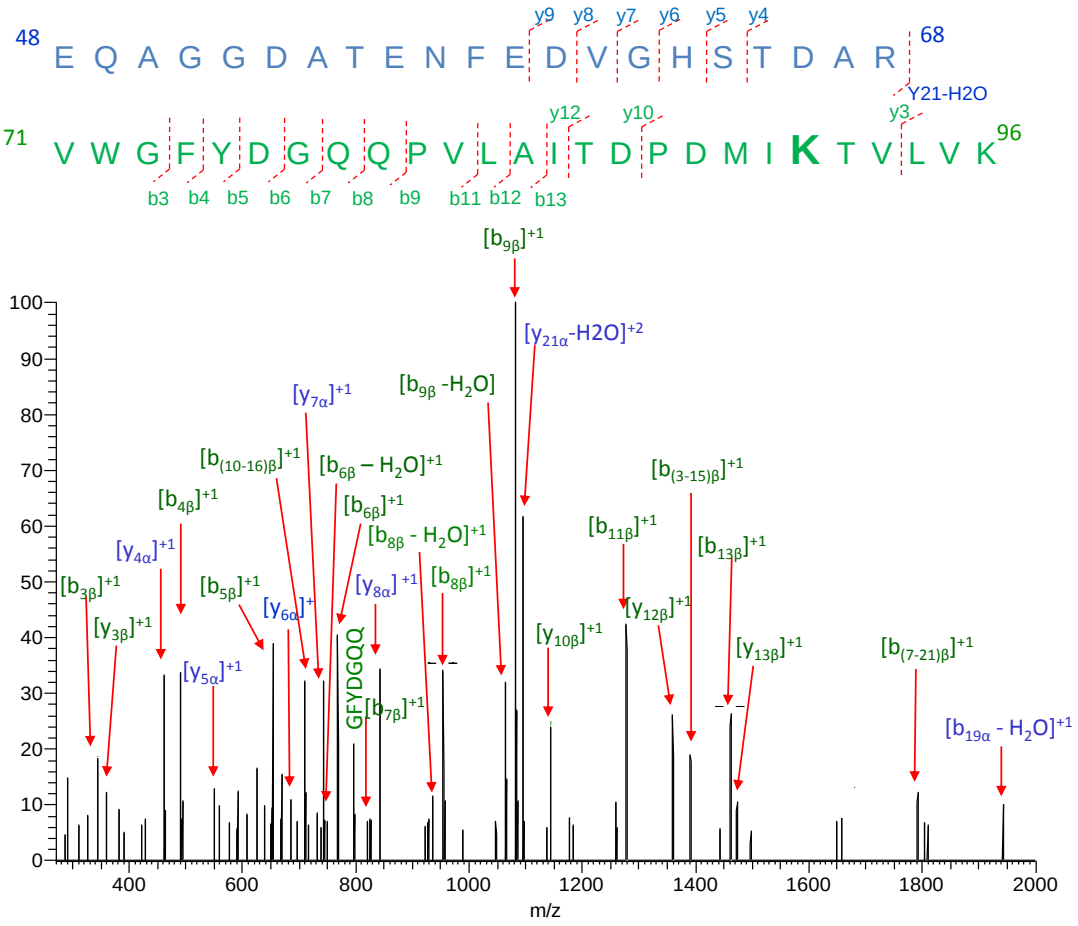

Figure 2.6. Tandem mass spectra for two cross-linked peptide precursor ions identified from apo b5-CYP3A4 complex. Fragment ions with superscript "x" represent the cross-linked fragment ions. Ions marked with subscript α are from cyt b5, and ions with subscript β are from CYP3A4. Identified cross-linked residue pairs are linked by bold black lines. (A) Ion $[M+4H]^{4+}$ =757.3763 for apo b5: ^{35}FLEEHPGGEEVLR^{47}-3A4: ^{116}SAISIAEDEEWKR^{128}. (B) Ion $[M+5H]^{5+}$ =1024.8989 for apo b5: ^{35}FLEEHPGGEEVLR^{47}-3A4: ^{71}VWGFYDGQQPVLAIT DPDMIKTVLVK^{96}.

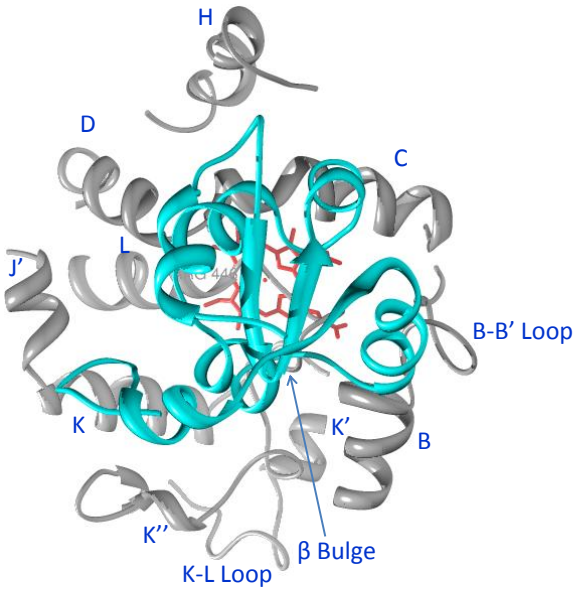

Figure 2.7. Top views of apo b5-CYP3A4 complex models. CYP3A4 is white; apo b5 is cyan. Protein regions on CYP3A4 far away from the interacting surfaces are truncated.

```
P00178_rabbit2B4   (431) LGKRICLGEGIARTELFLFFTTILQNFSIASPVPPEDIDLTPRESGVGNV
     P05182_h2E1   (432) AGKRVCVGEGLARMELFLLLSAILQHFNLKSLVDPKDIDLSPVTVGFGSI
    P33261_h2C19   (430) AGKRICVGEGLARMELFLFLTFILQNFNLKSLIDPKDLDTTPVVNGFASV
     P08684_h3A4   (434) PFGSGPRNCIGMRFALMNMKLALIRVLQNFSFKPCKETQIPLKLSLGGLL
     P20815_h3A5   (433) PFGTGPRNCIGMRFALMNMKLALIRVLQNFSFKPCKETQIPLKLDTQGLL
     P10635_h2D6   (438) AGRRACLGEPLARMELFLFFTSLLQHFSFSVPTGQPR-PSHHGVFAFLVS
     P51589_h2J2   (443) IGKRACLGEQLARTELFIFFTSLMQKFTFRPPNNEK--LSLKFRMGITIS
```

Figure 2.8. Sequence alignment of CYPs 2B4, 2E1, 2C19, 2D6, 3A4, 3A5 and 2J2. The protein access numbers as indicated in the protein names are according to the database of UniProtKB/Swiss-Prot. The star symbol above the sequences indicates the conserved residue of Arg in different CYP isoforms.

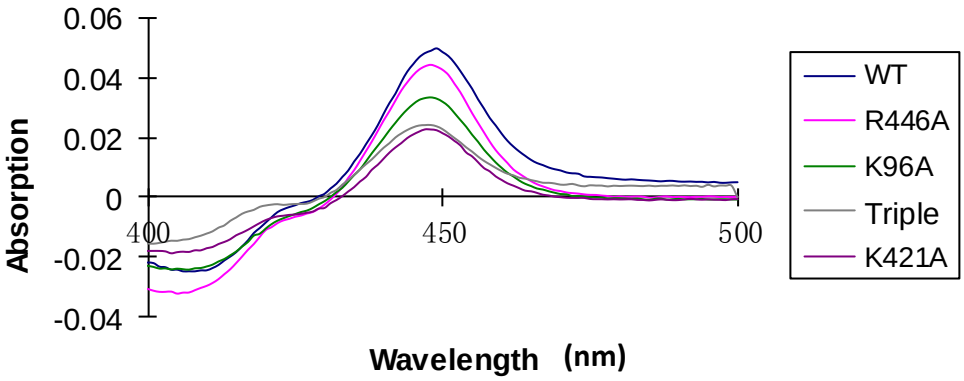

Figure 2.9. CO-ferrous binding difference spectra of wild-type CYP3A4 and its mutants. Spectra were measured in buffer containing 50 mM KPi, 20% glycerol, and pH 7.4.

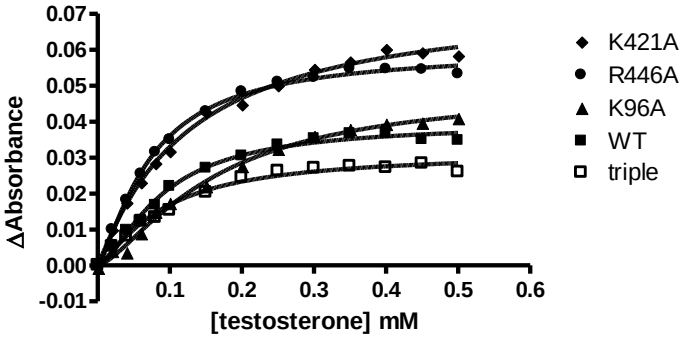

Figure 2.10. Testosterone binding affinity with CYP3A4 and its mutants. Binding of TST with CYP3A4 and mutants were measured by spectral changes with titrations of increasing concentrations of testosterone (from 20 nM to 0.5 mM), where equal volumes of vehicle (acetonitrile) were added to the reference cuvettes.

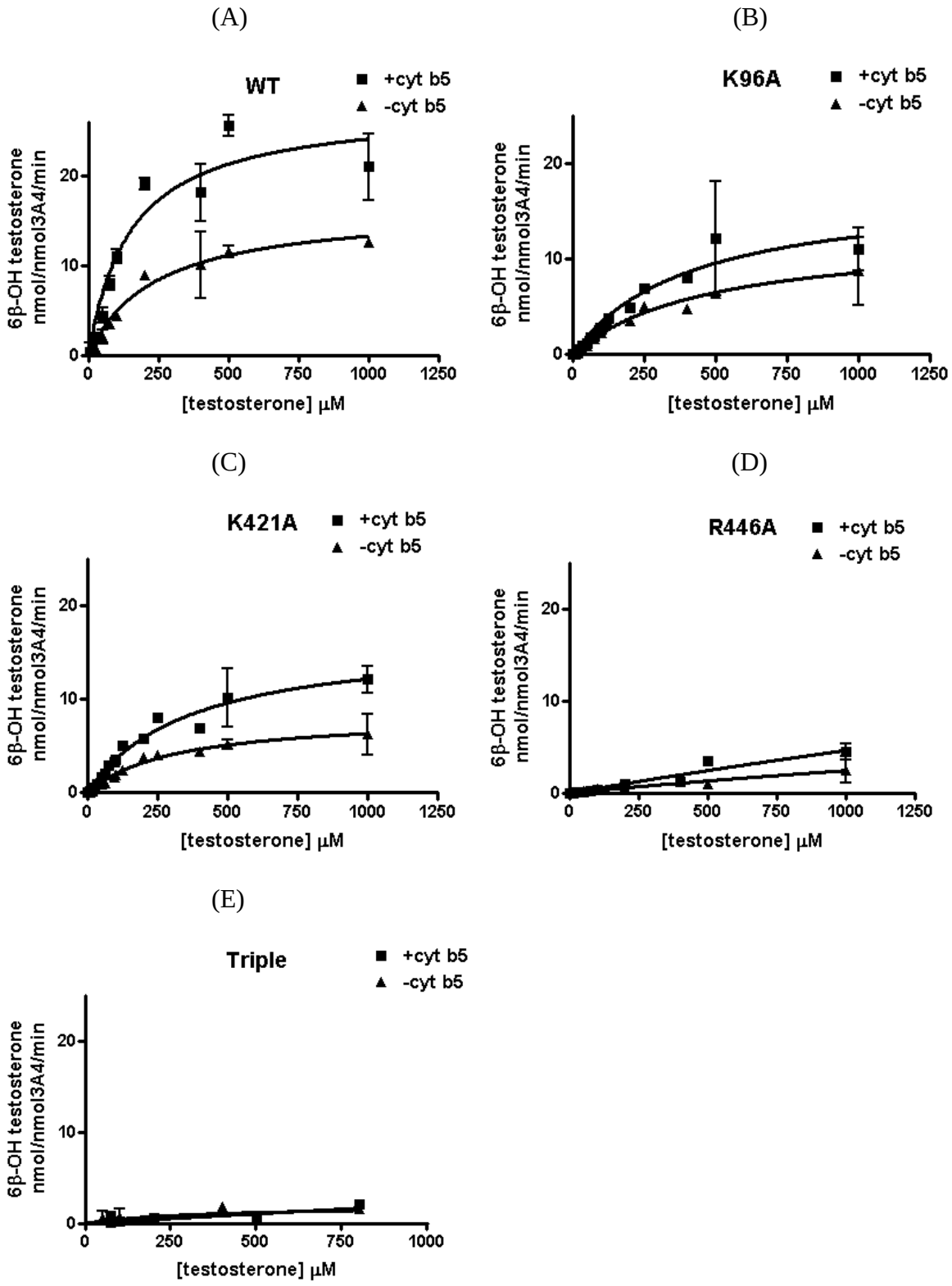

Figure 2. 11. NADPH-dependent formation of 6β-hydroxyl testosterone by CYP3A4 and its mutants. Reactions were carried out using 40 pmol CYP3A4, 80 pmol CPR and 40 pmol b5, in 200 uL reaction volume for 10 min.

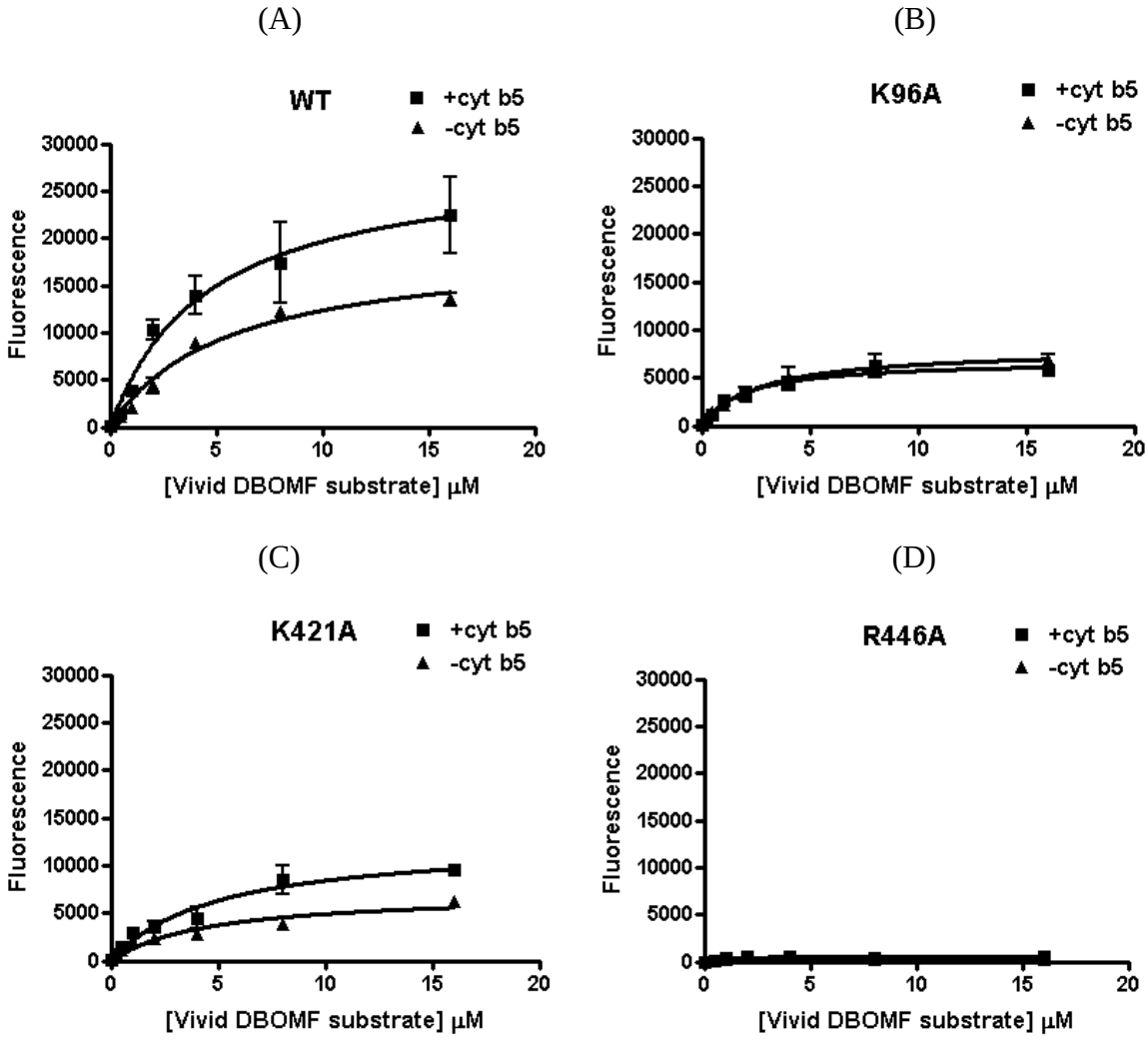

Figure 2.12. NADPH-dependent formation of Vivid Green® from Vivid DBOMF by CYP3A4 and its mutants. Reactions were carried out using 40 pmol CYP3A4/mutant, 80 pmol CPR, and 40 pmol b5, in 200 uL reaction volume for 15 min. (A) CYP3A4. (B) K96A. (C) K421A. (D) R446A.

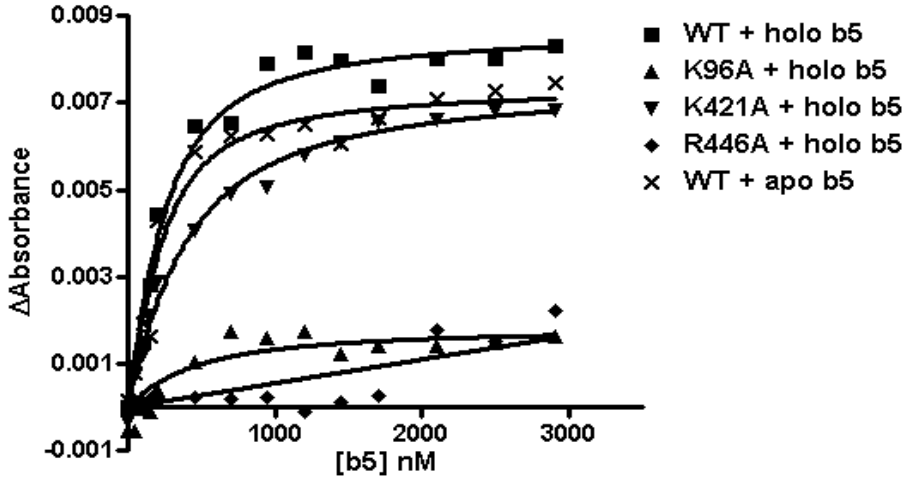

Figure 2.13. Titration of cyt b5 to wild-type CYP3A4 and mutants and apo b5 to wild-type CYP3A4. Spectral titration experiment was carried out using 200 nM CYP3A4/mutants and titration with cyt b5 or apo b5 in 0.5 mL total volume. The magnitude of the absorbance change at 390 minus 418 nm was measured following each addition of cyt b5 at room temperature.

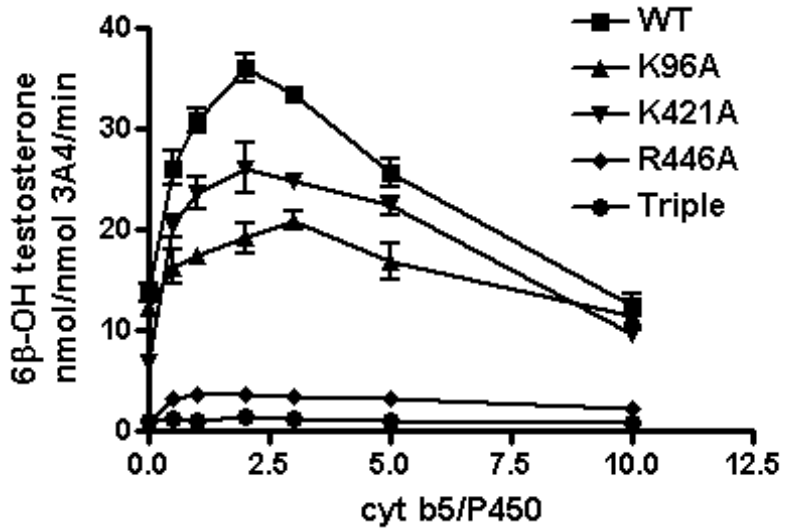

Figure 2.14. Effect of cyt b5 on formation of 6β-hydroxyl testosterone by CYP3A4 and its mutants. Reactions were carried out using varying concentrations of cyt b5 and constant ratio of CYP3A4 (40 pmol) /CPR (80 pmol) for 10 min in 200 uL reaction volume.

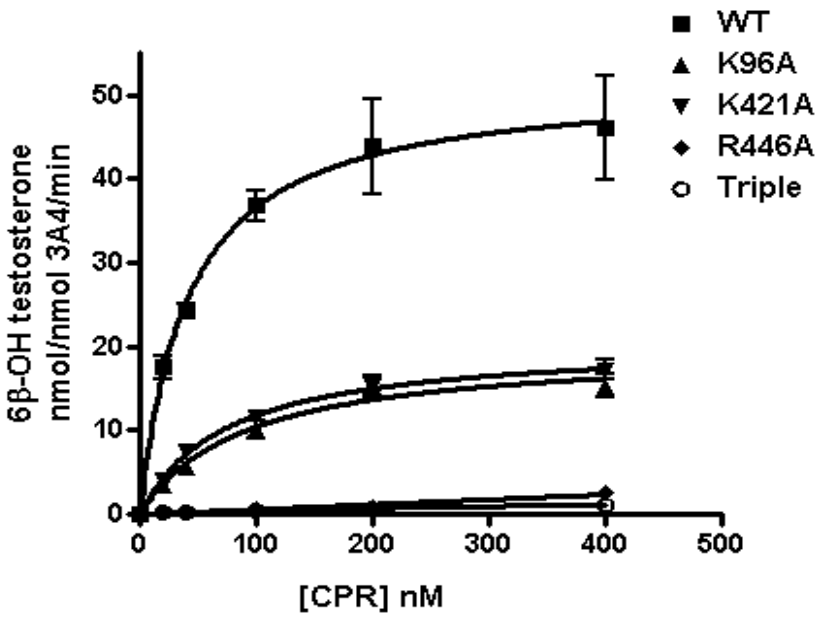

Figure 2.15. Effect of CPR on formation of 6β-hydroxyl testosterone by CYP3A4 and its mutants. Reactions were carried out using varying concentrations of CPR, constant ratio of CYP3A4 (40 pmol) / cyt b5 (40 pmol) for 10 min in 200 uL reaction volume.

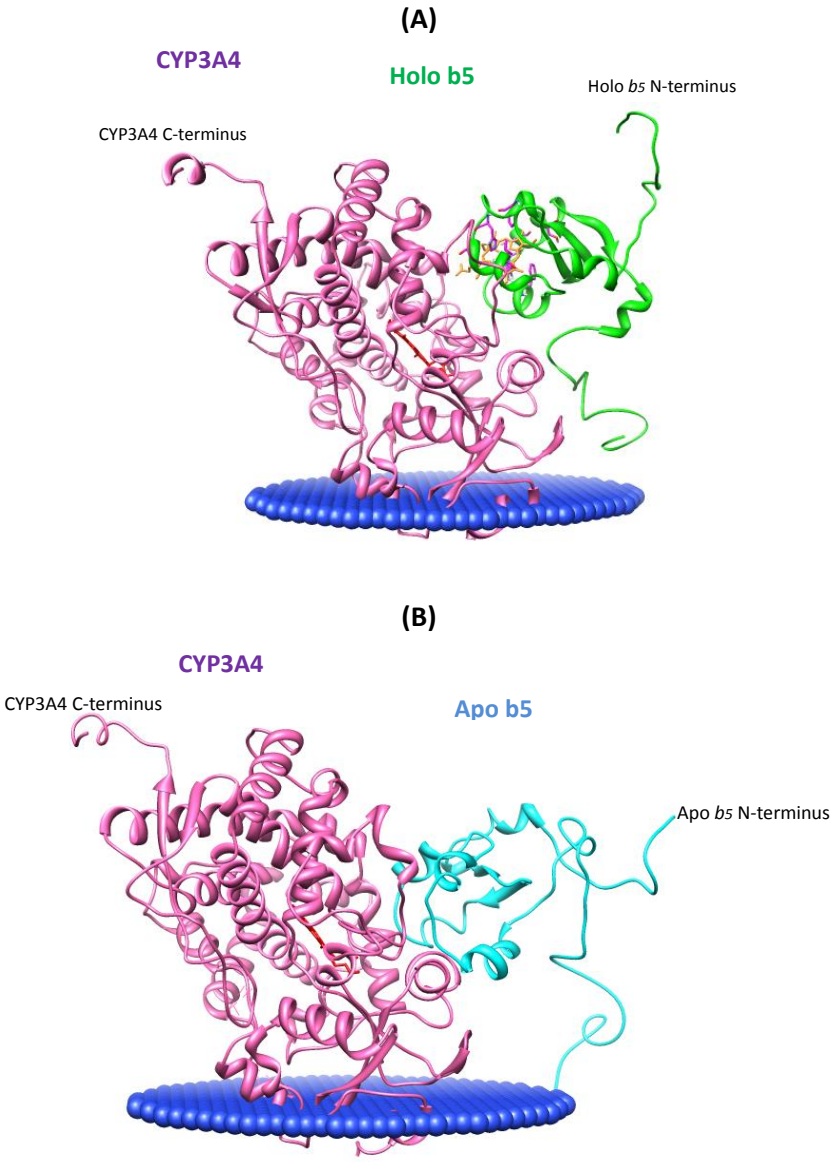

Figure 2.16. Orientations of CYP3A4 and holo/apo b5 in membranes. The angle between CYP3A4 heme (red) plane and the membrane slab (blue) was adjusted to 58°, a middle value between 38° and 78° according to (Ohta et al., 1992). Holo and apo b5 linker domain conformation was made flexible according to (Clarke et al., 2004), as well as the human and rabbit cyt b5 NMR structure (PDB: 2I96). CYP3A4 is light purple; holo b5 is green; apo b5 is cyan. (A) Holo b5-CYP3A4 interaction model position relative to the membrane; (B) Apo b5-CYP3A4 interaction model position relative to the membrane.

Table 2.1 Inter-molecular cross-linked peptide candidates in the complex of CYP3A4-apob_5. The peptide digests were analyzed on an LTQ-Orbitrap instrument.

Measured Mono-isotopic Peak (*m/z*)	Charge State	Measured Peptide Mass (Da)	Calculated peptide Mass (Da)	Error (ppm)	Mass Matches to Inter-molecular Cross-linked Peptides
757.3763	+4	3026.4814	3026.4854	1.3	(human b_5: ^{35}FLEEHPGGEEVLR^{47})-(CYP3A4: ^{116}SAISIAEDEEWKR^{128})
606.1026	+5	3026.4812		1.4	
1024.8989	+5	5120.4627	5120.4582	0.9	(human b_5: ^{48}EQAGGDATENFEDVGHSTDAR^{68})-(CYP3A4: ^{71}VWGFYDGQQPVLAITDPDMIKTVLVK^{96})

Table 2.2 Assignment of tandem mass spectrum for the quadruple-charged ion of cross-linked peptide apo b5:^{35}Phe-Arg^{47}-CYP3A4:^{116}Ser-Arg^{128} with m/z of 757.3763.

Measured m/z	Theoretical m/z	Assignment	Error (ppm)
254.1524	254.1499	$[b_{3\beta} - H_2O]^{+1}$	9.9
267.1107	267.1088	$[b_{(4-5)\alpha}]^{+1}$	7.1
272.1604	272.1605	$[b_{3\beta}]^{+1}$	-0.3
306.1456	306.1459	$[b_{4\beta} - 2H_2O\text{-}NH_3]^{+1}$	-1.0
323.1724	323.1713	$[b_{4\beta} - 2H_2O]^{+1}$	3.4
341.1820	341.1819	$[b_{4\beta} - H_2O]^{+1}$	0.3
359.1918	359.1925	$[b_{4\beta}]^{+1}$	-2.0
387.2722	387.2714	$[y_{3\alpha}]^{+1}$	2.0
428.7297	428.7301	$[y_{8\alpha}]^{+1}$	-0.8
454.2666	454.2660	$[b_{5\beta} - H_2O]^{+1}$	1.3
516.3142	516.3140	$[y_{4\alpha}]^{+1}$	0.3
525.3013	525.3031	$[b_{6\beta} - H_2O]^{+1}$	-3.4
552.7723	552.7755	$[y_{10\alpha} - H_2O]^{+2}$	-5.8
561.7825	561.7808	$[y_{10\alpha}]^{+2}$	3.0
645.3509	645.3566	$[y_{5\alpha}]^{+1}$	-8.9
702.3780	702.3781	$[y_{6\alpha}]^{+1}$	-0.1
759.4005	759.3995	$[y_{7\alpha}]^{+1}$	1.3
852.4094	852.4106	$[y_{13\alpha}/y_{8\beta}]^{+3}$	-1.4
856.4526	856.4523	$[y_{8\alpha}]^{+1}$	0.3
890.4261	890.4333	$[b_{(2-13)\alpha}/b_{(1-12)\beta}\text{-}2H_2O]^{+3}$	-8.1
919.4487	919.4493	$[y_{13\alpha}/y_{10\beta}]^{+3}$(C13)	-0.6
952.9784	952.9733	$[b_{3\alpha}/y_{13\beta}]^{+2}$	5.3
993.5079	993.5112	$[y_{9\alpha}]^{+1}$	-3.3
1086.0298	1086.0241	$[b_{5\alpha}/y_{13\beta}]^{+2}$	5.3

Table 2.3 Assignment of tandem mass spectrum for the quintuple-charged ion of the cross-linked peptide apo b5:^{48}Glu-Arg^{68}-CYP3A4: ^{71}Val-Lys^{96} with m/z of 1024.8989.

Measured (*m/z*)	Theoretical (*m/z*)	Assignment	Error (ppm)
343.1768	343.1765	$[b_{3\beta}]^{+1}$	0.9
359.2682	359.2653	$[y_{3\beta}]^{+1}$	8.1
490.2444	490.2449	$[b_{4\beta}]^{+1}$	-1.0
549.2604	549.2627	$[y_{5\alpha}]^{+1}$	-4.2
625.3098	625.3133	$[a_{5\beta}]^{+1}$	-5.6
653.3088	653.3082	$[b_{5\beta}]^{+1}$	0.9
669.2712	669.2667	$[b_{(2\text{-}6)\beta}]^{+1}$	6.7
686.3137	686.3104	$[y_{6\alpha}]^{+1}$	4.8
710.4137	710.4083	$[b_{(10\text{-}16)\beta}]^{+1}$	-7.6
743.3462	743.3431	$[y_{7\alpha}]^{+1}$	4.2
750.3257	750.3246	$[b_{6\beta} - H_2O]^{+1}$	1.5
768.334	768.3352	$[b_{6\beta}]^{+1}$	-1.6
796.3323	796.3260	$[b_{(3\text{-}9)\beta}]^{+1}$	-7.9
825.3599	825.3566	$[b_{7\beta}]^{+1}$	4.0
842.4138	842.4115	$[y_{8\alpha}]^{+1}$	2.7
953.4198	953.4152	$[b_{8\beta}]^{+1}$	4.8
1063.4709	1063.4632	$[b_{9\beta} - H_2O]$	7.2
1081.4753	1081.4738	$[b_{9\beta}]^{+1}$	1.4
1094.4622	1094.4626	$[y_{21\alpha} - H_2O]^{+2}$	-0.3
1143.678	1143.6806	$[y_{10\beta}]^{+1}$	-2.3
1277.597	1277.5949	$[b_{11\beta}]^{+1}$	1.6
1359.7583	1359.7552	$[y_{12\beta}]^{+1}$	2.3
1390.6974	1390.7001	$[b_{(3\text{-}15)\beta}]^{+1}$	-1.9
1461.7181	1461.7181	$[b_{13\beta}]^{+1}$	0.0
1790.9429	1790.9357	$[b_{(7\text{-}21]\beta}\text{-}NH_3]^{+1}$	4.0

Chapter 3. Cyt b5-CYP2C9 Interaction Study

3.1 CYP2C9 interaction with its redox partners

3.1.1 CYP2C9 introduction

Cytochrome P450 2C9 (CYP2C9) is a major hepatic P450 isoform, with estimated microsomal levels second only to CYP3A4. It accounts for the oxidation of up to 15% of all drugs that undergo Phase I metabolism (Rettie and Jones, 2005). CYP2C9 is the most important isoform in CYP2C family, which also includes CYP2C8, CYP2C18, and CYP2C19. CYP2C9 can catalyze the metabolism of a wide range of drugs, including nonsteroidal antiinflammatories, oral anticoagulants, and oral hypoglycemic (Rettie and Jones, 2005), with a selectivity of relatively small, lipophilic anions such as the non-steroidal anti-inflammatory drugs ibuprofen, flurbiprofen, naproxen and diclofenac as well as the hypolipidemic agent gemfibrozil (Schoch et al., 2004; Wester et al., 2004).

Several CYP2C9 substrates with low therapeutic index, such as (*S*)-warfarin, tolbutamide, and phenytoin, are frequently involved in drug-drug interactions, causing serious adverse events. In addition, CYP2C9 shows significant genetic polymorphism, with up to 40% of Caucasians carrying alleles that encode partially defective forms of the enzyme (Rettie and Jones, 2005). The defective enzyme expression may result in unpredictability of metabolizing enzymes of a drug in poor metabolizers..

Cytochrome b5 has been found to stimulate CYP2C9 activity and the extent of the effect is substrate-dependent (Yamazaki et al., 1997; Yamazaki et al., 2002). Although the in vitro-in vivo extrapolation strategies have been extensively used for drug interaction prediction, complications still exist. A thorough understanding of how cytochrome b5 modulates

CYP2C9 would greatly improve in vitro-in vivo prediction and eventually benefit management of therapeutics with a narrow therapeutic index.

3.1.2 Cyt b5 modulation effect on CYP2C9

CYP2C9's modulation by cyt b5 was first reported by Yamazaki et al, showing that both holo b5 and apo b5 can modestly increase CYP2C9 activity ~2-5 fold (Johnson and Guengerich, 1997; Yamazaki et al., 1997; Yamazaki et al., 2002). With respect to the mechanism of cyt b5 for interaction with CYP2C9, Yamazaki et al. proposed that protein-protein interactions between CYPs and cyt b5 are very important. However, there is a very limited literatures elucidating the mechanism of cyt b5 effect on CYP2C9, compared with CYP3A4 and CYP2B4.

The only study of cyt b5 effects on the coupling of CYP2C9 catalysis was reported by Locuson et al. (Locuson et al., 2007b). CYP2C9 activity in metabolizing diclofenac, (*S*)-wafarin, and (*S*)-flurbiprofen was investigated with varying ratios of cyt b5/CYP2C9 up to about 20. When cyt b5/CYP2C9 ratio was less than 4, the rates of the metabolism of all these substrates were invariably increased. However, when the ratio is above 4, the metabolite formation rates decreased with the increase of the cyt b5 to CYP2C9 ratio. The reaction coupling, as measured by the metabolite formation rate over NADPH consumption rate, was invariably increased with the increase of cyt b5 to CYP2C9 ratio up to 16. Though hydrogen peroxide formation rate showed a continuous decrease with varying ratios, hydrogen peroxide uncoupling, which is the hydrogen peroxide formation rate over NADPH consumption, showed a complex behavior. At cyt b5 to 2C9 ratios below 4, the hydrogen

peroxide uncoupling was increased with all three substrates. When the ratio is above 4, it was decreased with (*S*)-wafarin and diclofenac while increased with (*S*)-flurbiprofen. This suggested that cyt b5 affects multiple steps in the CYP2C9 catalytic cycle. Comparison of the holo b5 and apo b5 effect on CYP2C9 catalysis reveals that apo b5 has a similar profile in affecting the (*S*)-flurbiprofen metabolism, hydrogen peroxide formation, NADPH consumption and the reaction coupling, with a slightly different magnitude at various ratio of cyt b5/CYP2C9. This strongly suggests that cyt b5 can cause conformational change in CYP2C9 without directly affecting electron transfer. As for the apo b5 and holo b5 difference in CYP2C9 function, it was postulated that apo b5 could not induce the same extent of conformational change as the holo b5 due to disturbances of the structure after heme removal. This is based on the observation that the apo-b5 binding affinity to CYP2C9 is similar to that of holo b5 by spin equilibrium titration. Therefore, it binds to the CYP2C9 well but the allosteric effect is attenuated.

3.1.3 CYP2C9 structure and topology in interaction with its redox partners

CYP2C9 is the first human P450 to be crystallized. The crystal structure was resolved in 2004 by William et al. and Wester et al. independently, with three X-ray crystal structures reported (Wester et al., 2004; Williams et al., 2003). Among the three structures, one is substrate-free (1OG2 (PDB access number)), one is with substrate (*S*)-warfarin bound (1OG5), and the third one is with substrate (*S*)-flurbiprofen bound (1R9O). 1OG2 and 1OG5 were from a modified CYP2C9 protein containing seven amino acid substitutions, K206E, I215V, C216Y, S220P, P221A, I223L, and I224L corresponding to CYP2C5 protein, in addition to its N-terminal modification to facilitate expression and crystallization. The

structures therefore are similar to that of CYP2C5 in the specific region containing mutations. Comparison of the two substrate-bound structures 1OG5 and 1R9O show that though these two structures correspond to each other closely in many regions only with very small deviation (root mean square deviation of only 0.74 Å), significant differences in several segments of CYP2C9 exist, among which are the most prominent ones that the B-C loop region in 1R9O forms a random coil, but an α helix in 1OG5; the F-G loop region was disordered in 1R9O, but helical in 1OG5 (Wester et al., 2004; Williams et al., 2003). In addition, in 1R9O, residues Gly97-Lys121 on B-C loop adopt a distinct conformation from 1GO5 allowing Arg108 to interact with the (*S*)-flurbiprofen anion and Asn289 and Asp293 on helix I. Therefore, Arg108 on the B-C loop was predicted to be very important for CYP2C9 activity. Mutation of Arg108 to His or Phe drastically changed CYP2C9 activity (Dickmann et al., 2004). The substitution to His residue caused an intramolecular histidine coordination to the heme iron, resulting in the movement of several loop regions, including the F-G and B-C loop regions, the β1-1, β1-2 loop in the N-termini, the G-H loop, the H-I loop, the meander region, and the β3-3-β4-1 loop, the most significant ones being the F-G and B-C loops (Roberts et al., 2010). Wester et al. noticed that in the CYP2 family (with the exception of 2W1, 2U1, 2J2, 2R1 and 2D6), the B-C loop region contains the GXG motifs, which flank the flexible region, therefore, it can adopt alternative conformations without greatly perturbing the secondary structure immediately before and after. In a study on the human CYP2C9*13 variant, when the Leu90 is substituted with Pro residue, the backbone between Ala106-Arg108 on the B-C loop turned over against its original conformation, and blocked the substrate access channel, providing more evidence on the flexibility of the B-C loop and its role in substrate binding (Zhou et al., 2006). Indeed, the B-C loop region has

been identified by Gotoh (Gotoh, 1992) as a putative substrate recognition site (SRS-1) through analysis of CYP2 family sequence and appears to be important for substrate specificity through its contact with substrates. A random expulsion molecular dynamics investigation on CYP101 has indicated that the motion of this region can open the substrate access/egress channel bordered on B-C loop. Its motion can also result from global protein motions influenced by binding of the redox partners of P450s (Ludemann et al., 2000). Most recently, quite a few studies using computer dynamics simulations clearly show that the substrate access/egress channel to the active site of CYP2C9 are affected by the movement of the F-C loop and B-C loops (Cojocaru et al., 2007; 2012). Ligands exit from the buried active site of CYP2C9 using multiple routes depending on the type of the ligand (Cojocaru et al., 2012). The opening around the F-G and B-C region is necessary for ligand via this major channel (Cojocaru et al., 2012).

A search of the literature showed very limited studies on CYP2C9 topology in binding with its redox partners. Crespi et al. (Crespi and Miller, 1997) reported that an R144C variant of CYP2C9 has impaired binding for CPR, as when cumene hydroperoxide was added to bypass the first electron transfer step in the P450 catalytic cycle, R144C and wild-type showed no difference in catalyzing diclofenac 4'-hydroxylation. The Arg144 residue is located at the D helix on CYP2C9. Scott et al. proposed that the G/H and C/D loops interacting on the proximal face of the protein could affect the position of the C helix which is involved in redox partner binding (Cheng et al., 2004). In addition, comparing the open conformation of CYP2B4 and the closed form, it was proposed that interactions between the G/H and C/D loops could be involved in coordinating ligand-induced conformational changes on the distal side of the protein to electron delivery on the proximal side.

Another report on the redox binding site to P450s investigated CYP2C8 (Kaspera et al., 2011), a closely associated isoform with CYP2C9, which share 70% sequence homology and 80% sequence similarity. CYP2C8*3 contains two amino acid substitutions at R139K and K399R compared with wild-type CYP2C8*1, which are conserved among all CYP2C family. Recombinant CYP2C8.3 showed two- to five-fold higher clearance of amodiaquine, paclitaxel, rosiglitazone, and cerivastatin compared to wild-type CYP2C8. It was proposed that CYP2C8.3 has a higher affinity towards cyt b5 and CPR (Kd and Km,red), which resulted in increased reaction coupling and higher binding affinity of ligands. Among the two residues, R139 is suggested as an essential amino acid influencing CYP2C8-CPR interactions. R139 is at the C-D loop closed to the N-terminal D helix (Kaspera et al., 2011).

Other studies have indicated that the N-terminus of P450s contribute to the interaction of P450s with CPR by affecting the extent of membrane integration. The regions other than the N-terminal hydrophobic membrane anchor, , may also facilitate membrane attachment. The role of this region may differ for each individual P450s due to the different primary amino acid sequence (Shukla et al., 2009). The extent and orientation of P450s in the membrane affect their ability to interact with the redox partners CPR and cyt b5. Truncated form of CYP2C9 catalytic activity was affected as well as many other truncated form of P450s. CYPs 1A2(Δ1-25 or Δ1-36) (Dong et al., 1996), 2C9 (Δ3-20) , 2C11 (rat male specific isoform) (Δ3-20) (Licad-Coles et al., 1997), and 2C19 (Δ 3-20) showed a requirement for more CPR to reach maximal activity, while a CYP2C18 form containing a more intact N-terminal sequence (MALLLAVFL) did not. The CYP2C18 (MALLLAVFL) has a better membrane insertion which results in increased substrate availability and improved redox partner binding (Kinobe et al., 2005). Recombinant CYPs 2C9 and 2C19 with N-termini more similar to the

native sequence showed a better agreement in in vitro activity to the in vivo activity, as a result of more tightly binding to the membrane compared with the corresponding truncated forms (Kinobe et al., 2005).

3.1.4 Hypothesis for the study of cyt b5-CYP2C9 interaction

As discussed above, previous studies have suggested that cyt b5 modulation of CYP2C9 activity is through an allosteric effect. We hypothesize that when cyt b5 is devoid of heme, the surface contact region between holo b5-CYP2C9 and apo b5-CYP2C9 are similar, in order for both of them to exert similar stimulatory effect on CYP2C9 activity.

The goal of this study is to map the surface interaction between holo b5-CYP2C9 and apo b5-CYP2C9 using the chemical cross-linking coupled with mass spectrometric analysis,construct models of their interaction based on the cross-linking result, and compare their surface interactions.

3.2 Materials and experimental procedures

3.2.1 Materials

Escherichia coli strain DH5α $F'I^q$ cells containing the expression vector pCWhum2C9$(His)_6$ (N-terminus modified MALLLAVF) and strain BL21(DE3) containing the plasmid $(His)_4$HMWHuman-cyt b5 were provided by Dr. Allan E. Rettie and Dr. Richard J. Auchus (Guryev, 2001; Holmans, 1994). All other reagents are the same as those used for cyt b5-CYP3A4 interaction study.

3.2.2 Protein Expression and Purification

CYP2C9 was produced in *E. coli* DH5α F'I^q cells using the expression vector pCWhum2C9 $(His)_6$. Proteins were purified via nickel-nitrilotriacetic acid affinity columns essentially as described previously without the inclusion of stabilizing ligands, then further purified by hydroxyapatite column. Briefly, a single colony of freshly transformed *E. coli* DH5α F'I^q cells was inoculated into a ~3 mL LB-ampicillin medium for overnight culture at 37 ℃, then inoculated to 500 mL of Terrific Bloth medium supplemented with 50 μg/mL ampicillin and 0.5 mL of 1 M thiamine at 37 ℃ and shaken at 200 rpm for fast growth. When the OD_{600} of the mixture reached 0.4, 0.5 mL of 1 M δ-ALA was added, and cells were induced with 0.5 mL of 1 M IPTG with the temperature and rate of revolution reduced to 27 ℃ and 125 rpm, respectively. Cells were harvested after growing for a total of 40 hours, and stored at -80 ^{o}C until further purification.

Cells pellets were thawed and resuspended in ice-cold resuspension buffer (50 mM KPi, 20% glycerol, 20 mM β-mercaptoethanol (BME), pH 7.4) supplemented with protease inhibitor cocktail. The cell suspension was passed through the French Press cell twice at 600 psi, stirred at 4 ℃ for 1 h in the presence of 10% Emulgen 911, and centrifuged at 37000 rpm and 4 ℃ for 60 min. The resulting red supernatant was collected and loaded onto Ni-NTA affinity column equilibrated with resuspension buffer. The column was then washed extensively with wash buffer (50 mM KPi, 300 mM NaCl, 40 mM imidazole, 100 mM glycine, 20% glycerol, 2 mM BME, and 0.2% Emulgen 911, pH 7.4. Protein was eluted with elution buffer (50 mM KPi, 20% glycerol, 2 mM BME, 0.2% cholate, and 400 mM imidazole) and dialyzed against hydroxyapatite (HA) equilibration buffer (10 mM KPi, 2 mM BME, 0.2% cholate, and 20% glycerol) at 4 ℃. Dialyzed protein was loaded onto the HA column

and washed with HA wash buffer (25 mM KPi, 2 mM BME, and 20% glycerol, pH 7.4). Protein was eluted with 400 mM KPi and 20% glycerol, pH 7.4) and dialyzed against storage buffer (50 mM KPi, 20% glycerol, pH 7.4). The protein was aliquoted and stored at −80 °C for further use.

Protein concentrations were determined by CO-binding difference spectra using an extinction coefficient of 91 mM^{-1} cm^{-1}. Protein was determined to be greater than 95% pure by reducing SDS–PAGE using a 10% acrylamide gel and Coomassie brilliant blue staining.

Recombinant rat NADPH-cytochrome P450 reductase (rCPR) was expressed and purified using the method described in Chapter 2 according to published protocol (Shen et al., 1989). Human cyt b5 expression and purification was as described in Chapter 2 according to previously described protocol (Holmans et al., 1994; Naffin-Olivos and Auchus, 2006). Apo b5 was prepared according to previously published protocol (Yamazaki et al., 1996a).

3.2.3 Cross-linking Reactions

CYP2C9 and cyt b5 were reconstituted at a molar ratio of 1:1 in 100 uL 50 mM KPi (pH 7.4) buffer containing in the presence of liposome (DLPC, sonicated) with final concentration of 10 μM of each enzyme. The solution was gently stirred for 10 min and held at room temperature for 2 hr. Then the chemical cross-linking reagent EDC was added to a final concentration of 10 mM from a 100 mM stock in 50 mM KPi (pH 7.4) buffer. The reaction was allowed to proceed at room temperature for 2 hr followed by dialysis against 50 mM KPi (pH 7.4) buffer (2L) and then 50 mM ammonium bicarbonate (AB) buffer (2L) to move EDC

and isourea that was generated at 4 ^{o}C. After dialysis, the proteins were immediately processed for digestion.

3.2.4 Proteolytic Digestion and LTQ-Orbitrap Mass Spectrometric Analysis

Digestion of the cross-linked protein complex and subsequent mass spectrometric analysis were performed as previously described (Gao, 2006). Briefly, final concentration of 6M Urea was added to the protein mixture solution. Then a final concentration of 10 mM DTT was added into the solution with incubation at room temperature for 1 hour, followed by a final concentration of 60 mM IAM at room temperature for 1 hour. Then DTT was added again to the solution with a final concentration of 60 mM and incubated at room temperature for 1 hour. Then the protein mixture was dialyzed against 50 mM AB buffer. Then trypsin was added with a ratio of 1:50 w/w trypsin to protein and the digestion was allowed to proceed overnight for 12-16 hour. After digestion, the protein mixture was dried using SpeedVac.

Peptide digests were dissolved in 5% acetonitrile aqueous buffer containing 0.1% formic acid and analyzed by electrospray ionization in the positive ion mode on a hybrid linear ion trap-Oribtrap instrument, known as the LTQ-Orbitrap (Thermo Fisher, San Jose, CA). Peptides were trapped on a pre-column (100 μm i.d. ×15 mm) packed with 200 Å C18 stationary phase (5 μm, C18AQ; Michrom) for 10 min, followed by subsequent separation on an analytical column (75 μm i.d. × 150 mm) packed with 100 Å C18 stationary phase (5 μm, C18AQ; Michrom), coupled to the mass spectrometer. For each injection, an estimated amount of 2 μg of peptide mixture was loaded onto the pre-column in 5% acetonitrile aqueous buffer containing 0.1% (v/v) formic acid at a rate of 4 μL/min. Peptides were eluted

using an acetonitrile gradient flowing at 0.35 μL/min. The mobile phase consists of buffer A (water, 0.1% formic acid) and buffer (B, acetonitrile, 0.1% formic acid). A linear gradient program was used as follows: 0 min, A (95%), B (5%); 55 min, A (65%), B (35%); 60 min, A (15%), B (85%); 65 min, A (5%), B (95%); 75-90 min, A (95%), B (5%); (stop). All MS survey scans were performed in the Orbitrap from m/z 300-2000 at resolution of 60 000 (m/z 400). For tandem mass spectrometry with ion detection in the Orbitrap, the resolution was set to 7,500, and the precursor isolation width to 4 m/z units. Collision energy was set to 40% for CID in the LTQ. Data-dependent analyses were performed by data-dependent selection of the five most abundant precursors at a charge state of +3 and above for tandem mass spectrometry. Singly and doubly charged precursors were set to be rejected from the data-dependent mode. Data redundancy was minimized using the dynamic exclusion feature by excluding the previously selected precursor ions for 45 s before selected again for fragmentation.

3.2.5 Data Processing and Database Searching

Data processing and database searching was according to Singh et. al (Singh et al., 2008) and Goodlett lab protocols and scripts (http://goodlett.proteomics.washington.edu). Briefly, the data were converted into dta files with higher charge state precursors deconvoluted to the 2+ charge state precursors and 1+ charge state fragments. Deconvoluted spectra were searched using Phenyx (GeneBio SA, Geneva, Switzerland) to filter out the linear peptides. Methionine residues were considered as being present in the reduced and oxidized form and cysteine residues were considered alkylated by iodoacetamide. Popitam algorithm was then used to evaluate the tandem mass data and output the possible cross-linked peptide

candidates. A detailed description of the rationale of Popitam algorithm has been made by Hernandez et al. (Hernandez et al., 2003) and Singh et al. (Singh et al., 2008). As the LTQ-Orbitrap instrument is able to provide high mass accuracy, the error of the assignment is made within 10 ppm. Candidate peptides with higher error were excluded. The above ions were not identified to be any linear peptides when searched by phenyx, thus ruling out the possibility of mis-interpretation of a linear peptide.

3.2.6 Molecular Docking

X-ray crystallographic structures of human CYP2C9 (PDB "1R9O") and a homology model of human cyt b5 from bovine cyt b5 (PDB "1CYO") (Cunane et al., 1996) (Schoch et al., 2004) were used to construct the model of the CYP2C9-cyt b5 complex. Docking calcuations based on the structures (Pierce et al., 2011) with the cross-linking sites between cyt b5 and CYP2C9 as constraints was carried out using the software package Chimera. The distance between the residue pair in each identified crosslink was minimized.

3.3 Results

3.3.1 Chemical Cross-Linking

Treatment of an equimolar mixture of CYP2C9 and human cyt b5 or apo b5 with EDC resulted in the formation of cross-linked protein complexes, with the major complex being a binary complex at molecular weight of ~73 kDa on SDS-PAGE (Data not shown). CYP2C9 is ~56 kD and cyt b5 is about 16.7 kD. The occurrence of the ~73 kD band indicates that a cross-linked complex was formed by EDC covalently binding.

3.3.2 Holo b5 and CYP2C9 Interactions

Five inter-molecular cross-linked peptides were identified with cross-linking sites determined by corresponding tandem mass spectra (Table 3.1 and Fig. 3.1-3.6). Trypsin cleaves proteins at exclusively C-terminal to arginine or lysine (Olsen et al., 2004). When the Lys side chain is modified with cross-linking another peptide, it cannot fit into the trypsin binding pocket to be cleaved. Thus only non-C-terminal Lys residues can be the possible cross-linked residue with Glu or Asp residues.

In the cross-linked peptides holo cyt b5: ^{48}EQAGGDATENFEDVGHSTDAR^{58} - CYP2C9: ^{421}KSK^{423} , the cross-linking sites are determined to be Glu48 on cyt b5 and Lys421 on CYP2C9. Both quadruple-, and quintuple-charged ions of this cross-linked peptide were observed and the mass of the monoisotopic precursor ions are listed in Table 3.1. In the spectra, a series of y ions of cyt b5 peptide were shown, the longest y ion being y19. This helps in determining the acidic residue that is cross-linked with CYP2C9 peptide to be Glu48, the very first residue in this peptide. Because if the cross-linked residue is not the first one, y ions including the cross-linked acidic residue will not be formed, the mass of which has to be y minus an –OH group.

For the cross-linked peptide cyt b5: ^{35}FLEEHPGGEEVLR^{47} - CYP2C9: ^{421}KSK^{423}, triply, quadruple and quintuple charged precursor ions are all observed. The spectra indicate that the cross-linking sites on cyt b5 are both Glu37 and Glu43 with Lys421 on CYP2C9. Using the same criteria mentioned above, the Lys residue in cross-linking is determined to be the first Lys on CYP2C9. In the spectra, ion y10 of cyt b5 indicate that it has to be Glu37, the first acidic residue in this peptide that is cross-linked; however, cross-linking fragment y8/y3 was also found, indicating that it has to be one of the last two Glu residues that are cross-linked.

As b9/y3 is found, it might be likely that Glu43 is cross-linked though Glu44 cannot be excluded. Overall, the 1st and the 3rd acidic residues in the cyt b5 peptide are likely to be cross-linked. These two sites are right around the conserved His44 residue which ligates the heme iron, on a U-shaped loop turning at the site of the His44 residue. So in the three-dimension structure, the same Lys residue can be close enough to both Glu residues.

In a third cross-linked peptide cyt b5: ^{48}EQAGGDATENFEDVGHSTDAR^{68} - CYP2C9: ^{109}GFGIVFSNGKK^{119}, the quintuple charged precursor ion was observed. For this candidate, the instrument did not generate enough fragments to allow determining the cross-linking sites unambiguously. As shown in the spectra, no differentiation can be made between the acidic residues Asp53, 60, Glu48,56, 59, 66. Lys118 on CYP2C9 is determined to be the residue that is cross-linked according to the mentioned criteria and all fragments agree with this assignment.

A fourth cross-linked peptide is cyt b5: ^{35}FLEEHPGGEEVLR^{52} - 2C9: ^{158}KTK^{160}, in which Lys158 on CYP2C9 is cross-linked with Glu37 on cyt b5. In this spectrum, y10 of cyt b5 is found, indicating that the first Glu residue is cross-linked. The cross-linked fragments all agree with this assignment.

A fifth cross-linked peptide is cyt b5: ^{48}EQAGGDATENFEDVGHSTDAR^{58} - 2C9: ^{271}MEKEK^{275}, in which Lys273 on CYP2C9 is cross-linked with either Asp53 or Glu56, for in the cyt b5 fragments, y12 and b4 ions are identified, suggesting that only Asp53 and Glu56 in between the 4th and the 11th residues are possible cross-linked sites. All other fragments agree with the assignment.

3.3.3 Apo b5 and CYP2C9 Interactions by Mass Spectrometric Analysis

In apo b5-CYP2C9 complex, 5 cross-linked peptides were identified as shown in Table 3.2 and Fig. 3.7-3.11. The first cross-linked peptide is apo b5: ^{35}FLEEHPGGEEVLR^{47}- CYP2C9: ^{421}KSK^{423}. Only a quadruply charged peptide precursor was identified in apo b5-CYP2C9 complex. As y11 ion of apo b5 and cross-linked fragment y5α/y3β exist concomitantly (α stands for apo b5 and β stands for CYP2C9), it suggests that both Glu37 and 43 are cross-linked. The Lys421 on CYP2C9 was found cross-linked with the Glu37 and 43 on apo b5. This cross-linked peptide is the same as found in the holo b5-CYP2C9 cross-linked peptide.

The second cross-linked peptide is apo b5: ^{48}EQAGGDATENFEDVGHSTDAR^{68} - CYP2C9: ^{119}KWK^{121}. Similarly to the one found in holo b5-CYP2C9 complex, Lys118 on CYP2C9 was found cross-linked with Glu59 or Asp60 in the cross-linked peptide. In the fragmentation spectra, it shows y8 ion and b6 of apo b5, indicating that only acidic residues in between the Glu53 and Val61 are possible cross-linked sites. The observation of cross-linked fragment y11/y3 suggests that either Glu59 or Asp60 are the cross-linked site. No further differentiation is allowed based on the spectrum.

A third cross-linked peptide is cyt b5: ^{48}EQAGGDATENFEDVGHSTDAR^{68} - CYP2C9: ^{27}GKLPPGPTPLPVIGNILQIGIK^{48}. The precursor ion of it is quadruply charged. In its tandem mass spectrum, y8 of apo b5 is the longest y ion identified, and together with the cross-linked fragment y15α/y22β it suggests that it is Glu56, or Glu59, or Asp60 that is involved in the cross-linking. For CYP2C9 peptide, y19 ion is seen, indicating that it is the Lys28 that is cross-linked. The other fragmentation is in agreement with this assignment.

The fourth candidate is apo b_5: ^{48}EQAGGDATENFEDVGHSTDAR^{68}-CYP2C9: ^{233}LLKNVAFMK^{241}, the precursor of which is quintuply charged. For apo b5 peptide, the existence of b6 and y12 ions indicates that it has to be the Glu56 that is cross-linked; otherwise b and y ions containing the cross-linked acidic residue would not be formed. For CYP2C9 peptide, it is the Lys235 that is cross-linked according to previously mentioned criteria and the fragmentation pattern fully agrees with the assignment, e.g.,the longest y ion is y6 immediately after the Lys residues. Lys235 is at the middle of the G helix, a region that is generally considered to be very flexible and involved in conformational change upon substrate or redox partner binding. In addition, computer dynamic simulation has found that between the G helix, I helix and the B-C loop, a substrate egress channel is possible. However, this site is in the distal surface of CYP2C9, not within the traditionally agreed redox partners binding site. At this point, it is not clear whether it is an nonspecific interaction, or an indication of a second binding site of cyt b5 for CYP2C9.

3.3.4 Modeling of Holo b5-CYP2C9 and Apo b5-CYP2C9 Complex

Comparing the interaction sites between holo b5-CYP2C9 and apo b5-CYP2C9, it is found that there are residues in common that play an important role in the protein-protein interactions. 1) in both cases, Lys421 is identified to be cross-linked with Glu37 and Glu43. In the holo b5-CYP2C9 interaction, Lys421 is found cross-linked with Glu48 as well, which is not identified in the apo b5-CYP2C9 interaction. 2) Lys118 in holo b5 and Lys119 on apo b5, the two adjacent residues were found to interact with the same peptide segment on holo/apo b5. In apo b5, it is either Glu59 or Asp60 that is involved in cross-linking; for holo b5, due to the limited fragmentations, it is difficult to differentiate between these two and the

others. Differences in the cross-linking sites were also identified, as shown in the remaining cross-linked peptides. Lys 273 on the CYP2C9 H helix was found to cross-link with holo b5. The H helix is in close contact with helix C. Therefore, through contact with Lys273, cyt b5 may be able to affect helix C, the substrate recognition site as well as cause conformational change of CYP2C9. Lys158 on CP2C9 helix D was found cross-linked with Glu37 and 43 on holo b5. It is difficult to tell whether this interaction is specific or nonspecific at this point.

In the apo b5-CYP2C9 complex, Lys235 on the CYP2C9 helix G was cross-linked with apo b5. As mentioned earlier, a substrate egress channel between helices G, I and B-C loop was formed during dynamic simulations of CYP2C9. If apo b5 binds to this site through specific interaction, it might affect the product release process in the CYP2C9 catalytic cycle.Alternatively, this interaction is caused due to the perturbed structure of apo b5, and thus is non-specific. In either case, this pair is excluded from the docking calculation for the current study.

Another cross-linked site on CYP2C9 is Lys28, which crosslinked with Glu56/59/60. Lys28 is at the N-terminal region of CYP2C9 and is surrounded by hydrophobic residues. This region is considered to be membrane associated as an auxiliary support for CYP2C9 to be membrane associated. Under physiological conditions, Lys28 on P450s is very likely to dip in the membrane to contribute to locate and position the whole protein, and will not be able to be contacted by residues on the cyt b5 cytosolic domain. Therefore, in apo b5-CYP2C9 complex, the interaction of Lys28-Glu56/59/60 is considered to be nonspecific and excluded from the docking calculations.

Excluding the two pairs for apo b5-CYP2C9 and one pair for holo b5-CYP2C9 using the above mentioned criteria, the other interaction sites are considered specific and were used for the computer modeling of the holo/apo b5-CYP2C9 interaction. The three Lys residues on CYP2C9 are all on the proximal surface, and the very likely orientation of cyt b5 in interaction with CYP2C9 is shown as Fig 3.12A. This docking calculation for holo b5-CYP2C9 is based on the interacting pairs Lys421-Glu37/43/48, Lys118-Glu59/Asp60. In this orientation, Lys273 is close to the acidic residues 56-66 on cyt b5. Computer dynamic movement may allow it to interact with one or more of these acidic residues.

For apo b5-CYP2C9, the docking calculation is based on Lys421-Glu37/Glu43 with Lys119-Glu59/Asp60. It is evident that holo b5 and apo b5 bind to CYP2C9 with very similar orientations with these sites as primary contact sites (Fig. 3.12B), though without heme, apo b5 might be able to interact with CYP2C9 with these sites more "freely" and adjust itself further upon binding with CYP2C9. Dynamic simulation is needed to further elucidate this interaction.

Similar to the holo/apo b5-CYP3A4 interaction, the interacting surfaces on holo/apo b5 in binding to CYP2C9 are composed of the segments α2 -loop-α3 and α4 -loop-α5, and plus one propionate group of the heme in holo b5. Both holo and apo b5 bind to the same groove on CYP2C9 with the common contacting regions, despite the slightly different orientations according to their models (Fig. 3.12). The contact regions on CYP2C9 with holo b5 are the B helix, the B-B' loop, the C helix, the C-D loop, the K''-L meander region, the β-bulge and the L helix (Fig. 3.12). Those for apo b5 are the B helix, B-B' loop, C helix, C-D loop, H helix, K''-L meander region, and the β-bulge (Fig. 3.12). Both holo and apo b5 approach the B-B' loop region and the C helix of CYP2C9 via α3 and α4 helix, respectively. In holo b5-

CYP2C9 model, the CYP2C9 and cyt b5 heme groups have a distance of 11 Å, which is too far to facilitate a direct electron transfer. The apo b5 does not have the heme group, so the energy clash between apo b5 and CYP2C9 is less than with holo b5, which may result in the slight difference in the orientation of apo b5 from holo b5. In addition, the relatively more flexible structure of apo b5 may allow it to "adjust" its conformation more upon binding with CYP2C9. In another words, it cannot induce the same conformational change of CYP2C9 even though it binds to the same site as holo b5 as it can adapt its conformation to CYP2C9 more freely.

3.4 Discussion

P450s have overall similar secondary structures despite their quite different primary amino acid sequence; on the other hand, each P450 isoform is distinct in that they have "adapted" themselves for different substrate specificity. The active site of P450s is buried inside the protein next to the heme group, often isolated from the surrounding solvent. Consequently, it is expected that binding of substrate or coenzyme with P450s can influence the active site through conformational changes to affect its substrate specificity, product release and kinetic parameters (Cojocaru et al., 2007). Indeed, Cojocaru et al. analyzed the access and egress between the active site and the protein surface in P450 crystal structures available (by March 2006) with dynamic modeling simulation, and demonstrated that some channels in the structures can open or merge, resulting in a wide cleft leading to the active site, which is caused largely by movements of the F helix–loop–G helix and the B–C loop. A study of 300-ns molecular dynamics simulations of CYP2C9 showed that four main ligand exit channels from the active site to the surface of CYP2C9 were identified (Cojocaru et al., 2012). The

occurrence of these channels is dependent on both the ligand and the conformation of the border structure elements such the B-C loop and the F-G loop, which could be modulated by multiple factors such as the CYP-membrane interaction and redox partner binding. Aromatic residues dividing the active site and their relative movement function to direct ligand exit routes. The F-G and B-C loops determine the opening/merging of some channels and the degree of the opening/merging (Cojocaru et al., 2007).

Using Figure xx as a refernce, the opening of the substrate channel between the B-C loop and F-G loop can be facilitated by a rightwards movement of the B' helix and/or B–C loop, or by side chain motions. The conserved GxG motifs among CYP2 family members at the N- and C-termini of the B–C loop facilitate the flexibility of the B–C loop, resulting in the opening of channels that border this structural element. The B–C loop has the most variable primary sequence, length and the resulting flexibility in different P450 species, and has been predicated to account for the different substrate selectivity and specificity (Gotoh, 1992). Many studies of computer dynamic simulations have also predicated the flexibility of this region (Cojocaru et al., 2007; 2012; Mendieta-Wejebe et al., 2011). Mutagenesis of different residues on the B-C loop also showed an induction of conformational change, either resulting in closing of the substrate access channel and a significant decrease of CYP2C9 activity (Zhou et al., 2006), or forming a more "closed" conformation compared with 1R9O with the movement of several loops (Roberts et al., 2010).

In addition, NMR evidence has clearly shown that redox partner binding on the proximal surface of P450cam alters the protein dynamics on the distal side as mentioned before (Rui et al., 2006). Therefore, it is likely that the redox partner binding to the proximal surface of P450s could modulate channel opening even at their distal surface through the

conformational change, and help synchronize electron transfer, substrate binding, or product release in the P450 catalytic cycle.

In the current study, CYP2C9 and cyt b5 were reconstituted in an in vitro system. Their interactions are driven primarily by charge-charge interaction and were "trapped" by the specific cross-linking reagent EDC. Surface residues of CYP2C9 and holo/apo b5 in close contact were covalently cross-linked, and further identified by mass spectrometric analysis. Using these identified sites as constraints, the holo/apo b5-CYP2C9 complex models were constructed through protein docking calculations.

In the holo b5-CYP2C9 interaction model, similar to the cyt b5-CYP3A4 model, the heme groups of cyt b5 and CYP2C9 are not closely associated, with a distance of ~11 Å, suggesting that a direct electron-transfer between their heme iron is not likely. In the cyt b5-CYP2C9 model, the interacting interface on cyt b5 includes the heme prosthetic group that protrudes into the solvent, α2-loop-α3, α4-loop-α5. The acidic residues on these segments have long been suggested to be the driving force for electrostatic interactions (Schenkman and Jansson, 2003).

Interestingly, apo b5, which lacks the heme group, forms a highly overlapping interface with CYP2C9 compared with holo b5, with slightly different orientations due to lack of the clash between the heme group and the CYP2C9 proximal surface residues. Both holo and apo b5 contact nearly the same surface on CYP2C9, including the B helix, B-B' loop, C helix, C-D loop, K''-L meander region, and the β-bulge. The most prominent segments in contact on CYP2C9 would be the B-B' loop region and the C helix. As discussed above, the B-C loop region is located on the boundary of the P450s proximal and distal face, and has been widely

discussed as the substrate recognition site (SRSs) of P450s. This region is very flexible, forming different conformations upon substrate binding and functions to control several substrate channels connecting the active site to the surface solvent. It has been reported that in the CYP2C9 crystal structure, the B-B' loop region was identified to be involved in binding of the substrate warfarin (Williams et al., 2003). This flexible loop region serves as a modulator for several entrance and egress channels to the active site of CYP2C9, and is directly involved in the recognition and binding of substrate and/or effector molecules. It is likely that the contact of cyt b5 with CYP2C9 could cause a perturbation of the secondary structure of this region, and further, this perturbation can be transmitted to the many SRS's of CYP2C9 through conformational changes, thus affecting substrate access channels, active site size, and product release etc. This interaction is similar to that of cyt b5-CYP3A4 as discussed before. Consequently, association with cyt b5 gives rise to the allosteric effect on the CYP. This has been supported by the finding that apo b5 can increase the catalytic activity of CYP2C9 to the extent comparable to holo b5 (Locuson et al., 2007b; Yamazaki et al., 1997; Yamazaki et al., 2002).

P450s are different both in the distribution of charged residues on their surface and the composition and length of some secondary structures, such as the helices B, C, F, G, which can result in different driving forces for interaction. In the cases of cyt b5-CYP2E1 interaction, the cyt b5-CYP3A4 interaction and the cyt b5-CYP2C9 interactions, cyt b5 positions itself differently for each CYP.

(A)

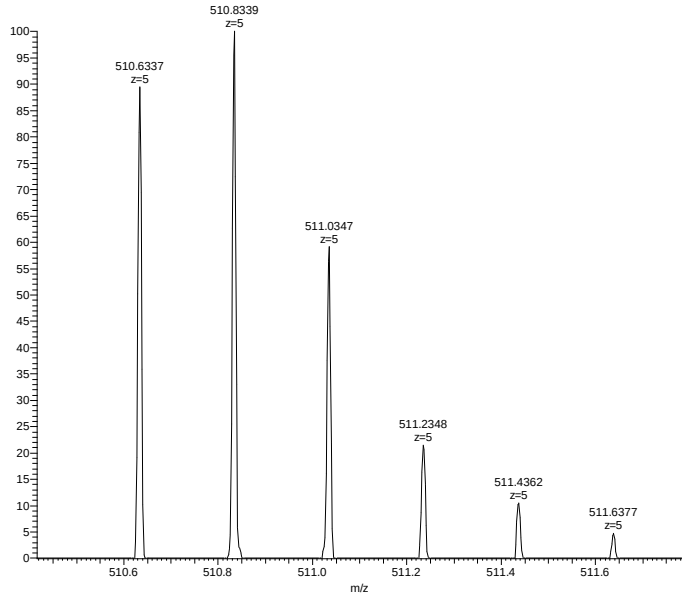

(B)

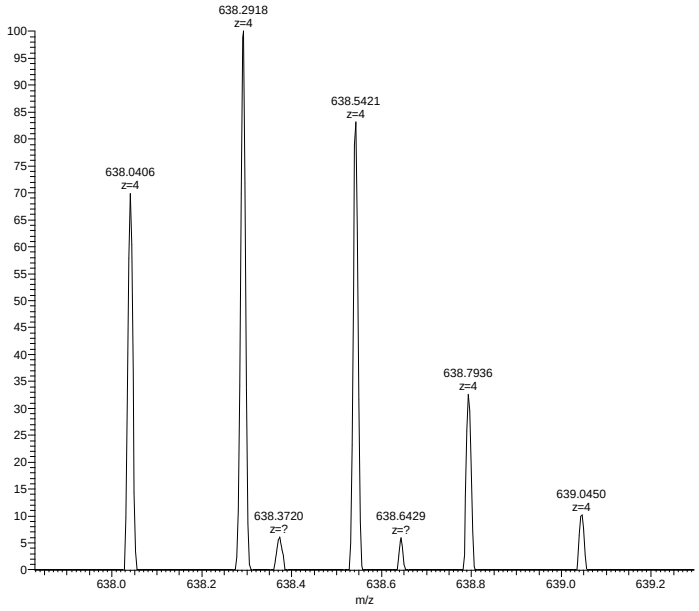

Figure 3.1. Precursor ion MS spectra for cross-linked peptide holo b_5: ^{48}EQAGGDATENFEDVGHSTDAR^{68} - CYP2C9: ^{421}KSK^{423}. (A) Measured quintuple charged ion $[M + 5H]^{5+}$ = 510.6337 for ion no.1 in Table 3.1. (B) Measured quadruple charged ion $[M + 4H]^{4+}$ = 638.0406 for ion no.2 in Table 3.1.

(A)

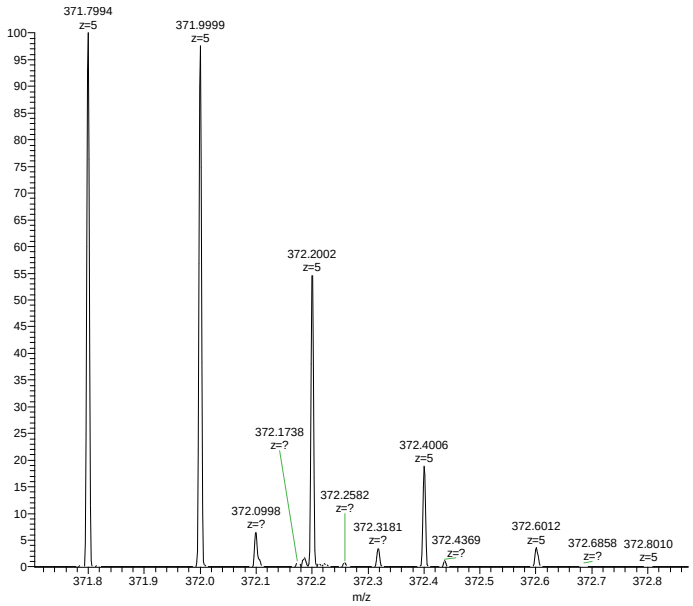
371.7994
z=5
371.9999
z=5
372.2002
z=5
372.1738
z=?
372.4006
z=5
372.2582
z=?
372.0998
z=?
372.3181
z=?
372.4369
z=?
372.6012
z=5
372.6858
z=?
372.8010
z=5
m/z

(B)

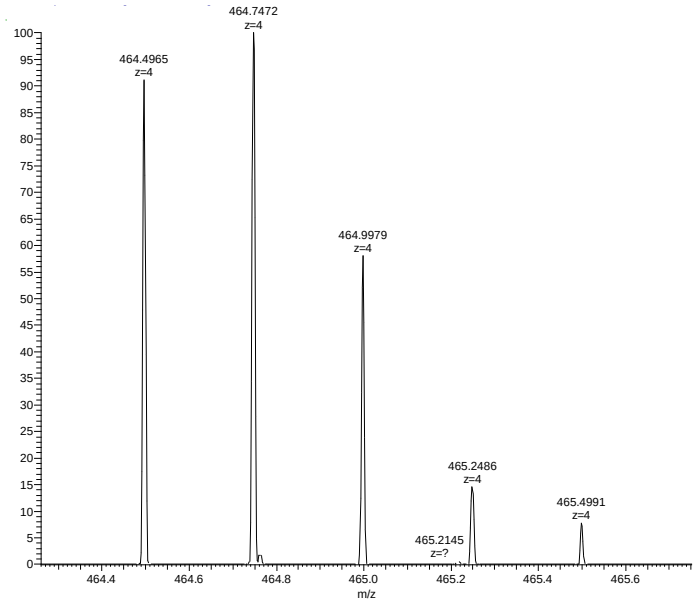
464.7472
z=4
464.4965
z=4
464.9979
z=4
465.2486
z=4
465.4991
z=4
465.2145
z=?
m/z

(C)

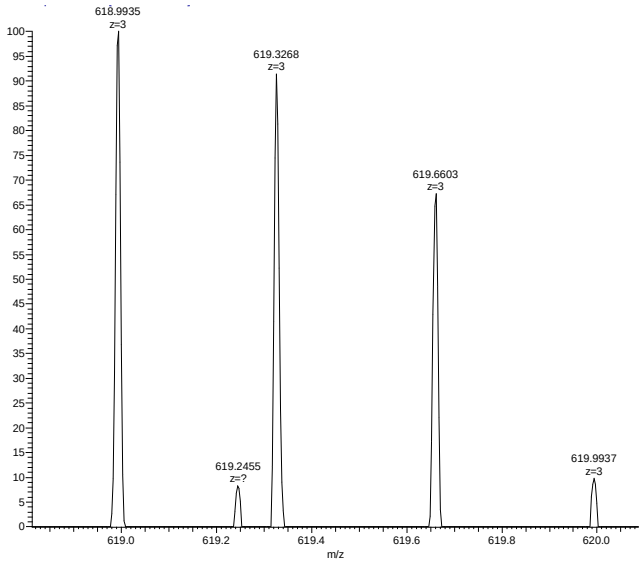

Figure 3.2. Precursor ion MS spectra for cross-linked peptide holo b_5: ^{35}FLEEHPGGEEVLR^{47} - CYP2C9: ^{421}KSK^{423}. (A) Measured quintuple charged ion $[M + 5H]^{5+}$ = 371.7994 for ion no.3 in Table 3.1. (B) Measured quadruple charged ion $[M + 4H]^{4+}$ = 464.4965 for ion no.4 in Table 3.1. (C) Measured triply charged ion $[M + 5H]^{5+}$ = 618.9935 for ion no.5 in Table 3.1.

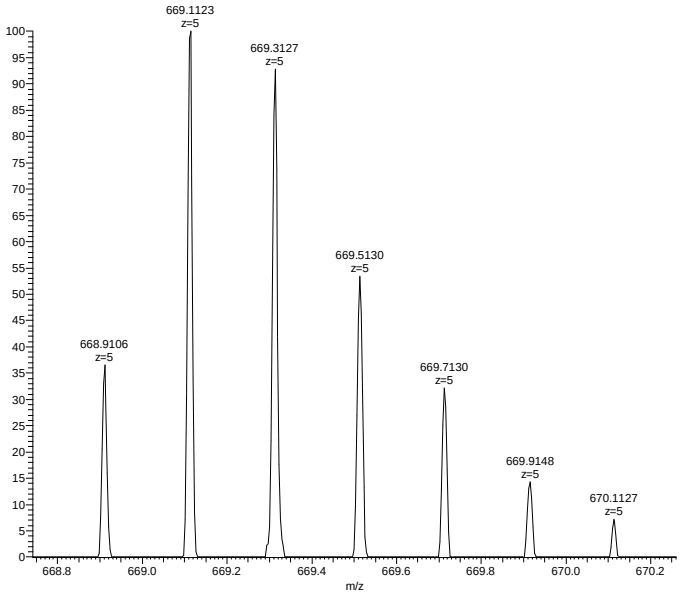

Figure 3.3. Precursor ion MS spectra for cross-linked peptide holo b5: ^{48}EQAGGDATENFEDVGHSTDAR^{68} - CYP2C9: ^{109}GFGIVFSNGKK^{119} (Measured quintuple charged ion $[M + 5H]^{5+}$ = 668.9106 for ion no.6 in Table 3.1)

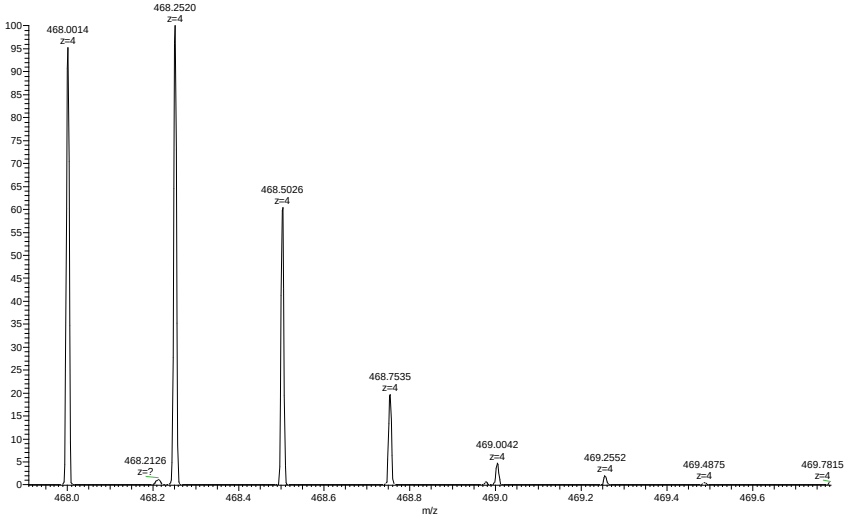

Figure 3.4. Precursor ion MS spectra for cross-linked peptide holo b5: ^{35}FLEEHPGGEEVLR^{47} - CYP2C9: ^{158}KTK^{160} (Measured quintuple charged ion $[M + 4H]^{4+}$ = 468.0014 for ion no.7 in Table 3.1)

(A)

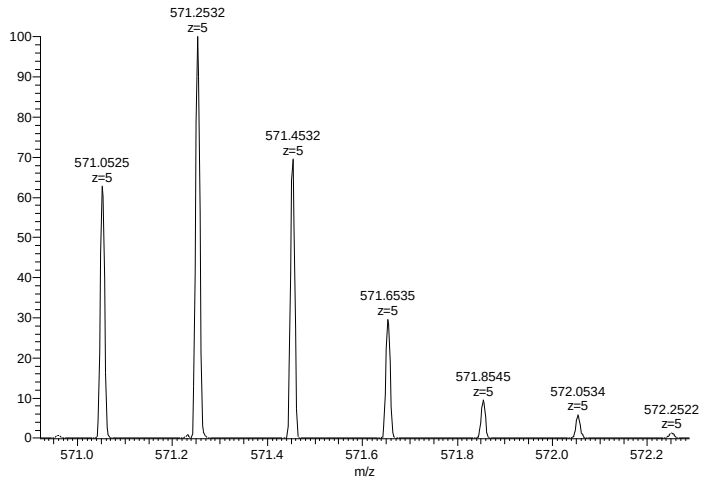

(B)

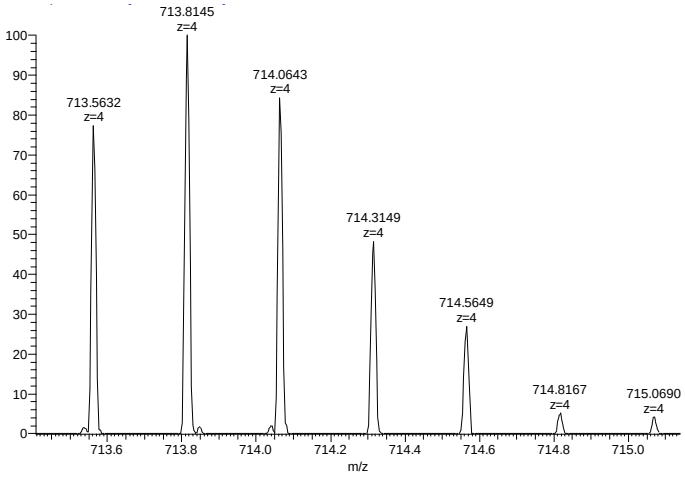

Figure 3.5. Precursor ion MS spectra for cross-linked peptide holo: ^{48}EQAGGDATENFEDVGHSTDAR^{68} - CYP2C9: ^{271}MEKEK^{275}. (A) Measured quintuple charged ion $[M + 5H]^{5+}$ = 571.0525 for ion no.8 in Table 3.1. (A) Measured quadruple charged ion [M + 4H]4+ = 713.5320 for ion no.9 in Table 3.1.

(A)

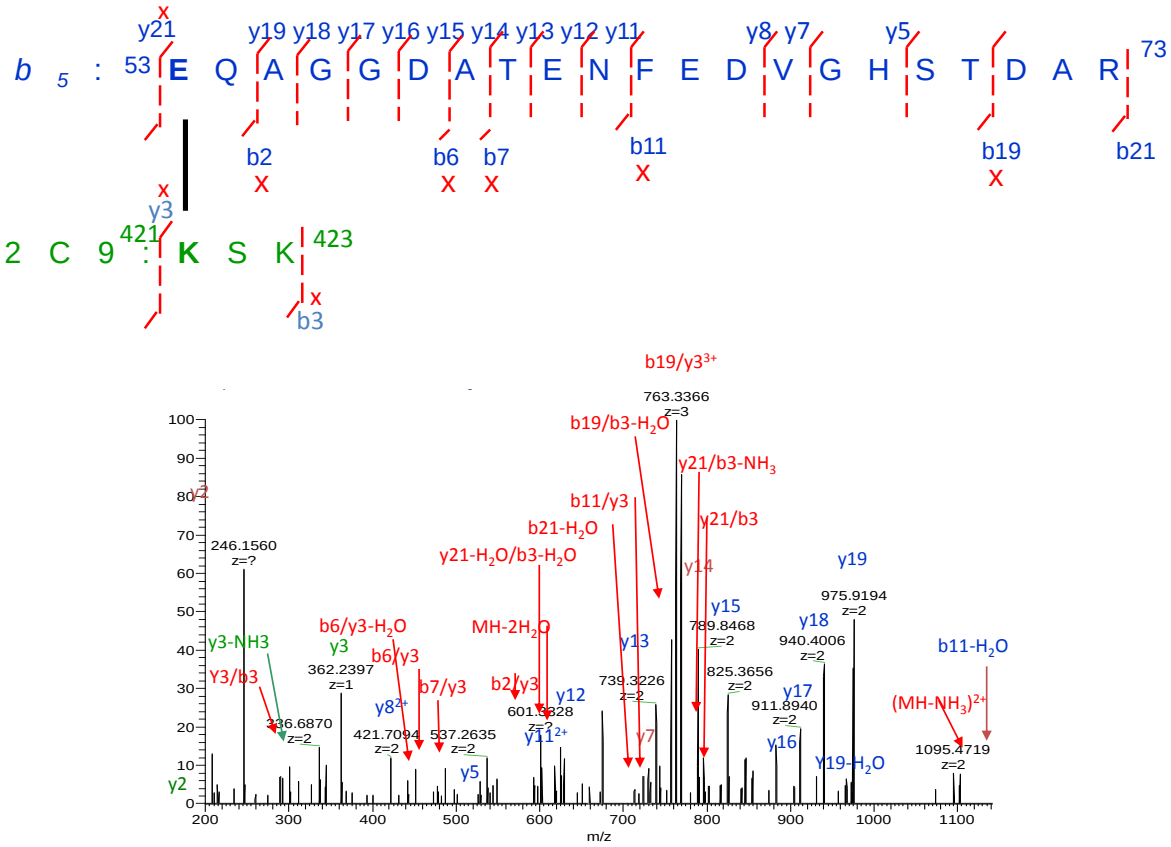
b 5 : 53 E Q A G G D A T E N F E D V G H S T D A R 73
y21 y19 y18 y17 y16 y15 y14 y13 y12 y11 y8 y7 y5
b2 b6 b7 b11 b19 b21
2 C 9 : 421 K S K 423
y3
b3
b19/y3 3+
763.3366 z=3
b19/b3-H2O
y21/b3-NH3
b11/y3
b21-H2O
y21/b3
y21-H2O/b3-H2O
y14
y19
975.9194 z=2
y15
789.8468 z=2
y18
940.4006 z=2
MH-2H2O
b6/y3-H2O
y3
b6/y3
y3-NH3
362.2397 z=1
Y3/b3
246.1560 z=?
y13
739.3226 z=2
825.3656 z=2
b11-H2O
y17
911.8940 z=2
(MH-NH3)2+
b2/y3
y12
y8 2+
y7
y16
y19-H2O
b7/y3
y11 2+
y5
y2
1095.4719 z=2
m/z

(B)

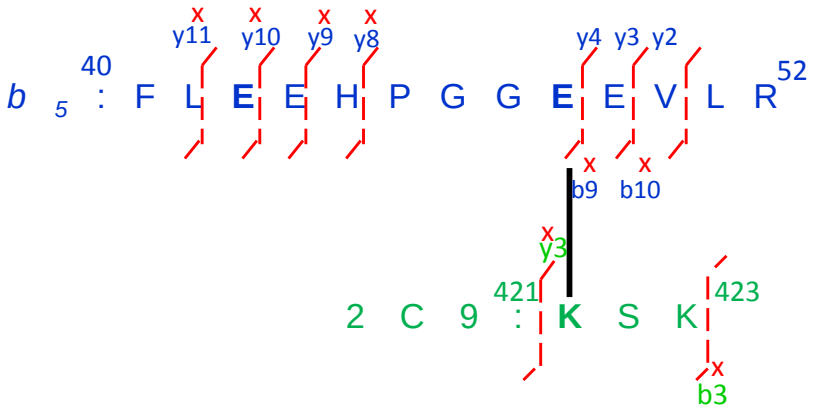
b 5 : 40 F L E E H P G G E E V L R 52
y11
y10
y9
y8
y4
y3
y2
b9
b10
y3
2 C 9 : 421 K S K 423
b3

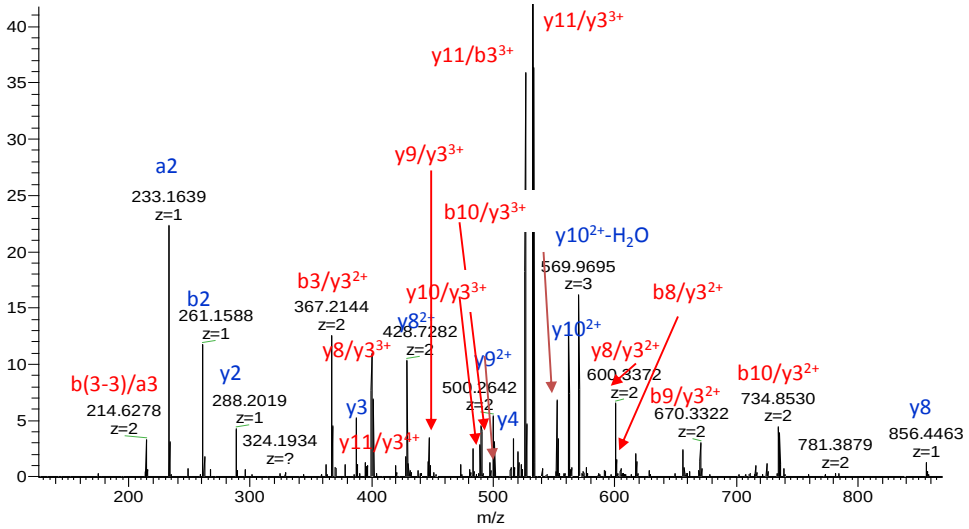
y11/y3^3+
y11/b3^3+
y9/y3^3+
a2
233.1639
z=1
b10/y3^3+
y10^2+-H2O
569.9695
z=3
b3/y3^2+
367.2144
z=2
y10/y3^3+
b8/y3^2+
b2
261.1588
z=1
y8^2+
428.7282
z=2
y10^2+
y8/y3^3+
y9^2+
y8/y3^2+
600.3372
z=2
b(3-3)/a3
214.6278
z=2
y2
288.2019
z=1
500.2642
z=2
b10/y3^2+
734.8530
z=2
b9/y3^2+
670.3322
z=2
y3
y4
y8
856.4463
z=1
324.1934
z=?
y11/y3^4+
781.3879
z=2
m/z

(C)

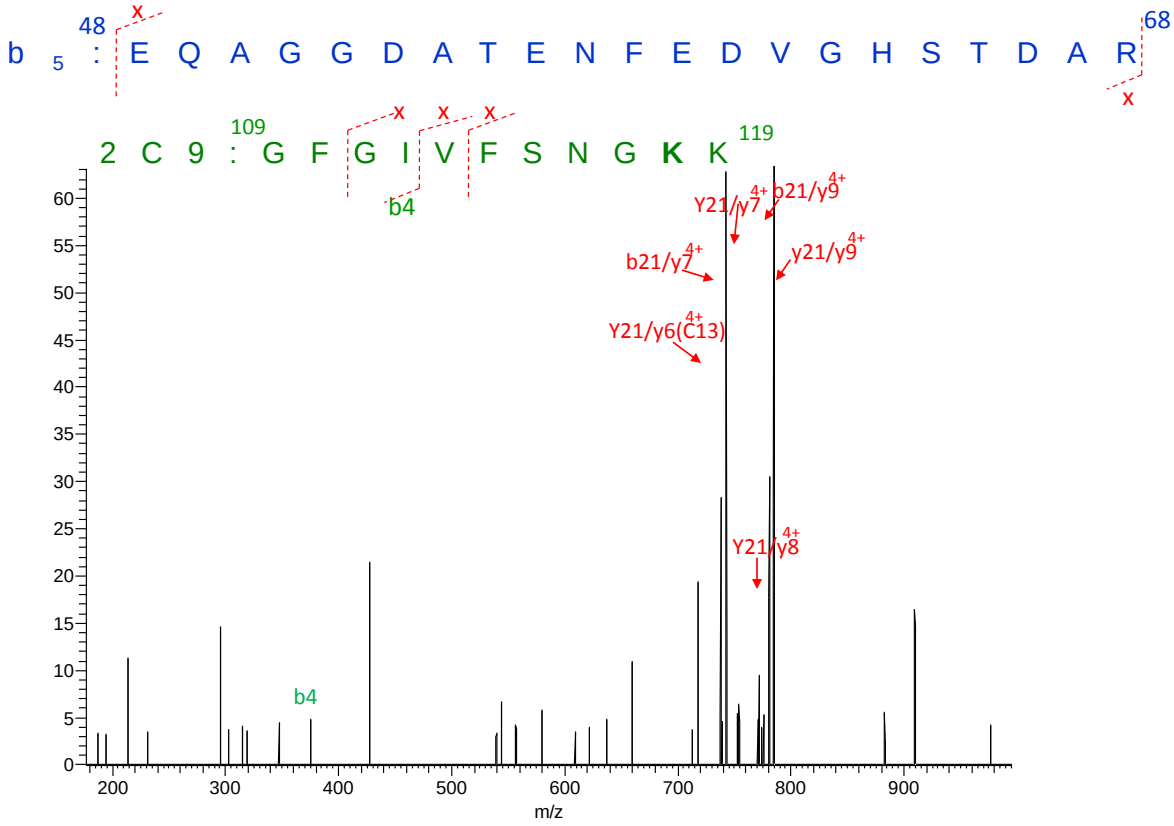
b 5 : E Q A G G D A T E N F E D V G H S T D A R
48
68
2 C 9 : G F G I V F S N G K K
109
119
b4
Y21/y7 4+
b21/y9 4+
b21/y7 4+
y21/y9 4+
Y21/y6(C13) 4+
Y21/y8 4+
b4
m/z

(D)

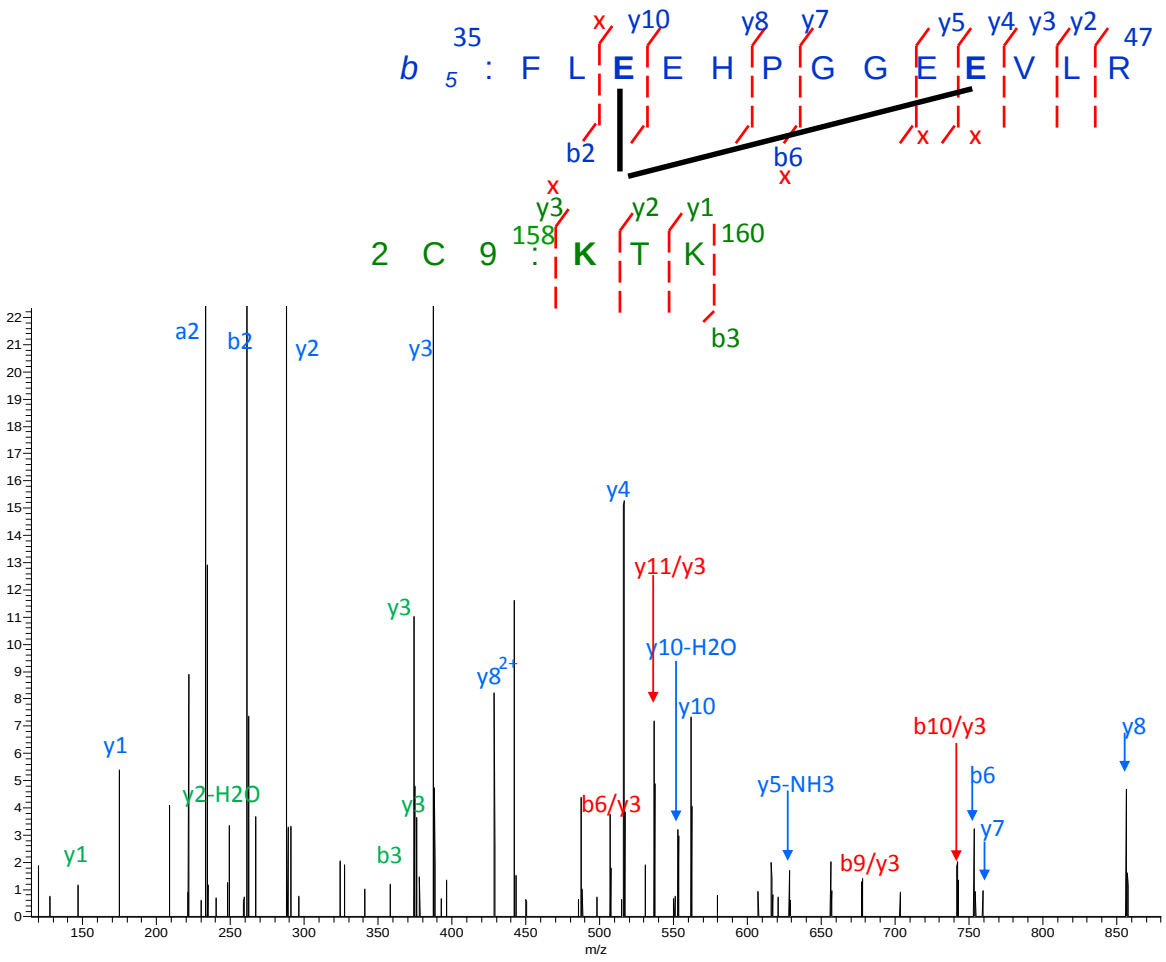
b 5 35 : F L E E H P G G E E V L R 47
x y10 y8 y7 y5 y4 y3 y2
b2 b6
x x x
2 C 9 158 : K T K 160
x y3 y2 y1
b3
a2 b2 y2 y3 y4 y11/y3 y10-H2O y10 y8 2+ y3 y1 y2-H2O y3 b3 b6/y3 y5-NH3 b10/y3 b6 y7 y8 y1 b9/y3
m/z

(E)

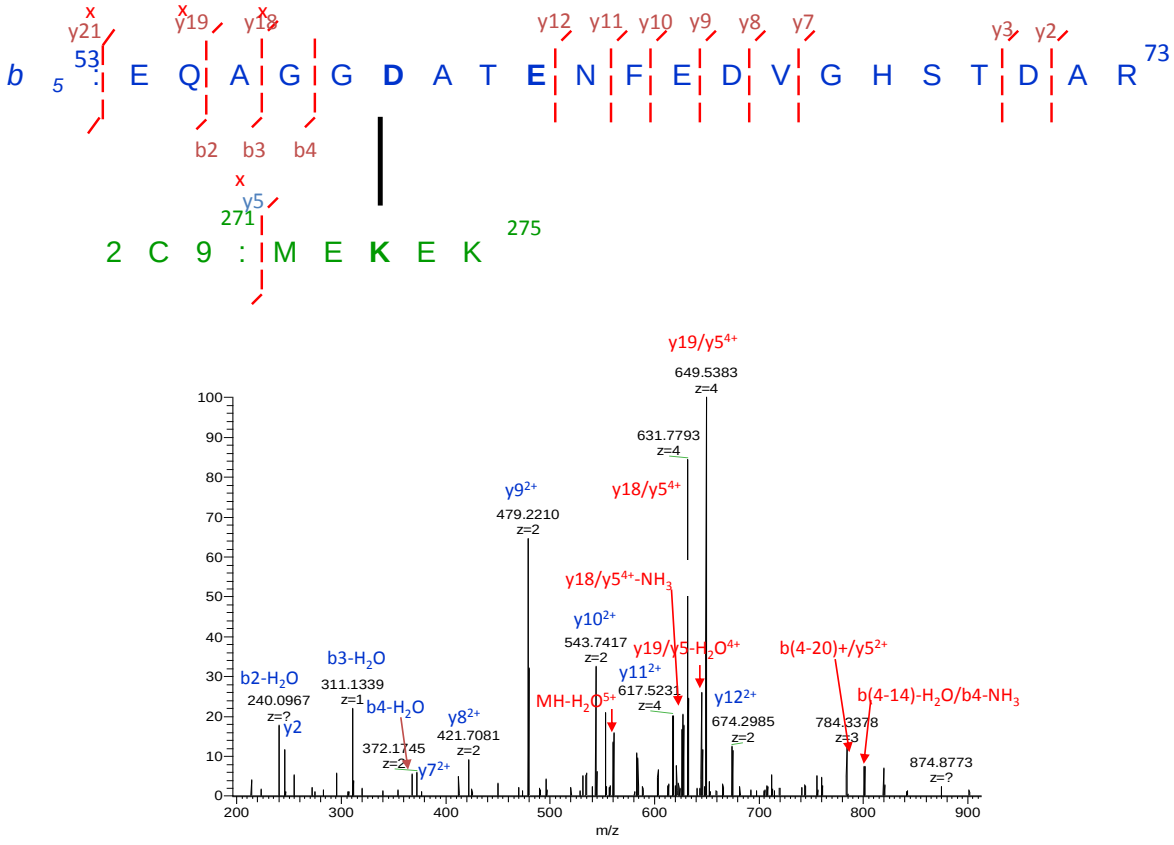

Figure 3.6. Tandem mass spectra for five cross-linked peptide precursor ions identified from holo b5-CYP2C9 complex. Fragment ions with superscript "x" represent the cross-linked fragment ions. Ions marked with subscript α are from cyt b5, and ions with subscript β are from CYP2C9. Identified cross-linked residue pairs are linked by bold black lines. (A) Ion No.1 in Table 3.1 with m/z of 510.6337 for holo b5: ^{48}EQAGGDATENFEDVGHSTDAR^{68}- CYP2C9: ^{421}KSK^{423}. B. Ion No.4 in Table 3.1 with m/z of 464.4965 for holo b_5: ^{35}FLEEHPGGEEVLR^{47} - CYP2C9: ^{421}KSK^{423}. (C) Ion No.6 in Table 3.1 with m/z of 668.9106 for holo b5: ^{48}EQAGGDATENFEDVGHSTDAR^{68} - CYP2C9: ^{109}GFGIVFSNGKK^{119}. (D) Ion No.7 in Table 3.1 with m/z of 468.0014 for holo b5: ^{35}FLEEHPGGEEVLR^{47} - CYP2C9: ^{158}KTK^{160}. (E) Ion No.7 in Table 3.1 with m/z of 468.0014 for holo b5: ^{48}EQAGGDATENFEDVGHSTDAR^{68} - CYP2C9: ^{271}MEKEK^{275}.

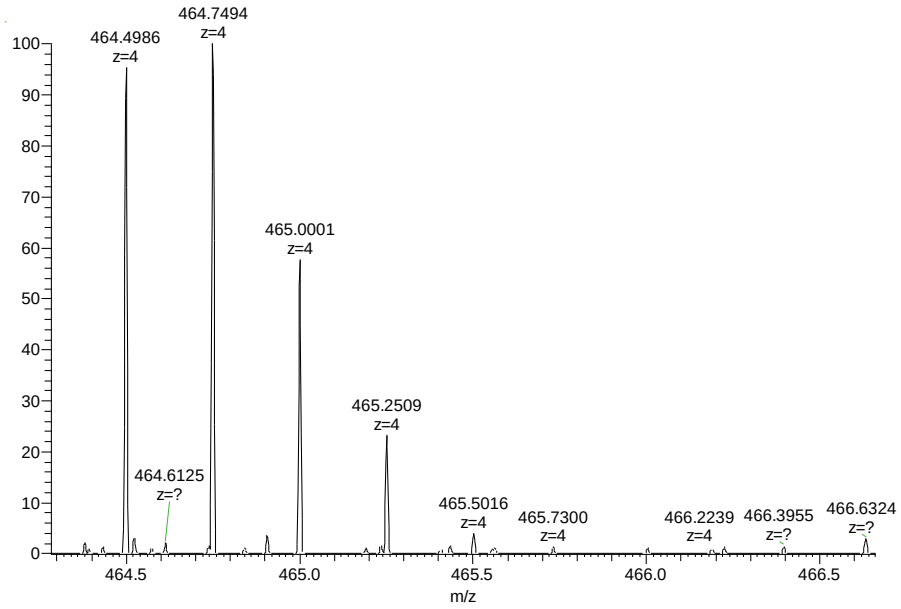

Figure 3.7. Precursor ion MS spectra for cross-linked peptide apo b_5: ^{35}FLEEHPGGEEVLR^{47} - CYP2C9: ^{421}KSK^{423} (Measured quadruple charged ion $[M + 4H]^{4+}$ = 464.4986 for ion no.1 in Table 3.2).

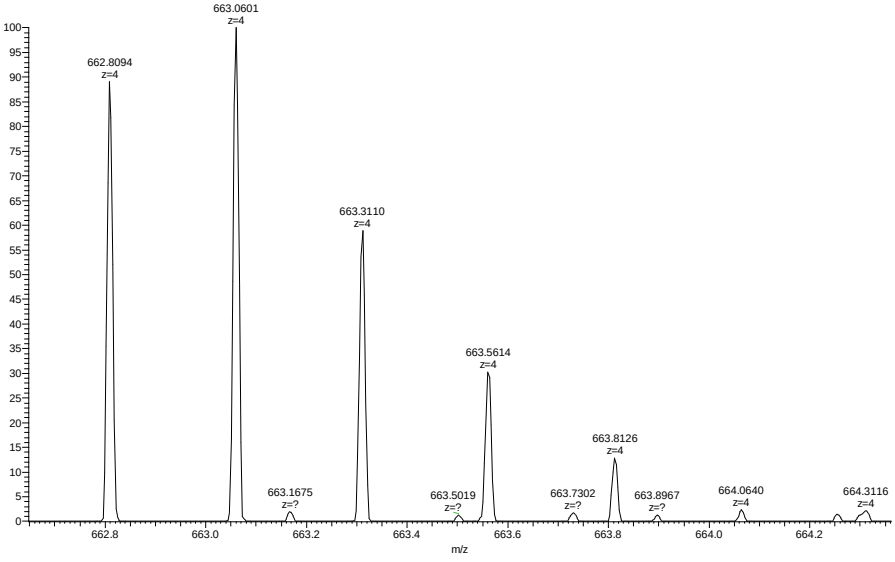

Figure 3.8. Precursor ion MS spectra for cross-linked peptide apo b_5: ^{48}EQAGGDATENFEDVGHSTDAR^{68} - CYP2C9: ^{119}KWK^{121} (Measured quadruple charged ion $[M + 4H]^{4+}$ = 662.8094 for ion no.2 in Table 3.2).

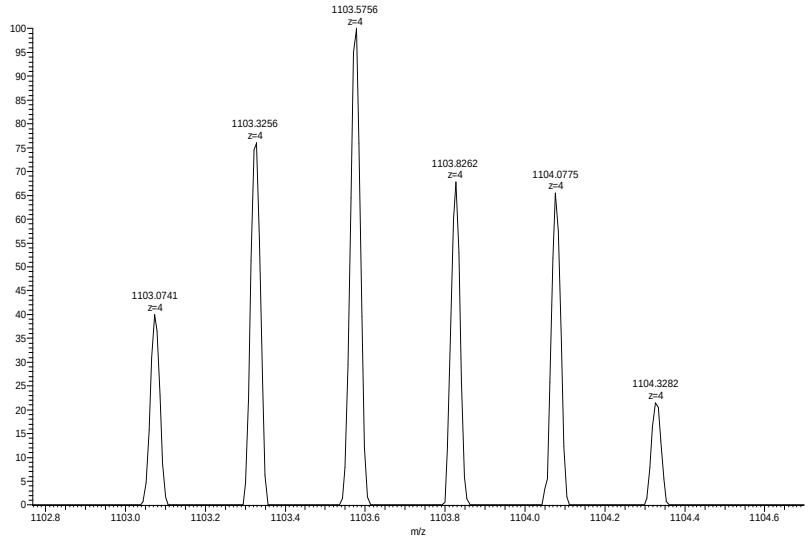

Figure 3.9. Precursor ion MS spectra for cross-linked peptide apo b_5: ^{48}EQAGGDATENFEDVGHSTDAR^{68} - CYP2C9: ^{27}GKLPPGPTPLPVIGNILQIGIK^{48} (Measured quadruple charged ion $[M + 4H]^{4+}$ = 1103.0741 for ion no.3 in Table 3.2).

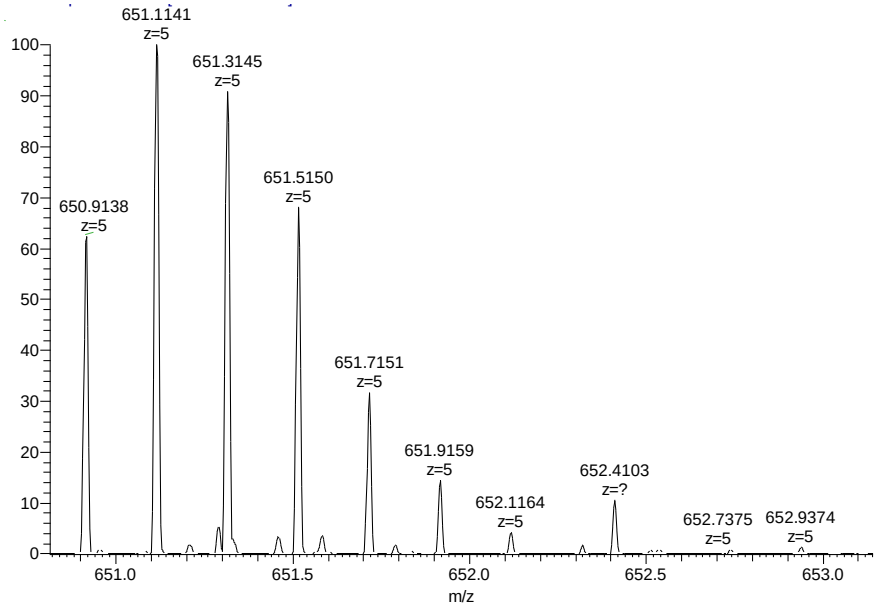

Figure 3.10. Precursor ion MS spectra for cross-linked peptide apo b_5: ^{48}EQAGGDATENFEDVGHSTDAR^{68} - CYP2C9: ^{233}LLKNVAFMK^{241} (Measured quadruple charged ion $[M + 5H]^{5+}$ = 650.9129 for ion no.4 in Table 3.2).

(A)

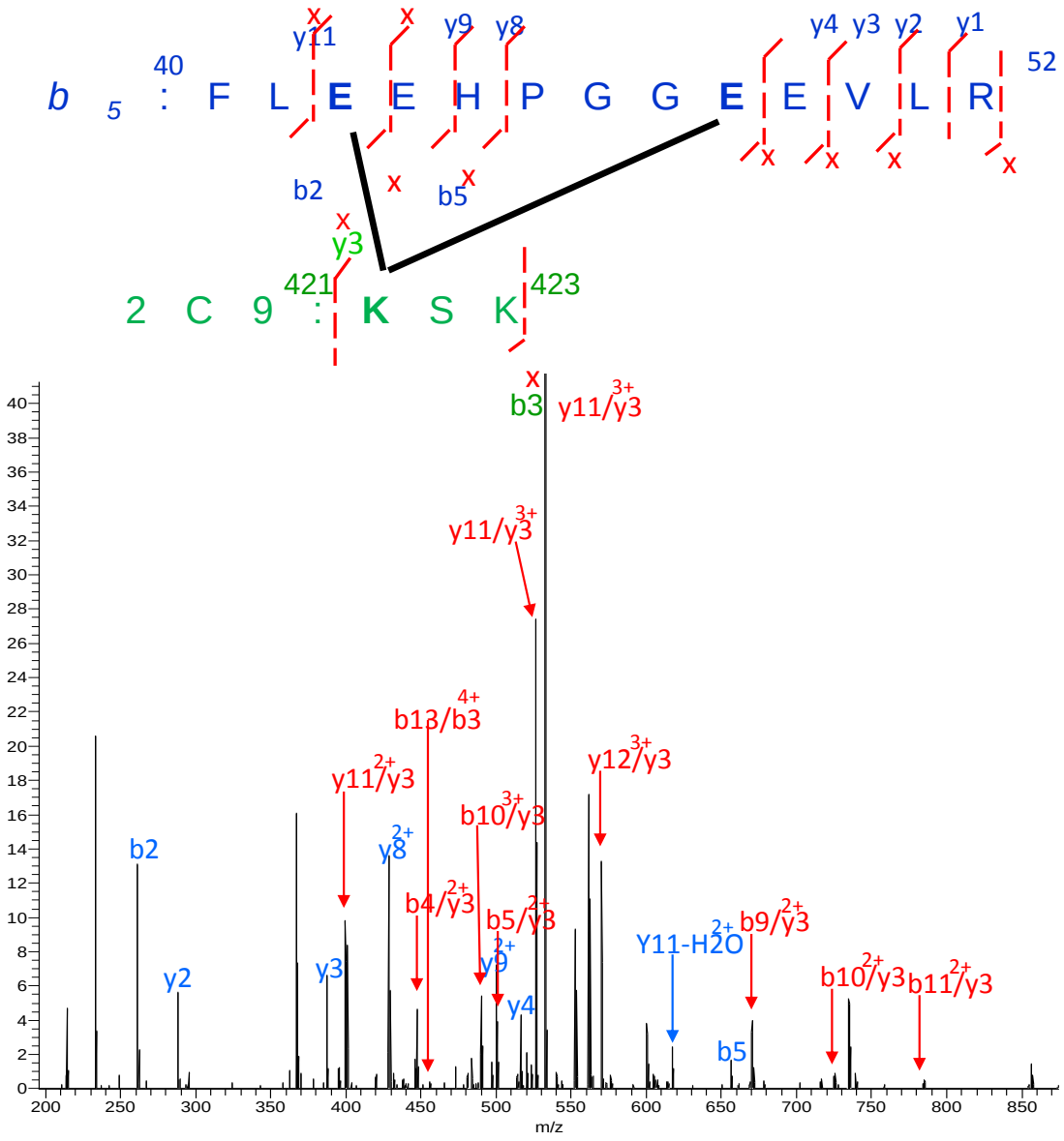
b 5 : F L E E H P G G E E V L R
40
52
y11
y9
y8
y4
y3
y2
y1
b2
b5
y3
421
423
2 C 9 : K S K
b3
y11/y3 3+
y11/y3 3+
b13/b3 4+
y12/y3 3+
y11/y3 2+
b10/y3 3+
y8 2+
b2
b4/y3 2+
b5/y3 2+
y9 2+
y3
y2
y4
Y11-H2O 2+
b9/y3 2+
b5
b10/y3 2+
b11/y3 2+
m/z

(B)

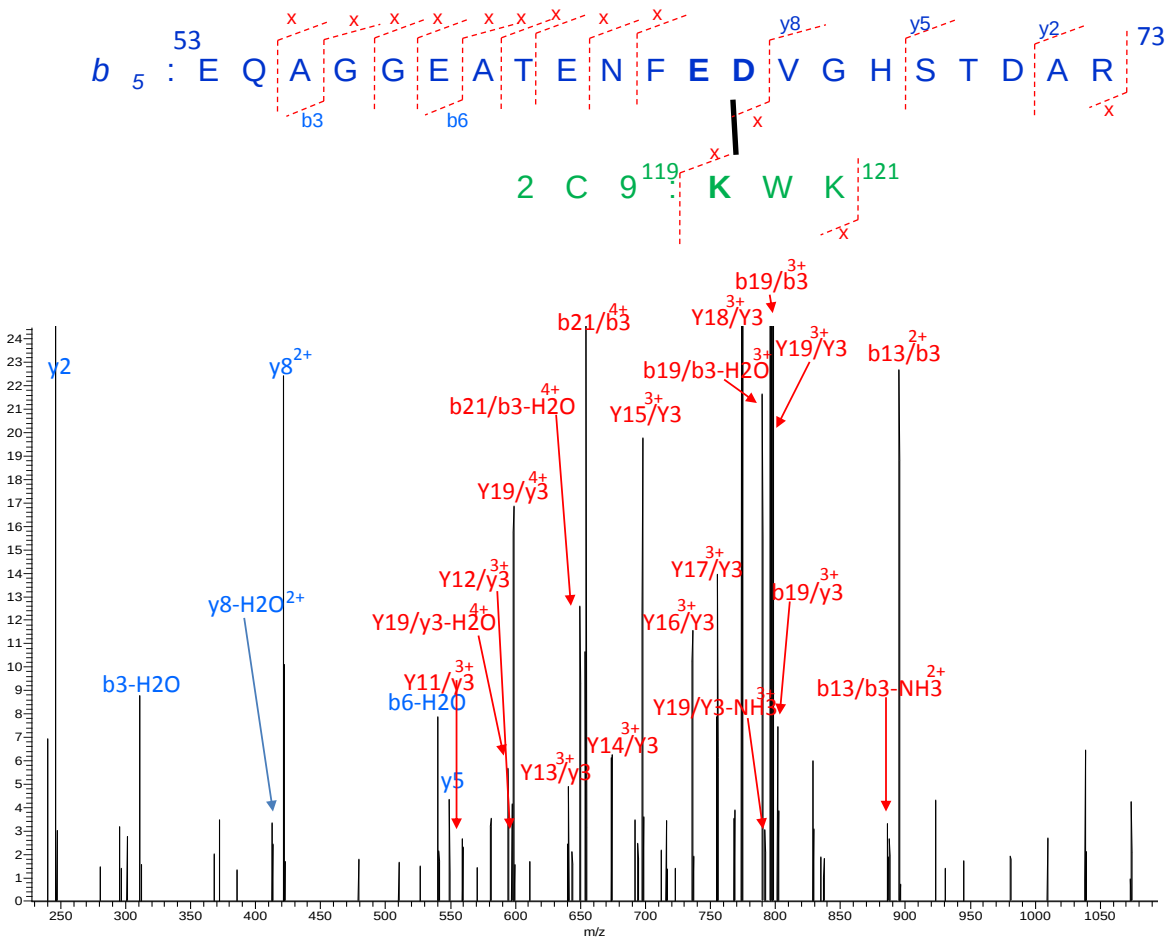
b 5 : 53 E Q A G G E A T E N F E D V G H S T D A R 73
b3
b6
y8
y5
y2
2 C 9 : 119 K W K 121
y2
y8 2+
b19/b3 3+
b21/b3 4+
Y18/Y3 3+
Y19/Y3 3+
b13/b3 2+
b19/b3-H2O 3+
b21/b3-H2O 4+
Y15/Y3 3+
Y19/y3 4+
Y12/y3 3+
Y17/Y3 3+
b19/y3 3+
y8-H2O 2+
Y19/y3-H2O 4+
Y16/Y3 3+
b3-H2O
Y11/y3 3+
b6-H2O
b13/b3-NH3 2+
Y19/Y3-NH3 3+
Y14/Y3 3+
Y13/y3 3+
y5
m/z

(C)

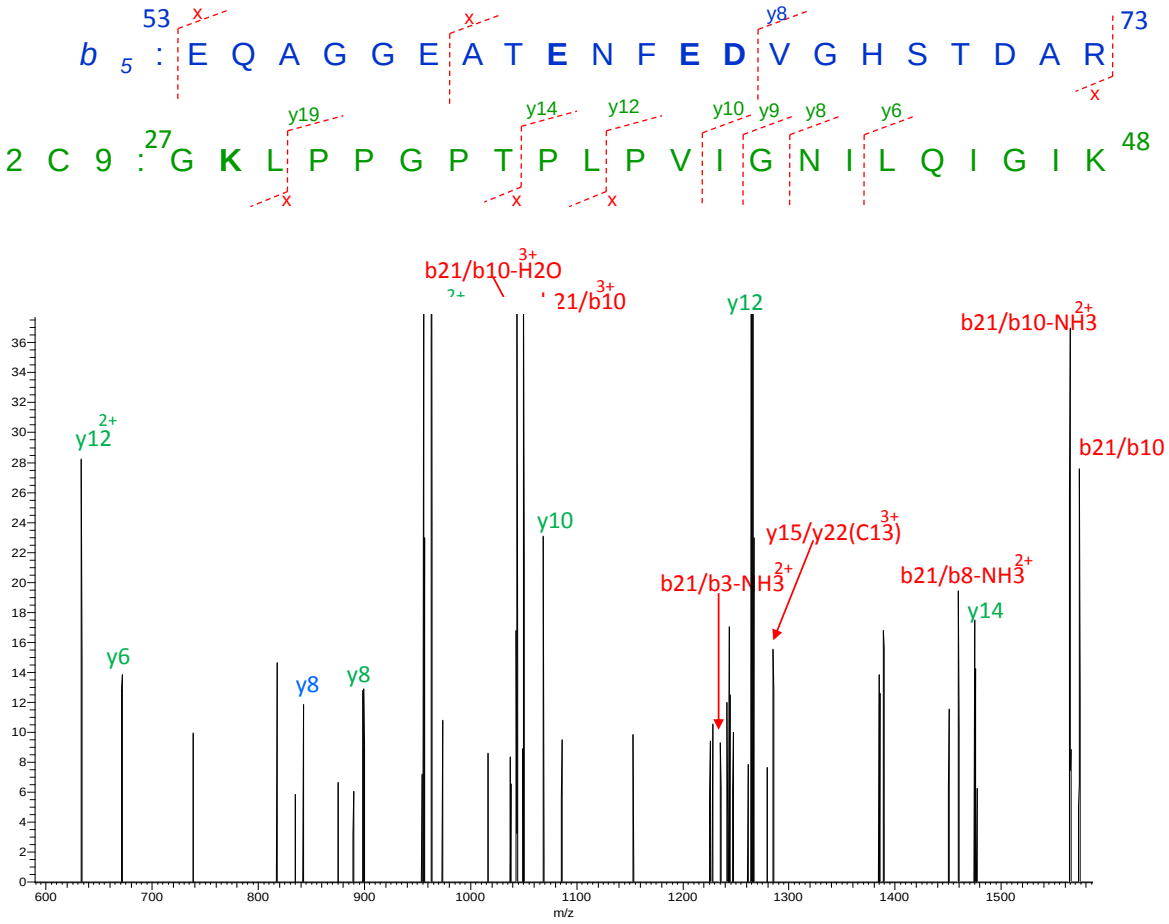
b 5 : E Q A G G E A T E N F E D V G H S T D A R
53
73
2 C 9 : G K L P P G P T P L P V I G N I L Q I G I K
27
48
y19
y14
y12
y10
y9
y8
y6
b21/b10-H2O 3+
b21/b10 3+
y12
b21/b10-NH3 2+
b21/b10
y12 2+
y10
y15/y22(C13) 3+
b21/b3-NH3 2+
b21/b8-NH3 2+
y14
y6
y8
y8
m/z

(D)

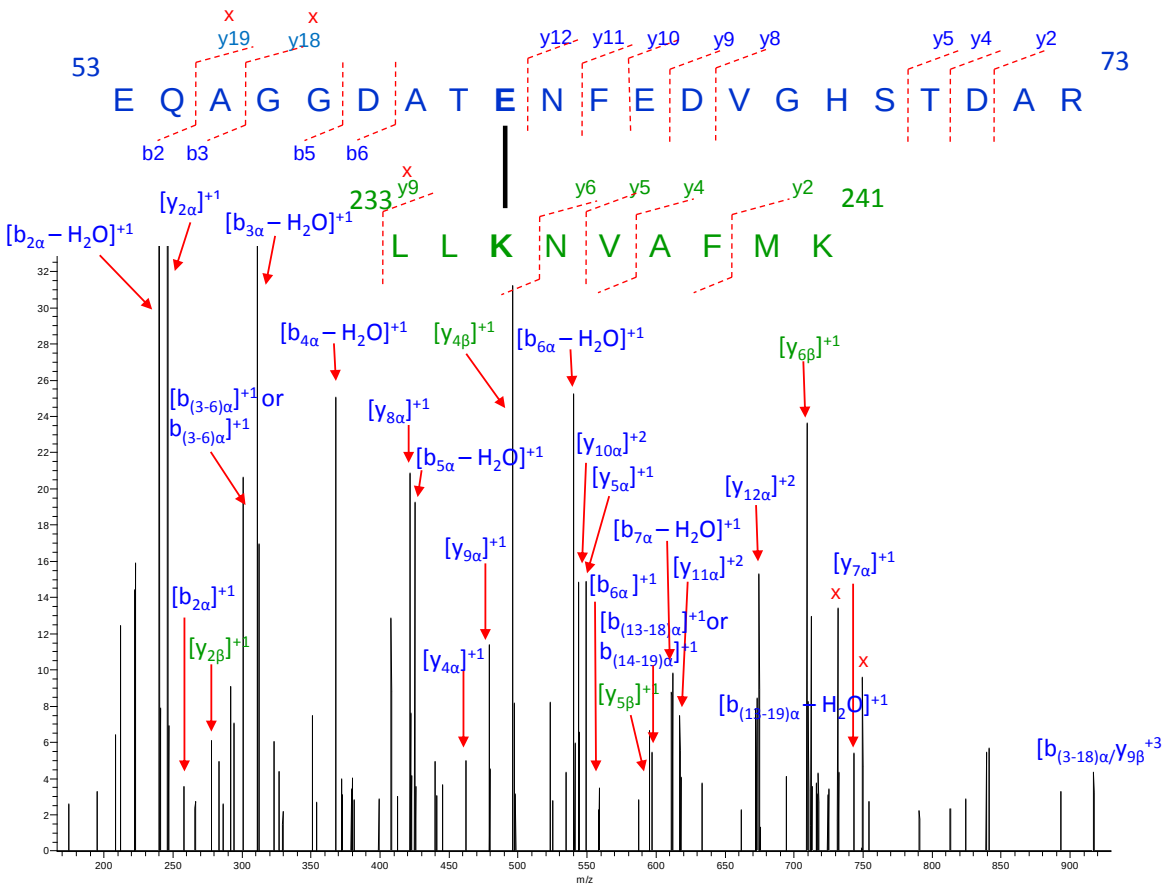

Figure 3.11. Tandem mass spectra for five cross-linked peptide precursor ions identified from apo b5-CYP2C9 complex. Fragment ions with superscript "x" represent the cross-linked fragment ions. Ions marked with subscript α are from cyt b5, and ions with subscript β are from CYP2C9. Identified cross-linked residue pairs are linked by bold black lines. (A) Ion No.1 in Table 3.2 with m/z of 464.4986 for apo b_5: ^{35}FLEEHPGGEEVLR^{47} - CYP2C9: ^{421}KSK^{423}. B. Ion No.2 in Table 2 with m/z of 662.8094 for apo b_5: ^{48}EQAGGDATENFEDVGHSTDAR^{68} - CYP2C9: ^{119}KWK^{121}. (C) Ion No.3in Table 3.2 with m/z of 1103.0741 for apo b5: ^{48}EQAGGDATENFEDVGHSTDAR^{68} - CYP2C9: ^{27}GKLPPGPTPLPVIGNILQIGIK^{48}. (D) Ion No.4 in Table 3.2 with m/z of 650.9129 for holo b5: ^{35}FLEEHPGGEEVLR^{47} - CYP2C9: ^{158}KTK^{160}. (E) Ion No.7 in Table 3.1 with m/z of 468.0014 for apo b5: ^{48}EQAGGDATENFEDVGHSTDAR^{68} - CYP2C9: ^{233}LLKNVAFMK^{241}.

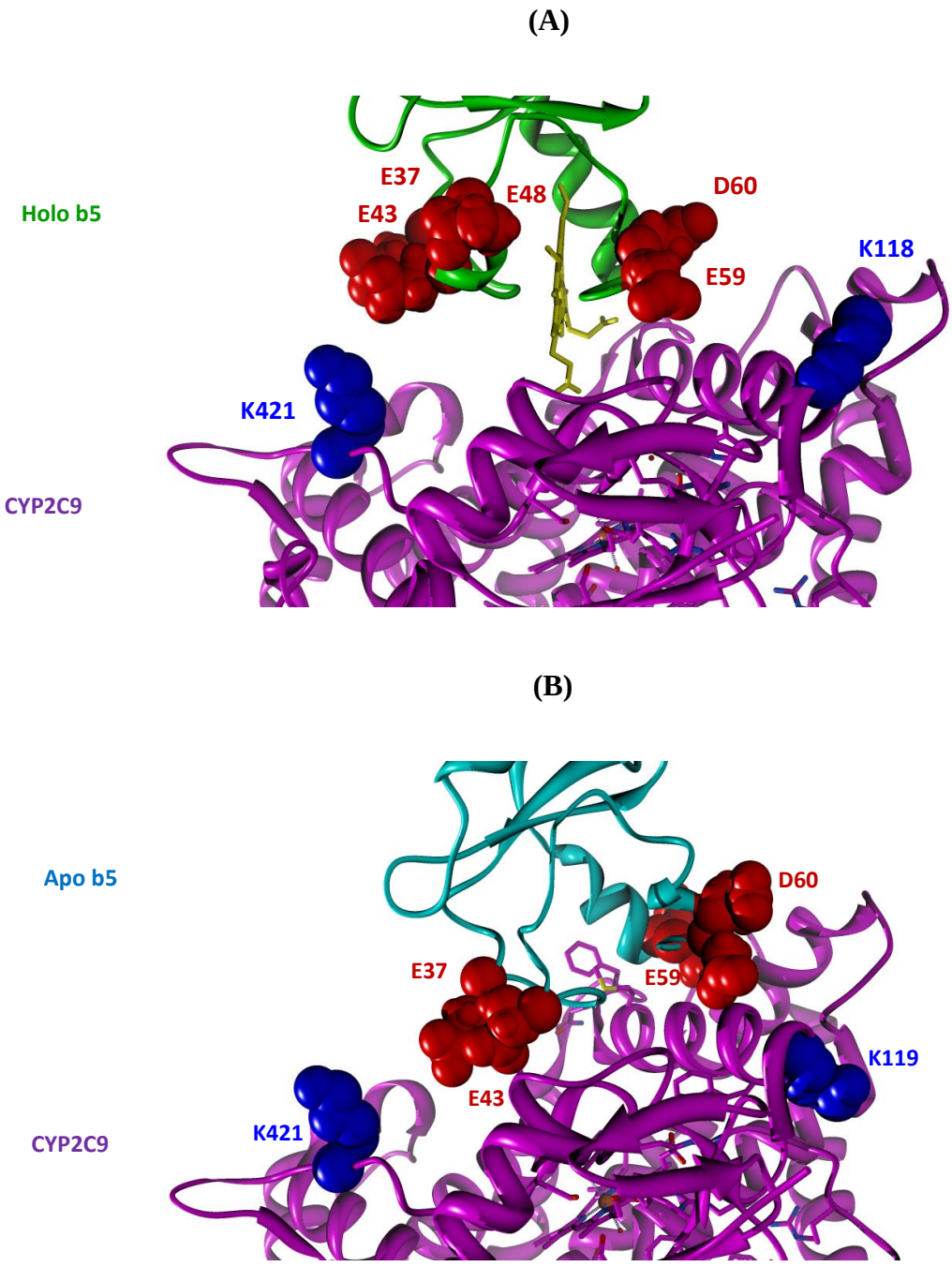

Figure 3.12. Holo/apo b5-CYP2C9 complex models. CYP2C9 is magenta; holo b5 is green; apo b5 is cyan. The interacting residues on CYP2C9 and holo/apo b5 are blue and red, respectively. (A) Holo b5 - CYP2C9 complex model. (B) Apo b5 – CYP2C9 complex model.

Table 3.1 Inter-molecular cross-linked peptides in the complex of holo cytb_5-CYP2C9.

No	Measured Mono-isotopic Peak (*m/z*)	Charge State	Measured Peptide Mass (Da)	Calculated peptide Mass (Da)	Error (ppm)	Mass Matches to Inter-molecular Cross-linked Peptides
1	510.6337	+5	2548.3907	2549.1499	4.4	(human b_5: ^{48}EQAGGDATENFEDVGHSTDAR^{68})-(CYP2C9: ^{421}KSK^{423})
2	638.0406	+4	2549.1386		5.2	
3	371.7994	+5	1854.9652	1854.9708	3.4	(human b_5: ^{35}FLEEHPGGEEVLR^{47})-(CYP2C9: ^{421}KSK^{423})
4	464.4965	+4	1854.9622		4.6	
5	618.9935	+3	1854.9646		3.3	
6	668.9106	+5	3340.5218	3340.5465	7.4	(human b_5: ^{48}EQAGGDATENFEDVGHSTDAR^{68})-(CYP2C9: ^{109}GFGIVFSNGKK^{119})
7	468.0014	+4	1868.9822	1868.9865	2.3	(human b_5: ^{35}FLEEHPGGEEVLR^{47})-(CYP2C9: ^{158}KTK^{160})
8	571.0525	+5	2851.2313	2851.2435	4.3	(human b_5: ^{48}EQAGGDATENFEDVGHSTDAR^{68})-(CYP2C9: ^{271}MEKEK^{275})
9	713.5632	+4	2851.2294		4.9	

Table 3.2 Inter-molecular cross-linked peptides in the complex of apo cytb_5-CYP2C9.

No	Measured Mono-isotopic Peak (*m/z*)	Charge State	Measured Peptide Mass (Da)	Calculated peptide Mass (Da)	Error (ppm)	Mass Matches to Inter-molecular Cross-linked Peptides
1	464.4986	+4	1854.971	1854.9708	0.1	(apo b_5: ^{35}FLEEHPGGEEVLR^{47})-(CYP2C9: ^{421}KSK^{423})
2	662.8094	+4	2648.2142	2648.1972	6.4	(apo b_5: ^{48}EQAGGDATENFEDVGHSTDAR^{68})-(CYP2C9: ^{119}KWK^{121})
3	1103.0741	+4	4409.2730	4409.2736	0.1	(apo b_5: ^{48}EQAGGDATENFEDVGHSTDAR^{68})-(CYP2C9: ^{27}GKLPPGPTPLPVIGNILQIGIK^{48})
4	650.9129	+5	3250.5333	3250.5433	3.1	(apo b_5: ^{48}EQAGGDATENFEDVGHSTDAR^{68})-(CYP2C9: ^{233}LLKNVAFMK^{241})

Table 3.3. Assignment tandem MS spectra of precursor ion $[M+4H]^{4+}$=638.0406 for holo b5: ^{48}EQAGGDATENFEDVGHSTDAR^{68} - CYP2C9: ^{421}KSK^{423} (candidate no. 1 in Table 3.1).

Measured monoisotopic peak (m/z)	Charge State	Measured monoisotopic MH^+	Calculated MH^+	Assignment	Error (ppm)
216.1334	1	216.1334	216.1343	b2β	4.2
234.1439	1	234.1439	234.1448	y1β	3.9
246.1560	1	246.1560	246.1561	Yα2	0.4
336.6870	2	672.3662	672.3675	b3α/y3β	1.9
421.7094	2	842.4110	842.4115	y8α	0.6
537.2635	2	1073.5192	1073.5222	b8α/y3β	2.8
543.7480	2	1086.4882	1086.481	y10α	6.6
549.2656	1	549.2656	549.2627	y5α	5.3
592.7861	2	1184.5644	1184.5534	b9α/b3β	9.3
617.2792	2	1233.5506	1233.5495	y11α	0.9
624.5370	4	2495.1246	2495.1172	b21α/b3β-H2O	3.0
629.0363	4	2513.1218	2513.1278	b21α/b3β	2.4
650.6168	3	1949.8348	1949.8268	y19α(C13)	4.1
674.2996	2	1347.5914	1347.5924	y12α	0.7
723.9712	3	2169.8980	2169.9067	b21α-H2O	4.0
729.8148	2	1458.6218	1458.6244	y13α-H2O	1.8
732.3400	2	1463.6722	1463.6761	b11α/y3β	2.7
738.8184	2	1476.6290	1476.635	y13α	4.1
743.3458	1	743.3458	743.3431	y7α	3.6
756.6683	3	2267.9893	2267.9799	b19α/b3β-H2O	4.1
762.6688	3	2285.9908	2285.9905	b19α/b3β	0.1
789.3456	2	1577.6834	1577.6827	y14α	0.4
796.0071	3	2386.0057	2386.0179	y21α/b2β-NH3	5.1
801.6953	3	2403.0703	2403.0808	y20α/y3β-NH3	4.4
816.3627	2	1631.7176	1631.7092	y15α-H2O(C13)	5.1
824.8637	2	1648.7196	1648.7198	y15α	0.1
845.3761	2	1689.7444	1689.735	b13α/b3β	5.6
854.3792	2	1707.7506	1707.7456	b13α/y3β	2.9
882.3713	2	1763.7348	1763.7467	y16α	6.7
910.8881	2	1820.7684	1820.7682	y17α	0.1
939.4014	2	1877.7950	1877.7896	y18α	2.9
965.9125	2	1930.8172	1930.8162	y19α-H2O	0.5
974.9156	2	1948.8234	1948.8268	y19α	1.7
1094.9597	2	2188.9116	2188.9173	y21α-H2O(C13)	2.6

Table 3.4 Assignment of tandem MS spectra of precursor ion $[M+4H]^{4+}$=464.4965 for holo b5: ^{35}FLEEHPGGEEVLR^{47} - CYP2C9: ^{421}KSK^{423} (candidate no. 4 in Table 3.1).

Measured monoisotopic peak (m/z)	Charge State	Measured monoisotopic MH+	Calculated MH+	Assignment	Error (ppm)
175.1177	1	175.1177	175.119	y1α	7.4
261.1588	1	261.1588	261.1598	b2α	3.8
288.2019	1	288.2019	288.203	y2α	3.8
367.2144	2	733.421	733.4243	bα3/y3β	4.5
387.2695	1	387.2695	387.2714	y3α	4.9
394.5564	3	1181.6536	1181.6636	y8α/b3β	8.5
394.9567	4	1576.8034	1576.8078	y11α/y3β-H2O	2.8
399.4584	4	1594.8102	1594.8184	y11α/y3β	5.1
400.5613	3	1199.6683	1199.6743	y8α/y3β	5.0
419.7219	2	838.436	838.4417	y8α-H2O	6.8
427.7297	4	1707.8954	1707.9024	y12α/y3β	4.1
428.7282	2	856.4486	856.4523	y8α	4.3
431.7366	2	862.4654	862.4669	b4α/y3β	1.7
446.2482	3	1336.729	1336.7332	y9α/y3β	3.1
447.2238	3	1339.6558	1339.6641	b9α/y3β	6.2
483.2582	3	1447.759	1447.7652	y10α/y3β-H2O	4.3
489.2616	3	1465.7692	1465.7757	y10α/y3β	4.4
490.2372	3	1468.696	1468.7067	b10α/y3β	7.3
497.2582	2	993.5086	993.5112	y9α	2.6
500.2642	2	999.5206	999.5258	b8α	5.2
516.3113	1	516.3113	516.314	y4α	5.2
520.2687	3	1558.7905	1558.7972	y11α/b3β-H2O	4.3
523.2625	3	1567.7719	1567.7751	b11α/y3β	2.0
526.2719	3	1576.8001	1576.8078	y11α/b3β	4.9
532.2748	3	1594.8088	1594.8184	y11α/y3β	6.0
551.8099	2	1102.612	1102.6215	y7α/y3β	8.6
552.7717	2	1104.5356	1104.5432	y10α-H2O	6.9
558.293	3	1672.8634	1672.8653	y12α/y3β	1.1
561.7778	2	1122.5478	1122.5538	y10α	5.3
569.9695	3	1707.8929	1707.9024	y12α/y3β	5.6
576.2944	3	1726.8676	1726.8759	y13α/b2β	4.8
591.3318	2	1181.6558	1181.6637	y8α/b3β	6.7
600.3372	2	1199.6666	1199.6743	y8α/y3β	6.4
608.2919	2	1215.576	1215.5752	y11α-2H2O	0.7
617.2933	2	1233.5788	1233.5858	y11α-H2O	5.7
656.299	1	656.299	656.3039	b5α	7.5
668.8638	2	1336.7198	1336.7332	y9α/y3β	10.0

670.3322	2	1339.6566	1339.6641	b9α/y3β	5.6
710.8587	2	1420.7096	1420.7067	b(2-11)α/b3β	2.0
715.385	2	1429.7622	1429.7546	b13α-H2O	5.3
724.8537	2	1448.6996	1448.7056	b12α/b1β-NH3	4.1
734.853	2	1468.6982	1468.7067	b10α/y3β	5.8
856.4463	1	856.4463	856.4523	y8α	7.0

Table 3.5 Assignment of tandem MS spectra of ion $[M+5H]^{5+}$=668.9106 for cross-linking peptide holo human b5: ^{48}EQAGGDATENFEDVGHSTDAR^{68} - CYP2C9: ^{109}GFGIVFSNGKK^{119} (candidate no. 6 in Table 3.1).

Measured monoisotopic peak (m/z)	Charge State	Measured monoisotopic MH+	Calculated MH+	Assignment	Error (ppm)
375.2042	1	375.2042	375.2027	b4β	4.0
717.8227	4	2868.267	2868.2827	y21α/y6β(C13)	5.3
737.8395	4	2948.335	2948.3405	y21α/y7β-H2O	2.0
742.3373	4	2966.326	2966.3511	y21α/y7β	8.5
770.6166	4	3079.443	3079.4352	y21α/y8β	2.5
771.8683	4	3084.45	3084.4453	y19α/y11β(C13)	1.5
780.3684	4	3118.45	3118.446	Y21α/Y9β-H2O	1.3
784.8684	4	3136.45	3136.4566	Y21α/Y9β	2.0

Table 3.6 Assignment of tandem MS spectra of ion $[M+4H]^{4+}$=468.0014 for cross-linked peptide holo b5: ^{35}FLEEHPGGEEVLR^{47} - CYP2C9: ^{158}KTK^{160} (candidate no. 7 in Table 3.1)

Measured monoisotopic peak (m/z)	Charge State	Measured monoisotopic MH+	Calculated MH+	Assignment	Error (ppm)
147.1136	1	147.1136	147.1128	y1β	5.4
175.1188	1	175.1188	175.119	y1α	1.1
261.1597	1	261.1597	261.1598	b2α	0.4
288.2028	1	288.2028	288.203	y2α	0.7
358.2439	1	358.2439	358.2448	b3β	2.5
374.2236	2	747.4393	747.4400	b6α	1.0
376.2535	1	376.2535	376.2554	y3β	5.0
387.2713	1	387.2713	387.2714	y3α	0.3
428.7289	2	856.44986	856.4523	y8α	2.8
487.2852	1	487.2852	487.2875	b(3-3)α/b3β	4.7
507.2771	2	1013.5463	1013.542	b5α/y3β	4.7
516.3135	1	516.3135	516.314	y4α	1.0
536.9492	3	1608.8317	1608.834	y11α/y3β	1.4
552.7775	2	1104.5471	1104.543	y10α-H2O	3.5
561.7809	2	1122.5539	1122.554	y10α	0.1
656.3055	1	656.3055	656.3039	b5α	2.4
677.3416	2	1353.6753	1353.68	b9α/y3β	3.3
741.8716	2	1482.7353	1482.722	b10α/y3β	8.7
753.3885	1	753.3885	753.3566	b(3-6)α/b3β	0.7
759.4029	1	759.4029	759.3995	y7α	4.5
856.4498	1	856.4498	856.4523	y8α	2.9

Table 3.7 Assignment of tandem MS spectra of ion $[M+5H]^{5+}$=571.0525 for cross-linked peptide holo human b5: ^{48}EQAGGDATENFEDVGHSTDAR^{68} - CYP2C9: ^{271}MEKEK^{275} (candidate no. 8 in Table 3.1).

Measured monoisotopic peak (m/z)	Charge State	Measured monoisotopic MH+	Calculated MH+	Assignment	Error (ppm)
240.0967	1	240.0967	240.0978	b2α-H2O	4.5
311.1339	1	311.1339	311.135	b3α-H2O	3.4
368.1560	1	368.1560	368.1564	b4α-H2O	1.1
372.1745	2	743.3412	743.3431	y7α	2.6
411.8524	3	1233.5416	1233.5495	y11α	6.4
421.7081	2	842.4084	842.4115	y8α	3.7
479.2210	2	957.4342	957.4384	y9α	4.4
543.7417	2	1086.4756	1086.4810	y10α	5.0
560.4463	5	2798.2003	2798.1958	b21α/b3-NH3	1.6
583.2562	3	1747.7530	1747.7592	b11α/b5β	3.5
603.0180	4	2409.0486	2409.0623	y16α/y5β	5.7
613.0241	4	2449.0730	2449.0573	y17α/y5β-NH3	6.4
617.2751	4	2466.0770	2466.0838	y17α/y5β	2.8
623.0261	4	2489.0810	2489.0522	y17α/y5β-2NH3	11.6
626.2698	3	1876.7938	1876.8017	b12α/b5β	4.2
627.2758	4	2506.0798	2506.0787	y18α/y5β-NH3	0.4
631.5292	4	2523.0934	2523.1052	y18α/y5β	4.7
644.7852	4	2576.1174	2576.0954	y21α/b3β	8.5
649.2878	4	2594.1278	2594.1424	y19α/y5β	5.6
674.2985	2	1347.5892	1347.5924	y12α	2.4
707.9917	3	2121.9595	2121.9506	y13α/y5β	4.2
743.8274	2	1486.6470	1486.6478	b9α/y5β-H2O	0.5
760.0002	3	2277.9850	2277.9564	y20α-17(C13)	10.4
784.0039	3	2349.9961	2348.9935	b(4-20)α/y5β(C13)	1.1
800.8493	2	1600.6908	1600.6907	b10α/b5β	0.1
1068.4642	1	1068.4642	1068.4704	y10α-H2O	5.8
1600.6913	1	1600.6913	1600.6907	b10α/b5β	0.4
1991.8309	1	1991.8309	1991.8287	b13α/b5β	1.1
2505.0893	1	2505.0893	2505.0946	y18α/b5β	2.1
2577.1181	1	2577.1181	2577.0954	y21α/b3β(C13)	8.8
2595.1082	1	2595.1082	2595.1424	y19α/y5β(C13)	13.2

Table 3.8 Assignment of tandem MS spectra of ion $[M+4H]^{4+}$=464.4986 for cross-linking peptide apo b_5: ^{35}FLEEHPGGEEVLR^{47} - CYP2C9: ^{421}KSK^{423} (candidate no. 1 in Table 3.2).

Measured monoisotopic m/z	Charge state	Measured MH	Calculated MH	Assignment	Error (ppm)
175.1187	1	175.1187	175.119	y1α	1.7
261.1591	1	261.1591	261.1598	b2α	2.8
288.2021	1	288.2021	288.203	y2α	3.3
367.2147	2	733.4222	733.4243	b3α/y3β	4.5
387.2701	1	387.2701	387.2714	y3α	3.4
394.9562	4	1576.8029	1576.808	y11α/y3β-H2O	3.1
399.4591	4	1594.8147	1594.818	y11α/y3β	2.3
400.5618	3	1199.6703	1199.6743	y8α/y3β	5.0
419.7221	2	838.4369	838.4417	y8α-H2O	6.8
428.7288	2	856.4504	856.4523	y8α	2.2
431.7347	2	862.4621	862.4669	b4α/y3β	5.6
446.2462	3	1336.7354	1336.7332	y9α/y3β	3.1
447.2253	3	1339.6594	1339.6641	b9α/y3β	6.2
455.4901	4	1818.9384	1818.95	b11α/b3β-H2O	6.2
483.2580	3	1447.7594	1447.7652	y10α/b3β	4.3
489.2619	3	1465.7692	1465.776	y10α/y3β	4.4
490.2379	3	1468.6992	1468.707	b10α/y3β	5.1
497.2581	2	993.5090	993.5112	y9α	2.3
500.2654	2	999.5235	999.5258	b5α/y3β	2.3
516.3126	1	516.3126	516.314	y4α	2.8
526.2728	3	1576.8001	1576.808	y11α/y3β-H2O	4.9
532.2756	3	1594.8088	1594.818	y11α/y3β	6.0
552.7728	2	1104.5383	1104.5432	y10α-H2O	6.9
561.7785	2	1122.5478	1122.5538	y10α	5.3
569.9703	3	1707.8963	1707.902	y12α/y3β	3.6
600.3388	2	1199.6666	1199.6743	y8α/y3β	6.4
617.2952	2	1233.5832	1233.586	y11α-H2O	2.1
656.2995	1	656.2995	656.3039	b5α	6.7
670.3333	2	1339.6566	1339.6641	b9α/y3β	5.6
724.8608	2	1448.7144	1448.7056	b12α/b1β-NH3	4.1
734.8529	2	1468.6982	1468.707	b10α/y3β	5.8
784.3964	2	1567.7854	1567.775	b11α/y3β	6.6

Table 3.9 Assignment of tandem MS spectra of ion $[M+4H]^{4+}$=662.8094 for apo b5: ^{48}EQAGGDAT ENFEDVGHSTDAR^{68} - CYP2C9: ^{119}KWK^{121} (candidate no. 2 in Table 3.2).

Measured monoisotopic m/z	Charge state	Monoisotopic MH	Calculated MH	Assignment	error
246.1558	1	246.1558	246.1561	y2α	1.2
311.1344	1	311.1344	311.1350	b3α-H2O	1.8
412.7007	2	824.39346	824.4009	y8α-H2O	9.0
421.7088	2	842.40966	842.4115	y8α	2.2
540.2055	1	540.2055	540.2048	b6α-H2O	1.3
549.2641	1	1.00794	549.2627	y5α	2.5
559.284	3	1675.8361	1675.8187	y11α/y3β	10.4
594.0354	4	2373.1178	2373.0854	y19α/y3β-H2O	13.6
597.3035	3	1789.8946	1789.8616	y12α/y3β	18.4
598.5344	4	2391.1138	2391.096	y19α/y3β	7.4
640.3152	3	1918.9297	1918.9042	y13α/y3β	13.3
649.3055	4	2594.1982	2594.1654	b21α/b3β-H2O	12.6
653.8007	4	2612.179	2612.176	b21α/b3β	1.1
673.9953	3	2019.97	2019.9519	y14α/y3β	9.0
697.6755	3	2091.0106	2090.989	y15α/y3β	10.3
736.0189	3	2206.0408	2206.016	y16α/y3β	11.3
755.0248	3	2263.0585	2263.0374	y17α/y3β	9.3
774.0303	3	2320.075	2320.0589	y18α/y3β	6.9
789.6859	3	2367.0418	2367.0272	b19α/b3β-H2O	6.2
792.0331	3	2374.0834	2374.0695	y19α/y3β-NH3	5.9
795.6879	3	2385.0478	2385.0378	b19α/b3β	4.2
797.7084	3	2391.1093	2391.096	y19α/y3β	5.6
801.6855	3	2403.0406	2403.0484	b19α/b3β	3.2
886.3883	2	1771.7687	1771.7558	b13α/b3β-NH3	7.3
894.9061	2	1788.8043	1788.78131	b13α/b3β	12.8

Table 3.10 Assignment of tandem MS spectra of ion $[M+4H]^{4+}$=1103.0741 for cross-linking peptide apo b5: ^{48}EQAGGDATENFEDVGHSTDAR^{68} - CYP2C9: ^{27}GKLPPGPTPLPVIGNILQIGI K^{48} (candidate no. 3 in Table 3.2).

Measured monoisotopic m/z	Charge state	Monoisotopic MH^+	Calculated MH^+	Assignment	Error (ppm)
632.8992	2	1264.7906	1264.7987	y12β	6.4
671.4482	1	671.4482	671.445	y6β	4.8
898.5766	1	898.5766	898.572	y8β	5.1
955.5921	1	955.5921	955.5935	y9β	1.5
962.5856	2	1924.1634	1924.163	y19β	0.2
1043.1619	3	3127.4701	3127.4715	b21α/b10β-H2O	0.4
1068.6726	1	1068.6726	1068.6776	y10β	4.7
1264.7987	1	1264.7987	1264.7987	y12β	0.0
1285.0275	3	3853.0669	3853.0654	y15α/y22β(C13)	0.4
1459.6675	2	2918.3272	2918.3188	b21α/b8β-NH3	2.9
1474.9426	1	1474.9426	1474.9356	y14β	4.7
1564.7343	2	3128.4608	3128.4556	b21α/b10β-NH4	1.7
1942.7585	1	1942.7585	1942.7685	b19α-H2O	5.1

Table 3.11 Assignment of tandem MS spectra of ion $[M+5H]^{5+}$=650.9129 for cross-linking peptide apo b5: ^{48}EQAGGDATENFEDVGHSTDAR^{68} - CYP2C9: ^{233}LLKNVAFMK^{241} (candidate no. 4 in Table 3.2).

Measured monoisotopic peak (m/z)	Charge state	Monoisotopic MH^+	Calculated MH^+	Assignment	Error (ppm)
240.0981	1	240.0981	240.0979	b2α-H2O	0.8
246.1562	1	246.1562	246.1561	y2α	0.4
258.1085	1	258.1085	258.1084	b2α	0.4
278.1545	1	278.1545	278.1533	y2β	4.3
301.1144	1	301.1144	301.1143	GGDA/AGGD	0.3
311.1353	1	311.1353	311.135	b3α-H2O	1.0
368.1565	1	368.1565	368.1564	b4α-H2O	0.3
421.7111	2	842.4144	842.4115	y8α	3.4
462.2306	1	462.2306	462.2307	y4α	0.2
479.2228	2	957.4378	957.4384	y9α	0.6
496.2614	1	496.2614	496.2588	y4β	5.2
540.2047	1	540.2047	540.2049	b6α-H2O	0.4
543.7457	2	1086.484	1086.481	y10α	2.4
549.2629	1	549.2629	549.2627	y5α	0.4
595.3257	1	595.3257	595.3272	y5β	2.5
617.283	2	1233.558	1233.55	y11α	7.1
694.2801	1	694.2801	694.2791	bα(13-19)-H2O	1.4
709.3718	1	709.3718	709.3716	y6β	0.3
712.2961	1	712.2961	712.2896	b8α-H2O	9.1
731.6034	4	2923.3902	2923.4050	y18α/y9β(C13)	5.1
743.3491	1	743.3491	743.3431	y7α	8.1
916.7761	3	2748.313	2748.2933	b(3-19)α/y9β	7.1

Chapter 4. Cyt b5-CYP2A6 Interaction Study

4.1 CYP2A6 interaction with its redox partners

4.1.1 CYP2A6 introduction

CYP2A6 accounts for ~4% of human liver P450s with the range from < 0.2% to 13% (Ortiz de Montellano, 2005; Porubsky et al., 2008). It is also expressed in other tissues, such as the nasopharyngeal region, trachea, lung, and esophageal mucosa. It is an important hepatic Phase I enzyme that contributes to the metabolism of over 30 drugs, accounting ~3% therapeutic drugs including valproic acid, ifosfamide, cyclophosphamide, nicotine, tamoxifen, propofol etc., environmental toxicants such as gasoline additives, and many procarcinogens such as nitrosamines and aflatoxin B1 (Di et al., 2009). In addition, CYP2A6 catalyzes the biotransformation of several endogenous compounds such as retinoid acids and steroids (Di et al., 2009). CYP2A6 belongs to human CYP2A family, which also includes CYP2A7 (nonfunctional) and 2A13 (Ortiz de Montellano, 2005). As for substrate specificity, CYP2A6 prefers small, often bicyclic molecules. Coumarin 7-hydroxylation is its characteristic and specific reaction, used both in vitro and in vivo as probe assay (Ortiz de Montellano, 2005).

CYP2A6 catalyzes nicotine metabolism and the activation of tobacco specific carcinogens such as N'-nitrosonornicotine and 4-(methylnitrosamino)-1-(3-pyridyl)-1-butanone to mutagenic products. Therefore, it is proposed to be associated with smoking behaviors and tobacco-related cancers. Defective CYP2A6 activity is suggested to correlate with lower smoking addiction and cancer risk (Ortiz de Montellano, 2005). Inhibitors of CYP2A6 are therefore considered useful in aiding smoke cessation and prevention of several cancers (Sellers et al., 2000). CYP2A6 also participates extensively in the metabolism of clinical

therapeutics such as fadrozole and losigamone (Sansen et al., 2007), as well as in activation of some prodrugs such as tegafur (Sansen et al., 2007).

CYP2A6 is genetically polymorphic, with 38 allele genes as of 2010 (http://www.cypalleles.ki.se). Individuals with defective CYP2A6 alleles showed significant reduction in tobacco-related lung cancer (Thorgeirsson et al., 2010), which was most pronounced in those homozygous for the CYP2A6*4 deletion allele (Mizutani, 2003). In East Asians, the CYP2A6*4 frequency is 11-18% (Kim et al., 2004).

4.1.2 Cyt b5 modulation on CYP2A6 activity

Soucek et al. showed that a 1:1 ratio of cyt b5 to CYP2A6 produced optimal activity in a purified recombinant system. In the presence of cyt b5, coumarin 7-hydroxylation and nicotine C-oxidation was stimulated ~2 fold (Yamazaki et al., 2002). Chen et al. found that not only acetaminophen metabolism by CYP2A6 was increased in the presence of cyt b5, but that the product ratio of GS-APAP to 3-OH-APAP was also slightly altered, indicating that cyt b5 might be able to conformationally change CYP2A6 and alter its substrate orientation (Chen et al., 1998).

As for the mechanism by which cyt b5 modulates CYP2A6 activity, very few studies are reported. Yamazaki et al. reported that apo b5 and holo b5 both stimulate CYP2A6 catalyzed coumarin 7-hydroxylation about 2 fold (Yamazaki et al., 2002), suggesting that cyt b5 might allosterically affect CYP2A6 conformation and result in the change of the substrate metabolism, instead of facilitating the second electron transfer step in the catalytic cycle.

4.1.3 CYP2A6 structure and topology in binding to redox partners

CYP2A6 crystal structure was first reported by Yano et al. in 2005 (Yano et al., 2005). Since then, twelve crystal structures of CYP2A6 have been available in the PDB bank as of March, 2012 (http://www.rcsb.org): 1Z10 with coumarin bound; inhibitors bound form 1Z11 with mathosalen, 2FDU with N,N-Dimethyl(5-(pyridin-3-yl)furan-2-yl)methanamine, 2FDV with N-Methyl(5-(pyridin-3-yl)furan-2-yl)methanamine, 2FDW with (5-(Pyridin-3-yl)furan-2-yl)methanamine, 2FDY with adrithiol, and 3T3R with pilocarpine, respectively; mutants 2PG5 (N297Q) with 1,2-ethanediol, 2PG6 (L240C/N297Q), 2PG7 (N297Q/I300V), 3T3Q/3EBS (I208S/I300F/ G301A/S369G with pilocarpine and phenacetin, respectively).

Comparing the CYP2A6 crystal structures complex with different substrates or inhibitors, their Cα backbone positions are very similar to each other, with an average RMSD of 0.24 Å. This suggests that CYP2A6 has a relatively lower flexibility in its active site, consistent with its narrow substrate range (DeVore et al., 2011). CYP2A6 has a compact active site, with an active site volume estimated about 230 $Å^3$, much smaller compared with other CYP isoforms such as 2C8, 2C9, and 3A4. It has a very hydrophobic active site, with Asn297 being the only polar residue in the active site (Arimoto, 2006). Residues contacting the ligand molecules in different CYP2A6 complex structures are almost identical, with a relatively more drastic repositioning of Phe209 in complex with 4-4'-dipyridyl disulfide, and only slight rearrangement of Phe107 in several crystal structures. These data indicate that CYP2A6 active site is relatively rigid though adaptable for small planar substrates (Sansen et al., 2007). Computer dynamic simulations have shown that CYP2A6 exhibits an overall rigidity with no remarkable structural changes observed. The most flexible regions are loops F-G, G-H and H-I in the distal surface of CYP2A6 (Hendrychova et al., 2012).

As for the topology of CYP2A6 for redox partner binding, there is very limited research reported. It was found that when Arg128 at the N-terminal of C helix was mutated to Leu, it showed altered heme binding, resulting in changes in coumarin 7-hydroxylation. L160H showed significantly enhanced coumarin 3-hydroxlation but lacked 7-hydroxylation activity indicating its importance in substrate orientation. Leu160 is at the C-terminal of D helix (Yamano et al., 1990).

Val117 and Ala372 were reported to be critical for coumarin 7-hydroxylation, the mutation of which resulted in 8- and 5-fold decrease in catalytic efficiencies, respectively, compared with the wild-type. Val117 is in the C helix and Ala372 is in the K-K' loop. In the crystal structure, these two residues are not in direct contact with the substrate, nor with solvent, but are on the "border" of the CYP2A6 active site (Di et al., 2009).

In a random mutagenesis study of CYP2A6 (Kim et al., 2005), the investigators found that the mutants D93H/D169N, F286L, and K476E showed decreased activity. These residues are not in the active site. Instead, their positions are: Asp93 in B-C loop, Asp169 in D-E loop, Phe286 in H-I loop, and Lys476 in β4-2 sheet. A further study on the K476E mutant indicated that Lys476 was important for CPR binding with CYP2A6. Mutation of this residue resulted in lower affinity and lack of productive binding with CPR (Di et al., 2009; Kim et al., 2005). Other mutants showed decreased coumarin binding affinities, which was believed to be the major reason causing decreased enzyme activity. These results suggest that structural elements outside of the active site may also play a role in regulating the catalytic activity of CYP2A6. The possible mechanism of their effect could be modulation of substrate access channels, altered CPR binding, altered substrate recognition site or causing non-productive binding modes (Di et al., 2009).

4.1.4 Goals of the study of cyt b5-CYP2A6 interaction

According to the discussion above, cyt b5 likely stimulates CYP2A6 through allosteric effect. Therefore, we hypothesize that apo b5 and holo b5 modulate CYP2A6 activity through similar surface contacts. The goal of this study is to map the surface interaction between holo b5/apo b5-CYP2A6 using the chemical cross-linking coupled with mass spectrometric analysis, and construct models of their interaction based on the cross-linking result.

4.2 Materials and experimental procedures

4.2.1 Materials

The expression plasmid of non-histagged N-terminal variant pCW/2A6 with the second amino acid Leu substituted to Ala was kindly provided by Dr. Pavel Souček, National Institute of Public Health in Prague, Czech Republic (Soucek, 1999). The expression plasmid containing $(His)_4$HMWHuman-cyt b5 were provided by Dr. Richard J. Auchus, University of Michigan (Guryev, 2001; Holmans, 1994). All other reagents are the same as those used for previous studies and indicated in the Material section in Chapter 2.

4.2.2 Protein Expression and Purification

The pCW/2A6 plasmid contains a mutation at the N-terminal to facilitate expression, which is Ala in substitution for Leu2. In addition, this plasmid contains a mutation of Val for Ile248 caused by PCR error. Though this mutation was found not to affect CYP2A6 activity (Gillam et al., 1999), the Val was corrected to Ile in the current study.

CYP2A6 was expressed in *E. coli* DH5α F'I^q cells using the expression plasmid according to previously published protocols (Soucek, 1999). Briefly, *E. coli* strain DH5α F'I^q cells were transformed with the expression plasmid and selected on Luria-Bertani agar plates containing 100 μg/mL ampicillin. A single colony was selected and grown overnight in Luria-Bertani medium supplemented with ampicillin (100 μg/ml) at 37°C. The overnight culture (~3ml) was used to seed 500 ml of expression medium of Terrific Bloth containing 100 μg/mL ampicillin, 1 mM thiamine, and trace elements and was allowed to grow until A_{600} reaches about 0.4. Then protein expression was induced by 1 mM IPTG and 0.5 mM δ-ALA was supplemented in the media. Cells were allowed to grow for a total 40 h at 27 ℃ with shaking at 160 rpm and then harvested and stored at -80 ^{o}C until further use.

Subsequent preparation of the membrane fraction was carried out using two passes through the French Press cell in resuspension buffer containing 50 mM KPi, 20% glycerol, 20 mM β-mercaptoethanol (BME) (pH 7.4) supplemented with protease inhibitor cocktail 250 μL per liter culture. The subcellular mixture was stirred at 4 ℃ for 1 h in the presence of 10% Emulgen 911, and centrifuged at 37 000 rpm and 4 ℃ for 60 min. The supernatant was collected and loaded onto Ni-NTA affinity column equilibrated with resuspension buffer. The column was then washed with 20 column volumes of wash buffer (50 mM KPi, 300 mM NaCl, 40 mM imidazole, 100 mM glycine, 20% glycerol, 2 mM BME, and 0.2% Emulgen 91, pH 7.4). Protein was eluted with elution buffer (50 mM KPi, 20% glycerol, 2 mM BME, 0.2% cholate, and 400 mM imidazole, pH 7.4) and dialyzed against dialysis buffer (50 mM KPi, 20% glycerol pH 7.4) for two times. The protein was aliquoted and stored at −80 °C for further use.

CYP2A6 concentration was determined using a previously described method of CO-binding difference spectra with extinction coefficient of 91 mM^{-1} cm^{-1}. Protein purity was examined by reducing SDS–PAGE using a 10% acrylamide gel and coomassie blue staining.

Rat CPR, cyt b5 and apo b5 were prepared as described in chapter 2.

4.2.3 Cross-linking reactions, mass spectrometric analysis and data processing

Chemical cross-linking reactions, mass spectrometric analysis and data processing were conducted using the same methods as described in Chapter 2.

4.2.4 Molecular Docking

X-ray crystallographic structures of human CYP2A6 (PDB "1Z10") and a homology model of human cyt b5 from bovine cyt b5 (PDB "1CYO") (Cunane et al., 1996) were used to construct the model of the holo/apo b5-CYP2A6 complex. CYP2A6 shows very low flexibility. Though the 9 crystal structures of wild-type CYP2A6 published so far were bound with different substrates, their backbones show very small deviations. Only active site residues show slightly different orientation allowing the different-sized substrates to occupy the active site. Therefore, docking calculations of CYP2A6-cyt b5 complex are not likely to vary with choice of CYP2A6 crystal structure.. Docking of the structures was accomplished manually using the software tool Chimera 1.5.3 with the cross-linking sites between cyt b5 and CYP2A6 as constraints.

4.3 Results

4.3.1 Chemical Cross-Linking

Equimolar mixture of CYP2A6 and holo cyt b5 or apo b5 in the presence of EDC showed formation of protein complexes, with the major complex at molecular weight of ~73 kDa detected by SDS-PAGE (Data not shown). CYP2A6 is ~56 kD and cyt b5 is ~16.7 kD.

4.3.2 Holo b5 and CYP2A6 Cross-linking Results

Nine inter-molecular cross-linked peptides were identified with cross-linking sites determined by corresponding tandem mass spectra (Table 4.1-4.10 and Fig. 4.1-4.16).

The first cross-linked peptide was confirmed to be from cross-linked peptides holo cyt b5: ^{48}EQAGGDATENFEDVGHSTDAR^{58} - CYP2A6: ^{124}AKQLR^{128}. The precursor ion is quintuple charged with m/z of 561.2653. According to the tandem MS spectrum. the cross-linked sites are Asp53 on cyt b5 and Lys125 on CYP2A6. In the spectrum, a series of linear y ions from holo b5 were observed with the longest liner y ion being y12α. In addition, the shortest cross-linked ion is b7α/y5β, indicating that either Glu48 or Asp53 is cross-linked. Furthermore, the observance of cross-linked fragment ion y16α/y5β-NH_3 indicates that it is Asp53 and not Glu48 that is cross-linked. Therefore, the first pair of cross-linked residue is Asp53 (holo b5) - Lys125 (CYP2A6).

The second quintuply charged precursor ion with m/z of 597.0750 was confirmed to be from the cross-linked peptide holo cyt b5: ^{48}EQAGGDATENFEDVGHSTDAR^{58} - CYP2A6: ^{376}KDTKFR^{381}. The cross-linking sites on cyt b5 are Asp53 with Lys379 on CYP2A6. The observance of linear y13α ion suggests that residues included in y13α are possibly not cross-

linked. The observance of cross-linked ion b7α/y6β suggests that it is either Glu48 or Asp53 that is cross-linked. Cross-linked ion b10α/y4β suggests that it is likely that Lys379 is cross-linked, which is the second Lys residue in the CYP2A6 peptide. No distinction between Glu48 and Asp53 is possible. Therefore, the second cross-linked pair is assigned to be Glu48/Asp53 (holo b5)-Lys379 (CYP2A6).

The third quintuply charged precursor ion with m/z of 728.5439 was confirmed to be from cross-linked peptide holo b_5: ^{48}EQAGGDATENFEDVGHSTDAR^{68} - CYP2A6: ^{425}KSDAFVPFSIGKR^{437}. Fragment ions y19α of holo b5 and cross-linked fragment b2α/y13β suggest that it is the very first acidic residue Glu48 on holo b5 that is cross-linked. In addition, fragment ion b8α/y6β suggests that it is the Lys436 on CYP2A6 that is cross-linked. All other fragments agree with this assignment. Therefore, the third cross-linked pair is Glu48 (holo b5) – Lys436 (CYP2A6).

Fourthly, the quintuply charged precursor ion for cross-linked peptide holo b_5: ^{48}EQAGGDATENFEDVGHSTDAR^{68} - CYP2A6: ^{462}LKSSQSPK^{469} was observed, with m/z of 613.0852. The cross-linked residue on holo b5 is determined to be Asp53. First, the linear fragment ion of y14α on cyt b5 indicates that only Glu48 and Asp53 are likely cross-linked. Furthermore, the cross-linked fragment y19α/b8β suggests that Glu48 is not the one that is involved in cross-linking. On CYP2A6, Lys463 is the only possible cross-linked residue. All other cross-linked fragments agree with this assignment well. So the fourth pair is identified to be Asp53 (holo b5) – Lys463 (CYP2A6).

The fifth quintuply charged precursor ion with m/z of 818.1609 is identified to be from cross-linked peptide holo b5: ^{48}EQAGGDATENF EDVGHSTDAR^{68} - CYP2A6:

^{275}MQEEEKNPNTEFYLK^{289}. Glu48 on holo b5 and Lys280 on CYP2A6 are identified to be the cross-linked residues. The observance of y19α ion of holo b5 indicates that it is the first acidic residue that is involved in the cross-linking. The Lys280 is the only residue on CYP2A6 that is possibly cross-linked. Therefore, the fifth pair is Glu48 (holo b5) - Lys280 (CYP2A6).

The sixth quardruply charged precursor ion with m/z of 697.8615 was confirmed to be from cross-linked peptide holo b_5: ^{35}FLEEHPGGEEVLR^{47} - CYP2A6: ^{425}KSDAFVPFSIGK^{436}. The cross-linked residue on cyt b5 is Glu37, as linear ion y10α of holo b5 was observed excluding Glu38 to be involved in cross-linking. The cross-linked residue on CYP2A6 is Lys425. The observation of cross-linked fragment y13α/b2β further confirmed the cross-linked site on CYP2A6 peptide can only be within the first two residues, which has to be the first Lys residue. Therefore, the pair identified in cross-linking is Glu37 (holo b5) – Lys425 (CYP2A6).

The seventh quintuply charged precursor ion with m/z of 458.2413 was confirmed to be from cross-linked peptide holo b_5: ^{35}FLEEHPGGEEVLR^{47} - CYP2A6: ^{376}KDTKFR^{381}. In its tandem MS spectrum, only two linear y ions of holo b5 were observed (y2α and y3α). Cross-linked fragments suggest that residues from the third to the ninth are all possibly involved in cross-linking. Spectrum does not allow further differentiation due to lack of enough fragments. Therefore, Glu37, 38, 43 and 44 all are possibily involved in cross-linking. The same situation is for cross-linked residues on CYP2A6. Therefore, Lys376 or Lys379 both are possible.

The eight identified cross-linked peptide was holo b_5: ^{35}FLEEHPGGEEVLR^{47} - CYP2A6: ^{334}VIGKNR^{339}, and both quadruple and quintuple charged precursor ions of it were observed. Lys337 on CYP2A6 is determined to be the residue involved in cross-linking with cyt b5. However, there were insufficient fragments to allow to determine the detailed crosslink arrangement between the acidic residues Glu37, Glu38 and Glu43 on cyt b5 and CYP2A6.

Any assignment of tandem MS data with an error > 10 ppm was excluded, as the LTQ-Orbitrap instrument is able to provide high mass accuracy within this error. In addition, the above ions were not identified to be any linear peptides when searched by phenyx, thus ruling out the possibility of mis-interpretation of a linear peptide.

4.3.3 Apo b5 and CYP2A6 Cross-linking Results

In apo b5-CYP2A6 complex, six cross-linked peptides were identified as shown in Table 4.10 and Fig. 4.17-4.28.

The first cross-linked peptide is similar to that found in holo b5-CYP2A6 complex. Its precursor ion is also quintuply charged with m/z of 561.2653. The cross-linked site on holo b5 is determined to be Glu56, as suggested by the linear fragment y11α and cross-linked fragments b10α/b5β, y18α/y5β, and b(7-10) α/b(1-4)β. Lys125 on CYP2A6 is the only possible residue that is cross-linked. So this pair is Glu56 (holo b5) - Lys125 (CYP2A6).

The second cross-linked peptide is apo b_5: ^{48}EQAGGDATENFEDVGHSTDAR^{68} - CYP2A6: ^{376}KDTK^{379}, with the precursor ion having an m/z of 670.3018 in a quadruple-charged state. It is in close association with the second candidates identified in holo b5-CYP2A6 complex, with CYP2A6 peptide two residues shorter compared the one in holo b5-CYP2A6. The

observance of linear y8α from apo b5 excludes the possibility of its composition residues involved in cross-linking. In addition, the observance of cross-linked fragment y15α/y4β suggests that residues Glu56, Glu59 or Asp60 on apo b5 all are possible contributors to the cross-linking. Lys376 is the only possible residue on CYP2A6 that is involved in cross-linking.

The third cross-linked peptide is apo b_5: ^{35}FLEEHPGGEEVLR^{47} - CYP2A6: ^{374}VKK^{376}, also similar to the seventh candidate identified in the holo b5-CYP2A6 complex with regard to the amino acid residues that are cross-linked. In the apo b5-CYP2A6 candidate, the cross-linked residue on CYP2A6 is Lys375, while in holo b5-CYP2A6, the cross-linked residue on CYP2A6 is Lys376 or Lys379 and both are on the same segament of holo/apo b5. For the current candidate, either Glu37 or Glu38 is cross-linked with CYP2A6, as suggested by the observation of linear y8α ion of apo b5 and cross-linked fragment ion b5α/y3β.

The fourth cross-linked peptide apo b_5: ^{35}FLEEHPGGEEVLR^{47}- CYP2A6: ^{334}VIGKNR^{339} also has been identified in the complex of holo b5-CYP2A6, listed as the 8th candidate in Table 4.11. The precursor ion shows an m/z of 545.5444 with a charge state of +4. Glu37 or Glu38 is cross-linked with Lys337 as suggested by the observation of y8α ion of apo b5 and b5α/y6β cross-linked fragment of the cross-linked candidate. Lys337 on CYP2A6 is the only residue that is possibly involved in cross-linking.

The fifth candidate is apo b_5: ^{48}EQAGGDATENFEDVGHSTDAR^{68} - CYP2A6: ^{334}VIGKNR^{339}, the precursor shows an m/z of 719.0888 with a charge state of +4. Compared with the fourth candidate, it shows that the same segment of CYP2A6 is cross-linked with a different segment of apo b5. The fragmentation suggest that it is Glu56 on apo b5 that is

cross-linked with Lys337 on CYP2A6, as determined by the linear y12α ion of apo b5 and cross-linked fragment y14α/y6β.

The sixth candidate is apo b5: ^{35}FLEEHPGGEEVLR^{47}- CYP2A6: ^{251}KVEHNQR^{257}, and the precursor ion is quintuply charged with an m/z of 481.4475. The observation of linear fragment y10α and b2α of apo b5, as well as cross-linked fragment ion b3α/y7β suggests that Glu37 on apo b5 is the cross-linked residue. However, the occurrence of y8α/y7β suggests another possibility that Glu43 or Glu44 is cross-linked. On CYP2A6, Lys251 is the only possible cross-linked residue.

All together six cross-linked pairs were identified, among which four pairs are highly similar to those identified in the holo b5-CYP2A6 complex.

4.3.4 Modeling of Holo b5-CYP2A6 and Apo b5-CYP2A6 Interactions

As mentioned above, comparing the cross-linking sites of holo b5-CYP2A6 with those of apo b5-CYP2A6 shows that there are residues on CYP2A6 that play important roles in interactions with both holo- and apo-b5, either the same residue or neighboring residues on CYP2A6 that cross-link with the same segment of holo-/apo- b5. These cases are summarized as the following.

First, in both cases, Lys125 is identified to be cross-linked with the same segment (Glu48-Arg68) of holo-/apo b5. In holo b5-CYP2A6, Asp53 is determined to be cross-linked, while in apo b5-CYP2A6, it is Glu56 that is cross-linked. Second, Lys379 and Lys376 on CYP2A6 are found cross-linked with the same segment of holo-/apo-b5 (Glu48-Arg68), respectively. In holo b5-CYP2A6, Glu48 or Asp53 is cross-linked, while in apo b5-CYP2A6, Glu56,

Glu59 or Asp60 is cross-linked. Third, Lys376 or Lys379 on CYP2A6 is also found cross-linked with another major segment of holo b5, Phe35-Arg47 in the holo b5-CYP2A6 complex, suggesting another possible orientation. Interestingly, in the apo b5-CYP2A6 interaction, Lys375 (adjacent to Lys376) on CYP2A6 is found cross-linked with the same segment, suggesting a similar orientation to apo b5 might also exist. Comparing with the aforementioned interaction of these residues with the segment Glu48-Arg68, it suggests that both holo-and apo-b5 may interact with CYP2A6 in two major orientations. Fourth, Lys337 on CYP2A6 is found to cross-link with the same segment (Phe35-Arg47) both in holo and apo b5. These above common residues on CYP2A6 are all in the proximal surface of CYP2A6. Lys125 is at the C-terminal of C helix; Lys375, Lys376 and Lys379 are at K-K' loop and close to Lys125 in three-dimensional position; Lys425 is at K''-L loop; Lys337 is at I-J loop, which borders the proximal surface.

There are also differences in cross-linking sites in holo b5-CYP2A6 compared with apo b5-CYP2A6. First, Lys425 is not identified in cross-linking between apo b5 and CYP2A6, but is found cross-linked with both of the major segments in holo b5 (Phe35-Arg47 and Glu48-Arg68). Second, in apo b5-CYP2A6, Lys337 is found cross-linked with both of the above segments while only Phe35-Arg47 in holo b5-CYP2A6. Third, in holo b5-CYP2A6 complex, Lys280 on CYP2A6 is found cross-linked with Glu48-Arg68 segment, but not identified in the apo b5-CYP2A6 complex. Lys280 is also a residue bordering the proximal surface of CYP2A6. In addition, one residue on CYP2A6 involved in cross-linking with holo b5 is not in the proximal surface. It is Lys463 on a β sheet following the L helix. At this point, it is not clear whether this is a non-specific interaction or an indication of another binding surface. As

discussed in the introduction, Lys476, the residue on the same loop was proposed to be involved in interaction with CPR as suggested by mutagenesis and binding affinity studies.

Based on the above analysis, the major common orientation of holo/apo b5 in interaction with CYP2A6 is modeled as shown in Fig. 4.29. The driving charge-pair interactions between holo b5-CYP2A6 are Lys125-Asp53, Lys379-Glu48/Asp53, Lys425-Glu37/Glu38, and Lys436/Glu48. It is clear that holo b5 interaction with CYP2A6 is similar to its interaction with CYP isoforms 2C9 and 3A4 as previously described, with regard to the region on cyt b5 and P450s involved in the interaction. The cytosolic domain of cyt b5 including the α2, α3, α3-loop-α4, α4 and the heme edge are in close contact with K''-L loop, K-K' loop, B helix, C helix and the meander region of CYP2A6. In the model, Lys337 is a little farther away from Glu37/Glu38. However, Lys337 is on J-K loop and has certain flexibility, it is possible that in the dynamic process of holo b5-CYP2A6 interaction, this residue interact with the corresponding acidic residues and contribute to the complex formation.

Apo b5-CYP2A6 interaction model was constructed with charge pairs Lys125-Glu56, Lys376-Glu56/ Glu59/Asp60, and Lys337-Glu37/Glu38 as constraints (Fig. 4.29). Considering the highly consistent interacting sites, it is not surprising that apo b5 interacts with CYP2A6 in an orientation similar to holo b5 (Fig 4.29(C)). Again, the cytosolic domain of apo b5 including the α2, α3, α3-loop-α4, α4 are in close contact with K''-L loop, K-K' loop, B helix, C helix and the meander region of CYP2A6.

With the alignment of CYP2A6 in the two models, it is clear that apo b5 and holo b5 adopt similar orientations when binding to CYP2A6 (Fig. 4.29(C)). Both apo b5 and holo b5

occupy the same groove on the proximal surface of CYP2A6, with very slight differences. In the holo b5-CYP2A6 interaction model, the heme groups of the two enzymes are not in close contact, with a distance ~11 Å between the closest atoms on their heme edges.

4.4 Discussion

Among the major hepatic CYP enzymes 3A4, 2C9 and 2A6, CYP2A6 shows the least flexibility in its structure (Hendrychova et al., 2011; Skopalik et al., 2008). It demonstrated very small change in UV/Vis spectroscopy at high hydrostatic pressure compared with the other CYPs such as 3A4 and 2C9 (Hendrychova et al., 2011), suggesting the least compressible heme active site. Resonance Raman (RR) spectra showed that CYP2A6 heme vinyl vibrations occurred mainly at 1631 cm^{-1}, which correspond to the out-of-plane conformations, suggesting the existence of relatively rigid constraints of the heme vinyls (Hendrychova et al., 2011). Moreover, recent computer dynamic simulations show that CYP2A6 fluctuations are localized mainly to the loops of F-G', G'-G, G-H, and H-I (Skopalik et al., 2008). Crystal structures of CYP2A6 with different substrates/inhibitors also show very little change in the positions of backbone as described in the introduction of this chapter.

In the cross-linking study of holo/apo b5 with CYP2A6, similar cross-linking sites between the two pairs of proteins were observed. In holo b5, residues Lys125 on helix C, Lys 376 on K-K' loop, Lys425 and Lys436 on K''-L loop were found involved in cross-linking; in apo b5, residues Lys125, Lys376 were also found to be cross-linked with the same segment of apo b5. These residues are scattered around the proximal surface which has a concave shape.

As in interactions with other CYPs discussed earlier, cyt b5 uses its cytosolic domain to interact with CYP2A6, including α2, α3, α4, α5 and the edge of the hemeproprionate group. The heme edge together with the α helixes surrounding the heme factor form a a convex shape, which interacts with the concave surface of CYP2A6. Cyt b5 interacts with the B, C, K helices and the loops of K-K', K''-L, as well as the meander region of CYP2A6. These regions, especially the helices B and C and the B-C loop border the major substrate access/egress pathway of P450s (Schleinkofer et al., 2005). Cyt b5 can affect the flexibility of B-C loop and result in the conformational change of this region to control the substrate access or egress. This affect might also be transferred to the distal surface, as suggested in the study of P450cam structure perturbations caused by cyt b5, a non-natural partner, to induce conformational changes globally. As CYP2A6 is relatively rigid with the highly compact active site as indicated by its high substrate selectivity and specificity, its conformational change upon cyt b5 binding may also be fairly small compared with CYPs 2C9 and 3A4. In other words, CYP2A6 maintains a rigid structure allowing apo b5 interacts with it in a way quite consistent with holo b5. Indeed, this is shown by the result of current study, shown in Fig. 4.29(C) the comparison of interaction models of the apo b5-CYP2A6 and holo b5-CYP2A6. With the alignment of CYP2A6 in the two models, the orientation of the holo and apo b5 show strong similarities. Given the many factors considered in the docking calculations as well as protein dynamics, it is reasonable to postulate that holo and apo b5 actually orient the same way in binding with CYP2A6 to exert their allosteric effect.

In addition, it is likely both holo- and apo b5 may have a similar second orientation in binding with CYP2A6 in addition to the orientation shown in Fig. 4.29. With the Glu48-Arg68 segment, Lys376 on holo b5 and Lys375 on apo b5 are both found in cross-linking

with the Phe35-Arg47 segment. Lys337 on apo b5 is also found cross-linked with both of the two above segments as well. According to the crystal structure and the relative positions of these residues, it is estimated that the second orientation is rotated ~180 degrees compared to the one discussed above. In this orientation, holo and apo b5 occupy the same region on the CYP2A6 proximal surface but the positions of the two major segments of cyt b5 exchanged with each other, resulting in an orientation ~180 degree different. Surface stabilizing forces between the two orientations might be different resulting in the different stability of the complex and thereby different conformational changes. The two orientations may not have the same efficiency in inducing productive conformational changes in the catalytic cycle to modulate CYP2A6.

There are cross-links that likely resulted from non-specific interactions. In the apo b5-CYP2A6 cross-link Lys251-Glu37/Glu43, Lys251 is in helix G, positioned at the opening of helix F, G and E-F loop, which is assigned as channel 3 by Cojocaru et al. (Cojocaru et al., 2007) in their study of the channels in P450s leading to the access and egress from the active site. This channel was only considered to be a potential secondary substrate/product egress route in dynamic simulations of P450cam and not observed i n most of the mammalian P450 crystal structures (Cojocaru et al., 2007).

In holo b5-CYP2A6, the Lys463 on CYP2A6 cross-linked with the segment Glu48-Arg68 is located at the β3 sheet, where no substrate access or egress channel has been identified in this region. Although there is a report of Lys476 residue in potential contribution to redox partner binding, Lys476 is closer to the active site in three dimensional structures compared with Lys463 and neither of them is located within the proximal surface of CYP2A6.

Overall, excluding the non-specific interactions, both holo and apo b5 interact with CYP2A6 in the highly similar orientations among the two possible orientations of each in binding to CYP2A6. CYP2A6 shows the least flexibility among the CYPs studied in the current investigation, providing a good template for study of holo b5 vs. apo b5 effect. It is because of the rigidity of CYP2A6 that results in the same orientation of holo and apo b5 in binding to it. When the CYPs structure fluctuation is higher such as in CYP2C9 and CYP3A4, this binding is highly affected by dynamic factors. As a result, more similar cross-linking sites between holo/apo b5-CYP2A6 are identified compared with other CYPs studied in this project.

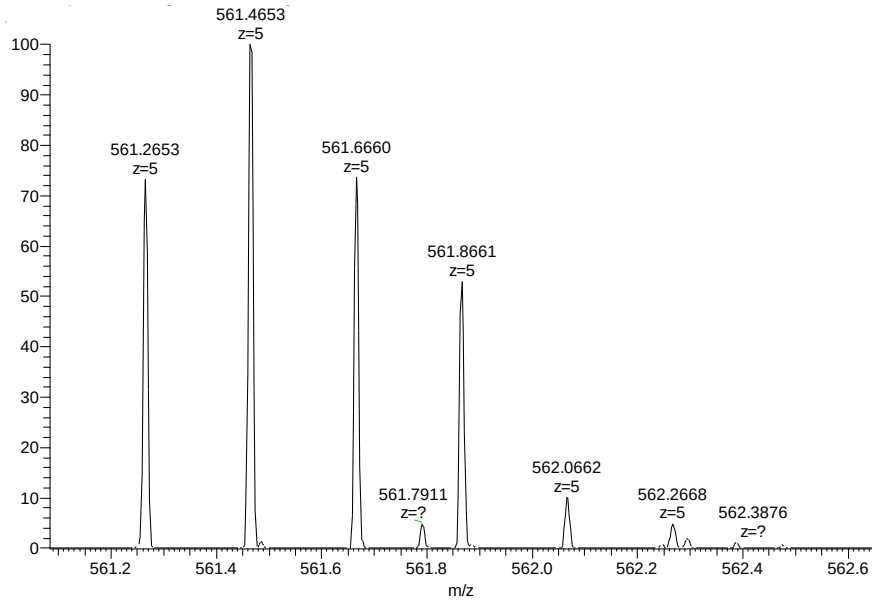

Figure 4.1. Precursor ion MS spectra for cross-linked peptide holo b_5: ^{48}EQAGGDATENFEDVGHSTDAR^{68} - CYP2A6: ^{124}AKQLR^{128}. Measured quintuple charged ion $[M + 5H]^{5+}$ = 561.2653 for ion no.1 in Table 4.1.

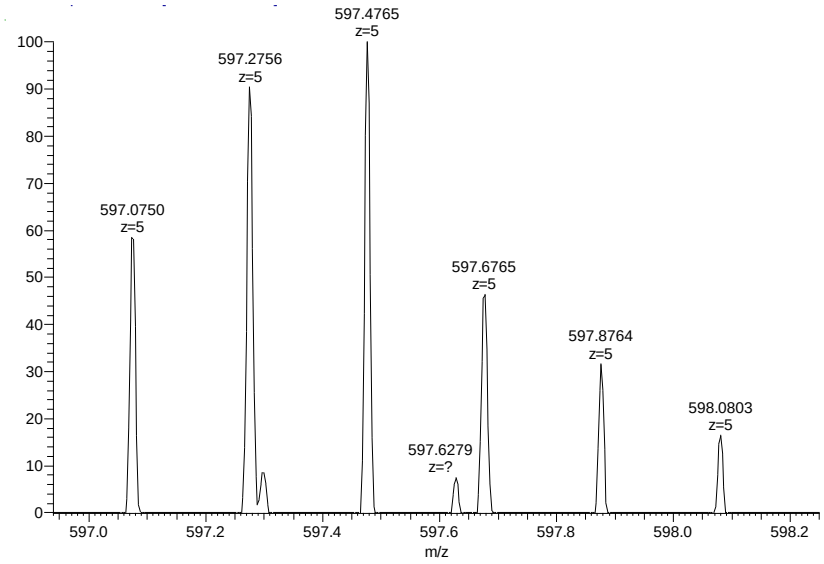

Figure 4.2 Precursor ion MS spectra for cross-linked peptide holo b_5: ^{48}EQAGGDATENFEDVGHSTDAR^{68} - CYP2A6: ^{376}KDTKFR^{381}. Measured quintuple charged ion $[M + 5H]^{5+}$ = 597.0750 for ion no.2 in Table 4.1.

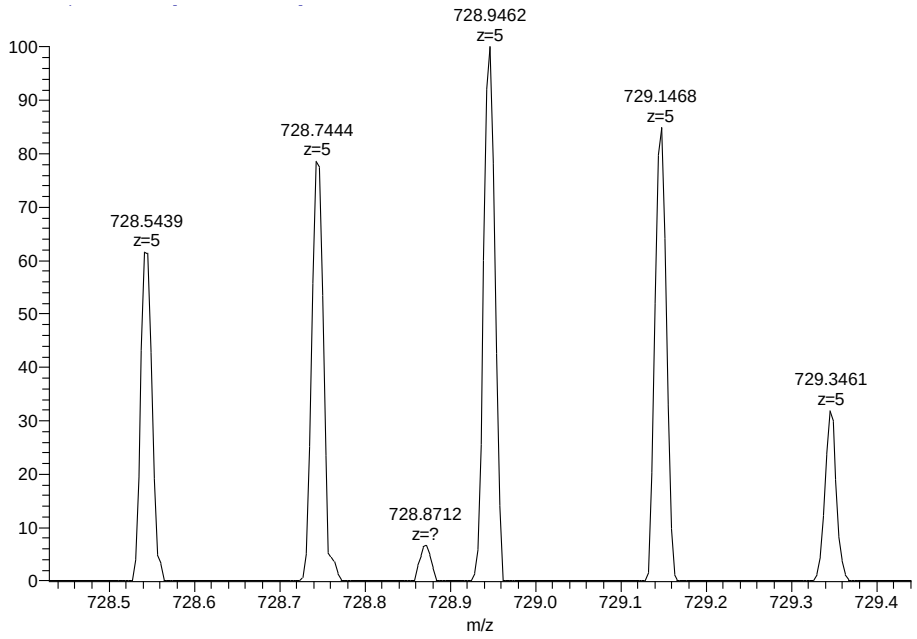

Figure 4.3 Precursor ion MS spectra for cross-linked peptide holo b_5: ^{48}EQAGGDATENFEDVGHSTDAR^{68} - CYP2A6: ^{425}KSDAFVPFSIGKR^{437}. Measured quintuple charged ion $[M + 5H]^{5+}$ = 728.5439 for ion no.3 in Table 4.1.

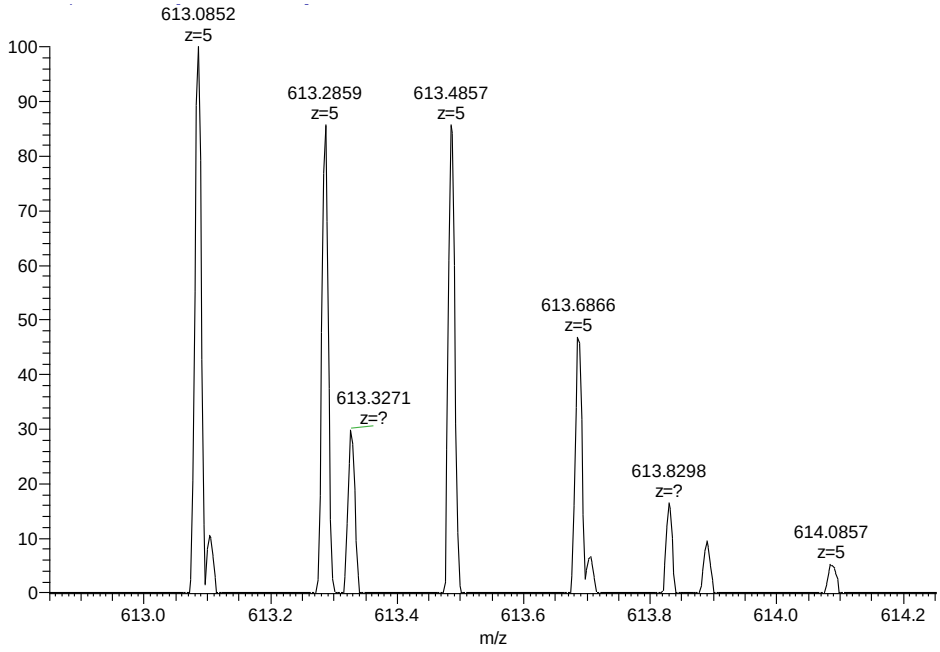

Figure 4.4. Precursor ion MS spectra for cross-linked peptide holo b_5: ^{48}EQAGGDATENFEDVGHSTDAR^{68} - CYP2A6: ^{462}LKSSQSPK^{469}. Measured quintuple charged ion $[M + 5H]^{5+}$ = 613.0852 for ion no.4 in Table 4.1.

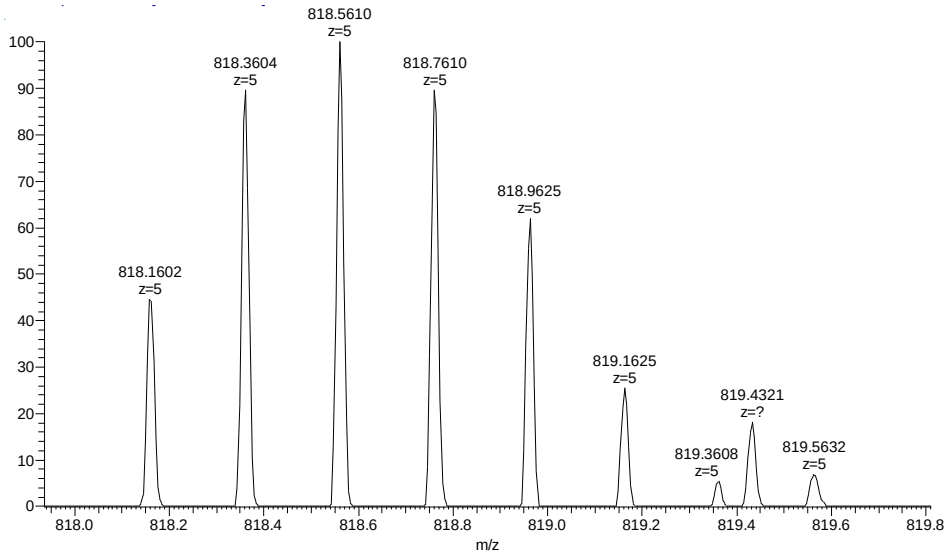

Figure 4.5. Precursor ion MS spectra for cross-linked peptide holo b5: 48EQAGGDATENFEDVGHSTDAR68 - CYP2A6: 275MQEEEKNPNTEFYLK289. Measured quintuple charged ion $[M + 5H]^{5+}$ = 818.1609 for ion no.5 in Table 4.1.

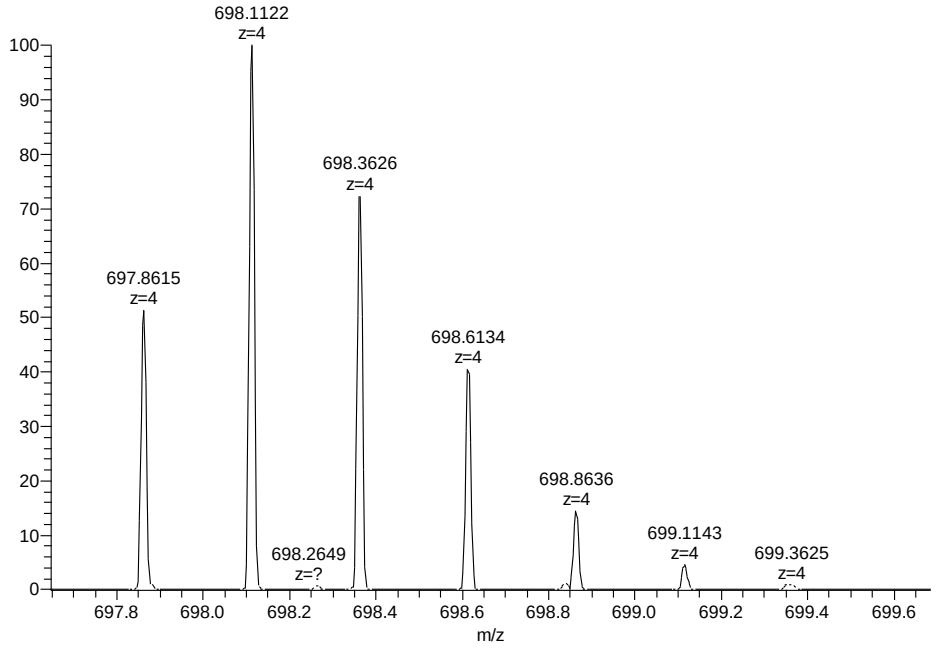

Figure 4.6. Precursor ion MS spectra for cross-linked peptide holo b_5: ^{35}FLEEHPGGEEVLR^{47} - CYP2A6: ^{425}KSDAFVPFSIGKR^{437}. Measured quintuple charged ion $[M + 4H]^{4+}$ = 696.8615 for ion no.6 in Table 4.1.

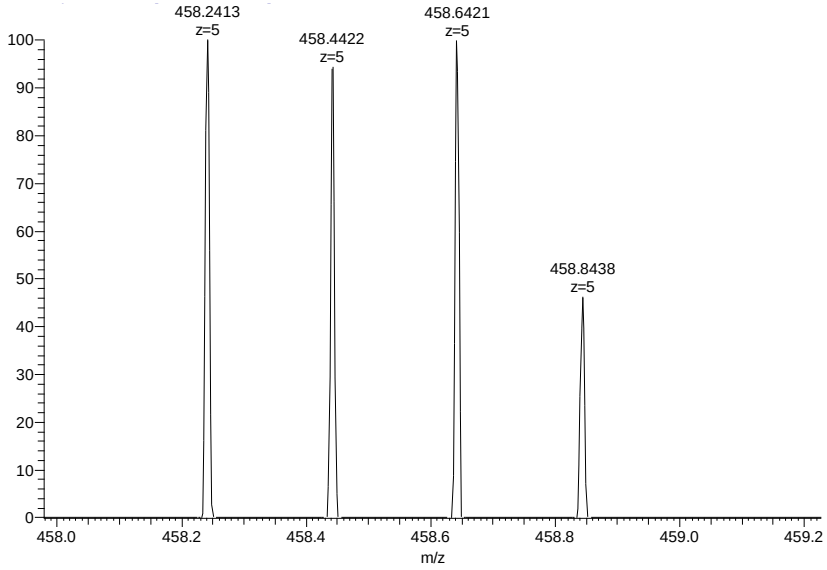

Figure 4.7. Precursor ion MS spectra for cross-linked peptide holo b_5: ^{35}FLEEHPGGEEVLR^{47} - CYP2A6: ^{376}KDTKFR^{381}. Measured quintuple charged ion $[M + 5H]^{5+}$ = 458.2413 for ion no.7 in Table 4.1.

(A)

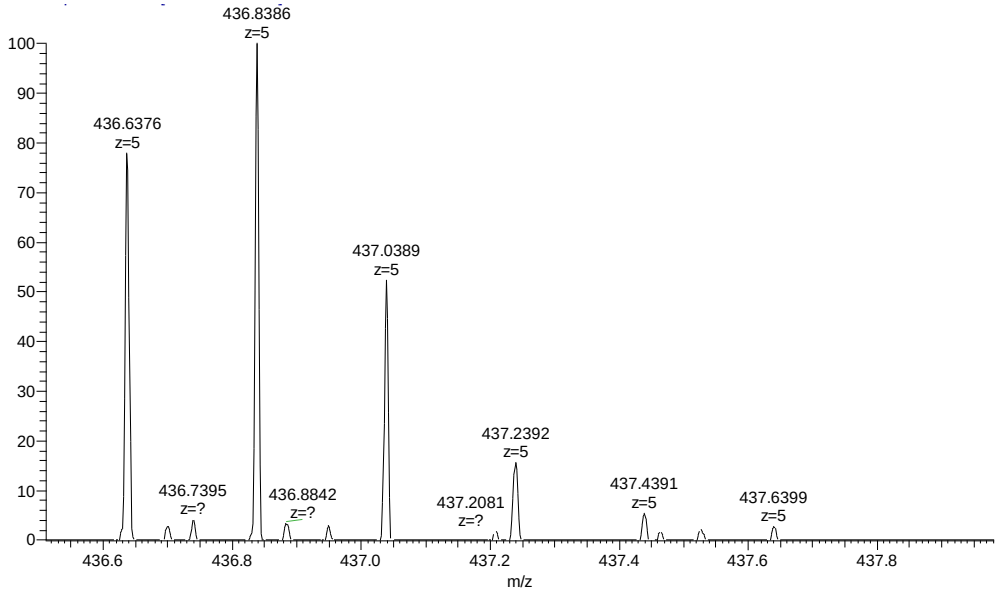

(B)

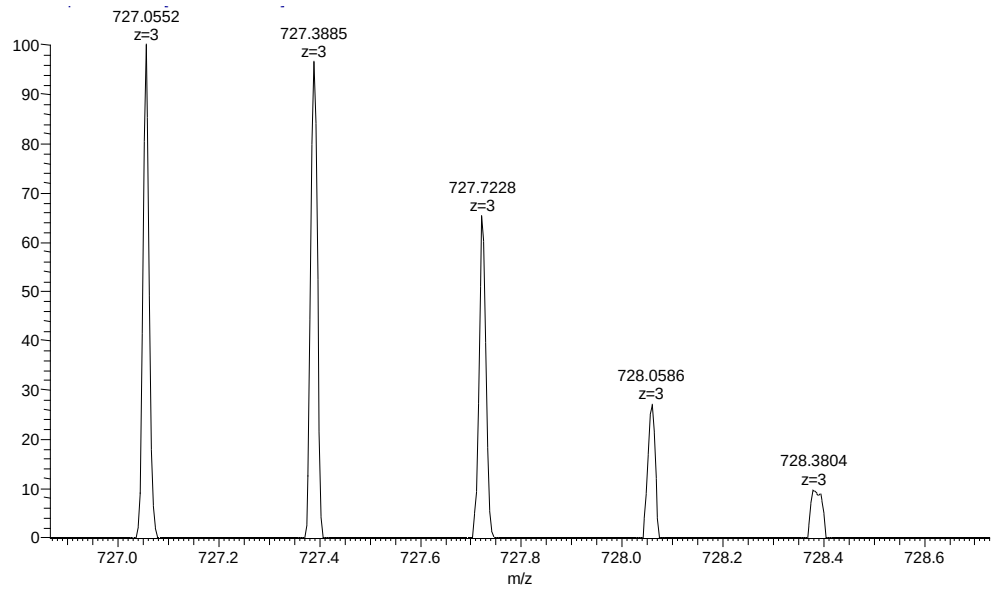

Figure 4.8. Precursor ion MS spectra for cross-linked peptide holo b_5: ^{35}FLEEHPGGEEVLR^{47} - CYP2A6: ^{334}VIGKNR^{339} for ion no.7 in Table 4.1. (A) Measured quintuple charged ion $[M + 5H]^{5+}$ = 436.6376. (B) Measured quintuple charged ion $[M + 3H]^{3+}$ = 727.0552.

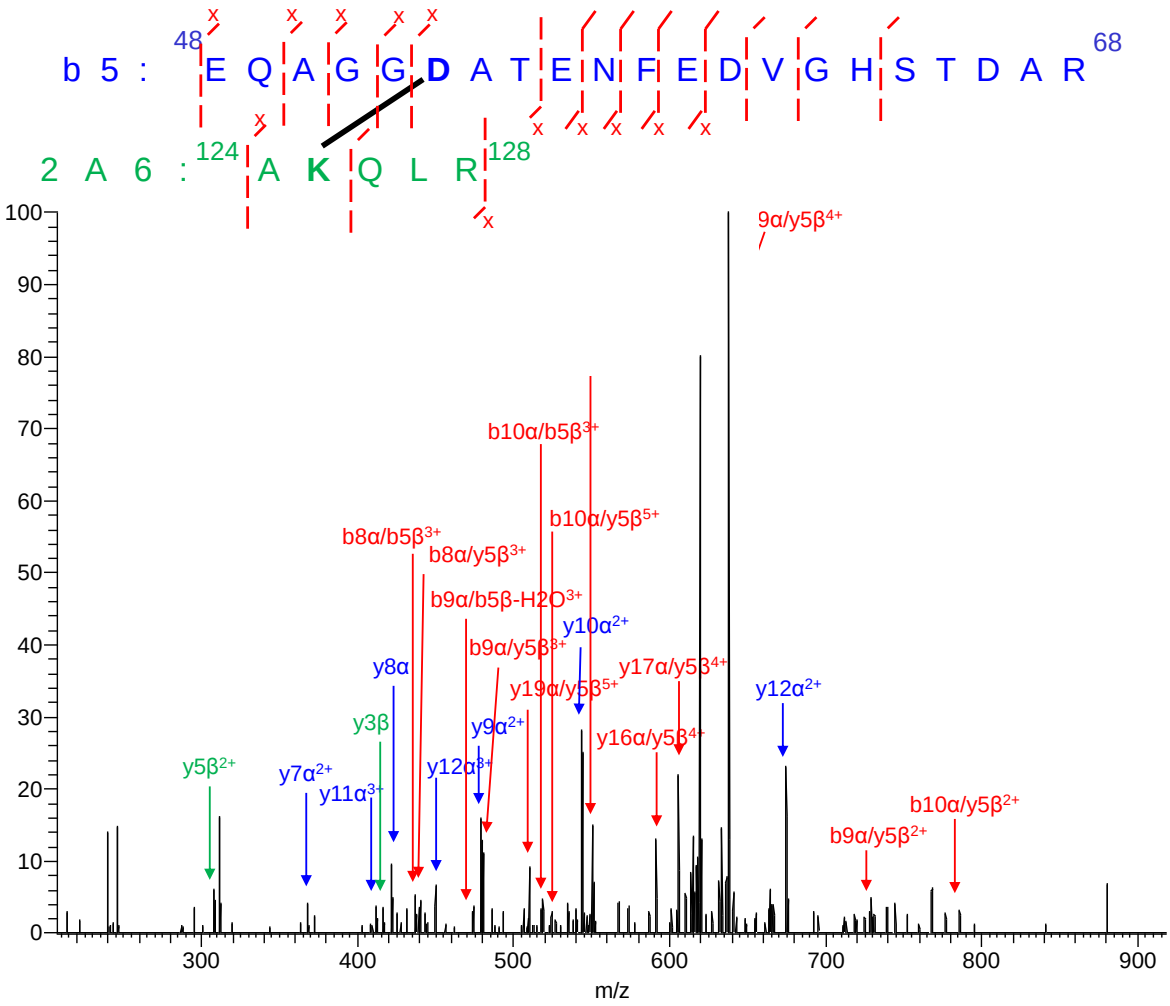

Figure 4.9. Tandem mass spectra for the cross-linked peptide precursor ion No.1 in Table 4.1 with m/z of 561.2653 z=5 for holo b_5: ^{48}EQAGGDATENFEDVGHSTDAR^{68} - CYP2A6: ^{124}AKQLR^{128} identified from holo b5-CYP2A6 complex. Peptide from holo b5 is designated as α, and peptide from CYP2A6 is designated as β. Fragment ions with superscript "x" represent the cross-linked fragment ions. Cross-linked residues are indicated in bold letter. Identified cross-linked residue pairs are linked by bold black lines.

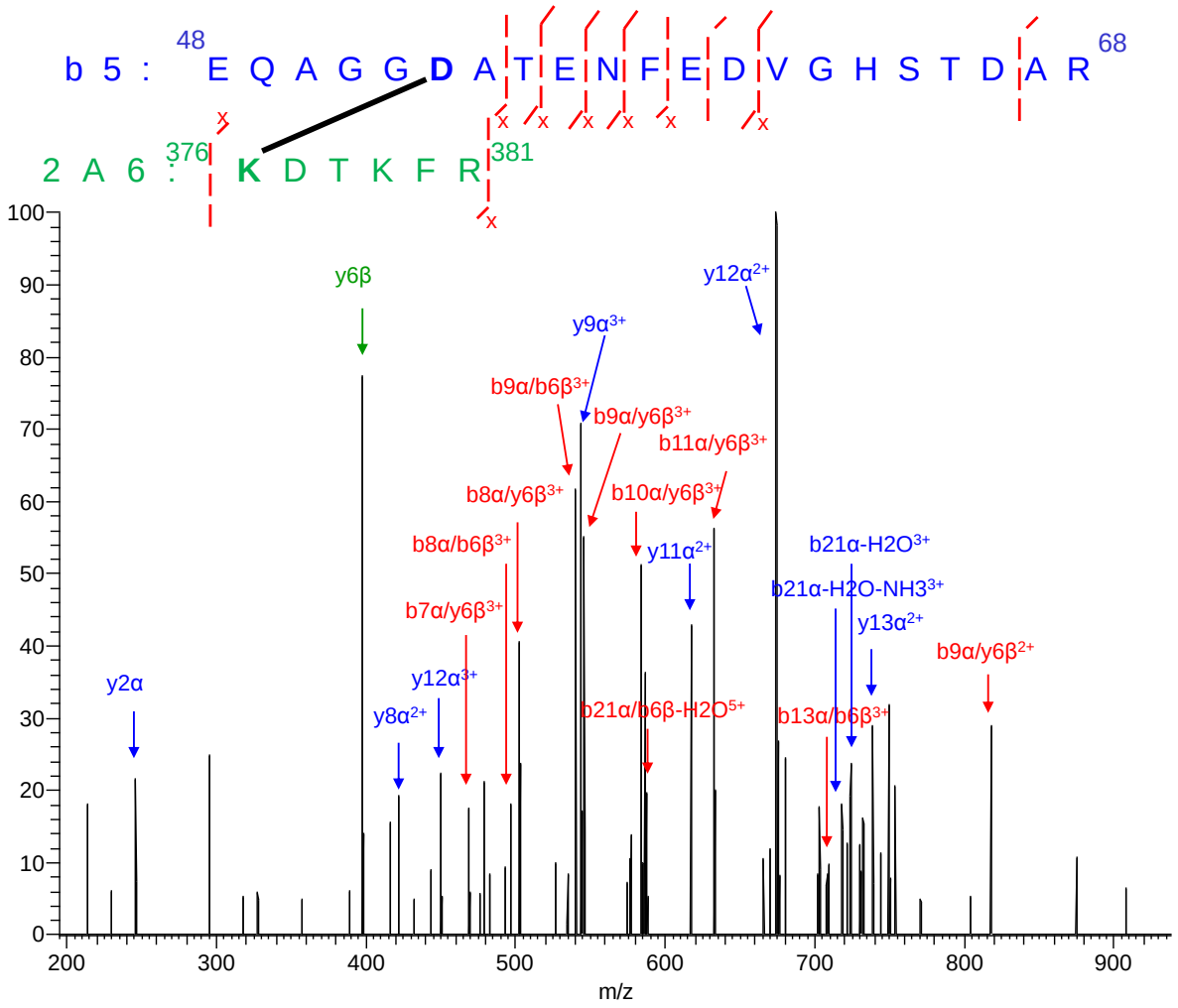

Figure 4.10. Tandem mass spectra for the cross-linked peptide precursor ion No.2 in Table 4.1 with m/z of 590.0750 z=5 for holo b_5: ^{48}EQAGGDATENFEDVGHSTDAR^{68} - CYP2A6: ^{376}KDTKFR^{381} identified from holo b5-CYP2A6 complex. Peptide from holo b5 is designated as α, and peptide from CYP2A6 is designated as β. Fragment ions with superscript "x" represent the cross-linked fragment ions. Identified cross-linked residue pairs are linked by bold black lines.

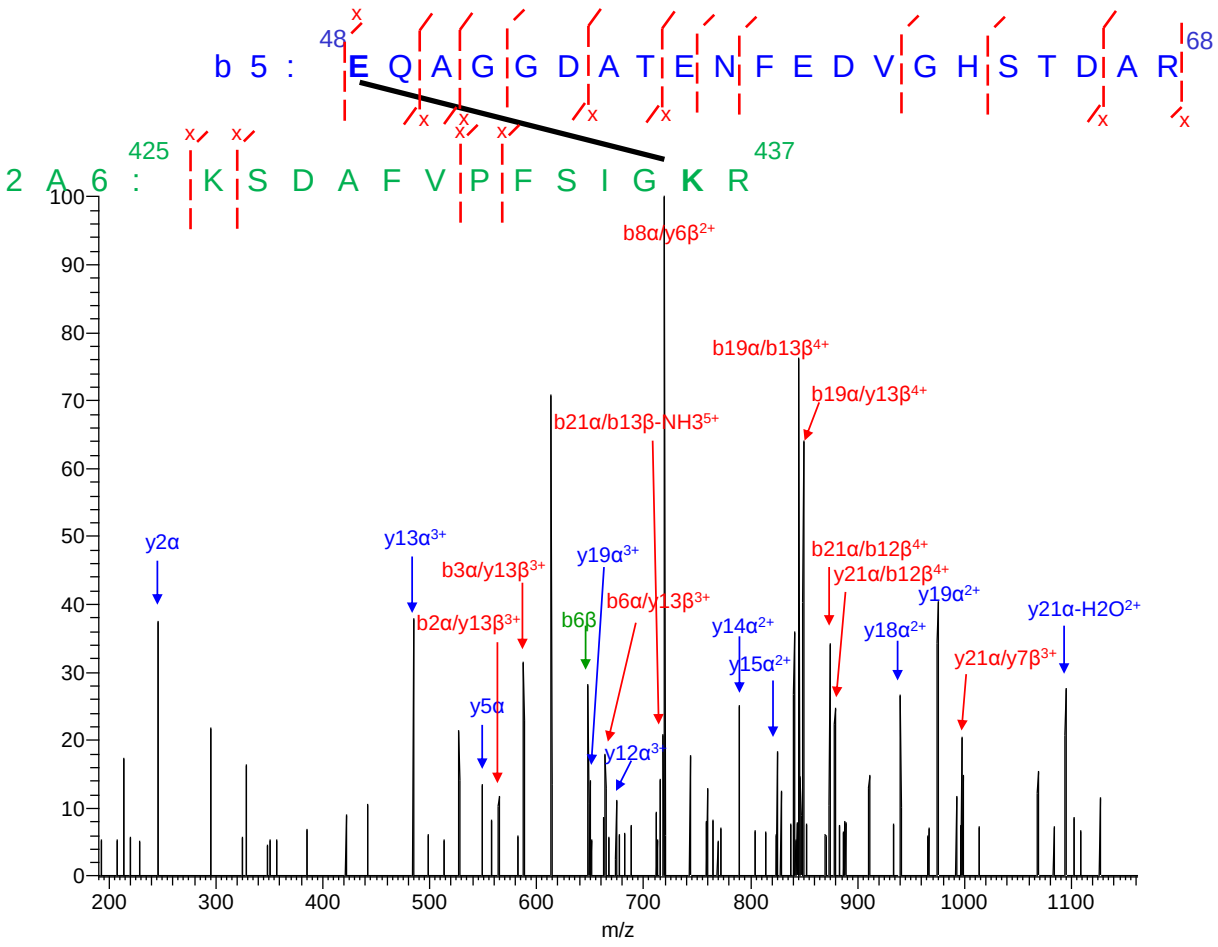

Figure 4.11. Tandem mass spectra for the cross-linked peptide precursor ion No.3 in Table 4.1 with m/z of 728.5439 z=5 for holo b_5: ^{48}EQAGGDATENFEDVGHSTDAR^{68} - CYP2A6: ^{425}KSDAFVPFSIGKR^{437} identified from holo b5-CYP2A6 complex. Peptide from holo b5 is designated as α, and peptide from CYP2A6 is designated as β. Fragment ions with superscript "x" represent the cross-linked fragment ions. Identified cross-linked residue pairs are linked by bold black lines.

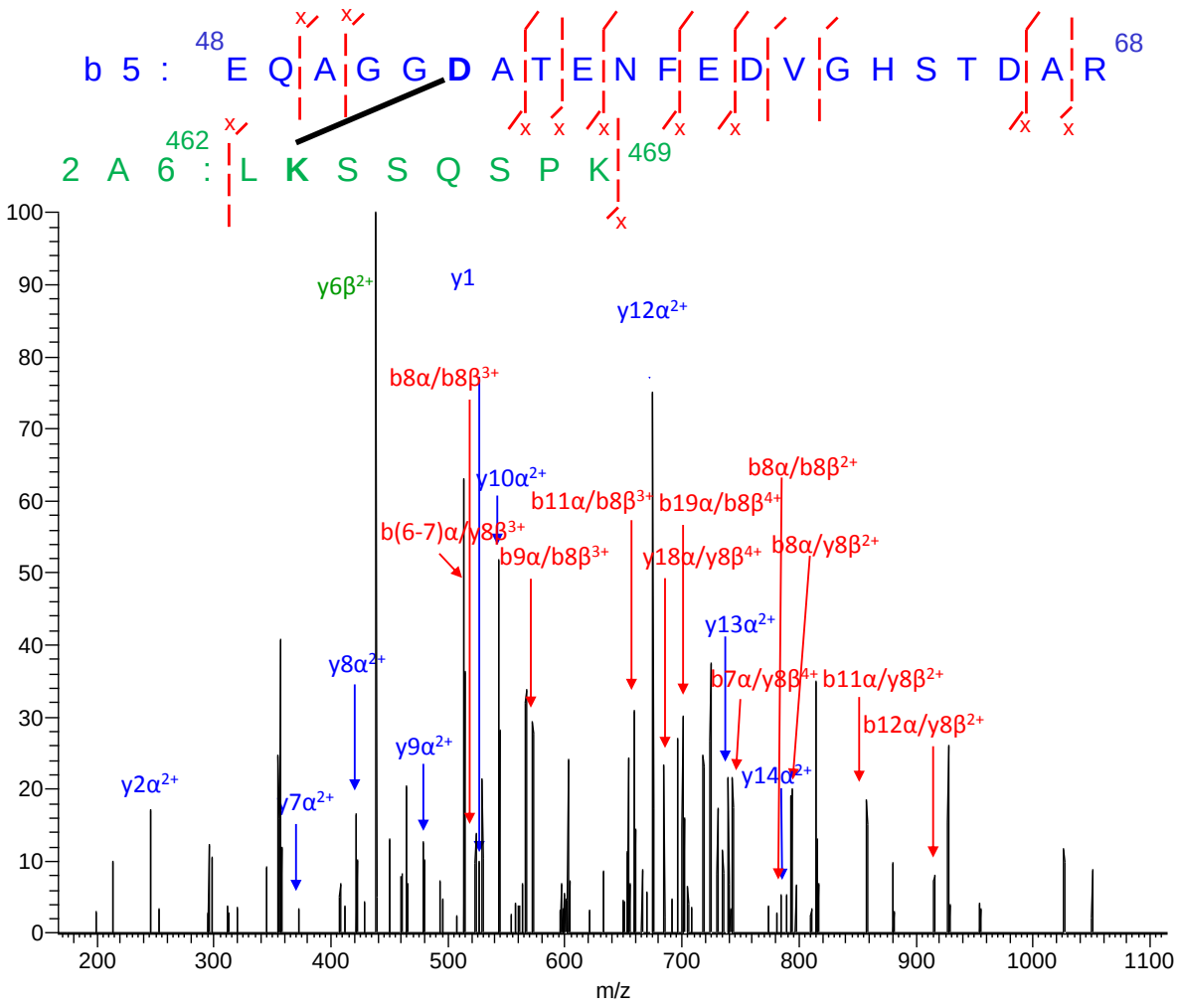

Figure 4.12 Tandem mass spectra for the cross-linked peptide precursor ion No.4 in Table 4.1 with m/z of 613.0852 z=5 for holo b_5: ^{48}EQAGGDATENFEDVGHSTDAR^{68} - CYP2A6: ^{462}LKSSQSPK^{469} identified from holo b5-CYP2A6 complex. Peptide from holo b5 is designated as α, and peptide from CYP2A6 is designated as β. Fragment ions with superscript "x" represent the cross-linked fragment ions. Identified cross-linked residue pairs are linked by bold black lines.

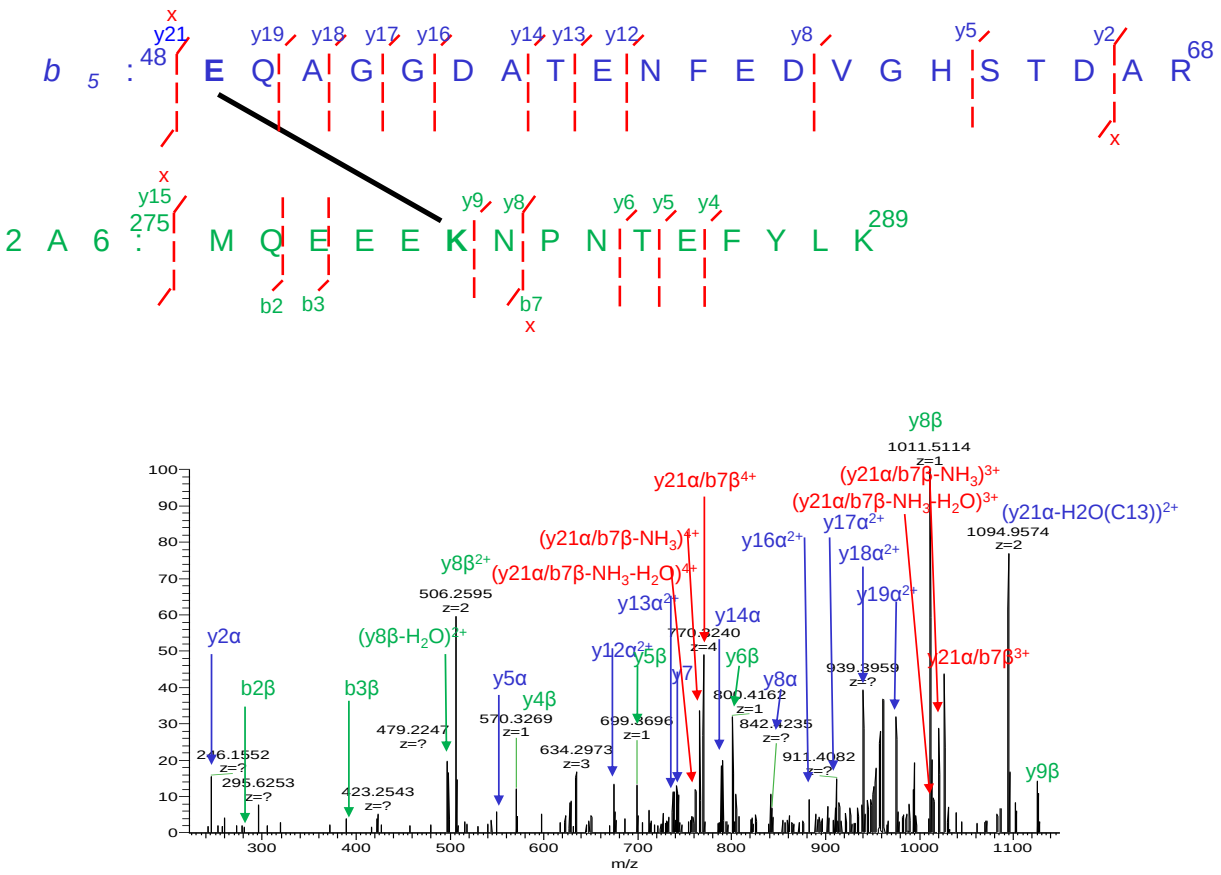

Figure 4.13 Tandem mass spectra for the cross-linked peptide precursor ion No.5 in Table 4.1 with m/z of 818.1609 z=5 for holo b5: ^{48}EQAGGDATENFEDVGHSTDAR^{68} - CYP2A6: ^{275}MQEEEKNPNTEFYLK^{289} identified from holo b5-CYP2A6 complex. Peptide from holo b5 is designated as α, and peptide from CYP2A6 is designated as β. Fragment ions with superscript "x" represent the cross-linked fragment ions. Identified cross-linked residue pairs are linked by bold black lines.

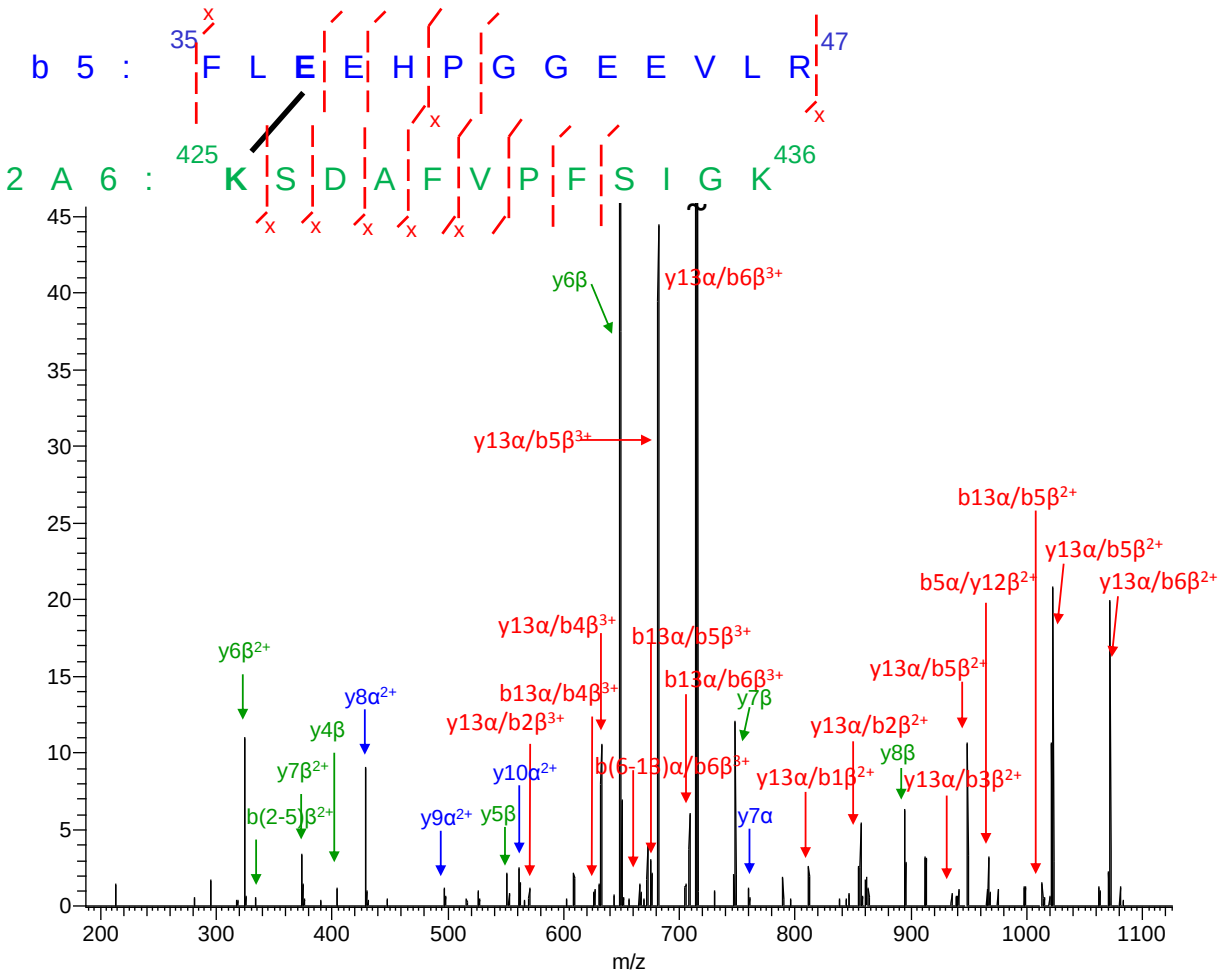

Figure 4.14. Tandem mass spectra for the cross-linked peptide precursor ion No.6 in Table 4.1 with m/z of 697.8615 z=4 for holo b_5: ^{35}FLEEHPGGEEVLR^{47} - CYP2A6: ^{425}KSDAFVPFSIGK^{436} identified from holo b5-CYP2A6 complex. Peptide from holo b5 is designated as α, and peptide from CYP2A6 is designated as β. Fragment ions with superscript "x" represent the cross-linked fragment ions. Identified cross-linked residue pairs are linked by bold black lines.

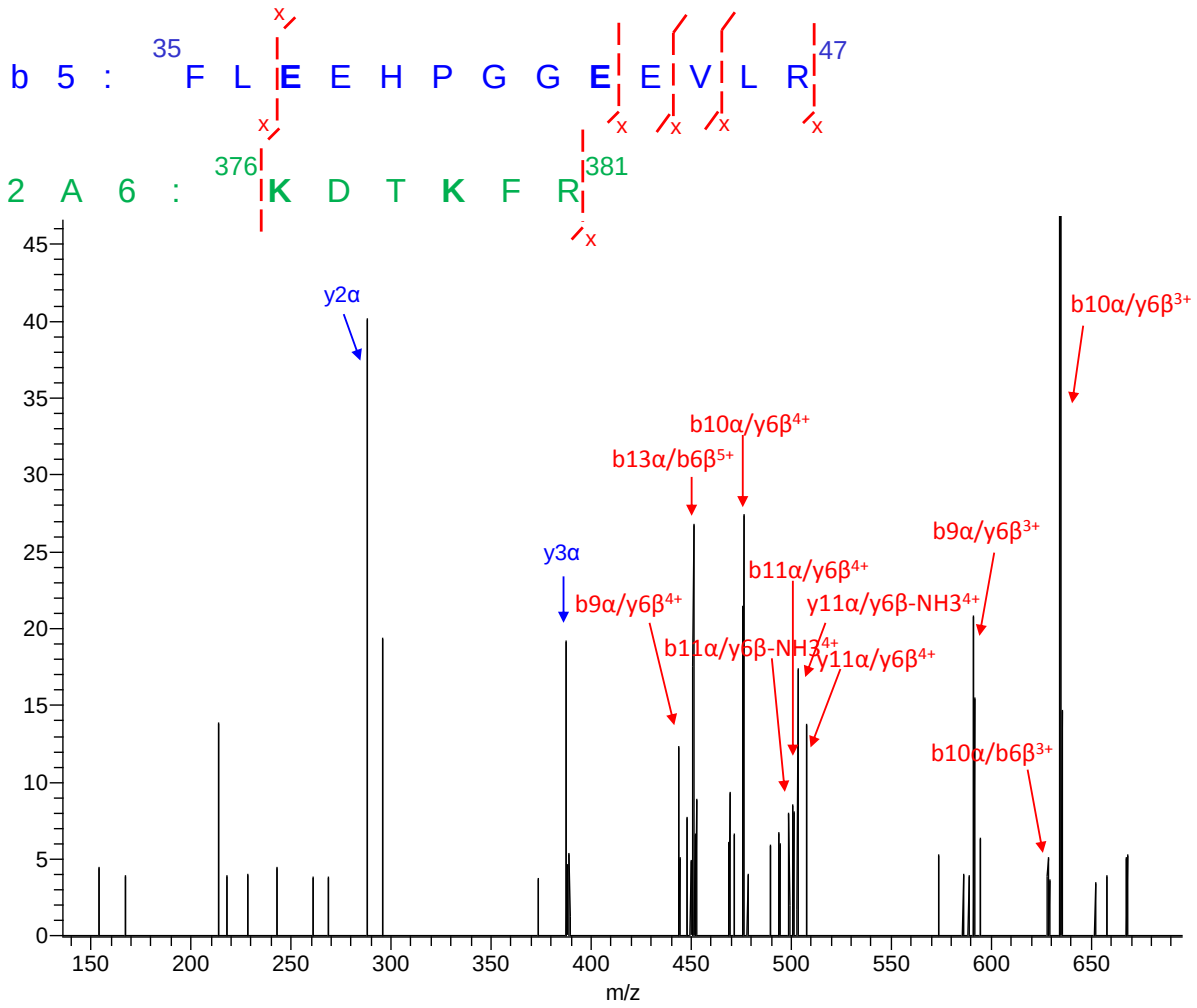

Figure 4. 15. Tandem mass spectra for the cross-linked peptide precursor ion No.7 in Table 4.1 with m/z of 458.2413 z=5 for holo b_5: ^{35}FLEEHPGGEEVLR^{47} - CYP2A6: ^{376}KDTKFR^{381} identified from holo b5-CYP2A6 complex. Peptide from holo b5 is designated as α, and peptide from CYP2A6 is designated as β. Fragment ions with superscript "x" represent the cross-linked fragment ions. Identified cross-linked residue pairs are linked by bold black lines.

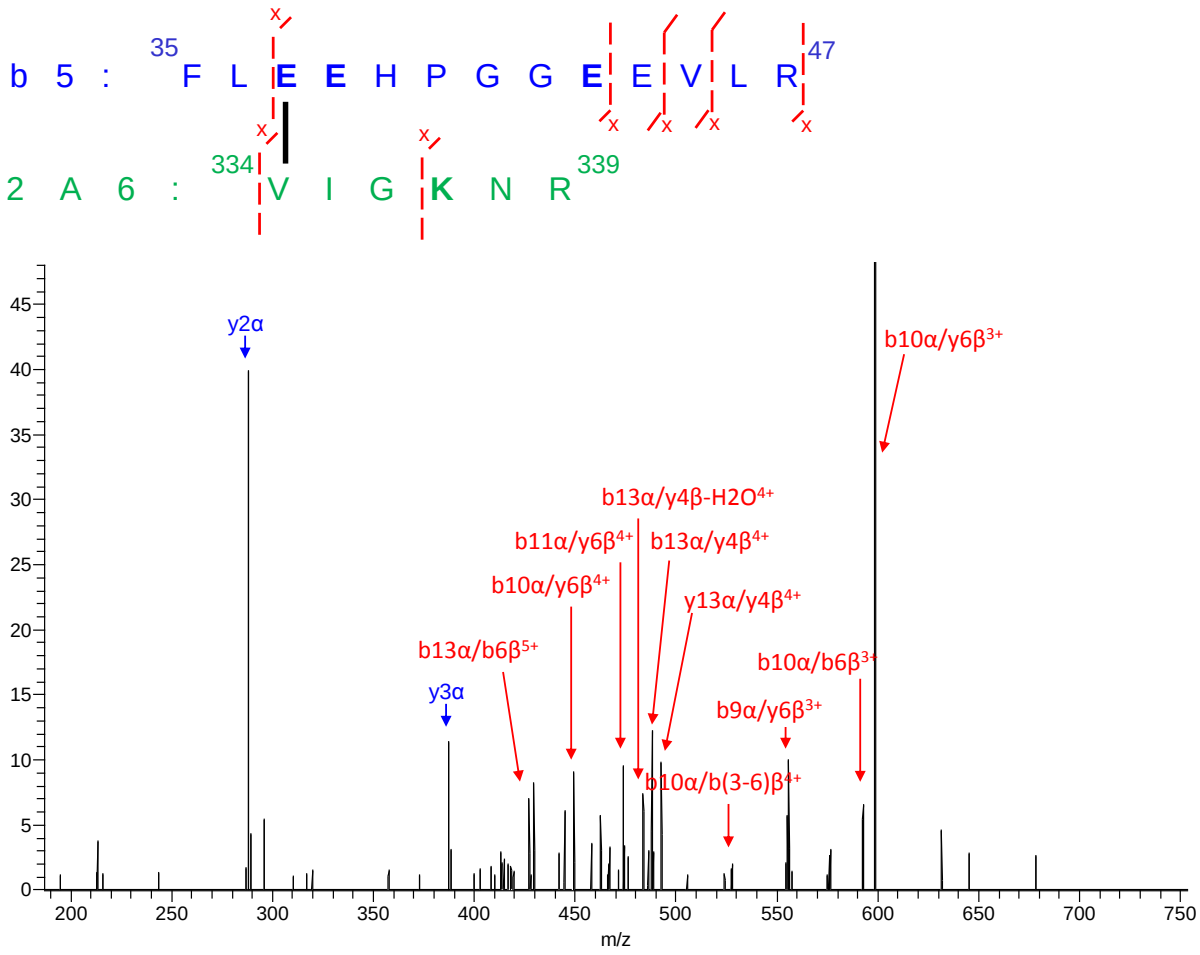

Figure 4.16. Tandem mass spectra for the cross-linked peptide precursor ion No.8 in Table 4.1 with m/z of 436.6376 z=5 for holo b_5: ^{35}FLEEHPGGEEVLR^{47} - CYP2A6: ^{334}VIGKNR^{339} identified from holo b5-CYP2A6 complex. Peptide from holo b5 is designated as α, and peptide from CYP2A6 is designated as β. Fragment ions with superscript "x" represent the cross-linked fragment ions. Identified cross-linked residue pairs are linked by bold black lines.

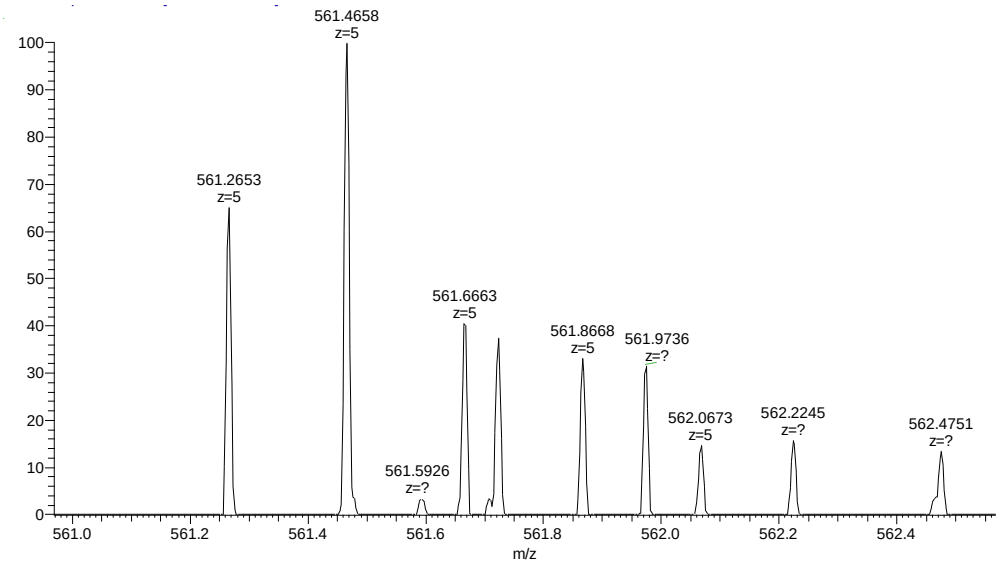

Figure 4.17. Precursor ion MS spectra for cross-linked peptide apo b_5: ^{48}EQAGGDATENFEDVGHSTDAR^{68} - CYP2A6: ^{124}AKQLR^{128} with measured quadruple charged ion $[M + 5H]^{5+}$ = 561.2653 for ion no.1 in Table 4.10.

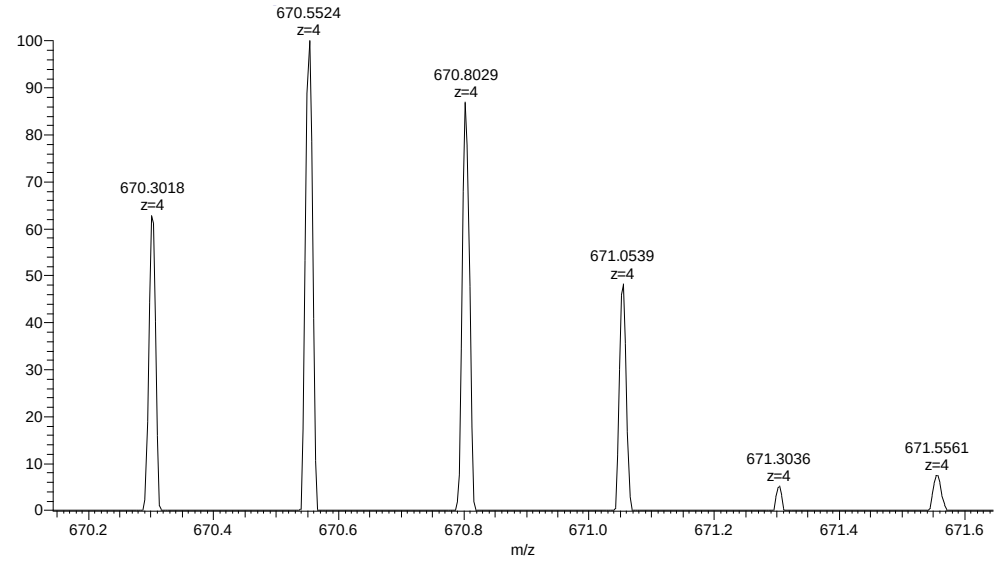

Figure 4.18. Precursor ion MS spectra for cross-linked peptide apo b_5: ^{48}EQAGGDATENFEDVGHSTDAR^{68} - CYP2A6: ^{376}KDTK^{379} with measured quadruple charged ion $[M + 4H]^{4+}$ = 670.3018 for ion no.2 in Table 4.10).

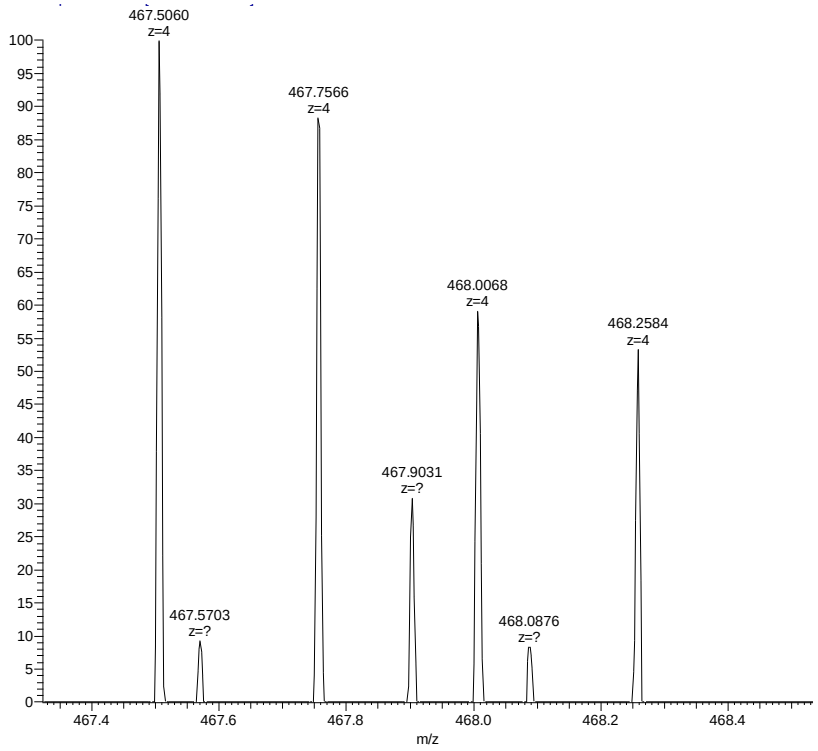

Figure 4.19. Precursor ion MS spectra for cross-linked peptide apo b_5: ^{35}FLEEHPGGEEVLR^{47} - CYP2A6: ^{374}VKK^{376} with measured quadruple charged ion $[M + 4H]^{4+}$ = 467.5060 for ion no.3 in Table 4.10).

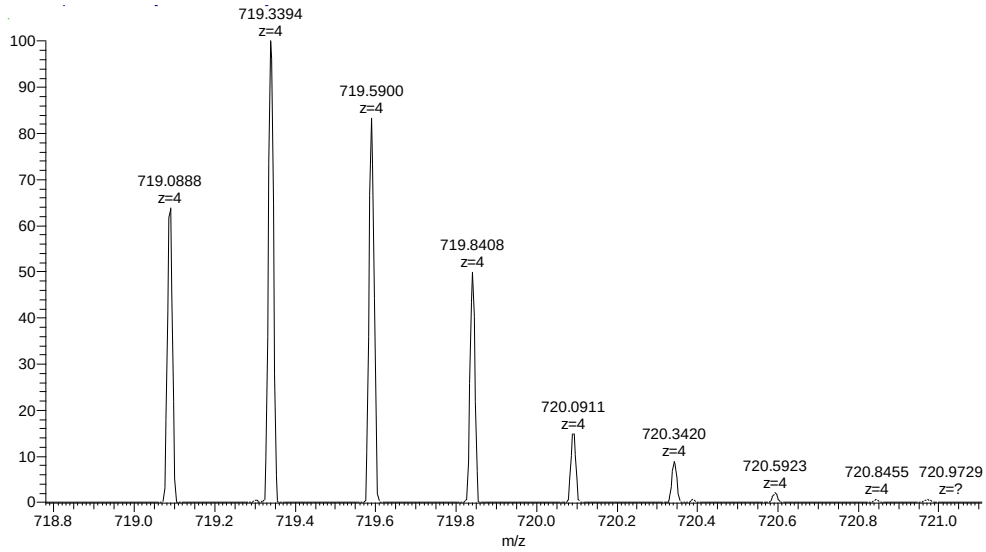

Figure 4.20. Precursor ion MS spectra for cross-linked peptide apo b_5: ^{35}FLEEHPGGEEVLR^{47}- CYP2A6: ^{334}VIGKNR^{339} with measured quadruple charged ion $[M + 4H]^{4+}$ = 545.5444 for ion no.4 in Table 4.10).

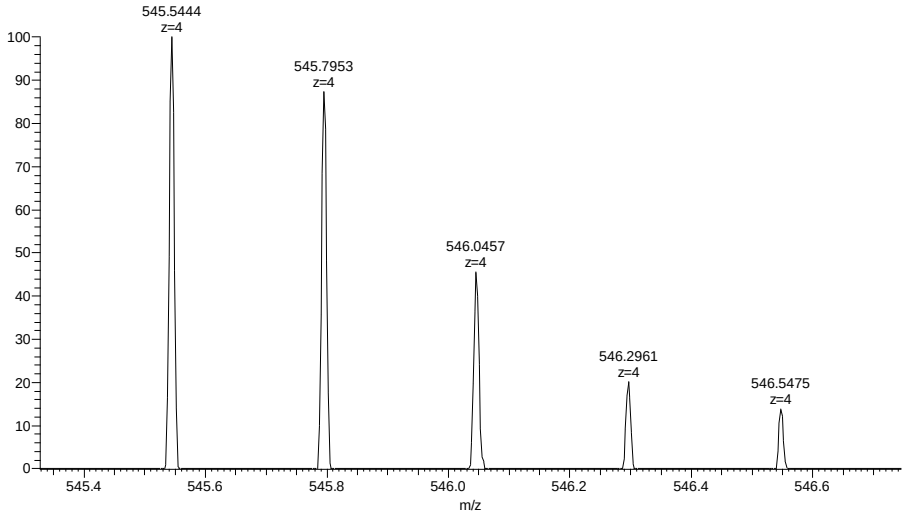

Figure 4.21. Precursor ion MS spectra for cross-linked peptide apo b_5: ^{35}FLEEHPGGEEVLR^{47} - CYP2A6: ^{334}VIGKNR^{339} with measured quadruple charged ion $[M + 4H]^{4+}$ = 719.0888 for ion no.5 in Table 4.10).

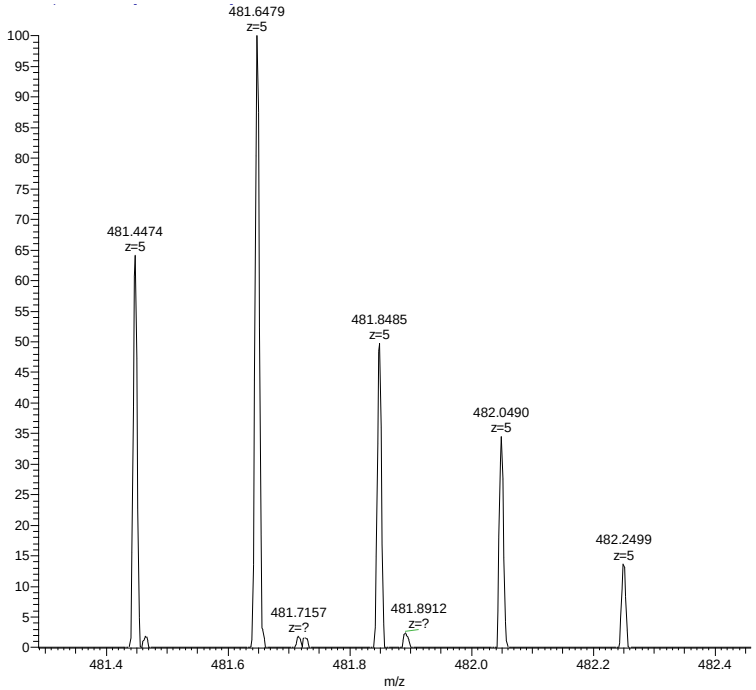

Figure 4.22. Precursor ion MS spectra for cross-linked apo b_5: ^{35}FLEEHPGGEEVLR^{47} - CYP2A6: ^{251}KVEHNQR^{257} with measured quintuple charged ion $[M + 5H]^{5+}$ = 481.4475 for ion no.6 in Table 4.10).

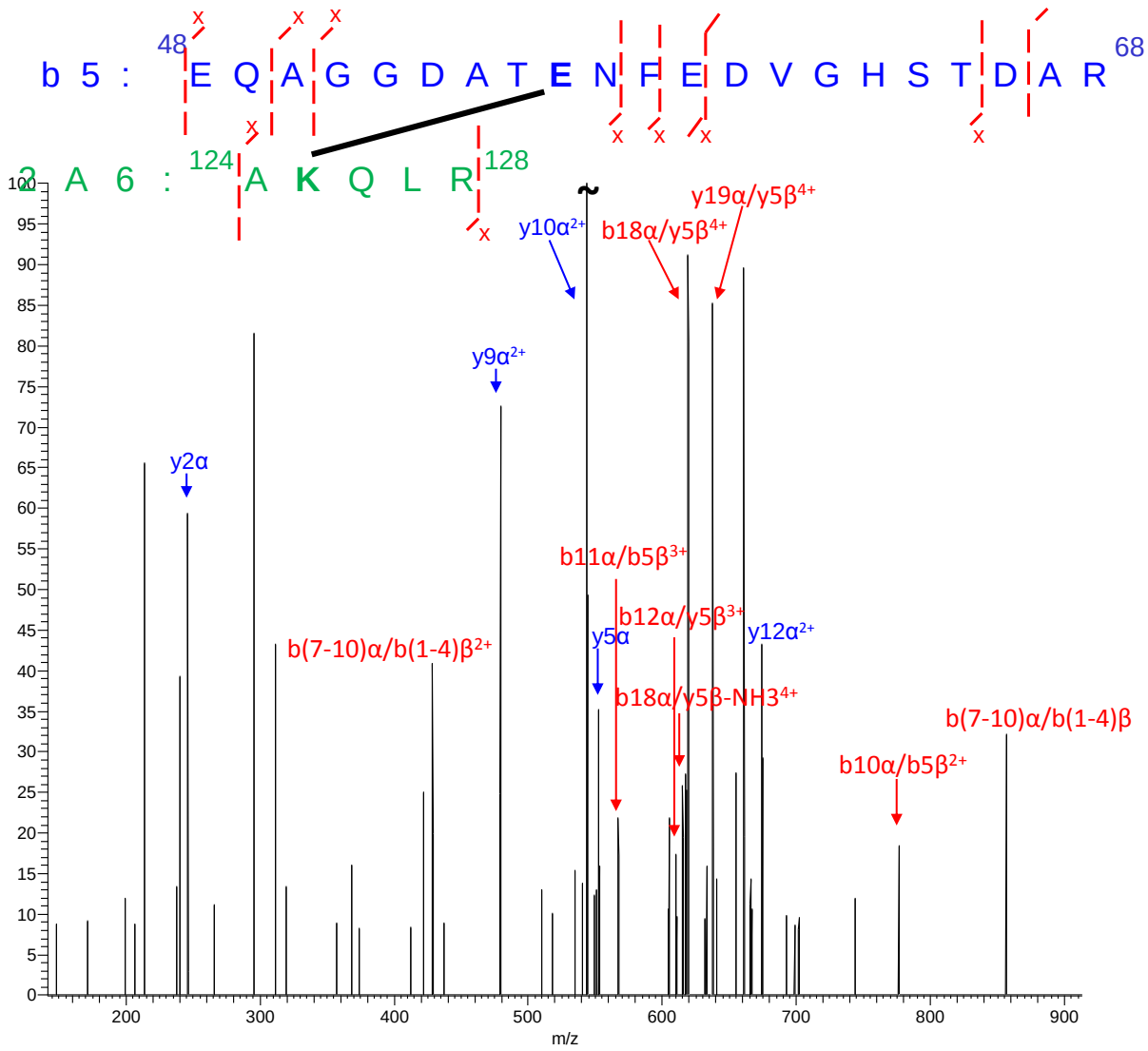

Figure 4.23 Tandem mass spectra for cross-linked peptide precursor ion No.1 in Table 4.2 with m/z of 561.2653 z=5 for peptide apo b_5: ^{48}EQAGGDATENFEDVGHSTDAR^{68} - CYP2A6: ^{124}AKQLR^{128} identified from apo b5-CYP2A6 complex. Peptide from apo b5 is designated as α, and peptide from CYP2A6 is designated as β. Fragment ions with superscript "x" represent the cross-linked fragment ions. Identified cross-linked residue pairs are linked by bold black lines.

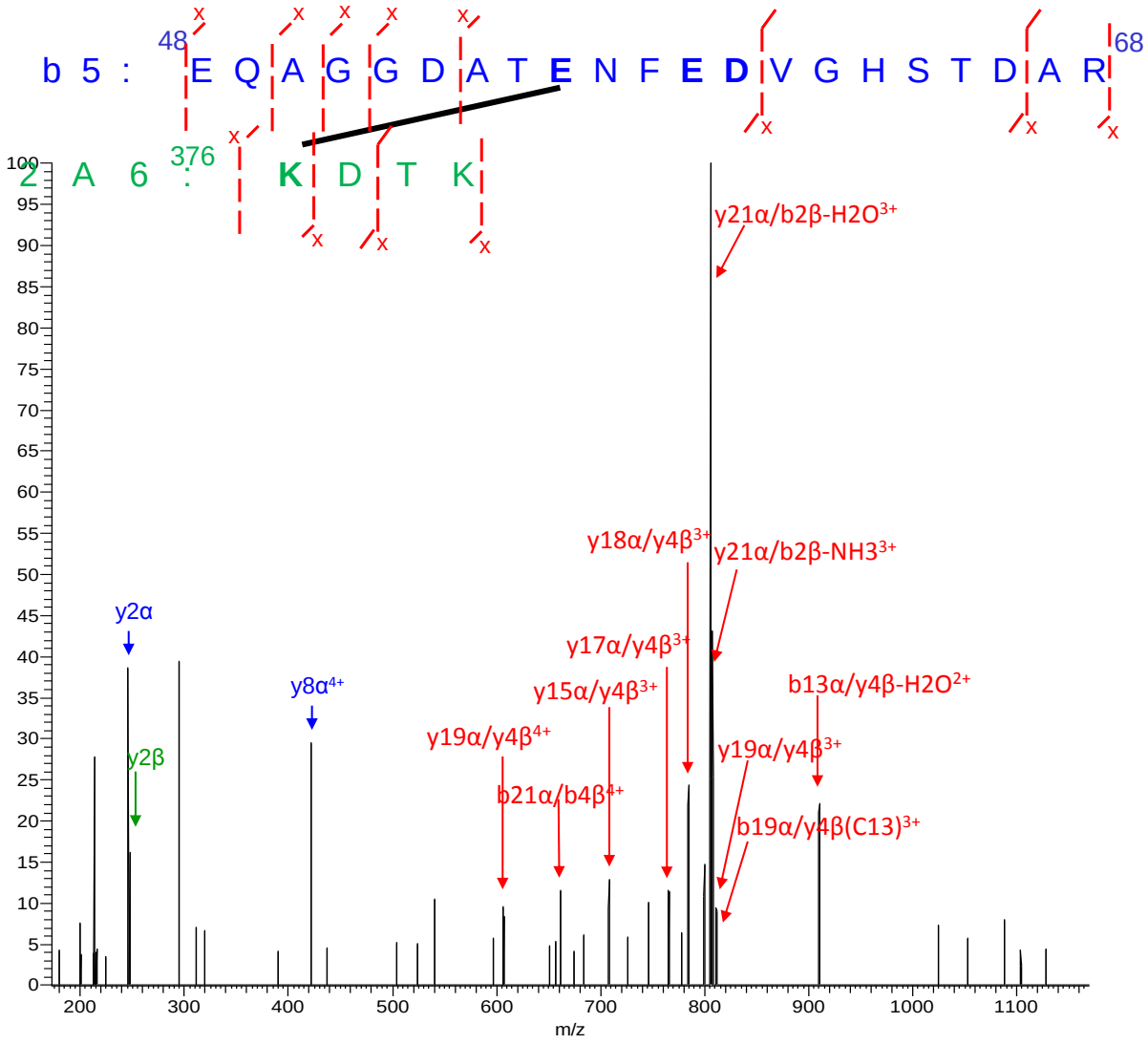

Figure 4.24. Tandem mass spectra for cross-linked peptide precursor ion No.2 in Table 4.2 with m/z of 670.3018 z=4 for apo b_5: ^{48}EQAGGDATENFEDVGHSTDAR^{68} - CYP2A6: ^{376}KDTK^{379} identified from apo b5-CYP2A6 complex. Peptide from apo b5 is designated as α, and peptide from CYP2A6 is designated as β. Fragment ions with superscript "x" represent the cross-linked fragment ions. Identified cross-linked residue pairs are linked by bold black lines.

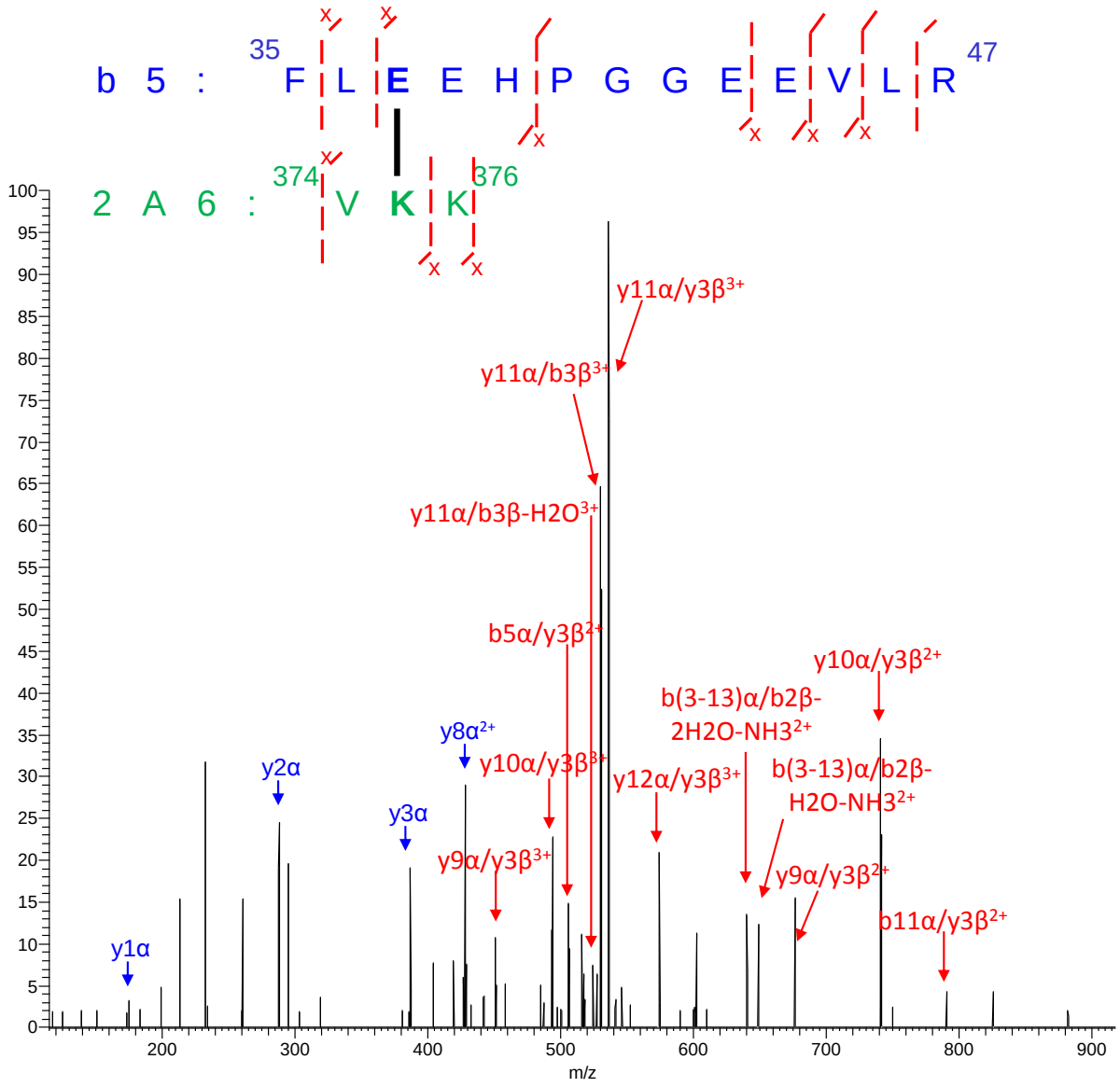

Figure 4.25. Tandem mass spectra for cross-linked peptide precursor ion No.3 in Table 4.10 with m/z of 467.5060 z=4 for apo b_5: ^{35}FLEEHPGGEEVLR^{47} - CYP2A6: ^{374}VKK^{376} identified from apo b5-CYP2A6 complex. Peptide from apo b5 is designated as α, and peptide from CYP2A6 is designated as β. Fragment ions with superscript "x" represent the cross-linked fragment ions. Identified cross-linked residue pairs are linked by bold black lines.

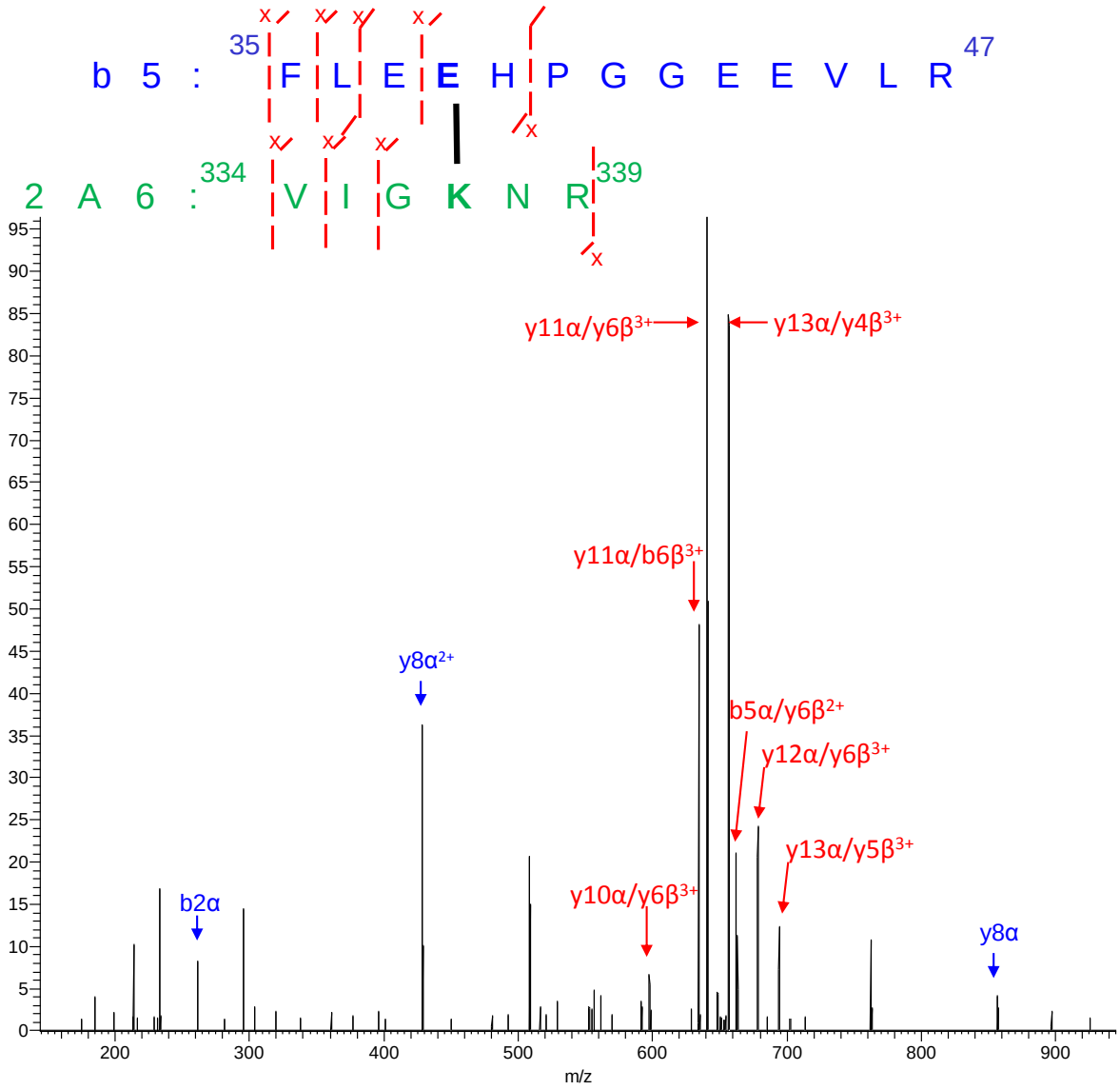

Figure 4.26. Tandem mass spectra for cross-linked peptide precursor ion No.4 in Table 4.10 with m/z of 545.5444 z=4 for apo b_5: ^{35}FLEEHPGGEEVLR^{47}- CYP2A6: ^{334}VIGKNR^{339} identified from apo b5-CYP2A6 complex. Peptide from apo b5 is designated as α, and peptide from CYP2A6 is designated as β. Fragment ions with superscript "x" represent the cross-linked fragment ions. Identified cross-linked residue pairs are linked by bold black lines.

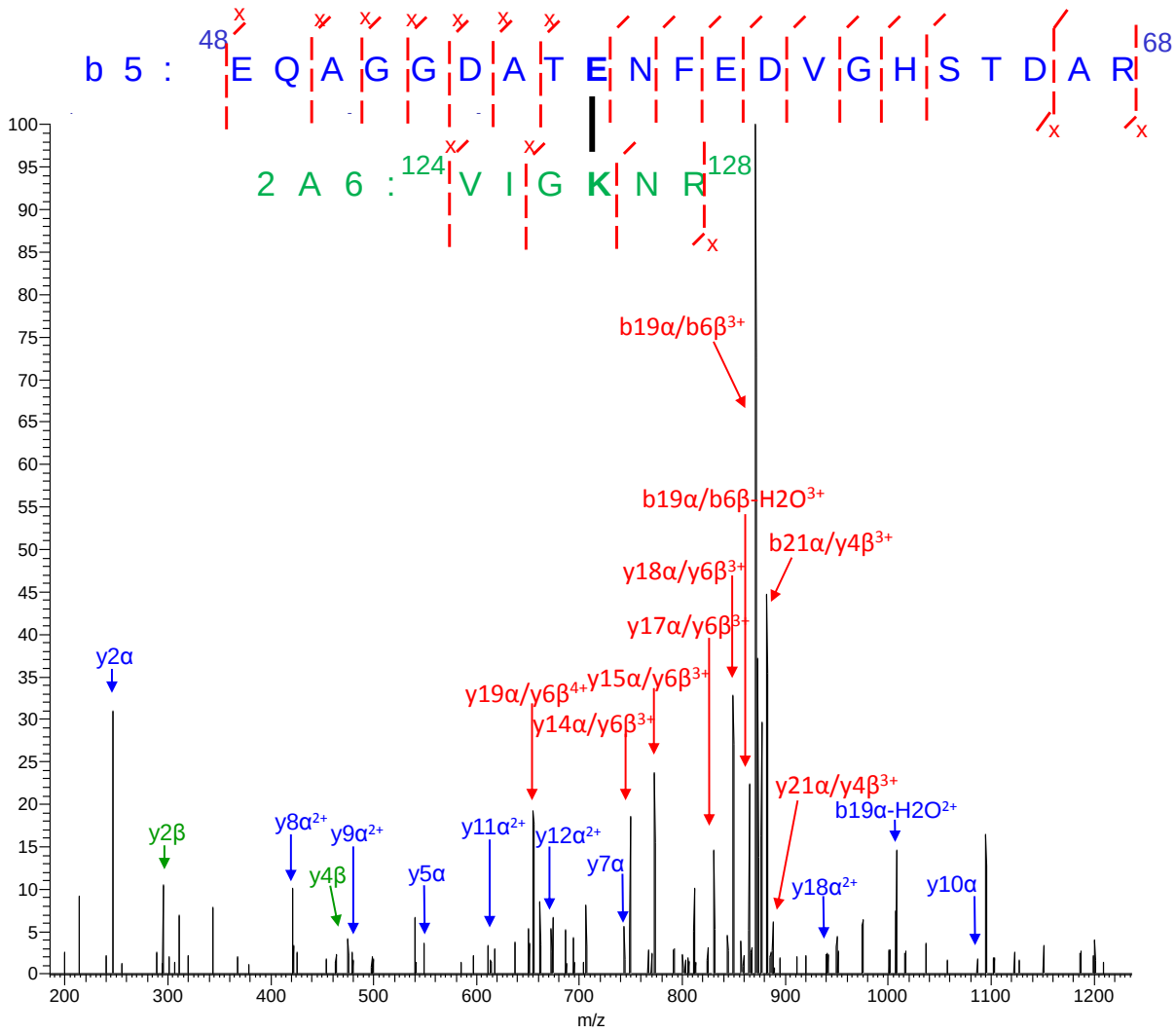

Figure 4.27. Tandem mass spectra for cross-linked peptide precursor ion No.5 in Table 4.1 with m/z of 719.0888 z=4 for apo b_5: ^{35}FLEEHPGGEEVLR^{47}-CYP2A6: ^{334}VIGKNR^{339} identified from apo b5-CYP2A6 complex. Peptide from apo b5 is designated as α, and peptide from CYP2A6 is designated as β. Fragment ions with superscript "x" represent the cross-linked fragment ions. Identified cross-linked residue pairs are linked by bold black lines.

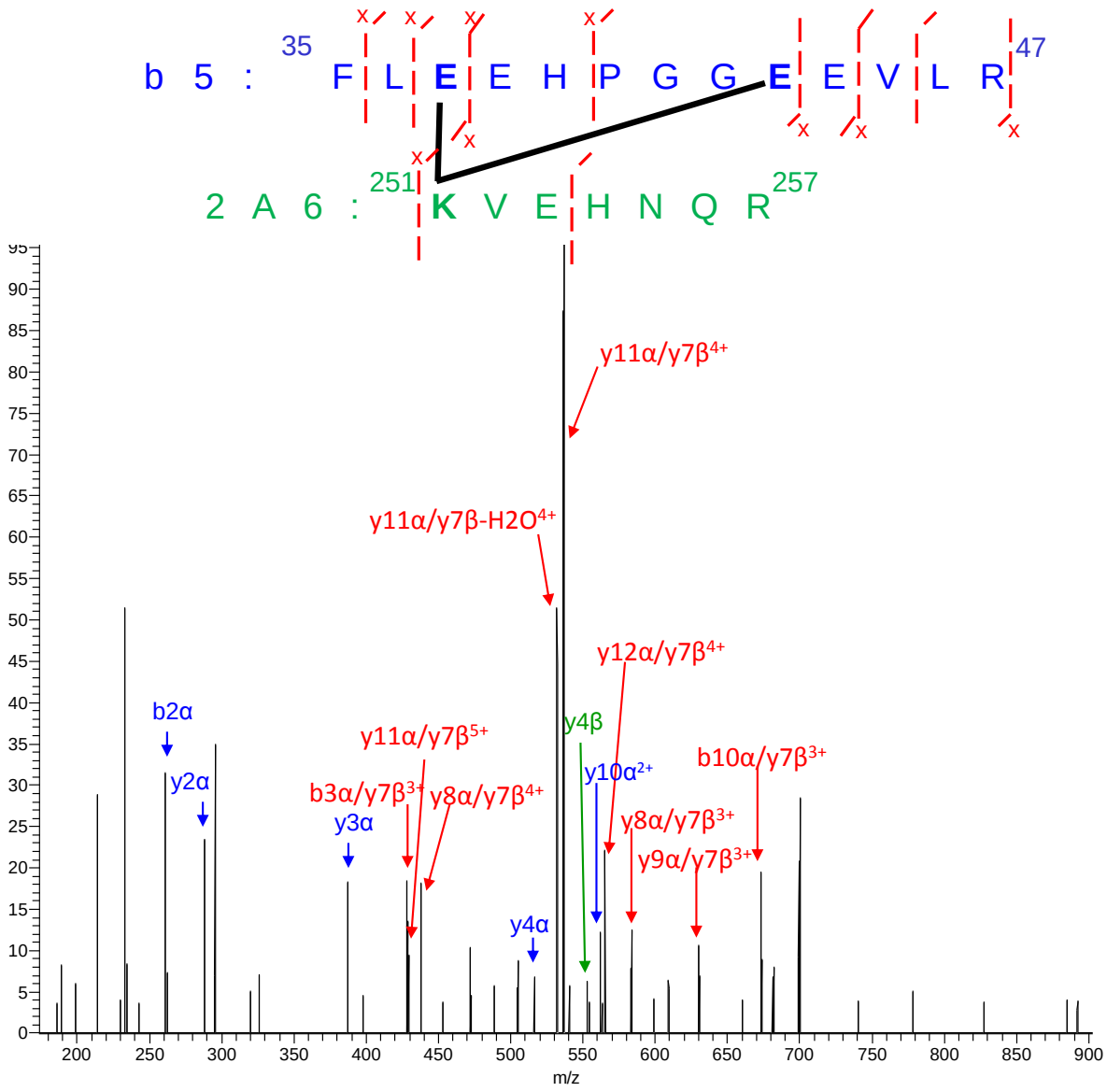

Figure 4.28. Tandem mass spectra for cross-linked peptide precursor ion No.6 in Table 4.10 with m/z of 481.4475 z=5 for apo b_5: ^{35}FLEEHPGGEEVLR^{47}-CYP2A6: ^{251}KVEHNQR^{257} identified from apo b5-CYP2A6 complex. Peptide from apo b5 is designated as α, and peptide from CYP2A6 is designated as β. Fragment ions with superscript "x" represent the cross-linked fragment ions. Identified cross-linked residue pairs are linked by bold black lines.

(A)

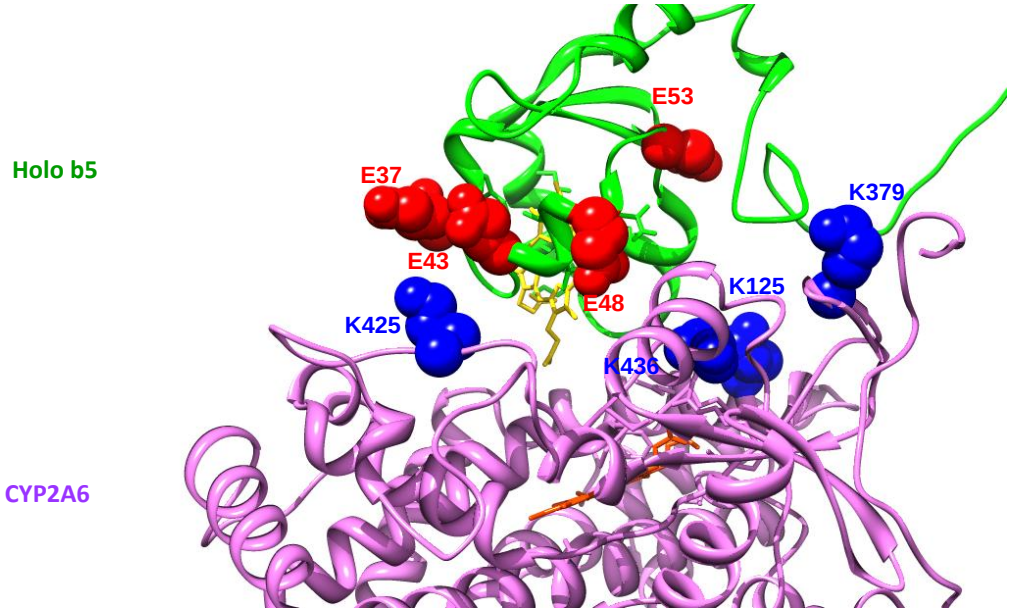
Holo b5
E53
E37
K379
E43
K125
E48
K425
K436
CYP2A6

(B)

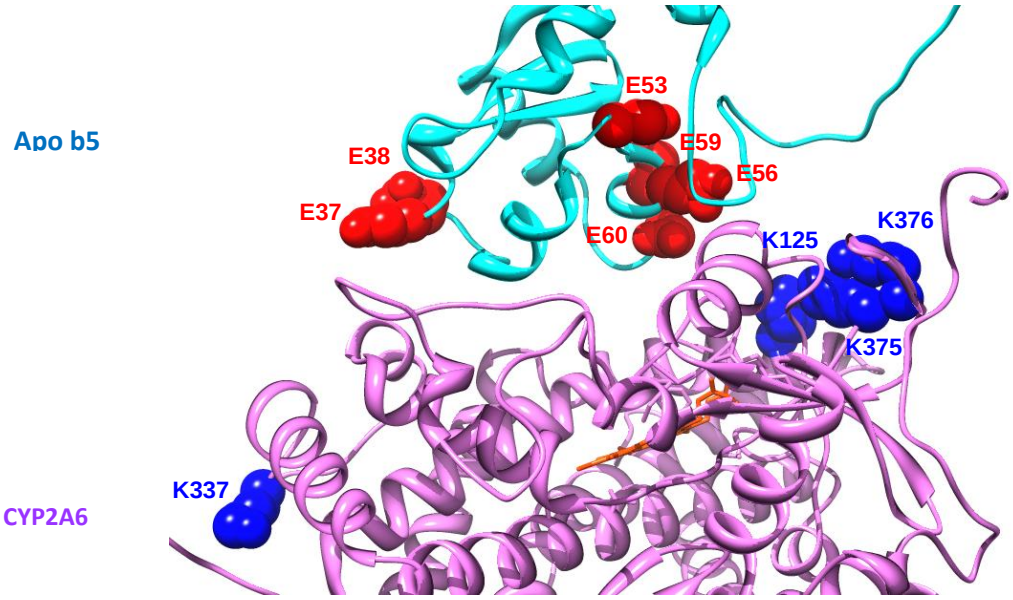
Apo b5
E53
E59
E38
E56
E37
K376
E60
K125
K375
K337
CYP2A6

(C)

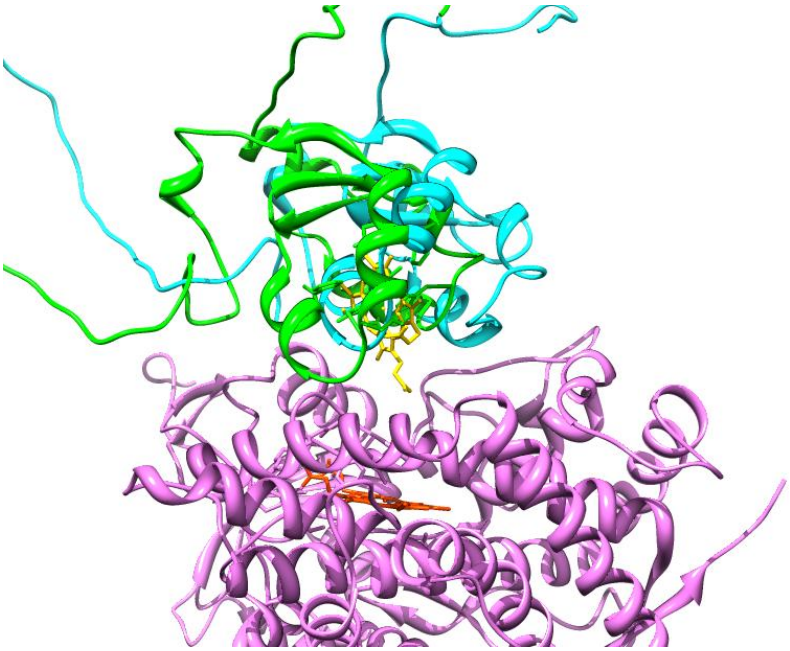

Figure 4.29. Holo/apo b5-CYP2A6 complex models. CYP2A6 is purple; holo b5 is green; apo b5 is cyan. The interacting residues on CYP2A6 and holo/apo b5 are blue and red, respectively. (A) Holo b5 - CYP2A6 complex model. (B) Apo b5 – CYP2A6 complex model. (C) Comparison of holo/apo b5 with CYP2A6 in the orientations.

Table 4.1 Inter-molecular cross-linked peptides in the complex of holo b_5-CYP2A6.

No	Measured Mono-isotopic Peak (*m/z*)	Charge State	Measured Peptide Mass (Da)	Calculated peptide Mass (Da)	Error (ppm)	Mass Matches to Inter-molecular Cross-linked Peptides
1	561.2653	+5	2802.2953	2802.3038	3.0	(holo b_5: ^{48}EQAGGDATENFEDVGHSTDAR^{68})-(CYP2A6: ^{124}AKQLR^{128})
2	597.0750	+5	2981.3438	2981.3620	6.1	(holo b_5: ^{48}EQAGGDATENFEDVGHSTDAR^{68})-(CYP2A6: ^{376}KDTKFR^{381})
3	728.5439	+5	3638.6883	3638.7106	6.1	(holo b_5: ^{48}EQAGGDATENFEDVGHSTDAR^{68})-(CYP2A6: ^{425}KSDAFVPFSIGKR^{437})
4	613.0852	+5	3061.3948	3061.4093	4.7	(holo b_5: ^{48}EQAGGDATENFEDVGHSTDAR^{68})-(CYP2A6: ^{462}LKSSQSPK^{469})
5	818.1609	+5	4086.7733	4086.7894	3.9	(holo b5: 48EQAGGDATENFEDVGHSTDAR68)-(CYP2A6: 275MQEEEKNPNTEFYLK289)
6	697.8615	+4	2788.4226	2788.4305	2.8	(holo b_5: ^{35}FLEEHPGGEEVLR^{47})-(CYP2A6: ^{425}KSDAFVPFSIGK^{436})
7	458.2413	+5	2287.1753	2287.1830	3.4	(holo b_5: ^{35}FLEEHPGGEEVLR^{47})-(CYP2A6: ^{376}KDTKFR^{381})
8	436.6376	+5	2179.1568	2179.1618	2.3	(holo b_5: ^{35}FLEEHPGGEEVLR^{47})-(CYP2A6: ^{334}VIGKNR^{339})
	727.0552	+3	2179.1500		5.4	

Table 4.2 Assignment tandem MS spectra of precursor ion 561.2653 z=5 for cross-linked peptide holo b_5: ^{48}EQAGGDATENFEDVGHSTDAR^{68} - CYP2A6: ^{124}AKQLR^{128} (candidate no. 1 in Table 4.1).

Observed m/z	Charge state	Observed MH	Theoretical MH	Assignment	Error (ppm)
308.1988	2	615.3898	615.3937	y5β	-6.3
368.1551	1	368.1551	368.1565	b4α-H2O	-3.8
372.1735	2	743.3392	743.3431	y7α	-5.2
411.8532	3	1233.5440	1233.5495	y11α	-4.5
416.2591	1	416.2591	416.2616	y3β	-6.0
421.7084	2	842.4090	842.4115	y8α	-3.0
436.8909	3	1308.6571	1308.6655	b8α/b5β	-6.4
442.8952	3	1326.6700	1326.6761	b8α/y5β	-4.6
449.8695	3	1347.5929	1347.5924	y12α	0.4
473.9026	3	1419.6922	1419.6974	b9α/b5β-H2O	-3.7
479.2208	2	957.4338	957.4384	y9α	-4.8
479.9048	3	1437.6988	1437.7080	b9α/b5β	-6.4
493.2169	3	1477.6351	1477.6350	y13α(C13)	0.1
509.8447	5	2545.1923	2545.2026	y19α/y5β	-4.0
517.9174	3	1551.7366	1551.7510	b10α/b5β	-9.3
523.9243	3	1569.7573	1569.7616	b10α/y5β	-2.7
534.7340	2	1068.4602	1068.4704	y10α-18	-9.5
543.7413	2	1086.4748	1086.4810	y10α	-5.7
547.2540	5	2732.2388	2732.2296	b21α/b5β-2NH3-H2O	3.4
549.2588	1	549.2588	549.2627	y5α	-7.1
550.8582	5	2750.2598	2750.2402	b21α/b5β-2NH3	7.1
567.2741	3	1699.8067	1699.8194	b11α/b5β(C13)	-7.5
573.2815	3	1717.8289	1717.8300	b11α/y5β(C13)	-0.6
586.5274	4	2343.0862	2343.0960	y16α/y5β-17	-4.2
600.7824	4	2400.1062	2400.1175	y17α/y5β-17	-4.7
604.2867	3	1810.8445	1810.8355	b12α/y5β-17	5.0
605.0422	4	2417.1454	2417.1440	y17α/y5β	0.6
613.3157	2	1225.6236	1225.6284	b7α/y5β	-3.9
615.0421	4	2457.1450	2457.1390	y18α/y5β-17	2.4
617.2739	2	1233.5400	1233.5495	y11α	-7.7
619.2939	4	2474.1522	2474.1655	y18α/y5β	-5.4
632.8041	4	2528.1930	2528.1761	y19α/y5β-H2O	6.7
637.0527	4	2545.1874	2545.2026	y19α/y5β	-6.0
640.2966	4	2558.1630	2558.1550	b19α/y5β(C13)	3.1
654.8335	2	1308.6592	1308.6655	b8α/b5β	-4.8
663.8410	2	1326.6742	1326.6761	b8α/y5β	-1.4
665.7811	2	1330.5544	1330.5659	y12α-17	-8.6
674.2970	2	1347.5862	1347.5924	y12α	-4.6
728.3611	2	1455.7144	1455.7186	b9α/y5β	-2.9
785.3839	2	1569.7600	1569.7616	b10α/y5β	-1.0

Table 4.3 Assignment tandem MS spectra of precursor ion 597.0750 z=5 for cross-linked peptide holo b_5: ^{48}EQAGGDATENFEDVGHSTDAR^{68} - CYP2A6: ^{376}KDTKFR^{381} (candidate no. 2 in Table 4.1).

Observed m/z	Charge state	Observed MH	Theoretical MH	Assignment	Error (ppm)
246.1551	1	246.1551	246.1561	y2α	-4.1
397.7275	2	794.4472	794.4519	y6β	-5.9
421.7076	2	842.4074	842.4115	y8α	-4.9
449.8672	3	1347.5860	1347.5924	y12α	-4.7
468.8987	3	1404.6805	1404.6866	b7α/y6β	-4.3
496.5776	3	1487.7172	1487.7237	b8α/b6β	-4.4
502.5810	3	1505.7274	1505.7343	b8α/y6β	-4.6
539.5925	3	1616.7619	1616.7663	b9α/b6β	-2.7
543.7418	2	1086.4758	1086.4810	y9α	-4.8
545.5963	3	1634.7733	1634.7769	b9α/y6β	-2.2
583.6089	3	1748.8111	1748.8198	b10α/y6β	-5.0
617.2749	2	1233.5420	1233.5495	y11α	-6.1
632.6325	3	1895.8819	1895.8882	b11α/y6β	-3.3
674.2966	2	1347.5854	1347.5924	y12α	-5.2
718.2990	3	2152.8814	2152.8803	b21α-18-17	0.5
723.9695	3	2169.8929	2169.9068	b21α-18	-6.4
730.3084	2	1459.6090	1459.6084	y13α-17	0.4
738.8194	2	1476.6310	1476.6350	y13α	-2.7
753.3595	2	1505.7112	1505.6979	b10α/y4β	8.8
817.8902	2	1634.7726	1634.7769	b9α/y6β	-2.6

Table 4.4 Assignment tandem MS spectra of precursor ion 728.5439 z=5 for cross-linked peptide holo b_5: ^{48}EQAGGDATENFEDVGHSTDAR^{68} - CYP2A6: ^{425}KSDAFVPFSIGKR^{437}) (candidate no. 3 in Table 4.1).

Observed m/z	Charge state	Observed MH	Theoretical MH	Assignment	Error (ppm)
246.1553		246.1553	246.1561	y2α	-3.2
484.6053	3	1451.8003	1451.8005	y13α	-0.1
549.2607	1	549.2607	549.2627	y5α	-3.6
564.3021	3	1690.8907	1690.8911	b2α/y13β	-0.2
587.9758	3	1761.9118	1761.9282	b3α/y13β	-9.3
648.3324	1	648.3324	648.3352	b6β	-4.3
650.2819	3	1948.8301	1948.8268	y19α	1.7
664.3337	3	1990.9855	1990.9981	b6α/y13β	-6.3
674.2975	2	1347.5872	1347.5924	y12α	-3.9
717.9409	5	3585.6733	3585.6629	b21α/b13β-NH3	2.9
718.8650	2	1436.7222	1436.7128	b8α/y6β	6.5
743.3369	1	743.3369	743.3431	y7α	-8.3
789.3432	2	1577.6786	1577.6827	y14α	-2.6
844.6371	4	3375.5250	3375.5512	b19α/b13β	-7.8
849.1442	4	3393.5534	3393.5618	b19α/y13β	-2.5
873.9066	4	3492.6030	3492.605	b21α/y12β	-0.6
878.4083	4	3510.6098	3510.6156	y21α/y12β	-1.7
939.3919	2	1877.7760	1877.7896	y18α	-7.2
974.9103	2	1948.8128	1948.8268	y19α	-7.2
997.7992	3	2991.3820	2991.3827	y21α/y7β	-0.2
1094.4663	2	2187.9248	2187.9173	y21α-H2O	3.4

Table 4.5 Assignment tandem MS spectra of precursor ion 613.0852 z=5 for cross-linked peptide holo b_5: ^{48}EQAGGDATENFEDVGHSTDAR^{68} - CYP2A6: ^{462}LKSSQSPK^{469} (candidate no. 4 in Table 4.1).

Observed m/z	Charge state	Observed MH	Theoretical MH	Assignment	Error (ppm)
421.7078	2	842.4078	842.4115	y8α	-4.4
437.7517	2	874.4956	874.4993	y6β	4.3
450.2014	3	1348.5886	1348.5924	y9α(C13)	2.8
479.2222	2	957.4366	957.4384	y9α	-1.9
492.8820	3	1476.6304	1476.6350	y13α	-3.1
495.5786	3	1484.7202	1484.7340	b7α/y8β	-9.3
513.7593	2	1026.5108	1026.5103	b(6-7)α/y8β-2NH3	0.5
523.2610	3	1567.7674	1567.7710	b8α/b8β	2.3
529.2640	3	1585.7764	1585.781641	b8α/y8β	3.3
543.7433	2	1086.4788	1086.4810	y10α	-2.0
566.2729	3	1696.8031	1696.8137	b8α/y8β	6.2
572.2776	3	1714.8172	1714.8242	b9α/y8β	-4.1
653.3152	3	1957.9300	1957.9250	b11α/b8β	2.6
659.3153	3	1975.9303	1975.9356	b11α/y8β	-2.7
665.7898	2	1330.5718	1330.5659	y12α-NH3	4.4
674.2975	2	1347.5872	1347.5924	y12α	-3.9
684.0714	4	2733.2622	2733.2711	y18α/y8β	-3.3
691.3137	4	2762.2314	2762.2288	b19α/b8β-2H2O	0.9
695.8132	4	2780.2294	2780.2394	b19α/b8β-H2O	3.6
700.3201	4	2798.2570	2798.2500	b19α/b8β	2.5
701.8267	4	2804.2834	2804.3081	y19α/y8β	-8.8
704.8224	4	2816.2662	2816.2606	b19α/y8β	2.0
718.2982	3	2152.8790	2152.8802	b21α-H2O-NH3	-0.6
723.9713	3	2169.8983	2169.9067	b21α-H2O	-3.9
730.3044	2	1459.6010	1459.6085	y13α-H2O	-5.1
738.8176	2	1476.6274	1476.6350	y13α	-5.1
742.8679	2	1484.7280	1484.7340	b7α/y8β	-4.0
784.3926	2	1567.7774	1567.7710	b8α/b8β	4.1
793.3976	2	1585.7874	1585.7816	b8α/y8β	3.7
857.9128	2	1714.8178	1714.8242	b11α/y8β	-3.7
914.9396	2	1828.8714	1828.8672	b12α/y8β	2.3

Table 4.6 Assignment tandem MS spectra of precursor ion 818.1609 z=5 for holo b5: ^{48}EQAGGDATENFEDVGHSTDAR^{68} - CYP2A6: ^{275} MQEEEKNPNTEFYLK ^{289} (candidate no. 5 in Table 4.1).

Observed m/z	Charge state	Observed MH	Theoretical MH	Assignment	Error (ppm)
246.1552	1	246.1552	246.1561	y2α	-3.5
497.2536	2	993.4994	993.5040	y8β-H2O	-4.6
506.2595	2	1011.5112	1011.5115	y8α	-0.3
506.2595	2	1011.5112	1011.5146	y8β	-3.4
549.2602	1	549.2602	549.2627	y5α	-4.6
570.3269	1	570.3269	570.3286	y4β	-3.0
622.2847	3	1864.8385	1864.8422	b15β-17	-2.0
627.9616	3	1881.8692	1881.8687	b15β	0.3
633.9605	3	1899.8659	1899.8793	y15β	-7.1
650.2803	3	1948.8253	1948.8268	y19α	-0.8
674.2979	2	1347.5880	1347.5924	y12α	-3.3
686.3283	1	686.3283	686.3216	y6α	9.8
699.3696	1	699.3696	699.3712	y5β	2.2
738.8176	2	1476.6274	1476.6350	y13α	-5.1
741.3149	4	2962.2362	2962.2392	b21α/b6β	1.0
743.3433	1	743.3433	743.3431	y7α	0.2
756.8130	4	3024.2286	3024.2184	b21α/b15β-2NH3	3.4
761.0659	4	3041.2402	3041.2449	b21α/b15β-NH3	1.5
765.3226	4	3058.2670	3058.2714	y21α/b7β-H2O	-1.4
769.8245	4	3076.2746	3076.2820	y21α/b7β	-2.4
789.3434	2	1577.6790	1577.6827	y14α	-2.3
794.0862	4	3173.3214	3173.3349	y21α/b8β	-4.3
800.4162	1	800.4162	800.4189	y6β	-3.4
842.4144	1	842.4144	842.4115	y8α	3.5
882.3745	2	1763.7412	1763.7467	y16α	-3.1
889.3788	1	889.3788	889.3720	b7β	7.7
910.8854	2	1820.7630	1820.7682	y17α	-2.9
914.4692	1	914.4692	914.4618	y7β	8.1
925.6592	4	3699.6134	3699.5954	y21α/b(3-14)β	4.9
930.4017	2	1859.7956	1859.7790	y18α-H2O	8.9
939.3959	2	1877.7840	1877.7896	y18α	-3.0
957.1591	4	3825.6130	3825.614	y19α/y15β-NH3	0.3
958.1743	4	3829.6738	3829.6882	y19α/y15β	-3.8
961.1631	4	3841.6290	3841.6406	b19α/y15β	-3.0
975.4154	2	1949.8230	1949.8268	y19α(C13)	-1.9
993.5031	1	993.5031	993.5040	y8β-H2O	-0.9
1011.5114	1	1011.5114	1011.5146	y8β	-3.2
1026.4269	3	3077.2651	3077.2820	y21α/b7β(C13)	5.5
1094.9574	2	2188.9070	2188.9014	y21α-17	2.6

1125.5569	1	1125.5569	1125.5575	y9β	-0.5
1860.7554	1	1860.7554	1860.7731	y18α-NH3	-9.5
1899.8670	1	1899.8670	1899.8793	y15β	-6.5
1948.8143	1	1948.8143	1948.8268	y19α	-6.4

Table 4.7 Assignment tandem MS spectra of precursor ion 697.8615 z=4 for cross-linked peptide holo b_5: ^{35}FLEEHPGGEEVLR^{47} - CYP2A6: ^{425}KSDAFVPFSIGK^{436} (candidate no. 6 in Table 4.1).

Observed m/z	charge state	Observed MH	Theoretical MH	Assignment	Error (ppm)
324.6887	2	648.3696	648.3715	y6β	-2.9
334.1377	1	334.1377	334.1397	b(2-5)β	-6.0
374.2224	2	747.4370	747.4400	y7β	-4.0
404.2502	1	404.2502	404.2504	y4β	-0.5
428.7288	2	856.4498	856.4523	y8α	-2.9
497.2602	2	993.5126	993.5112	y9α	1.4
551.3166	1	551.3166	551.3187	y5β	-3.8
561.7809	2	1122.5540	1122.5538	y10α	0.2
608.6313	3	1823.8783	1823.8923	y13α/b2β	-7.7
626.3141	3	1876.9267	1876.9188	b13α/b4β	4.2
632.3143	3	1894.9273	1894.9294	y13α/b4β	-1.1
648.3695	1	648.3695	648.3715	y6β	-3.1
665.3395	3	1994.0029	1993.9978	b(2-13)α/b6β	2.6
675.3322	3	2023.9810	2023.9872	b13α/b5β	-3.1
681.3357	3	2041.9915	2041.9978	y13α/b4β	-3.1
708.3565	3	2123.0539	2123.0556	b13α/b5β	-0.8
714.011	3	2140.0174	2141.0662	y13α/b5β	3.4
747.4382	1	747.4382	747.4400	y7β	-2.4
759.4004	1	759.4004	759.3995	y7α	1.2
811.4204	2	1621.8330	1621.8332	y13α/b1β	-0.1
854.9358	2	1708.8638	1708.8653	y13α/b2β	-0.9
894.5075	1	894.5075	894.5084	y8β	-1.0
912.444	2	1823.8802	1823.8923	y13α/b3β	-6.6
947.9688	2	1894.9298	1894.9294	y13α/b5β	0.2
966.9933	2	1932.9788	1932.9854	b5α/y12β	-3.4
1012.5	2	2023.9918	2023.9872	b13α/b6β	2.3
1021.501	2	2041.9936	2041.9978	y13α/b5β	-2.1
1062.037	2	2123.0654	2123.0556	b13α/b6β	4.6
1071.034	2	2141.0606	2141.0662	y13α/b6β	-2.6

Table 4.8 Assignment tandem MS spectra of precursor ion 458.2413 z=5 for cross-linked peptide holo b_5: ^{35}FLEEHPGGEEVLR^{47} - CYP2A6: ^{376}KDTKFR^{381} (candidate no. 7 in Table 4.1).

Observed m/z	Charge state	Observed MH	Theoretical MH	Assignment	Error (ppm)
288.2014	1	288.2014	288.203	y2α	-5.6
387.2710	1	387.2710	387.2714	y3α	-1.0
443.7228	4	1771.8678	1771.8762	b9α/y6β	-4.7
451.0406	5	2251.1718	2251.1618	b13α/b6β	4.4
475.9855	4	1900.9186	1900.9188	b10α/y6β	-0.1
498.7546	4	1991.9950	1991.9934	y11α/b6β-17	0.8
500.7472	4	1999.9654	1999.9872	b11α/y6β	-10.9
503.2574	4	2010.0062	2010.0040	y11α/y6β-17	1.1
507.5100	4	2027.0166	2027.0305	y11α/y6β	-6.9
591.2917	3	1771.8595	1771.8762	b9α/y6β	-9.4
628.3120	3	1882.9204	1882.9082	b10α/b6β	6.5
634.3082	3	1900.9090	1900.9188	b10α/y6β	-5.2
667.6707	3	2000.9965	2000.9872	b11α/y6β(C13)	4.6

Table 4.9 Assignment tandem MS spectra of precursor ion 436.6376 z=5 for cross-linked peptide holo b_5: ^{35}FLEEHPGGEEVLR^{47} - CYP2A6: ^{334}VIGKNR^{339} (candidate 8 in Table 4.1)**.**

Observed m/z	charge state	Observed MH	Theoretical MH	Assignment	Error (ppm)
175.1182	1	175.1182	175.11895	y1α	-4.3
288.2018	1	288.2018	288.20302	y2α	-4.2
387.2695	1	387.2695	387.27143	y3α	-5.0
429.4326	5	2143.1318	2143.1407	b13α/b6β	-4.1
448.9778	4	1792.8878	1792.8977	b10α/y6β	-5.5
473.7465	4	1891.9626	1891.9661	b11α/y6β	-1.8
483.4999	4	1930.9762	1930.9882	b13α/y4β-H2O	-6.2
488.0033	4	1948.9898	1948.9988	b13α/y4β	-4.6
492.5063	4	1967.0018	1967.0093	y13α/y4β	-3.8
527.5842	3	1580.7370	1580.7452	b10α/b(3-6)β	-5.2
555.2862	3	1663.8430	1663.8551	b9α/y6β	-7.3
592.3007	3	1774.8865	1774.8871	b10α/b6β	-0.3
598.3011	3	1792.8877	1792.8977	b10α/y6β	-5.6

Table 4.10 Inter-molecular cross-linked peptides in the complex of apo cytb_5-CYP2A6.

No	Measured Mono-isotopic Peak (*m/z*)	Charge State	Measured Peptide Mass (Da)	Calculated peptide Mass (Da)	Error (ppm)	Mass Matches to Inter-molecular Cross-linked Peptides
1	561.2653	+5	2802.2953	2802.3038	3.0	(apo b_5: ^{48}EQAGGDATENFEDVGHSTDAR^{68})-(CYP2A6: ^{124}AKQLR^{128})
2	670.3018	+4	2678.1838	2678.1925	3.2	(apo b_5: ^{48}EQAGGDATENFEDVGHSTDAR^{68})-(CYP2A6: ^{376}KDTK^{379})
3	467.5060	+4	1867.0006	1867.0072	3.5	(apo b_5: ^{35}FLEEHPGGEEVLR^{47})-(CYP2A6: ^{374}VKK^{376})
4	719.0888	+4	2179.1542	2179.1618	3.5	(apo b_5: ^{48}EQAGGDATENFEDVGHSTDAR^{68})-(CYP2A6: ^{334}VIGKNR^{339})
5	545.5444	+4	2873.3318	2873.3409	3.2	(apo b_5: : ^{35}FLEEHPGGEEVLR^{47}-(CYP2A6: ^{334}VIGKNR^{339})
6	481.4475	+5	2403.2063	2403.2164	4.2	(apo b_5: : ^{35}FLEEHPGGEEVLR^{47}-(CYP2A6: ^{251}KVEHNQR^{257})

Table 4.11 Assignment tandem MS spectra of precursor ion 561.2653 z=5 for cross-linked peptide apo b_5: ^{48}EQAGGDATENFEDVGHSTDAR^{68} - CYP2A6: ^{124}AKQLR^{128} (candidate no. 1 in Table 4.10).

Observed m/z	Charge state	Observed MH	Theoretical MH	Assignment	Error
246.1553	1	246.1553	246.1561	y2α	-3.2
428.7278	2	856.4478	856.4523	b(7-10)α/b(1-4)β	5.3
479.2211	2	957.4344	957.4384	y9α	-4.2
543.7419	2	1086.476	1086.481	y10α	-4.6
566.9426	3	1698.8122	1698.8194	b11α/b5β	4.2
609.9535	3	1827.8449	1827.8620	b12α/y5β	9.4
615.0449	4	2457.1562	2457.1390	b18α/y5β-NH3	7.0
619.296	4	2474.1606	2474.1655	y18α/y5β	-2.0
637.0517	4	2545.1834	2545.2026	y19α/y5β	-7.5
674.2972	2	1347.5866	1347.5924	y12α	-4.3
776.377	2	1551.7462	1551.7509	b10α/b5β	-3.0
856.4502	1	856.4502	856.4523	b(7-10)α/b(1-4)β	2.5

Table 4.12 Assignment tandem MS spectra of precursor ion 597.0750 z=5 for cross-linked peptide apo b_5: ^{48}EQAGGDATENFEDVGHSTDAR^{68} - CYP2A6: ^{376}KDTK^{379} (candidate no. 2 in Table 4.10).

Observed m/z	Charge state	Observed MH	Theoretical MH	Assignment	Error (ppm)
246.1556	1	246.1556	246.1561	y2α	-1.9
248.16	1	248.1600	248.1605	y2β	-1.9
421.7084	2	842.4090	842.4115	y8α	-3.0
606.0269	4	2421.0842	2421.0913	y19α/y4β	-2.9
661.2943	4	2642.1538	2642.1713	b21α/b4β	-6.6
707.6613	3	2120.9683	2120.9843	y15α/y4β	-7.6
765.012	3	2293.0204	2293.0327	y17α/y4β	-5.4
784.0224	3	2350.0516	2350.0542	y18α/y4β	-1.1
799.0173	3	2395.0363	2395.0181	b21α/b2β-H2O	7.6
799.3353	3	2395.9903	2396.0022	b21α/b2β-NH3	5.0
805.0078	3	2413.0078	2413.0287	y21α/b2β-H2O	-8.6
805.349	3	2414.0314	2414.0128	y21α/b2β-NH3	7.7
807.6997	3	2421.0835	2421.0913	y19α/y4β	-3.2
811.3474	3	2432.0266	2432.0393	b19α/y4β(C13)	-5.2
909.8925	2	1818.7772	1818.7776	b13α/y4β-H2O	-0.2

Table 4.13 Assignment tandem MS spectra of precursor ion 728.5439 z=5 for cross-linked peptide apo b_5: ^{35}FLEEHPGGEEVLR^{47} - CYP2A6: ^{374}VKK^{376} (candidate no. 3 in Table 4.10).

Observed m/z	Charge state	Observed MH	Theoretical MH	Assignment	Error (ppm)
175.1182	1	175.1182	175.1190	y1α	-4.6
288.2016	1	288.2016	288.2030	y2α	-4.9
387.2695	1	387.2695	387.2714	y3α	-5.0
428.7275	2	856.4472	856.4523	y8α	-6.0
451.2372	3	1351.6960	1351.7005	b9α/y3β	-3.3
494.2493	3	1480.7323	1480.7431	b10α/y3β	-7.3
506.2808	2	1011.5538	1011.5622	b5α/y3β	-8.3
524.2813	3	1570.8283	1570.8335	y11α/b3β-H2O	-3.3
527.2721	3	1579.8007	1579.8115	b11α/y3β	-6.8
530.2837	3	1588.8355	1588.8441	y11α/b3β	-5.4
536.2867	3	1606.8445	1606.8547	y11α/y3β	-6.4
573.9802	3	1719.9250	1719.9388	y12α/y3β	-8.0
639.837	2	1278.6662	1278.6589	b(3-13)α/b2β-NH3-2H2O	5.7
648.8396	2	1296.6714	1296.6695	b(3-13)α/b2β-NH3-H2O	1.5
676.3491	2	1351.6904	1351.7005	b9α/y3β	-7.5
740.8728	2	1480.7378	1480.7431	b10α/y3β	-3.6
790.4092	2	1579.8106	1579.8115	b11α/y3β	-0.6

Table 4.14 Assignment tandem MS spectra of precursor ion 613.0852 z=5 for cross-linked peptide apo b_5: ^{48}EQAGGDATENFEDVGHSTDAR^{68} - CYP2A6: ^{334}VIGKNR^{339} (candidate no. 4 in Table 4.10).

Observed m/z	Charge state	Observed MH	Theoretical MH	Assignment	Error (ppm)
246.1552	1	246.1552	246.15607	y2α	-3.5
289.1604	1	289.1604	289.16188	y2β	-5.1
343.7173	2	686.4268	686.4308	y6β	5.8
421.7061	2	842.4044	842.41151	y8α	-8.4
474.2742	1	474.2742	474.27831	y4β	-8.7
479.2243	2	957.4408	957.43845	y9α	2.5
540.2017	1	540.2017	540.2048	b6α-H2O	5.8
549.2616	1	549.2616	549.26272	y5α	-2.0
617.2781	2	1233.5484	1233.5495	y11α	-0.9
654.8143	4	2616.2338	2616.2397	y19α/y6β	2.3
661.5541	4	2643.1930	2643.1778	y21α/y4β-H2O	5.8
674.2967	2	1347.5856	1347.5924	y12α	-5.0
686.4282	1	686.4282	686.4308	y6β	3.8
694.2763	1	694.2763	694.2791	b(13-19)α	4.0
705.8307	4	2820.2994	2820.2932	b21α/b7β-NH3	2.2
743.3447	1	743.3447	743.3431	y7α	2.2
749.0375	3	2245.0969	2245.0956	y14α/y6β	0.6
766.7094	3	2298.1126	2298.1221	y15α/b6β	4.1
772.7125	3	2316.1219	2316.1327	y15α/y6β	-4.7
830.0601	3	2488.1647	2488.1811	y17α/y6β	-6.6
849.0702	3	2545.1950	2545.2026	y18α/y6β	-3.0
864.7285	3	2592.1699	2592.1709	b19α/y6β-2h2O	-0.4
870.7275	3	2610.1669	2610.1815	b19α/y6β-H2O	-5.6
872.7457	3	2616.2215	2616.2397	y19α/y6β	-7.0
876.0558	3	2626.1518	2626.1513	b21α/y4β-NH3	0.2
876.7310	3	2628.1774	2628.1921	b19α/y6β	-5.6
881.7245	3	2643.1579	2643.1778	y21α/y4β-H2O	-7.5
887.7328	3	2661.1828	2661.1884	y21α/y4β	-2.1
1007.4630	2	2013.9182	2013.9261	b19α-H2O	-3.9
1086.4818	1	1086.4818	1086.481	y10α	0.7
1102.4330	1	1102.4330	1102.4436	b11α-H2O	9.6

Table 4.15 Assignment tandem MS spectra of precursor ion 818.1609 z=5 for apo b_5: : ^{35}FLEEHPGGEEVLR^{47}- CYP2A6: ^{334}VIGKNR^{339} (candidate no. 5 in Table 4.10).

Observed m/z	Charge state	Observed MH	Theoretical MH	Assignment	Error
261.1584	1	261.1584	261.1598	b2α	-5.4
428.7278	2	856.4478	856.4523	y8α	-5.3
556.2831	2	1111.5584	1111.5643	b5α/b(3-6)β	-5.3
591.3216	3	1771.9492	1771.9562	y10α/b6β	-4.0
597.3255	3	1789.9609	1789.9668	y10α/y6β	-3.3
628.6637	3	1883.9755	1883.9722	y11α/b6β-NH3	1.8
634.3348	3	1900.9888	1900.9987	y11α/b6β	-5.2
640.3384	3	1918.9996	1919.0093	y11α/y6β	-5.1
656.34	3	1967.0044	1967.0093	y13α/y4β	-2.5
662.3589	2	1323.71	1323.7168	b5α/y6β	-5.1
678.0327	3	2032.0825	2032.0934	y12α/y6β	-5.4
694.0364	3	2080.0936	2080.0934	y13α/y5β	0.1
856.4528	1	856.4528	856.4523	y8α	0.6

Table 4.16 Assignment tandem MS spectra of precursor ion 818.1609 z=5 for apo b_5: ^{35}FLEEHPGGEEVLR^{47}- CYP2A6: ^{251}KVEHNQR^{257} (candidate no 6 in Table 4.10).

Observed m/z	Charge state	Observed MH	Theoretical MH	Assignment	Error (ppm)
261.1584	1	261.1584	261.1598	b2α	-5.2
288.2011	1	288.2011	288.2030	y2α	-6.6
387.2714	1	387.2714	387.2714	y3α	-0.1
427.8954	3	1281.6706	1281.6698	b3α/y7β	0.6
429.4182	5	2143.0598	2143.0639	y11α/y7β	-1.9
437.7335	4	1747.9106	1747.9198	y8α/y7β	-5.3
516.3140	1	516.3140	516.3140	y4α	0.0
532.0158	4	2125.0398	2125.0533	y11α/y7β-H2O	-6.4
536.5171	4	2143.0450	2143.0639	y11α/y7β	-8.8
554.2794	1	554.2794	554.2794	Y4β	0.1
561.7761	2	1122.5444	1122.5538	y10α	-8.4
564.7885	4	2256.1306	2256.1480	y12α/y7β	-7.7
583.3066	3	1747.9042	1747.9198	y8α/y7β	-8.9
672.9829	3	2016.9331	2016.9522	b10α/y7β	-9.5

Chapter 5. CYP2D6 Interactions with Cyt b5 and Conclusions

5.1 Control experiments for crosslinking studies using CYP2D6-cyt b5 and CYPs-C-terminal truncated cyt b5

5.1.1 Rationale for control experiments

Previous studies have shown that CYP2D6 activity is not modulated by holo cyt b5 (Yamazaki et al., 1997; Yamazaki et al., 2002). Therefore, we hypothesize that cyt b5 and CYP2D6 do not have specific productive interactions. Cyt b5-CYP2D6 cross-linking experiment could serve as a negative control for the cross-linking study, to exclude artificial non-specific interaction introduced by the in-vitro conditions.

In addition, it has been reported that C-terminally truncated cyt b5 can not stimulate CYP activity (Vergeres and Waskell, 1992). Thus, truncated cyt b5 instead of holo b5 in all the holo b5-CYPs cross-linking experiments can also serve as control experiments.

5.1.2 Methods

5.1.2.1 CYP2D6 and truncated cyt b5 preparation

The pSP19T7LT plasmid containing human CYP2D6 (wild type) with a C-terminal His6-tag and human CPR was kindly provided by Dr. Magnus Ingelman-Sundberg (Karolinska Institute, Stockholm, Sweden). The expression and purification were according to (Keizers et al., 2004).Truncated cyt b5 was prepared according to (Holmans et al., 1994).

5.1.2.2 Cross-linking studies of cyt b5-CYP2D6 and CYPs-truncated cyt b5

For cyt b5-CYP2D6, cyt b5 and CYP2D6 were reconstituted as previously described and the cross-linking experiment was carried out using the same method as described in chapters 3 and 4. Truncated cyt b5 and CYP2C9, CYP2D6, CYP3A4 and CYP2A6 were also reconstituted in the same way, respectively, and cross-linking experiments between truncated cyt b5 and each CYP isoform were carried out. Mass spectrometric analysis was done as described in chapters 2-4.

5.1.3 Results

CYP2D6 and cyt b5 cross-linking result showed that only the C-terminus of holo cyt b5 is cross-linked with CYP2D6 surface residues. The cross-linked peptides are holo b5: LYMAED - CYP2D6: ^{389}IPKGTTLITNLSSVLK^{404} and holo b5: LYMAED - CYP2D6: ^{141}NLGLGKK^{147}, in which Lys391 and Lys146 were cross-linked with the C-terminal acidic residues. Lys391 and Lys146 are on the loop between β2-2 and β1-3, and the beginning of D helix, respectively. In physiological conditions, cyt b5 is anchored on the membrane by its C-terminus α-helix domain with its tail located in the lumen side of the membrane. Therefore, the identified cross-linking of cyt b5 C-terminal residues with CYP2D6 surface residues can only be caused by non-specific interactions. There were no other cross-linking peptides seen in the experiments.

Likewise, no specific cross-linked peptides were identified by mass spectrometric analysis between truncated b5 and any of the CYPs tested (CYP2C9, CYP2D6, CYP3A4 and CYP2A6).

5.1.4 Discussion

It is unlikely that the identified cross-linked peptides are from any specific interactions between CYP2D6 and cyt b5, as only C-terminal residues of cyt b5 in the lumen side of the membrane was found cross-linked, rather than residues in the cytosolic functional domain of cyt b5. The formation of non-specific cross-linking peptides is very likely due to the non-physiological conditions in the in vitro system. This result is consistent with the literature reports that CYP2D6 does not need cyt b5 to fully exert its catalytic activity. Therefore, the cyt b5-CYP2D6 cross-linking experiment served as a negative control for our studies.

In addition, no cross-linked peptide was detected between truncated cyt b5 and any of the CYPs investigated in this study. C-terminally truncated cyt b5 lacks the potential for membrane association. Therefore, it is not able to properly orient in the liposomes to interact with CYPs. Mass spectrometric analysis failed to detect any cross-linked peptides between truncated b5 and any CYPs tested.

In holo/apo b5-CYP3A4/2C9/2A6 cross-linking experiments, the C-terminus of cyt b5 was also found to cross-link with surface residues on the CYPs. These cross-links also resulted from non-specific interactions.

5.2 Summary of cyt b5-CYP interactions

The current study provides for the first time the orientations of cyt b5 in the complexes of cyt b5-CYP isoforms. For holo b5 interaction with the CYPs (3A4, 2C9 and 2A6), the models show that the heme groups of holo b5 and each CYP isoform are not closely associated, with

a distance between the heme groups about 11-14 Å. Electron transfer would require the heme groups in a close contact or in the form of an electron tunneling. Through the current models, it is reasonable to speculate that allosteric effect of cyt b5 dominates its modulation effect on CYPs, in addition to its possible electron transfer role. Allosteric effects of cyt b5 on CYPs were first suggested in the studies by Lipscomb et al. (Lipscomb et al., 1976) and Guengerich et al (Guengerich et al., 1976), and have gained support recently (Porter, 2002; Schenkman and Jansson, 2003). Our results on the surface interaction between cyt b5 and CYPs 2A6, 2C9 and 3A4 also support the allosteric effect of cyt b5 on these isoforms, which are consistent with previously reported enzyme activity studies by Yamazaki et al (Yamazaki et al., 1997; Yamazaki et al., 1996a; Yamazaki et al., 2002).

Comparing the interaction models of holo/apo b5 interaction with CYP2A6, CYP2C9, CYP3A4, it can be seen that both holo and apo b5 bind to these CYP isoforms on the proximal surface of CYPs. The orientation of holo b5 and apo b5 on the same CYP differ slightly depending on the structural flexibility of the CYPs. Molecular dynamics simulations showed that active site flexibility of CYPs was as the follows: the most rigid is that of CYP2A6, followed by CYP2E1; CYP2C9 active sites are significantly more flexible (Arimoto, 2006); CYP3A4 is the most malleable (Skopalik et al., 2008). Therefore, the model shows that the orientation of holo b5 and apo b5 differ the most with CYP3A4, but the least with CYP2A6. For more rigid structure such as CYP2A6, it seems holo and apo b5 can recognize the binding sites more consistently. As a comparison, for structures with higher flexibility such as CYP3A4, holo and apo b5 seem to recognize the binding sites with higher degree of disparity in the bound orientations. Considering the relatively small structure disturbance of apo b5 upon removal of heme, it is reasonable to postulate that the similar

stimulatory effects of holo and apo b5 on CYPs result from their similar regulation of the various SRSs on the CYP.

In terms of the membrane orientations of CYPs and cyt b5, there are several reports (Berka et al., 2011; Clarke et al., 2004; Ohta et al., 1992; Schleinkofer et al., 2005; Williams et al., 2000). According to these studies, other than the N-terminal membrane anchor domain, the CYP F-G loops containing hydrophobic residues likely immerse into the membrane and provide a driving force for protein-membrane interaction. The CYPs height above the membrane is calculated to be approximately 3.5 ± 0.9 nm, e.g., for CYP2C9, the maximal height above the membrane is estimated to be ~4 nm. The heme plane of CYPs is estimated to tilt relative to the membrane, with the angle reported to be 38-78 ^{o} by Ohta et al. (Ohta et al., 1992), 90^{o} by William et al. (Williams et al., 2000), and 30 ± 5^{o} by Berka et al. (Berka et al., 2011). The proximal surface where redox partners of CYPs are proposed to bind is fully exposed to the hydrophilic environment of the cytosol. Cyt b5 has a linker domain of 15 amino acid between the cytosolic functional domain and the C-terminal membrane anchor domain, which has a length of 22.5-51 Å between the α helix form and the fully extended β sheet form. This linker domain has significant flexibility as shown in the different NMR conformations (PDB: 2I96 (human cyt b5), 1DO9 (rabbit cyt b5)) (Banci et al., 2000) and allows the functional domain to adopt different orientations when interacting with partners. In the models of holo/apo b5-CYPs interaction, when using an NMR solution conformation of cyt b5 to substitute its conformation in crystal structure, holo/apo b5 linker domains are capable of reaching the membrane, while having effective interaction with CYPs anchored in the membrane (Fig. 2.16). This suggests that under physiological conditions, it is possible for cyt b5 and CYPs to adopt the orientations as in the models to interact with each other.

5.3 Future direction of cyt b5-CYP interaction study

Mechanisms of cyt b5 modulation of CYPs are very complex. Surface interactions of cyt b5 and CYPs may result in the motion of structural elements of CYPs related to substrate binding, as well as the change of active site topology. Therefore, cyt b5 may affect multiple catalytic steps. In order to understand what conformational changes cyt b5 causes on the CYPs, it is important to perform molecular docking calculations based on the surface interaction identified by mass spectrometry. In the past, molecular dynamics simulations have been used to study CYP flexibility, substrate access/egress, membrane association, etc. (Berka et al., 2011; Cheng et al., 2006; Cojocaru et al., 2007; 2012; Conner et al., 2011; Davis and Lecomte, 2006). With the surface charge-pair interactions identified, calculation of protein association kinetics may be feasible. Selzer and Schreiber have shown that relative association rate constants of the proteins are highly correlated with the electrostatic interaction in the complex, as demonstrated in a number faster associating proteins (Elcock, 2001). The current study has identified the electrostatic binding sites, which provide the basis for further molecular dynamics simulation to understand the complex interactions between CYPs and their redox partner cyt b5 in the membrane.

Bibliography

Anzenbacherova E, Bec N, Anzenbacher P, Hudecek J, Soucek P, Jung C, Munro AW and Lange R (2000) Flexibility and stability of the structure of cytochromes P450 3A4 and BM-3. *European journal of biochemistry / FEBS* **267**:2916-2920.

Archakov AI, Karyakin AV and Skulachev VP (1974) Intermembrane electron transfer in mitochondrial and microsomal systems. *FEBS letters* **39**:239-242.

Arimoto R (2006) Computational models for predicting interactions with cytochrome p450 enzyme. *Current topics in medicinal chemistry* **6**:1609-1618.

Auchus RJ, Geller DH, Lee TC and Miller WL (1998a) The regulation of human P450c17 activity: relationship to premature adrenarche, insulin resistance and the polycystic ovary syndrome. *Trends in endocrinology and metabolism: TEM* **9**:47-50.

Auchus RJ, Lee TC and Miller WL (1998b) Cytochrome b5 augments the 17,20-lyase activity of human P450c17 without direct electron transfer. *J Biol Chem* **273**:3158-3165.

Backes WL and Eyer CS (1989) Cytochrome P-450 LM2 reduction. Substrate effects on the rate of reductase-LM2 association. *J Biol Chem* **264**:6252-6259.

Backes WL and Kelley RW (2003) Organization of multiple cytochrome P450s with NADPH-cytochrome P450 reductase in membranes. *Pharmacol Ther* **98**:221-233.

Banci L, Bertini I, Rosato A and Scacchieri S (2000) Solution structure of oxidized microsomal rabbit cytochrome b5. Factors determining the heterogeneous binding of the heme. *European journal of biochemistry / FEBS* **267**:755-766.

Berka K, Hendrychova T, Anzenbacher P and Otyepka M (2011) Membrane position of ibuprofen agrees with suggested access path entrance to cytochrome P450 2C9 active site. *The journal of physical chemistry A* **115**:11248-11255.

Bernhardt R, Makower A, Janig GR and Ruckpaul K (1984) Selective chemical modification of a functionally linked lysine in cytochrome P-450 LM2. *Biochimica et biophysica acta* **785**:186-190.

Bernhardt R, Pommerening K and Ruckpaul K (1987) Modification of carboxyl groups on NADPH-cytochrome P-450 reductase involved in binding of cytochromes c and P-450 LM2. *Biochemistry international* **14**:823-832.

Black SD, French JS, Williams CH, Jr. and Coon MJ (1979) Role of a hydrophobic polypeptide in the N-terminal region of NADPH-cytochrome P-450 reductase in complex formation with P-450LM. *Biochem Biophys Res Commun* **91**:1528-1535.

Bozina N, Bradamante V and Lovric M (2009) Genetic polymorphism of metabolic enzymes P450 (CYP) as a susceptibility factor for drug response, toxicity, and cancer risk. *Arhiv za higijenu rada i toksikologiju* **60**:217-242.

Bridges A, Gruenke L, Chang YT, Vakser IA, Loew G and Waskell L (1998) Identification of the binding site on cytochrome P450 2B4 for cytochrome b5 and cytochrome P450 reductase. *J Biol Chem* **273**:17036-17049.

Canova-Davis E, Chiang JY and Waskell L (1985) Obligatory role of cytochrome b5 in the microsomal metabolism of methoxyflurane. *Biochemical pharmacology* **34**:1907-1912.

Chen W, Koenigs LL, Thompson SJ, Peter RM, Rettie AE, Trager WF and Nelson SD (1998) Oxidation of acetaminophen to its toxic quinone imine and nontoxic catechol

metabolites by baculovirus-expressed and purified human cytochromes P450 2E1 and 2A6. *Chem Res Toxicol* **11**:295-301.
Cheng D, Kelley RW, Cawley GF and Backes WL (2004) High-level expression of recombinant rabbit cytochrome P450 2E1 in Escherichia coli C41 and its purification. *Protein Expr Purif* **33**:66-71.
Cheng Q, Benson DR, Rivera M and Kuczera K (2006) Influence of point mutations on the flexibility of cytochrome b5: molecular dynamics simulations of holoproteins. *Biopolymers* **83**:297-312.
Chudaev MV, Gilep AA and Usanov SA (2001) Site-directed mutagenesis of cytochrome b5 for studies of its interaction with cytochrome P450. *Biochemistry Biokhimiia* **66**:667-681.
Clarke TA, Im SC, Bidwai A and Waskell L (2004) The role of the length and sequence of the linker domain of cytochrome b5 in stimulating cytochrome P450 2B4 catalysis. *J Biol Chem* **279**:36809-36818.
Cojocaru V, Winn PJ and Wade RC (2007) The ins and outs of cytochrome P450s. *Biochimica et biophysica acta* **1770**:390-401.
Cojocaru V, Winn PJ and Wade RC (2012) Multiple, Ligand-dependent Routes from the Active Site of Cytochrome P450 2C9. *Current drug metabolism* **13**:143-154.
Conner KP, Woods CM and Atkins WM (2011) Interactions of cytochrome P450s with their ligands. *Arch Biochem Biophys* **507**:56-65.
Correia MA and Mannering GJ (1973) Reduced diphosphopyridine nucleotide synergism of the reduced triphosphopyridine nucleotide-dependent mixed-function oxidase system of hepatic microsomes. II. Role of the type I drug-binding site of cytochrome P-450. *Molecular pharmacology* **9**:470-485.
Crespi CL and Miller VP (1997) The R144C change in the CYP2C9*2 allele alters interaction of the cytochrome P450 with NADPH:cytochrome P450 oxidoreductase. *Pharmacogenetics* **7**:203-210.
Cunane LM, Chen ZW, Durley RC and Mathews FS (1996) X-ray structure of the cupredoxin amicyanin, from Paracoccus denitrificans, refined at 1.31 A resolution. *Acta crystallographica Section D, Biological crystallography* **52**:676-686.
Cvrk T, Hodek P and Strobel HW (1996) Identification and characterization of cytochrome P4501A1 amino acid residues interacting with a radiolabeled photoaffinity diazido-benzphetamine analogue. *Arch Biochem Biophys* **330**:142-152.
Davis RB, Jr. and Lecomte JT (2006) A dynamic N-capping motif in cytochrome b5: evidence for a pH-controlled conformational switch. *Proteins* **63**:336-348.
Davydov DR (2001) Microsomal monooxygenase in apoptosis: another target for cytochrome c signaling? *Trends in biochemical sciences* **26**:155-160.
Davydov DR, Knyushko TV, Kanaeva IP, Koen YM, Samenkova NF, Archakov AI and Hui Bon Hoa G (1996) Interactions of cytochrome P450 2B4 with NADPH-cytochrome P450 reductase studied by fluorescent probe. *Biochimie* **78**:734-743.
Denisov IG, Makris TM, Sligar SG and Schlichting I (2005) Structure and chemistry of cytochrome P450. *Chemical reviews* **105**:2253-2277.
Di Primo C, Deprez E, Sligar SG and Hui Bon Hoa G (1997) Origin of the photoacoustic signal in cytochrome P-450cam: role of the Arg186-Asp251-Lys178 bifurcated salt bridge. *Biochemistry* **36**:112-118.

Di YM, Chow VD, Yang LP and Zhou SF (2009) Structure, function, regulation and polymorphism of human cytochrome P450 2A6. *Current drug metabolism* **10**:754-780.

Dickmann LJ, Locuson CW, Jones JP and Rettie AE (2004) Differential roles of Arg97, Asp293, and Arg108 in enzyme stability and substrate specificity of CYP2C9. *Molecular pharmacology* **65**:842-850.

Dong MS, Yamazaki H, Guo Z and Guengerich FP (1996) Recombinant human cytochrome P450 1A2 and an N-terminal-truncated form: construction, purification, aggregation properties, and interactions with flavodoxin, ferredoxin, and NADPH-cytochrome P450 reductase. *Arch Biochem Biophys* **327**:11-19.

Ekroos M and Sjogren T (2006) Structural basis for ligand promiscuity in cytochrome P450 3A4. *Proceedings of the National Academy of Sciences of the United States of America* **103**:13682-13687.

Elcock AH, Sept,D., and McCammon,J.A. (2001) Computer Simulation of Protein-Protein Interactions. *J Phys Chem B* **105**:1504-1518.

Ellis J, Gutierrez A, Barsukov IL, Huang WC, Grossmann JG and Roberts GC (2009) Domain motion in cytochrome P450 reductase: conformational equilibria revealed by NMR and small-angle x-ray scattering. *J Biol Chem* **284**:36628-36637.

Emoto C and Iwasaki K (2007) Approach to predict the contribution of cytochrome P450 enzymes to drug metabolism in the early drug-discovery stage: the effect of the expression of cytochrome b(5) with recombinant P450 enzymes. *Xenobiotica; the fate of foreign compounds in biological systems* **37**:986-999.

Estabrook RW, Franklin MR, Cohen B, Shigamatzu A and Hildebrandt AG (1971) Biochemical and genetic factors influencing drug metabolism. Influence of hepatic microsomal mixed function oxidation reactions on cellular metabolic control. *Metabolism: clinical and experimental* **20**:187-199.

Eyer CS and Backes WL (1992) Relationship between the rate of reductase-cytochrome P450 complex formation and the rate of first electron transfer. *Arch Biochem Biophys* **293**:231-240.

Falzone CJ, Mayer MR, Whiteman EL, Moore CD and Lecomte JT (1996) Design challenges for hemoproteins: the solution structure of apocytochrome b5. *Biochemistry* **35**:6519-6526.

Farooq Y and Roberts GC (2010) Kinetics of electron transfer between NADPH-cytochrome P450 reductase and cytochrome P450 3A4. *The Biochemical journal* **432**:485-493.

Finn RD, McLaughlin LA, Ronseaux S, Rosewell I, Houston JB, Henderson CJ and Wolf CR (2008) Defining the in Vivo Role for cytochrome b5 in cytochrome P450 function through the conditional hepatic deletion of microsomal cytochrome b5. *J Biol Chem* **283**:31385-31393.

Forrester LM, Henderson CJ, Glancey MJ, Back DJ, Park BK, Ball SE, Kitteringham NR, McLaren AW, Miles JS, Skett P and et al. (1992) Relative expression of cytochrome P450 isoenzymes in human liver and association with the metabolism of drugs and xenobiotics. *The Biochemical journal* **281 (Pt 2)**:359-368.

French JS, Guengerich FP and Coon MJ (1980) Interactions of cytochrome P-450, NADPH-cytochrome P-450 reductase, phospholipid, and substrate in the reconstituted liver microsomal enzyme system. *J Biol Chem* **255**:4112-4119.

Gao Q (2007) An Investigation of Interactions of Cytochrome b5 with Cytochrome P450s and Mechanisms of Cytochrome b5 on Cytochrome P450 Reactions.

Gao Q, Doneanu CE, Shaffer SA, Adman ET, Goodlett DR and Nelson SD (2006) Identification of the interactions between cytochrome P450 2E1 and cytochrome b5 by mass spectrometry and site-directed mutagenesis. *J Biol Chem* **281**:20404-20417.

Geller DH, Auchus RJ and Miller WL (1999) P450c17 mutations R347H and R358Q selectively disrupt 17,20-lyase activity by disrupting interactions with P450 oxidoreductase and cytochrome b5. *Mol Endocrinol* **13**:167-175.

Gigon PL, Gram TE and Gillette JR (1969) Studies on the rate of reduction of hepatic microsomal cytochrome P-450 by reduced nicotinamide adenine dinucleotide phosphate: effect of drug substrates. *Molecular pharmacology* **5**:109-122.

Gilep AA, Guryev OL, Usanov SA and Estabrook RW (2001) Apo-cytochrome b5 as an indicator of changes in heme accessability: preliminary studies with cytochrome P450 3A4. *Journal of inorganic biochemistry* **87**:237-244.

Gillam E. M. BT, Kim B., Ohmori S., and Guengerich F. P. (1993) Expression of modified human cytochrome P450 3A4 in *Escherichia coli* and purification and reconstitution of the enzyme. *Arch Biochem Biophys* **305**:123-131.

Gillam EM, Aguinaldo AM, Notley LM, Kim D, Mundkowski RG, Volkov AA, Arnold FH, Soucek P, DeVoss JJ and Guengerich FP (1999) Formation of indigo by recombinant mammalian cytochrome P450. *Biochem Biophys Res Commun* **265**:469-472.

Giordano SJ, Kaftory A and Steggles AW (1994) A splicing mutation in the cytochrome b5 gene from a patient with congenital methemoglobinemia and pseudohermaphrodism. *Human genetics* **93**:568-570.

Gorsky LD, Koop DR and Coon MJ (1984) On the stoichiometry of the oxidase and monooxygenase reactions catalyzed by liver microsomal cytochrome P-450. Products of oxygen reduction. *J Biol Chem* **259**:6812-6817.

Gotoh O (1992) Substrate recognition sites in cytochrome P450 family 2 (CYP2) proteins inferred from comparative analyses of amino acid and coding nucleotide sequences. *J Biol Chem* **267**:83-90.

Graham-Lorence S and Peterson JA (1996) P450s: structural similarities and functional differences. *The FASEB journal : official publication of the Federation of American Societies for Experimental Biology* **10**:206-214.

Graham SE and Peterson JA (1999) How similar are P450s and what can their differences teach us? *Arch Biochem Biophys* **369**:24-29.

Gruenke LD, Konopka K, Cadieu M and Waskell L (1995) The stoichiometry of the cytochrome P-450-catalyzed metabolism of methoxyflurane and benzphetamine in the presence and absence of cytochrome b5. *J Biol Chem* **270**:24707-24718.

Guengerich FP (1983) Oxidation-reduction properties of rat liver cytochromes P-450 and NADPH-cytochrome p-450 reductase related to catalysis in reconstituted systems. *Biochemistry* **22**:2811-2820.

Guengerich FP, Ballou DP and Coon MJ (1976) Spectral intermediates in the reaction of oxygen with purified liver microsomal cytochrome P-450. *Biochem Biophys Res Commun* **70**:951-956.

Guengerich FP, Martin, M. V., Beaune, P. H., Kremers, P., Wolff, T. and Waxman, D. J. (1986) *J Biol Chem* **261**:5051-5060.

Guryev OL, Gilep AA, Usanov SA and Estabrook RW (2001) Interaction of apo-cytochrome b5 with cytochromes P4503A4 and P45017A: relevance of heme transfer reactions. *Biochemistry* **40**:5018-5031.

Guryev OL, Gilep, A. A., Usanov, S. A. and Estabrook, R. W. (2001) *Biochemistry* **40**:5018–5031.

Hackett CS and Strittmatter P (1984) Covalent cross-linking of the active sites of vesicle-bound cytochrome b5 and NADH-cytochrome b5 reductase. *J Biol Chem* **259**:3275-3282.

Hamdane D, Xia C, Im SC, Zhang H, Kim JJ and Waskell L (2009) Structure and function of an NADPH-cytochrome P450 oxidoreductase in an open conformation capable of reducing cytochrome P450. *J Biol Chem* **284**:11374-11384.

Harlow GR and Halpert JR (1998) Analysis of human cytochrome P450 3A4 cooperativity: construction and characterization of a site-directed mutant that displays hyperbolic steroid hydroxylation kinetics. *Proceedings of the National Academy of Sciences of the United States of America* **95**:6636-6641.

Hendrychova T, Anzenbacherova E, Hudecek J, Skopalik J, Lange R, Hildebrandt P, Otyepka M and Anzenbacher P (2011) Flexibility of human cytochrome P450 enzymes: molecular dynamics and spectroscopy reveal important function-related variations. *Biochimica et biophysica acta* **1814**:58-68.

Hendrychova T, Berka K, Navratilova V, Anzenbacher P and Otyepka M (2012) Dynamics and hydration of the active sites of Mammalian cytochromes p450 probed by molecular dynamics simulations. *Current drug metabolism* **13**:177-189.

Hernandez P, Gras R, Frey J and Appel RD (2003) Popitam: towards new heuristic strategies to improve protein identification from tandem mass spectrometry data. *Proteomics* **3**:870-878.

Hildebrandt A and Estabrook RW (1971) Evidence for the participation of cytochrome b 5 in hepatic microsomal mixed-function oxidation reactions. *Arch Biochem Biophys* **143**:66-79.

Hlavica P, Schulze J and Lewis DF (2003) Functional interaction of cytochrome P450 with its redox partners: a critical assessment and update of the topology of predicted contact regions. *Journal of inorganic biochemistry* **96**:279-297.

Holmans PL, Shet MS, Martin-Wixtrom CA, Fisher CW and Estabrook RW (1994) The high-level expression in Escherichia coli of the membrane-bound form of human and rat cytochrome b5 and studies on their mechanism of function. *Arch Biochem Biophys* **312**:554-565.

Holmans PL, Shet, M. S., Martin-Wixtrom, C. A., Fisher, C. W. and Estabrook, R. W. (1994) *Arch Biochem Biophys* **312**:554-565.

Idkowiak J, Randell T, Dhir V, Patel P, Shackleton CH, Taylor NF, Krone N and Arlt W (2012) A Missense Mutation in the Human Cytochrome b5 Gene causes 46,XY Disorder of Sex Development due to True Isolated 17,20 Lyase Deficiency. *The Journal of clinical endocrinology and metabolism* **97**:E465-475.

Im SC and Waskell L (2011) The interaction of microsomal cytochrome P450 2B4 with its redox partners, cytochrome P450 reductase and cytochrome b(5). *Arch Biochem Biophys* **507**:144-153.

Imai Y and Sato R (1977) The roles of cytochrome b5 in a reconstituted N-demethylase system containing cytochrome P-450. *Biochem Biophys Res Commun* **75**:420-426.

Jansson I and Schenkman JB (1987) Influence of cytochrome b5 on the stoichiometry of the different oxidative reactions catalyzed by liver microsomal cytochrome P-450. *Drug Metab Dispos* **15**:344-348.

Jansson I and Schenkman JB (1996) Substrate influence on interaction between cytochrome P450 and cytochrome b5 in microsomes. *Arch Biochem Biophys* **325**:265-269.

Johnson EF and Muller-Eberhard U (1977) Resolution of two forms of cytochrome P-450 from liver microsomes of rabbit treated with 2,3,7,8-tetrachlorodibenzo-p-dioxin. *J Biol Chem* **252**:2839-2845.

Johnson WW and Guengerich FP (1997) Reaction of aflatoxin B1 exo-8,9-epoxide with DNA: kinetic analysis of covalent binding and DNA-induced hydrolysis. *Proceedings of the National Academy of Sciences of the United States of America* **94**:6121-6125.

Johnson WW, Yamazaki H, Shimada T, Ueng YF and Guengerich FP (1997) Aflatoxin B1 8,9-epoxide hydrolysis in the presence of rat and human epoxide hydrolase. *Chem Res Toxicol* **10**:672-676.

Jung C, de Vries S and Schunemann V (2011) Spectroscopic characterization of cytochrome P450 Compound I. *Arch Biochem Biophys* **507**:44-55.

Kaspera R, Naraharisetti SB, Evangelista EA, Marciante KD, Psaty BM and Totah RA (2011) Drug metabolism by CYP2C8.3 is determined by substrate dependent interactions with cytochrome P450 reductase and cytochrome b5. *Biochemical pharmacology* **82**:681-691.

Keizers PH, Lussenburg BM, de Graaf C, Mentink LM, Vermeulen NP and Commandeur JN (2004) Influence of phenylalanine 120 on cytochrome P450 2D6 catalytic selectivity and regiospecificity: crucial role in 7-methoxy-4-(aminomethyl)-coumarin metabolism. *Biochemical pharmacology* **68**:2263-2271.

Kenaan C, Zhang H, Shea EV and Hollenberg PF (2011) Uncovering the role of hydrophobic residues in cytochrome P450-cytochrome P450 reductase interactions. *Biochemistry* **50**:3957-3967.

Khan KK, He YQ, Domanski TL and Halpert JR (2002) Midazolam oxidation by cytochrome P450 3A4 and active-site mutants: an evaluation of multiple binding sites and of the metabolic pathway that leads to enzyme inactivation. *Molecular pharmacology* **61**:495-506.

Kim D, Wu ZL and Guengerich FP (2005) Analysis of coumarin 7-hydroxylation activity of cytochrome P450 2A6 using random mutagenesis. *J Biol Chem* **280**:40319-40327.

Kim K, Johnson JA and Derendorf H (2004) Differences in drug pharmacokinetics between East Asians and Caucasians and the role of genetic polymorphisms. *Journal of clinical pharmacology* **44**:1083-1105.

Kinobe RT, Parkinson OT, Mitchell DJ and Gillam EM (2005) P450 2C18 catalyzes the metabolic bioactivation of phenytoin. *Chem Res Toxicol* **18**:1868-1875.

Kok RC, Timmerman MA, Wolffenbuttel KP, Drop SL and de Jong FH (2010) Isolated 17,20-lyase deficiency due to the cytochrome b5 mutation W27X. *The Journal of clinical endocrinology and metabolism* **95**:994-999.

Kurian JR, Longlais BJ and Trepanier LA (2007) Discovery and characterization of a cytochrome b5 variant in humans with impaired hydroxylamine reduction capacity. *Pharmacogenetics and genomics* **17**:597-603.

Kuwahara S and Omura T (1980) Different requirement for cytochrome b5 in NADPH-supported O-deethylation of p-nitrophenetole catalyzed by two types of microsomal cytochrome P-450. *Biochem Biophys Res Commun* **96**:1562-1568.

Li W, Liu H, Luo X, Zhu W, Tang Y, Halpert JR and Jiang H (2007) Possible pathway(s) of metyrapone egress from the active site of cytochrome P450 3A4: a molecular dynamics simulation. *Drug Metab Dispos* **35**:689-696.

Licad-Coles E, He K, Yin H and Correia MA (1997) Cytochrome P450 2C11: Escherichia coli expression, purification, functional characterization, and mechanism-based inactivation of the enzyme. *Arch Biochem Biophys* **338**:35-42.

Lipscomb JD, Sligar SG, Namtvedt MJ and Gunsalus IC (1976) Autooxidation and hydroxylation reactions of oxygenated cytochrome P-450cam. *J Biol Chem* **251**:1116-1124.

Locuson CW, Gannett PM, Ayscue R and Tracy TS (2007a) Use of simple docking methods to screen a virtual library for heteroactivators of cytochrome P450 2C9. *J Med Chem* **50**:1158-1165.

Locuson CW, Wienkers LC, Jones JP and Tracy TS (2007b) CYP2C9 protein interactions with cytochrome b(5): effects on the coupling of catalysis. *Drug Metab Dispos* **35**:1174-1181.

Louerat-Oriou B, Perret A and Pompon D (1998) Differential redox and electron-transfer properties of purified yeast, plant and human NADPH-cytochrome P-450 reductases highly modulate cytochrome P-450 activities. *European journal of biochemistry / FEBS* **258**:1040-1049.

Loughran PA, Roman LJ, Miller RT and Masters BS (2001) The kinetic and spectral characterization of the E. coli-expressed mammalian CYP4A7: cytochrome b5 effects vary with substrate. *Arch Biochem Biophys* **385**:311-321.

Ludemann SK, Lounnas V and Wade RC (2000) How do substrates enter and products exit the buried active site of cytochrome P450cam? 1. Random expulsion molecular dynamics investigation of ligand access channels and mechanisms. *Journal of molecular biology* **303**:797-811.

Mathews FS, Czerwinski, E. W., Argos, P. (1979) The Porphyrins. **7**:107-147.

McLaughlin LA, Ronseaux S, Finn RD, Henderson CJ and Roland Wolf C (2010) Deletion of microsomal cytochrome b5 profoundly affects hepatic and extrahepatic drug metabolism. *Molecular pharmacology* **78**:269-278.

Mendieta-Wejebe JE, Correa-Basurto J, Garcia-Segovia EM, Ceballos-Cancino G and Rosales-Hernandez MC (2011) Molecular modeling used to evaluate CYP2C9-dependent metabolism: homology modeling, molecular dynamics and docking simulations. *Current drug metabolism* **12**:533-548.

Mendonca BB, Domenice S, Arnhold IJ and Costa EM (2009) 46,XY disorders of sex development (DSD). *Clinical endocrinology* **70**:173-187.

Miwa GT and Lu AY (1984) The association of cytochrome P-450 and NADPH-cytochrome P-450 reductase in phospholipid membranes. *Arch Biochem Biophys* **234**:161-166.

Miwa GT, West SB, Huang MT and Lu AY (1979) Studies on the association of cytochrome P-450 and NADPH-cytochrome c reductase during catalysis in a reconstituted hydroxylating system. *J Biol Chem* **254**:5695-5700.

Mizutani T (2003) PM frequencies of major CYPs in Asians and Caucasians. *Drug metabolism reviews* **35**:99-106.

Moore CD and Lecomte JT (1990) Structural properties of apocytochrome b5: presence of a stable native core. *Biochemistry* **29**:1984-1989.
Morgan ET and Coon MJ (1984) Effects of cytochrome b5 on cytochrome P-450-catalyzed reactions. Studies with manganese-substituted cytochrome b5. *Drug Metab Dispos* **12**:358-364.
Naffin-Olivos JL and Auchus RJ (2006) Human cytochrome b5 requires residues E48 and E49 to stimulate the 17,20-lyase activity of cytochrome P450c17. *Biochemistry* **45**:755-762.
Nisimoto Y and Lambeth JD (1985) NADPH-cytochrome P-450 reductase-cytochrome b5 interactions: crosslinking of the phospholipid vesicle-associated proteins by a water-soluble carbodiimide. *Arch Biochem Biophys* **241**:386-396.
Ohta Y, Kawato S, Tagashira H, Takemori S and Kominami S (1992) Dynamic structures of adrenocortical cytochrome P-450 in proteoliposomes and microsomes: protein rotation study. *Biochemistry* **31**:12680-12687.
Olsen JV, Ong SE and Mann M (2004) Trypsin cleaves exclusively C-terminal to arginine and lysine residues. *Molecular & cellular proteomics : MCP* **3**:608-614.
Ortiz de Montellano PR (2005) *Cytochrome P450: Structure, Mechanism, and Biochemistry*.
Paine MF, Hart HL, Ludington SS, Haining RL, Rettie AE and Zeldin DC (2006) The human intestinal cytochrome P450 "pie". *Drug Metab Dispos* **34**:880-886.
Perret A and Pompon D (1998) Electron shuttle between membrane-bound cytochrome P450 3A4 and b5 rules uncoupling mechanisms. *Biochemistry* **37**:11412-11424.
Peterson JA, Ebel RE, O'Keeffe DH, Matsubara T and Estabrook RW (1976) Temperature dependence of cytochrome P-450 reduction. A model for NADPH-cytochrome P-450 reductase:cytochrome P-450 interaction. *J Biol Chem* **251**:4010-4016.
Phizicky EM and Fields S (1995) Protein-protein interactions: methods for detection and analysis. *Microbiological reviews* **59**:94-123.
Pierce BG, Hourai Y and Weng Z (2011) Accelerating protein docking in ZDOCK using an advanced 3D convolution library. *PloS one* **6**:e24657.
Pierce Biotechnology I (2005) Cross-Linking Reagents technical handbook.
Porter TD (2002) The roles of cytochrome b5 in cytochrome P450 reactions. *J Biochem Mol Toxicol* **16**:311-316.
Porubsky PR, Meneely KM and Scott EE (2008) Structures of human cytochrome P-450 2E1. Insights into the binding of inhibitors and both small molecular weight and fatty acid substrates. *J Biol Chem* **283**:33698-33707.
Qian W, Sun YL, Wang YH, Zhuang JH, Xie Y and Huang ZX (1998) The influence of mutation at Glu44 and Glu56 of cytochrome b5 on the protein's stabilization and interaction between cytochrome c and cytochrome b5. *Biochemistry* **37**:14137-14150.
Rettie AE and Jones JP (2005) Clinical and toxicological relevance of CYP2C9: drug-drug interactions and pharmacogenetics. *Annual review of pharmacology and toxicology* **45**:477-494.
Rittle J and Green MT (2010) Cytochrome P450 compound I: capture, characterization, and C-H bond activation kinetics. *Science* **330**:933-937.
Rittle J, Younker JM and Green MT (2010) Cytochrome P450: the active oxidant and its spectrum. *Inorganic chemistry* **49**:3610-3617.

Roberts AG, Campbell AP and Atkins WM (2005) The thermodynamic landscape of testosterone binding to cytochrome P450 3A4: ligand binding and spin state equilibria. *Biochemistry* **44**:1353-1366.

Roberts AG, Cheesman MJ, Primak A, Bowman MK, Atkins WM and Rettie AE (2010) Intramolecular heme ligation of the cytochrome P450 2C9 R108H mutant demonstrates pronounced conformational flexibility of the B-C loop region: implications for substrate binding. *Biochemistry* **49**:8700-8708.

Roussel F KK, Halpert JR (2000) The importance of SRS-1 residues in catalytic specificity of human cytochrome P450 3A4. *Arch Biochem Biophys* **374**:269-278.

Rui L, Pochapsky SS and Pochapsky TC (2006) Comparison of the complexes formed by cytochrome P450cam with cytochrome b5 and putidaredoxin, two effectors of camphor hydroxylase activity. *Biochemistry* **45**:3887-3897.

Sansen S, Hsu MH, Stout CD and Johnson EF (2007) Structural insight into the altered substrate specificity of human cytochrome P450 2A6 mutants. *Arch Biochem Biophys* **464**:197-206.

Schenkman JB and Jansson I (2003) The many roles of cytochrome b5. *Pharmacol Ther* **97**:139-152.

Schilling B, Row RH, Gibson BW, Guo X and Young MM (2003) MS2Assign, automated assignment and nomenclature of tandem mass spectra of chemically crosslinked peptides. *Journal of the American Society for Mass Spectrometry* **14**:834-850.

Schleinkofer K, Sudarko, Winn PJ, Ludemann SK and Wade RC (2005) Do mammalian cytochrome P450s show multiple ligand access pathways and ligand channelling? *EMBO reports* **6**:584-589.

Schoch GA, Yano JK, Wester MR, Griffin KJ, Stout CD and Johnson EF (2004) Structure of human microsomal cytochrome P450 2C8. Evidence for a peripheral fatty acid binding site. *J Biol Chem* **279**:9497-9503.

Schrag ML and Wienkers LC (2000) Topological alteration of the CYP3A4 active site by the divalent cation Mg(2+). *Drug Metab Dispos* **28**:1198-1201.

Schrag ML and Wienkers LC (2001) Triazolam substrate inhibition: evidence of competition for heme-bound reactive oxygen within the CYP3A4 active site. *Drug Metab Dispos* **29**:70-75.

Sellers EM, Kaplan HL and Tyndale RF (2000) Inhibition of cytochrome P450 2A6 increases nicotine's oral bioavailability and decreases smoking. *Clin Pharmacol Ther* **68**:35-43.

Sevrioukova IF and Poulos TL (2012) Structural and mechanistic insights into the interaction of cytochrome P4503A4 with bromoergocryptine, a type I ligand. *J Biol Chem* **287**:3510-3517.

Shaw PM, Hosea, N. A., Thompson, D. V., Lenius, J. M. and Guengerich, F. P. (1997) *Arch Biochem Biophys* **348**:107-115.

Shen AL, Porter TD, Wilson TE and Kasper CB (1989) Structural analysis of the FMN binding domain of NADPH-cytochrome P-450 oxidoreductase by site-directed mutagenesis. *J Biol Chem* **264**:7584-7589.

Shukla A, Huang W, Depaz IM and Gillam EM (2009) Membrane integration of recombinant human P450 forms. *Xenobiotica; the fate of foreign compounds in biological systems* **39**:495-507.

Singh P, Shaffer SA, Scherl A, Holman C, Pfuetzner RA, Larson Freeman TJ, Miller SI, Hernandez P, Appel RD and Goodlett DR (2008) Characterization of protein cross-

links via mass spectrometry and an open-modification search strategy. *Anal Chem* **80**:8799-8806.
Sinz A (2003) Chemical cross-linking and mass spectrometry for mapping three-dimensional structures of proteins and protein complexes. *Journal of mass spectrometry : JMS* **38**:1225-1237.
Skopalik J, Anzenbacher P and Otyepka M (2008) Flexibility of human cytochromes P450: molecular dynamics reveals differences between CYPs 3A4, 2C9, and 2A6, which correlate with their substrate preferences. *The journal of physical chemistry B* **112**:8165-8173.
Soucek P (1999) Expression of cytochrome P450 2A6 in Escherichia coli: purification, spectral and catalytic characterization, and preparation of polyclonal antibodies. *Arch Biochem Biophys* **370**:190-200.
Storch EM and Daggett V (1995) Molecular dynamics simulation of cytochrome b5: implications for protein-protein recognition. *Biochemistry* **34**:9682-9693.
Sugiyama T, Miki N, Miyake Y and Yamano T (1982) Interaction and electron transfer between cytochrome b5 and cytochrome P-450 in the reconstituted p-nitroanisole O-demethylase system. *J Biochem* **92**:1793-1803.
Tamburini PP and Schenkman JB (1987) Purification to homogeneity and enzymological characterization of a functional covalent complex composed of cytochromes P-450 isozyme 2 and b5 from rabbit liver. *Proceedings of the National Academy of Sciences of the United States of America* **84**:11-15.
Tamburini PP, White RE and Schenkman JB (1985) Chemical characterization of protein-protein interactions between cytochrome P-450 and cytochrome b5. *J Biol Chem* **260**:4007-4015.
Tang X, Munske GR, Siems WF and Bruce JE (2005) Mass spectrometry identifiable cross-linking strategy for studying protein-protein interactions. *Anal Chem* **77**:311-318.
Thermo Scientific I (2009) Thermo Scientific Pierce Crosslinking Technical Handbook.
Thorgeirsson TE, Gudbjartsson DF, Surakka I, Vink JM, Amin N, Geller F, Sulem P, Rafnar T, Esko T, Walter S, Gieger C, Rawal R, Mangino M, Prokopenko I, Magi R, Keskitalo K, Gudjonsdottir IH, Gretarsdottir S, Stefansson H, Thompson JR, Aulchenko YS, Nelis M, Aben KK, den Heijer M, Dirksen A, Ashraf H, Soranzo N, Valdes AM, Steves C, Uitterlinden AG, Hofman A, Tonjes A, Kovacs P, Hottenga JJ, Willemsen G, Vogelzangs N, Doring A, Dahmen N, Nitz B, Pergadia ML, Saez B, De Diego V, Lezcano V, Garcia-Prats MD, Ripatti S, Perola M, Kettunen J, Hartikainen AL, Pouta A, Laitinen J, Isohanni M, Huei-Yi S, Allen M, Krestyaninova M, Hall AS, Jones GT, van Rij AM, Mueller T, Dieplinger B, Haltmayer M, Jonsson S, Matthiasson SE, Oskarsson H, Tyrfingsson T, Kiemeney LA, Mayordomo JI, Lindholt JS, Pedersen JH, Franklin WA, Wolf H, Montgomery GW, Heath AC, Martin NG, Madden PA, Giegling I, Rujescu D, Jarvelin MR, Salomaa V, Stumvoll M, Spector TD, Wichmann HE, Metspalu A, Samani NJ, Penninx BW, Oostra BA, Boomsma DI, Tiemeier H, van Duijn CM, Kaprio J, Gulcher JR, McCarthy MI, Peltonen L, Thorsteinsdottir U and Stefansson K (2010) Sequence variants at CHRNB3-CHRNA6 and CYP2A6 affect smoking behavior. *Nature genetics* **42**:448-453.

Vatsis KP, Theoharides AD, Kupfer D and Coon MJ (1982) Hydroxylation of prostaglandins by inducible isozymes of rabbit liver microsomal cytochrome P-450. Participation of cytochrome b5. *J Biol Chem* **257**:11221-11229.

Vergeres G, Ramsden J and Waskell L (1995) The carboxyl terminus of the membrane-binding domain of cytochrome b5 spans the bilayer of the endoplasmic reticulum. *J Biol Chem* **270**:3414-3422.

Vergeres G and Waskell L (1992) Expression of cytochrome b5 in yeast and characterization of mutants of the membrane-anchoring domain. *J Biol Chem* **267**:12583-12591.

Vergeres G and Waskell L (1995) Cytochrome b5, its functions, structure and membrane topology. *Biochimie* **77**:604-620.

Voznesensky AI and Schenkman JB (1992) The cytochrome P450 2B4-NADPH cytochrome P450 reductase electron transfer complex is not formed by charge-pairing. *J Biol Chem* **267**:14669-14676.

Voznesensky AI and Schenkman JB (1994) Quantitative analyses of electrostatic interactions between NADPH-cytochrome P450 reductase and cytochrome P450 enzymes. *J Biol Chem* **269**:15724-15731.

Wang JF, Zhang CC, Chou KC and Wei DQ (2009) Structure of cytochrome p450s and personalized drug. *Current medicinal chemistry* **16**:232-244.

Wang M, Roberts DL, Paschke R, Shea TM, Masters BS and Kim JJ (1997) Three-dimensional structure of NADPH-cytochrome P450 reductase: prototype for FMN- and FAD-containing enzymes. *Proceedings of the National Academy of Sciences of the United States of America* **94**:8411-8416.

Wen B, Doneanu, C. E., Gartner, C. A., Roberts, A. G., Atkins, W. M. and Nelson, S. D. (2005) *Biochemistry* **44**:1833-1845.

Wen B, Lampe JN, Roberts AG, Atkins WM, David Rodrigues A and Nelson SD (2006) Cysteine 98 in CYP3A4 contributes to conformational integrity required for P450 interaction with CYP reductase. *Arch Biochem Biophys* **454**:42-54.

Wester MR, Yano JK, Schoch GA, Yang C, Griffin KJ, Stout CD and Johnson EF (2004) The structure of human cytochrome P450 2C9 complexed with flurbiprofen at 2.0-A resolution. *J Biol Chem* **279**:35630-35637.

Williams PA, Cosme J, Sridhar V, Johnson EF and McRee DE (2000) Mammalian microsomal cytochrome P450 monooxygenase: structural adaptations for membrane binding and functional diversity. *Molecular cell* **5**:121-131.

Williams PA, Cosme J, Vinkovic DM, Ward A, Angove HC, Day PJ, Vonrhein C, Tickle IJ and Jhoti H (2004) Crystal structures of human cytochrome P450 3A4 bound to metyrapone and progesterone. *Science* **305**:683-686.

Williams PA, Cosme J, Ward A, Angove HC, Matak Vinkovic D and Jhoti H (2003) Crystal structure of human cytochrome P450 2C9 with bound warfarin. *Nature* **424**:464-468.

Xia C, Hamdane D, Shen AL, Choi V, Kasper CB, Pearl NM, Zhang H, Im SC, Waskell L and Kim JJ (2011) Conformational changes of NADPH-cytochrome P450 oxidoreductase are essential for catalysis and cofactor binding. *J Biol Chem* **286**:16246-16260.

Yamaguchi Y, Khan KK, He YA, He YQ and Halpert JR (2004) Topological changes in the CYP3A4 active site probed with phenyldiazene: effect of interaction with NADPH-cytochrome P450 reductase and cytochrome b5 and of site-directed mutagenesis. *Drug Metab Dispos* **32**:155-161.

Yamano S, Tatsuno J and Gonzalez FJ (1990) The CYP2A3 gene product catalyzes coumarin 7-hydroxylation in human liver microsomes. *Biochemistry* **29**:1322-1329.

Yamazaki H, Gillam EM, Dong MS, Johnson WW, Guengerich FP and Shimada T (1997) Reconstitution of recombinant cytochrome P450 2C10(2C9) and comparison with cytochrome P450 3A4 and other forms: effects of cytochrome P450-P450 and cytochrome P450-b5 interactions. *Arch Biochem Biophys* **342**:329-337.

Yamazaki H, Johnson WW, Ueng YF, Shimada T and Guengerich FP (1996a) Lack of electron transfer from cytochrome b5 in stimulation of catalytic activities of cytochrome P450 3A4. Characterization of a reconstituted cytochrome P450 3A4/NADPH-cytochrome P450 reductase system and studies with apo-cytochrome b5. *J Biol Chem* **271**:27438-27444.

Yamazaki H, Nakamura M, Komatsu T, Ohyama K, Hatanaka N, Asahi S, Shimada N, Guengerich FP, Shimada T, Nakajima M and Yokoi T (2002) Roles of NADPH-P450 reductase and apo- and holo-cytochrome b5 on xenobiotic oxidations catalyzed by 12 recombinant human cytochrome P450s expressed in membranes of Escherichia coli. *Protein Expr Purif* **24**:329-337.

Yamazaki H, Nakano M, Gillam EM, Bell LC, Guengerich FP and Shimada T (1996b) Requirements for cytochrome b5 in the oxidation of 7-ethoxycoumarin, chlorzoxazone, aniline, and N-nitrosodimethylamine by recombinant cytochrome P450 2E1 and by human liver microsomes. *Biochemical pharmacology* **52**:301-309.

Yamazaki H, Nakano M, Imai Y, Ueng YF, Guengerich FP and Shimada T (1996c) Roles of cytochrome b5 in the oxidation of testosterone and nifedipine by recombinant cytochrome P450 3A4 and by human liver microsomes. *Arch Biochem Biophys* **325**:174-182.

Yamazaki H, Shimada T, Martin MV and Guengerich FP (2001) Stimulation of cytochrome P450 reactions by apo-cytochrome b5: evidence against transfer of heme from cytochrome P450 3A4 to apo-cytochrome b5 or heme oxygenase. *J Biol Chem* **276**:30885-30891.

Yano JK, Hsu MH, Griffin KJ, Stout CD and Johnson EF (2005) Structures of human microsomal cytochrome P450 2A6 complexed with coumarin and methoxsalen. *Nat Struct Mol Biol* **12**:822-823.

Yano JK, Wester, M. R., Schoch, G. A., Griffin, K. J., Stout, C. D. and Johnson, E. F. (2004) *J Biol Chem* **279**:38091-38094.

Young MM, Tang N, Hempel JC, Oshiro CM, Taylor EW, Kuntz ID, Gibson BW and Dollinger G (2000) High throughput protein fold identification by using experimental constraints derived from intramolecular cross-links and mass spectrometry. *Proceedings of the National Academy of Sciences of the United States of America* **97**:5802-5806.

Yu ET, Hawkins A, Kuntz ID, Rahn LA, Rothfuss A, Sale K, Young MM, Yang CL, Pancerella CM and Fabris D (2008) The collaboratory for MS3D: a new cyberinfrastructure for the structural elucidation of biological macromolecules and their assemblies using mass spectrometry-based approaches. *Journal of proteome research* **7**:4848-4857.

Zangar RC, Davydov DR and Verma S (2004) Mechanisms that regulate production of reactive oxygen species by cytochrome P450. *Toxicology and applied pharmacology* **199**:316-331.

Zhang H, Hamdane D, Im SC and Waskell L (2008) Cytochrome b5 inhibits electron transfer from NADPH-cytochrome P450 reductase to ferric cytochrome P450 2B4. *J Biol Chem* **283**:5217-5225.

Zhang H, Im SC and Waskell L (2007) Cytochrome b5 increases the rate of product formation by cytochrome P450 2B4 and competes with cytochrome P450 reductase for a binding site on cytochrome P450 2B4. *J Biol Chem* **282**:29766-29776.

Zhang H, Kenaan C, Hamdane D, Hoa GH and Hollenberg PF (2009) Effect of conformational dynamics on substrate recognition and specificity as probed by the introduction of a de novo disulfide bond into cytochrome P450 2B1. *J Biol Chem* **284**:25678-25686.

Zhang H, Myshkin E and Waskell L (2005) Role of cytochrome b5 in catalysis by cytochrome P450 2B4. *Biochem Biophys Res Commun* **338**:499-506.

Zhou YH, Zheng QC, Li ZS, Zhang Y, Sun M, Sun CC, Si D, Cai L, Guo Y and Zhou H (2006) On the human CYP2C9*13 variant activity reduction: a molecular dynamics simulation and docking study. *Biochimie* **88**:1457-1465.

Vita

Chunsheng Zhao was born in Henan province, China. She earned a Bachelor of Science degree at Tongji Medical University in Pharmacy in 1999 and a Master of Science degree at Shanghai Institute of Materia Medica, Chinese Academy of Sciences, in 2002. She then worked in biopharmaceutical industry in Shanghai for two years and came to US in 2004. She enrolled in the PhD program in Department of Medicinal Chemistry in University of Washington at Seattle in 2006. In 2012, she earned a Doctor of Philosophy at the University of Washington in Medicinal Chemistry.